Beam-plasma interaction in randomly inhomogeneous solar wind

Andrii Voshchepynets

UNIVERSITÉ D'ORLÉANS

ÉCOLE DOCTORALE ENERGIE - MATERIAUX - SCIENCES DE LA TERRE ET DE L'UNIVERS

LABORATOIRE : LPC2E

THÈSE présentée par :

Andrii Voshchepynets

soutenue le : **09 Novembre 2015**

pour obtenir le grade de : **Docteur de l'université d'Orléans**

Discipline/ Spécialité : **Physique de Plasmas**

Interaction faisceau-plasma dans un plasma aleatoirement non-homogene du vent solaire

THÈSE dirigée par :

Vladimir Krasnosselskikh	Directeur de Recherche, LPC2E/CNRS, Orleans, France

RAPPORTEURS :

Eduard Kontar	Reader, University of Glasgow, Glasgow, UK
Milan Maksimovic	Directeur de Recherche, Observatoire de Paris, Paris, France

---

JURY :

Laïfa Boufendi	Professeur, Université d'Orléans, Orléans, France, Président du jury
Eduard Kontar	Reader, University of Glasgow, Glasgow, UK
Vladimir Krasnosselskikh	Directeur de Recherche, LPC2E/CNRS, Orléans, France
Milan Maksimovic	Directeur de Recherche, Observatoire de Paris, Paris, France
Didier Mourenas	Ingénieur, CEA, DAM, DIF, F-91297, Arpajon, France
Michel Tagger	Chercheur, CEA/LPC2E, Orléans, France
Alexander Volokitin	Dr, senior research scientist, Space Research Institute, Moscow, Russia

Andrii Voshchepynets

Interaction faisceau-plasma dans un plasma aleatoirement non-homogene du vent solaire

Résumé : Dans cette thèse nous avons présenté un modèle probabiliste auto cohérent décrivant la relaxation d'un faisceau d'électrons dans un vent solaire dont les fluctuations aléatoires de la densité ont les mêmes propriétés spectrales que celles mesurées à bord de satellites. On a supposé que, le système possèdait différentes échelles caractéristiques en plus de l'échelle caractéristique des fluctuations de densité. Ceci nous a permis de décrire avec précision l'interaction onde-particule à des échelles inférieures à l'échelle caractéristique des fluctuations de densité en supposant que des paramètres d'onde sont connus: notamment, la phase, la fréquence et l'amplitude. Cependant, pour des échelles suffisamment plus grandes que l'échelle caractéristique des irrégularités de densité, l'interaction des ondes et des particules ne peut être caractérisée déterminé que par des quantités statistiques moyennes dans l'espace des vitesses à savoir: le taux de croissance/amortissement et le coefficient de diffusion des particules. En utilisant notre modèle, nous décrivons l'évolution de la fonction de distribution des électrons et d'énergie des ondes de Langmuir. Le schéma 1D suggérée est applicable pour des paramètres physiques de plasma du vent solaire à différentes distances du Soleil. Ainsi, nous pouvons utiliser nos calculs pour décrire des émissions solaires de Type III, ainsi que les interactions de faisceau avec le plasma, à des distances d'une Unité Astronomique du Soleil dans l'héliosphère et au voisinage des chocs planétaires.
Mots clés : accélération des particules, plasma, vent solaire

Beam-plasma interaction in randomly inhomogeneous solar wind

Résumé : This thesis is dedicated to effects of plasma density fluctuations in the solar wind on the relaxation of the electron beams ejected from the Sun. The density fluctuations are supposed to be responsible for the changes in the local phase velocity of the Langmuir waves generated by the beam instability. Changes in the wave phase velocity during the wave propagation can be described in terms of probability distribution function determined by distribution of the density fluctuations. Using these probability distributions we describe resonant wave particle interactions by a system of equations, similar to well known quasi-linear approximation, where the conventional velocity diffusion coefficient and the wave growth rate are replaced by the averaged in the velocity space. It was shown that the process of relaxation of electron beam is accompanied by transformation of significant part of the beam kinetic energy to energy of the accelerated particles via generation and absorption of the Langmuir waves. We discovered that for the very rapid beams the relaxation process consists of two well separated steps. On first step the major relaxation process occurs and the wave growth rate almost everywhere in the velocity space becomes close to zero or negative. At the seconde stage the system remains in the state close to state of marginal stability enough long to explain how the beam may be preserved traveling distances over 1 AU while still being able to generate the Langmuir waves. Keywords : acceleration of particles, plasma, solar wind

LPC2E, 3A, Avenue de la Recherche Scientifique, 45071 Orléans, France

Remerciements

Ma reconnaissance profonde va à mon directeur de thèse V.Krasnosselskikh, pour partage avec moi sa compréhension originale de la physique des plasmas et les traditions de son école scientifique.

Je veux remercier le professeur qui m'a invité à la physique des plasmas, O. Agapitov.

Le travail de cette thèse a aussi bénéficié de conversations et d'échanges avec A. Artemyev, A. Volokitin et C. Krafft.

Je suis reconnaissante envers mes rapporteurs, E. Kontar et M. Maksimovic, et les membres de mon jury de thèse, L. Boufendi et D. Mourenas.

Je remercie monsieur M. Tagger, Directeur du LPC2E qui m'a ouvert la porte du laboratoire pendant ces trois dernières années.

Je tiens à remercier personnes du LPC2E, pour leur aide, en particulier, T. Dudok De Wit, J.-L. Pinçon, M. Kretzschmar, C. Revillet, L. Jourdain, P. Henri, O. Randriamboarison, I. Langer , C. Revil , L. Royer F. Elie, A. Mattei.

Enfin, je suis reconnaissante envers mes parents et mon amie Sophie.

Contents

Chapter 1

Introduction

1.1 Solar electron beams

The Sun is most efficient accelerator of the charged particles in the solar system. Solar flares and their associated coronal mass ejections are the most violent examples of the acceleration of electrons. Solar flares are the manifestation of a sudden, intense and spatially concentrated release of energy in the solar corona, causing localized heating up to temperatures of $\sim 10^7 K$, as evidenced by the copious emissions of short-wavelength (soft X-ray, $0.1-10$ nm) radiation. The association of largest flares with magnetic active regions, and their very short onset time, leave little doubt that magnetic reconnection is the mechanism responsible for the dynamical release of magnetic energy [see, for instance, Kulsrud, 1998, Priest and Forbes, 2000].

All solar flare models involve magnetic reconnection in one or the other form [see Aschwanden, 2002, as review]. Magnetic reconnection changes the topology of the magnetic field by reconfiguring the connectivities between opposite magnetic polarities. During magnetic reconnection, the connectivity between opposite polarities is switched and the new-configured field lines snap back into a lower energy state. Reconfiguration of the unstable magnetic field configuration of the solar atmosphere to lower energy states results in the acceleration of charged particles up to relativistic energies. Over a period of tens of seconds to minutes, energy up to 10^{32} ergs can be transferred into accelerated electrons. [e.g., Emslie et al., 2012].

Accelerated electrons can escape the Sun before they lose their energy and slow down. In situ observations in the heliosphere provide the opportunity to directly detect solar flare accelerated electrons [e.g., van Allen and Krimigis, 1965, Anderson and Lin, 1966]. From the in situ observations in the interplanetary medium near 1 AU it was shown that solar impulsive $\sim 1 - 100$ keV electron events occur 10^3 times per year near solar maximum over the whole Sun [see Lin, 1985]. An analysis of the detailed observations of energetic electrons from the ISEE 3 spacecraft has revealed that electron distribution is highly anisotropic and is beamed along the background magnetic field lines. The impulsive electron events often show a clear scatter-free velocity dispersion

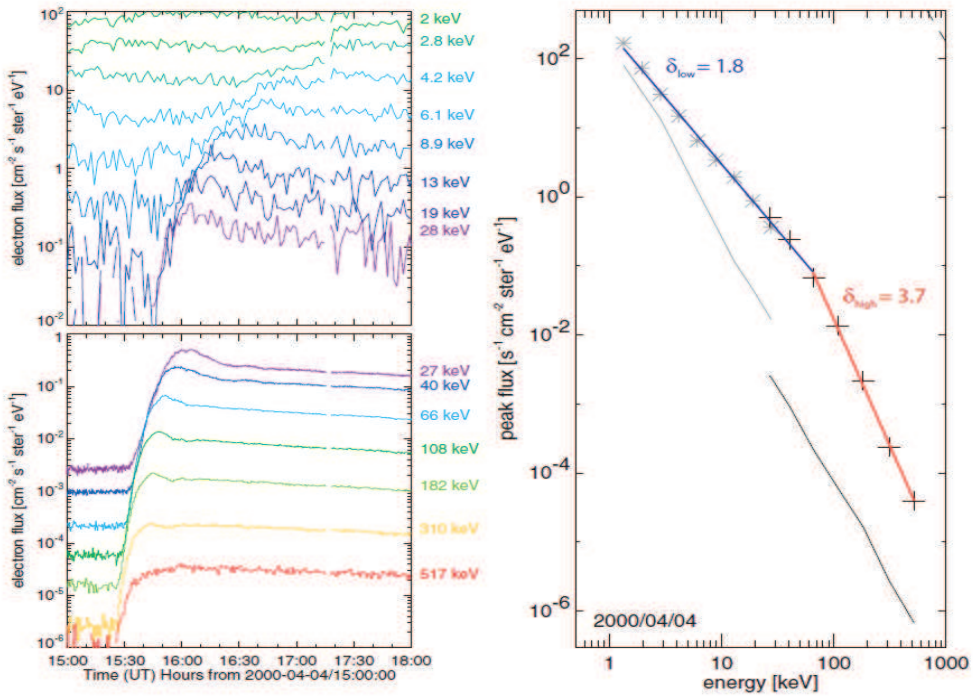

Figure 1.1: Example of a typical solar impulsive electron event observed from the keV range up to 500 keV. Left: time profiles at different energies as indicated. The top panel shows data from the electrostatic analyzer (EESA-H) and the bottom panel shows data from the SST. Note the much higher sensitivity of SST. Right: derived electron peak flux spectrum of the same event. EESA-H data are shown in gray (asterisk), while the SST measurements are given in black (crosses). The thin curves below give an estimate of the background emission. The red and blue curves are the power-law fits to the data, with a pronounced break around 60 keV [from Krucker et al., 2009].

when the higher energy electrons arrive earlier than electrons at lower energy [Krucker et al., 2007, 2009]. This is consistent with a simple ballistic transport model, when after simultaneous injection the electron beams propagate near scatter-free along the interplanetary Archimedean spiral field line to $1 A.U.$ [Lin, 1985].

Example of typical solar impulsive electron event observed by WIND spacecraft is shown in Figure 1.1[from Krucker et al., 2009]. Observed electron spectra show a broken power law dependencies. The break in the spectrum is around 60 keV and the spectra above break are significantly steeper. The values of the power-law index below the break, δ_{low}, is 1.8 and above the break, δ_{high}, is 3.7. A statistical study of the observations from the IMP 6, 7, and 8 spacecrafts [Lin et al., 1982] showed δ_{low} between 0.6 and 2.0 and δ_{high} 2.4 and 4.3, while the values obtained from the WIND observations [Krucker et al., 2009] were $\delta_{low} = 1.9 \pm 0.3$ and $\delta_{high} = 3.6 \pm 0.7$. The observed energies of the break lie in the range from $30keV$ to $100keV$ but typically are of approximately $\sim 60keV$. It is speculated that the observed breaks in spectrum are direct signatures of the acceleration mechanism [Wild et al., 1963, van Allen and

Krimigis, 1965, Anderson and Lin, 1966, Lin, 1974]. However, many processes such as energy losses in the electric field induced by electrons during precipitation into the flaring atmosphere and associated Ohmic heating of the ambient electrons [e.g Haydock et al., 2001, Zharkova and Gordovskyy, 2006],nonuniform ionization [e.g Kontar et al., 2002], albedo Compton backscattering [e.g Kašparová et al., 2007], could influence the spectral shape as well. The observed spectral breaks therefore do not necessarily have to be a signature of the acceleration mechanism.

Remote sensing, hard X-ray observations provide the electron spectra near the Sun. Near the Sun, nonthermal electrons produce bremsstrahlung emissions in the hard X-ray (HXR) range. Inversion of the observed photon spectrum provides information on the spectrum of the non-thermal electrons. The electron spectra derived from these observations show power-law or broken-power shapes [e.g., Lin and Schwartz, 1987, Krucker and Lin, 2002, Conway et al., 2003]. Comparison of the statistical properties of electron spectra near the Sun and near Earth showed two main differences: (1) the number of escaping electrons is much lower, and (2) the escaping electrons have flatter/harder spectra [Krucker et al., 2009]. It was shown [Krucker et al., 2007] that spectral indices, and number of the escaping electrons with energies above 50 keV and electrons producing the HXR emission near the Sun are correlated. This may indicate the single process accelerating both the escaping and HXR-producing electrons. The spectral shape of the electrons near 1 A.U. could be altered by an energy-dependent escape and/or transport effects. For instance, wave-particle interactions during the beam propagation within the interplanetary medium could distort the spectrum significantly [e.g., Kontar, 2001b].

1.2 Solar type III radio bursts

Electron beams, ejected from the Sun during solar flares, are widely accepted to be responsible for the generation of solar Type III radio bursts [Lin, 1970, Alvarez et al., 1972, Frank and Gurnett, 1972, Ergun et al., 1998]. These bursts are amongst the strongest radio emissions found within the solar system. Radio bursts have a characteristic frequency near the fundamental frequency (local electron plasma frequency) and/or its harmonic. Both the fundamental and the harmonic emissions are characterized by a rapid drift, from high frequency to low, that can be assigned to the decreasing electron density of the solar wind [Lin et al., 1981]. Since they can provide an important information about the acceleration and transport of Solar energetic electrons, as well as information regarding the conditions of the background plasma, Type III radio bursts have been the object of scientific study for the past 60 years [see the review of Reid and Ratcliffe, 2014].

Ginzburg and Zhelezniakov [1958] were the first to propose a generation mechanism for Type III radio bursts. The theory was later refined by many authors [Goldman,

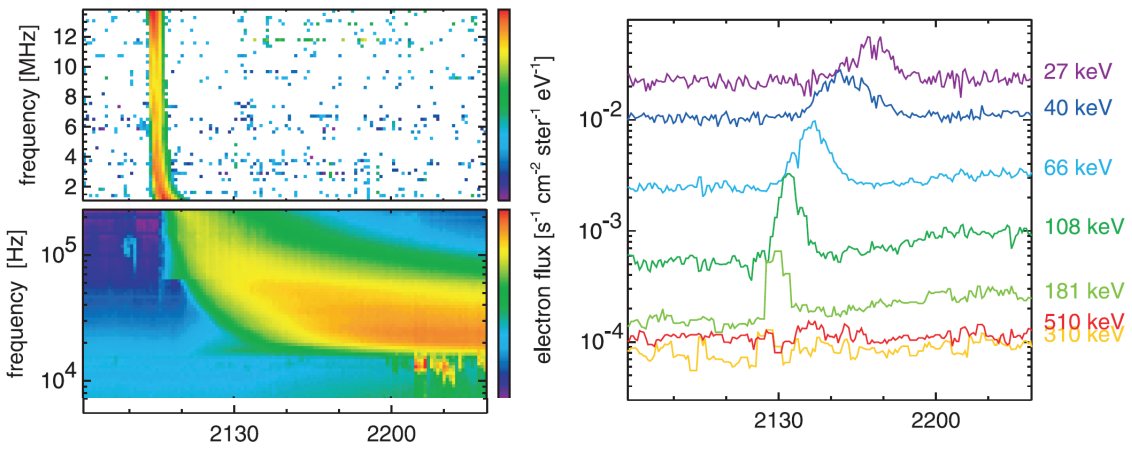

Figure 1.2: Left panels: An expanded view of the WIND/WAVES data including low frequency observations. Right panel: In situ observed energetic electrons from 30 to 500 keV detected by WIND/3DP[from Krucker et al., 2007].

1983, Dulk, 1985, Melrose, 1987]. Today, it is widely accepted that the Type III radio bursts are the result of a two steps process. In the first step, electrostatic plasma waves (Langmuir waves) are generated by electron fbeam. In the second step, due to scattering on plasma ions or density fluctuations, Langmuir waves can be converted to an electromagnetic emission with a plasma frequency, while harmonic emissions appear as a result of the coalescence of two Langmuir waves. Figure 1.2 shows simultaneous observations from WIND spacecraft of the electron beam and electro-magnetic emission.

The Langmuir waves have been observed and studied on many spacecrafts, because they are known to be responsible for converting accelerated electron beam energy into the electromagnetic energy of type III radio bursts [Gurnett et al., 1978, Lin et al., 1981, Mangeney et al., 1999, Kellogg et al., 1992, Ergun et al., 2008]. Analysis of the measurements of the three-dimensional structure of solar wind Langmuir waves made by the STEREO spacecraft showed that the waves can be classified into three major types having different three-dimensional electric field hodograms [Malaspina and Ergun, 2008]. One-dimensional wave structures are observed aligned with the local magnetic field and compose nearly 75% of the 2000 waveforms of Langmuir waves captured by time domain sampling instrument. Two- and three-dimensional wave structures are also observed, and make up a minority of the total samples.

The canonical plasma emission mechanism is the nonlinear wave-wave interaction of Langmuir, ion-acoustic, and electromagnetic waves [Melrose, 1980a]. In the wave-wave mechanism, existing Langmuir waves L couples with the backward propagating ion-acoustic wave S and these two waves generate an electromagnetic wave $t \Longrightarrow L+S=t$. It is worth noting here that the process also often observed is the decay of the primarily generated by the beam Langmuir wave onto another backward propagating Langmuir wave and ion acoustic wave. However so generated acoustic wave in general can not be

directly involved onto generation of the electromagnetic emission, its k-vector typically is too large to ensure the satisfaction of the resonant condition $k_t = k_L + k_S$. As $k_t \sim \omega_p/c$, and $k_L \sim \omega_p/v_b >> k_t$, the $k_S \simeq -k_L$, thus the presence of intense density fluctuations in the plasma can make the coupling sufficiently more efficient.

Harmonic emissions appear as a result of the coupling of forward and backward-propagating Langmuir waves. There were several alternative mechanisms proposed to explain electromagnetic emissions, between those, the direct conversion of the beam-driven Langmuir waves into electromagnetic radiation in the presence of the inhomogeneities, [Hinkel-Lipsker et al., 1992], quasi-mode processes [Yoon et al., 1994], and the radiation by localized bunches of the Langmuir waves by means of the antenna radiation [Papadopoulos and Freund, 1978, Goldman et al., 1980]. The antenna radiation mechanism considers the radiation by nonlinear currents at twice plasma frequency, driven by plasma oscillations. Recently, an alternative formulation based of the idea that a significant fraction of solar wind Langmuir waves are localized as eigenmodes of solar wind density cavities was proposed [Ergun et al., 2008, Malaspina et al., 2012]. In this mechanism, eigenmode-localized Langmuir waves drive localized, nonlinear electrostatic modes at $2f_p$, which, in turn, emit coherent electromagnetic radiation with an efficiency dependent on local plasma parameters and wave packet characteristics such as amplitude and length scale. However one should take into account the theorem shown in Landau and Lifshitz [1960] course that there are no dipolar emission in non-relativistic case if only electron motions are taken into account due to the fact that for the particles with the same ratio of e/m, the dipolar moment is equal to zero. Thus only quadrupole emission can exist. Further discussion of this topic comes beyond the scope of our consideration.

1.3 Beam plasma interaction

A long standing theoretical problem corresponds to the question how the electron beam may be preserved while traveling distances over $1AU$ still being able to generate Langmuir waves. The standard quasi linear (QL) theory, which describes the relaxation of the electron beams in a homogeneous plasma [Vedenov et al., 1962, Drummond and Pines, 1964] , considers the interaction of Langmuir waves with beam particles under conditions of exact resonance: the phase velocity of the waves should be equal to the velocity of the electrons. As a result, waves are stated to only grow in the domain of the velocity space where the electron velocity distribution function has a positive slope. Relaxation finishes when the back-reaction of waves on particles forms a plateau type distribution and stops wave growth. An application of the QL theory to conditions of the solar corona indicated that the spatial length for the saturation of beam-plasma instability was about several hundreds kilometers [Sturrock, 1964].

Detailed in situ measurements from ISEE 1 and 2 [Anderson et al., 1981] and from

ISEE 3 [Lin et al., 1981] spacecrafts at $1AU$ have indicated the simultaneous presence of the positive slope for the electron distribution function and the growth of plasma waves above the background level. The positive slope on the electron distribution function, $f(v)$, was observed in the range of velocities from $3 \cdot 10^7 ms^{-1}$ to $13 \cdot 10^7 ms^{-1}$. Typical observed values of $\partial f(v)/\partial v$ were in the range from $10^{-18} m^{-5} s^{-2}$ to $10^{-14} m^{-5} s^{-2}$. Strong positive slopes $\sim 10^{-15} m^{-5} s^{-2}$ were observed to persist for periods of > 10 minutes. The plasma wave intensity showed close correlation with variations in $\partial f(v)/\partial v$. However, the observed plasma waves level was many orders of magnitude below the the level predicted by the QL theory for parameters of observed beams. This fact indicates that some physical mechanism should be present that can decrease the level of generated Langmuir waves and suppress the beam relaxation process.

Zaitsev et al. [1972] considered the time-of-fly effects on the relaxation process. At the given distance from the source of the energetic electrons, the bump in the distribution function moves from high to low velocities with time. The relaxation can be slowed down because the plasma waves produced by the positive slope portion of the distribution function may not build up to sufficient amplitudes to cause back-reaction on the bump before the bump has moved to the lower velocities. Also the Langmuir waves produced by a positive slope at time t_1 may be reabsorbed at the later time t_2 when a negative slope is present. Reabsorption allows a reduction in the energy losses of beam particles and, as a result, the process of 'plateauing' is slowed. However, numerical simulations [Takakura and Shibahashi, 1976] have demonstrated that the spatial scale of the relaxation is still too small to explain the observations of the positive slope for the electron distribution at $1AU$.

To explain smaller levels of wave energy density than those predicted by QL theory, additional physical processes were invoked that could evacuate Langmuir waves from the velocity range resonant with particles. Such an outflow of wave energy to other regions of velocity space could be related to nonlinear processes. They could also play an important role in the evolution of generated Langmuir waves [Melrose, 1980b]. During $1970's$, beam plasma interaction was studied in the framework of weak [Sagdeev and Galeev, 1969, Kaplan and Tsytovich, 1973] and strong [Zakharov, 1972, Papadopoulos et al., 1974, Galeev et al., 1977a] turbulence theory. In the frame of weak turbulence theory the process of electrostatic decay of Langmuir waves, consisting of the decay of a primary Langmuir wave on a secondary Langmuir wave and an ion sound wave, was considered. Since a secondary Langmuir wave is far from the resonance with the beam particles, the wave energy density in the resonance region of the velocity space significantly decreases. The strong turbulence theory ensures an even more rapid outflow of wave energy from the resonant interaction region. The theory is based on modulation instability and wave collapse. The modulational instability, also known as the oscillating two stream instability, excites a low-frequency ion density perturbation

which can be either a freely propagating ion sound wave or a strongly damped quasi-mode. This can beat with two of the initial pump Langmuir waves and produce high-frequency down-shifted and up-shifted sidebands. The spatial collapse, on the other hand, occurs due to intensification of the localized Langmuir wave packet in the self-generated shrinking density cavity. The level of wave saturation becomes smaller and the corresponding beam relaxation length longer [Galeev et al., 1977b]. The first semi-quantitative models for type III solar radio bursts in the solar wind from 0.1 to 1 AU were developed on the basis of these models [Smith et al., 1976]. Recently, [Thejappa et al., 2012, 2013] has presented observational evidence for the oscillating two stream instability and spatial collapse of Langmuir waves in the source region of a solar type III radio burst. However, Graham et al. [2012] has analyzed the same event using all three electric components and showed that, while the wave packet has structure consistent with collapse simulations and theory, the field strength is well below that required for collapse to proceed.

1.4 Langmuir waves clumping

From the very first measurements onboard satellites it was determined that Langmuir waves were not homogeneously distributed in space but rather clumped into spikes with peak amplitudes typically three orders of magnitude above the mean level [Gurnett et al., 1978]. Smith and Sime [1979] after analyzing plasma waves in the source region of solar type III ratio bursts, argued that no evidence existed in the data regarding non-linear processes such as a wave collapse or soliton formation and proposed a clumping phenomenon associated with the presence of density irregularities in plasma. Density irregularities can cause changes in the phase velocity of Langmuir waves, and, as a result, can lead to a rapid break-down in the conditions for beam-plasma instability. If the characteristic spatial scales of the inhomogeneities are comparable with the spatial growth rate, a wave along its path can consequently pass regions where it can grow and regions where the resonance conditions for wave-particle interactions are violated. As a result, sufficient amplification may only occur along certain paths where the successive inhomogeneities present allow significant amplification for the formation of spikes [Muschietti et al., 1985, Melrose et al., 1986, Robinson, 1992]. Waveforms of large-amplitude Langmuir oscillations recorded by the Wind spacecraft are shown in Figure 1.3.

The observations of the large scale electron density fluctuations in the solar wind gave strong argument in favor of such an interpretation. In situ measurements of the density fluctuations spectrum onboard ISEE 1 and 2 satellites [Celnikier et al., 1983] revealed that characteristic density fluctuations as high as 10^{-2} may exist on the scale range of the order of $100km$, while interplanetary scintillations measurements from extragalactic radio sources give an average value for density fluctuation of the order of

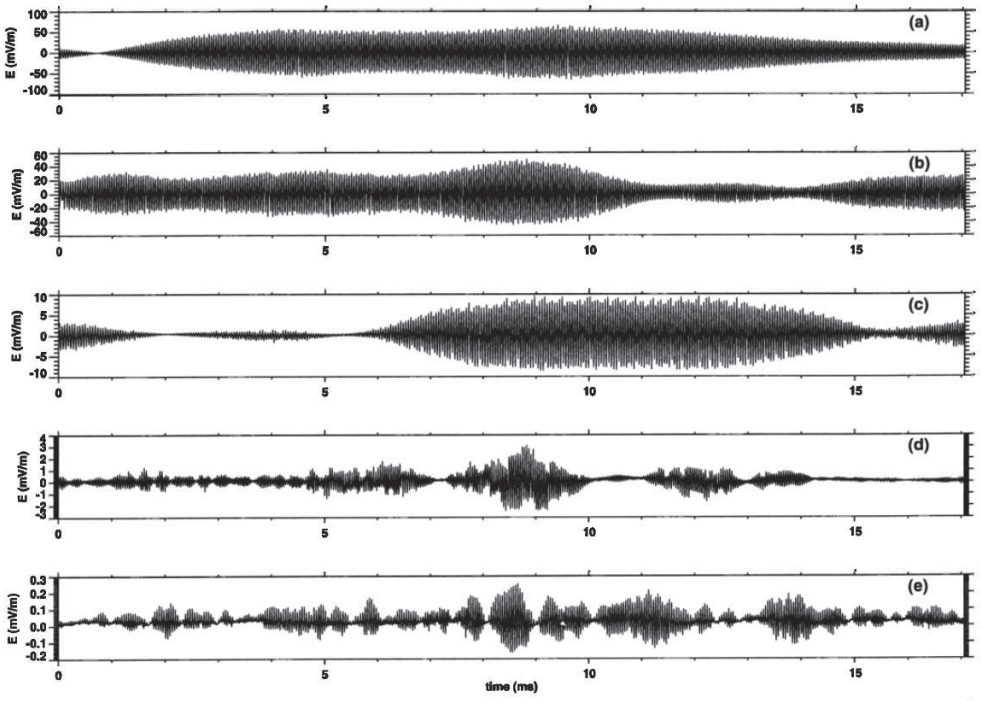

Figure 1.3: Typical Langmuir waveforms for various amplitudes. Panels (a), (b), and (c) show large amplitude Langmuir waves. Weaker Langmuir wave packets are shown in panels (d) and (e) [from Bale et al., 1997].

10^{-3} [Cronyn, 1970]. The electron density power spectrum can be presented in the form of a double-power with different spectral indices, with a breaking frequency of approximately $6 \cdot 10^2 Hz$ [Celnikier et al., 1983]. In the low frequency (long wavelengths) part of the spectrum, it can be approximated quite well using the Kolmogorov power law. The power index for high frequencies is variable, typically lying in the rage $-0.39 \sim -0.94$. The spectrum was found to be isotropic, indicating that the direction of the magnetic field is irrelevant. The result was obtained by Celnikier et al. [1987], making use the technique of active sounding between two satellites. Similar results were obtained by Kellogg and Horbury [2005] by deducing density fluctuation spectra from EFW probe potential variations measured aboard Cluster spacecraft in the free solar wind.

The presence of such fluctuations can result in several physical effects that can affect beam-plasma interaction dynamics. Certain effects were identified recently making use of direct measurements of high frequency electric fields in space. Bale et al. [1998] and Kellogg et al. [1999] have reported that the waves observed in the vicinity of the electron foreshock region have quite often elliptical polarization, rather than linear, and can belong to the Z-mode rather than the Langmuir mode. They suggested that the transformation of primarily generated Langmuir waves to the slow electromagnetic mode can occur due to plasma inhomogeneities.

1.5 Beam-plasma interaction in the non-homogeneous solar wind

A very similar problem related to the interaction of electron beam with a nonhomogeneous plasma was studied in laboratory plasma. Breizman and Ryutov [1970] considered the case of plasma with a monotonously increasing/decreasing density profile along the path of beam propagation and indicated that due to changes in the k vector of Langmuir waves the presence of density inhomogeneity leads to effective outflow for the wave energy from regions of the velocity space where the waves are primarily generated. As a result, the efficiency of beam-plasma instability is significantly reduced. For the case of monotonously increasing density, the beam was also determined to spread not only to lower but also to higher velocities. The outcome is the formation of a tail of accelerated electrons. Ryutov [1969] proposed a model describing electron beam relaxation in a plasma with relatively deep density cavities. He argued that if the depth of the potential hole formed by the cavity is sufficiently deep, wave activity is mainly localized to an area near the bottom of the well. The k vector of waves undergoes oscillations around zero. For this case, beam instability can be stopped even when a positive slope on the beam particle velocity distribution occurs [Ryutov, 1969, Voshchepynets and Krasnoselskikh, 2013]. Nishikawa and Ryutov [1976] considered the development of beam-plasma instability in a plasma with weak random density fluctuations. The amplitudes of the density irregularities were thought to be small enough to exclude possible wave reflection. The angular diffusion of Langmuir waves on density fluctuations on timescales smaller than the typical growth time were shown to be able to strongly suppress the beam-plasma instability.

Relaxation of the electron beam in the non-homogeneous solar wind has been investigated by many authors in the framework of QL theory, week and strong turbulence theories [Kontar, 2001a, Li et al., 2006, Krasnoselskikh et al., 2007, Reid and Kontar, 2010, Ziebell et al., 2011]. Recent numerical simulations take into account various effects, including Landau and collisional damping, the reflection of waves on large density gradients, angular scattering, non-linear wave processes, expansion of the solar magnetic field from the corona to the interplanetary space, the generation of the electromagnetic emissions, etc [Reid and Kontar, 2010, Krafft et al., 2013, 2014, Ratcliffe et al., 2014, Reid and Kontar, 2015]. These studies confirm that density irregularities strongly affect the dynamics of beam and plasma wave activity.

Numerical simulations of the beam plasma interaction in a monotonically inhomogeneous plasma containing negative gradient of the plasma density profile [Kontar, 2001a, Kontar and Reid, 2009, Reid and Kontar, 2010, 2013] indicate that electron beams ejected from the Sun lose their energy much more slowly than for the homogeneous case and can propagate over distances larger than 1 AU. The relaxation is

slowed down because the waves driven by the beam are refracted in decreasing plasma density towards high wave numbers (lower phase velocities), thereby reducing the level of waves that can react with the beam [Kontar, 2001b]. The results are in a good agreement with the recent observations from the STEREO spacecraft [Krupar et al., 2015]. Additionally, in the presence of large scale density fluctuations, a shift of the k-vector for primarily generated waves to the lower k has been demonstrated [Reid and Kontar, 2010]. Subsequent reabsorption by energetic electrons can provide quite an efficient mechanism of particle acceleration. Several recent numerical simulations for beam-plasma interactions by means of different techniques in randomly inhomogeneous plasmas [Ratcliffe et al., 2012, Krafft et al., 2013, Ratcliffe et al., 2014] have shown that significant portion of the beam energy can be transferred to accelerated particles.

Kontar and Reid [2009] have investigated the corresponding energy spectrum of the electron beam after it has propagated 1 AU [see also Reid and Kontar, 2010, 2013]. It was shown that the level of density fluctuations has a direct effect on the spectral characteristics of the electron beam near the Earth. Authors have found a direct correlation between the spectrum of the double power-law below the break energy and the turbulent intensity of the background plasma. The numerical simulations allowed to reproduce two-knee power electron energy spectrum observed near the Earth. The effects of the diffusion of Langmuir waves in wave-number space was considered in [Ratcliffe et al., 2012, 2014, Kontar et al., 2012]. It was found that this effect has the potential to suppress the beam-plasma instability when the diffusion is sufficiently fast, namely, when the timescale for diffusion of Langmuir waves in wave-number space is close to the quasi-linear time.

The idea that the local growth rate of Langmuir waves in a plasma with random density irregularities can behave as a random variable was suggested by Robinson [1992]. Stochastic growth theory (SGT) [Robinson et al., 1993, Robinson, 1995, Cairns and Robinson, 1999], deals with an electron beam that propagates through the solar wind close to the state of marginal stability. For such a case, the growth rate of waves only depends on the local characteristics of the plasma. SGT suggests that a significant amplification of waves may only take place along certain paths that contain many regions where the local growth rates for waves are positive, thus, the total growth rate characterizing a gain in wave energy should behave in a manner similar to that of the sum of random variables. By applying the central limit theorem to the sum of growth rates, SGT predicts a log-normal distribution for the wave amplitudes. Different experimental data registered onboard various spacecraft and in laboratory plasma [Cairns and Robinson, 1999, Cairns and Menietti, 2001, Austin et al., 2007] have indicated that the observed distributions for Langmuir wave amplitudes are rather similar to the log-normal distribution. Recent simulations, which include Langmuir-beam evolution in an inhomogeneous plasma background, incorporate angular scattering, and take into ac-

count nonlinear wave processes, demonstrate the evolution of the beam plasma system to a final state predicted by the stochastic growth theory [Li et al., 2006]. However, a statistical study of the large database onboard Cluster satellites [Krasnoselskikh et al., 2007] unambiguously demonstrated that deviations from the log-normal distribution are rather significant [Vidojević et al., 2011, see also].

Recently, Voshchepynets et al. [2015] proposed a self-consistent probabilistic model that describes beam-plasma instability in a plasma with random density fluctuations. In contrast to the model proposed by Nishikawa and Ryutov [1976], density fluctuations were thought to be high enough to cause changes in the k in the direction of wave propagation. As a result, the wave phase velocity can change, allowing the wave to resonantly interact with beam electrons that have different velocities within a quite large range. An assumption that the phase velocity is a random quantity that obeys a predetermined distribution allows one to describe the energy exchange between the waves and the beam in terms of an averaged in the velocity space growth rate of the waves, and the similarly averaged electron velocity diffusion coefficient (Chapter 3). The averaged growth rate and diffusion coefficient depend on the form of distribution function for the wave phase velocity that is determined by the distribution function of the density fluctuations. We have proposed a technique for evaluating the distribution function of density fluctuations using density fluctuations obtained from measurements onboard satellites. We used the Pearson technique for classifying different distributions [Pearson, 1895] in order to determine what type of distribution can represent the best fit for observed variations in the solar wind plasma density and how it's form affects the beam relaxation process. Using the Pearson type II distribution found to be the best fit, we determined the distribution function of wave phase velocities and applied this distribution in our model for beam plasma interaction (Chapter 4). The model, applied for a realistic conditions in solar wind, allowed us to investigate how key parameters of the relaxation process, such as the energy of particles at the end of relaxation, the saturation level of the wave energy density, the characteristic time of the relaxation, etc., depend on the level of density fluctuations and on the initial velocity of the beam. It is worth noting that the results obtained in the model are in a good agreement with weak turbulence theory.

At the end we have investigated the statistical properties of the amplitudes of the Langmuir waves in the clumping regions by making use of our model and of the Hamiltonian based approach taking data of simulations by Krafft et al. [2013](Chapter5). The Hamiltonian models are used to describe self-consistently wave-particle and wave-wave interactions in homogeneous or inhomogeneous magnetized plasmas. Various physical problems could be efficiently studied by such methods, concerning nonlinear and turbulent stages of different instabilities of electron or ion distributions, wave-particle interactions at multiple resonances, quasi-linear diffusion processes of particles interact-

ing with waves, wave turbulence in randomly inhomogeneous plasmas, wave focusing, scattering, reflection and decay [Krafft et al., 2015]. Recently, [Volokitin et al., 2013, Krafft et al., 2013, 2014, 2015] the self-consistent model was applied to the problem of the resonant interaction of an electron beam with Langmuir wave packets in plasma with density fluctuations under conditions close to the typical solar type III bursts region. A Hamiltonian model describes the properties of the waves propagating in a plasma with large and random density fluctuations by the Zakharov's equations and the energetic beam by means of particles moving self-consistently in the fields of the excited Langmuir waves. The approach supposes that the particles' distribution is split into (1) a so-called non-resonant bulk formed by the background plasma, which interacts weakly with the waves and can be described using linear theory, and (2) the resonant beam particles, which experience strong energy exchanges with the waves and whose motion follows the Newton equations. Comparison of the wave-form of the Langmuir waves obtained in the simulations with recent measurements by the STEREO and WIND satellites shows that their characteristic features are very similar [Krafft et al., 2014].

The remainder of the manuscript is organized as follows. Chapter 2 provides a brief introduction to essentials of beam-plasma interaction in homogeneous plasma as well as in plasma with large scale density irregularities. Part of this material can be found in various textbooks dedicated to plasma physics [Artsimovich and Sagdeev, 1979, Akhiezer, 1975, Melrose, 1980b] and in original papers [Breizman and Ryutov, 1970, Ryutov, 1969, Vedenov and Ryutov, 1975]. In the Chapter 3 we present recently published statistical model for beam plasma interaction in a plasma with relatively small scale ($10^2\lambda_D$-$10^5\lambda_D$) density fluctuations [Voshchepynets et al., 2015]. The model, applied for a case with a normal distribution for the fluctuations, allowed us to investigate how key parameters of the relaxation process, such as the energy of particles at the end of relaxation, the saturation level of the wave energy density, the characteristic time of the relaxation, etc., depend on the level of density fluctuations and on the initial velocity of the beam. In Chapter 4 we perform a statistical study of density fluctuations, deduced from measurements onboard satellites when they were in the solar wind. Our analysis indicates that on spatial scales of approximately $10^2\lambda_D$, the distribution of the fluctuations obeys a Pearson type II distribution. Numerical simulations for the electron beam plasma interaction for both cases of the Gaussian and non-Gaussian distribution does not lead to substantial difference. In Chapter 5 we present preliminary statistical analysis of the results of simulations carried out using equations derived in our probabilistic model of beam plasma interaction with probability distribution of density fluctuations corresponding to observed in solar wind. The results we obtain in our simulations are statistical distributions of the wave intensities in the process of development and evolution of the beam plasma instability in inhomogeneous plasma. It was shown that the statistical characteristics of wavefields strongly depends on the

levels of density fluctuations.

1.6 Resume in French

Pendant plusieurs décennies, les ondes de Langmuir dans le vent solaire et en amont du choc de la Terre et d'autres planètes ont fait l'objet d'études intensives [Kellogg, 2003, Brain, 2004, Soucek et al., 2009]. Il est largement admis que les faisceaux d'électrons éjectés du soleil pendant les éruptions solaires sont responsables de la génération d'ondes de Langmuir par intermédiaire de l'instabilité de faisceau-plasma [Anderson et al., 1981, Lin et al., 1981]. Les premières études mettant en évidence ce processus étaient effectuées dans la région source des émissions radio de type III qui sont parmi les émissions radio les plus intenses observées dans le système solaire. Ginzburg et Zhelezniakov [1958] ont suggéré que des ondes électromagnétiques peuvent être générées lorsque des ondes électrostatiques de Langmuir sont diffusées par des ions ou par des fluctuations de densité. Dans ces conditions, la fréquence d'émission sera égale à la fréquence de plasma locale. Les émissions d'harmoniques (ayant une fréquence d'environ deux fois la fréquence de plasma) apparaissent à la suite de la coalescence de deux ondes de Langmuir. La théorie d'un mécanisme en deux étapes de la génération des émissions solaire de type III a été affinée par de nombreux auteurs [Cairns and Melrose, 1985, Melrose, 1987, Yoon et al., 1994, Malaspina et al., 2012].

Il reste encore un problème théorique de longue date, notamment, comment un faisceau d'électrons peut être préservé jusqu'à des distances plus grandes que 1 AU, en restant capable de générer des ondes de Langmuir. La relaxation d'un faisceau d'électrons dans un plasma homogène est décrit par la théorie quasi linéaire [Vedenov et al., 1962, Drummond and Pines, 1964], qui ne prend en compte que l'interaction des ondes de Langmuir avec les particules du faisceau se trouvant sous la condition de résonance exacte: c'est-à-dire, la vitesse de phase des ondes doit être égale à la vitesse des électrons. En conséquence, les ondes sont supposées à croître seulement dans le domaine de l'espace des vitesses où la fonction de distribution des électrons possède une pente positive. La relaxation prend fin lorsque la réaction des ondes sur les particules résonantes formera une distribution de type plateau et la croissance d'onde s'arrête. Une application de la théorie QL aux conditions de la couronne solaire a donnée un résultat très surprenant, la longueur spatiale de la saturation de l'instabilité faisceau-plasma se produit à une distance de quelques centaines de kilomètres [Sturrock, 1964]. Des mesures in situ à la distance de 1 AU [Anderson et al., 1981, Lin et al., 1981] ont indiqué la présence simultanée de pente positive de la fonction de distribution d'électrons et des ondes de Langmuir de niveau au-dessus du niveau de bruit.

Zaitsev et al. [1972] a considéré un effet supplémentaire, notamment, la possibilité, pour que l'onde de Langmuir générée par le faisceau soit ensuite réabsorbée par des groupes d'électrons retardataires. Le processus de réabsorption permet de réduire les

pertes d'énergie des particules du faisceau et, par conséquent, le processus de formation du plateau est ralenti. Cependant, des simulations numériques [Takakura and Shibahashi, 1976] ont démontré que l'échelle spatiale de relaxation reste encore trop petite pour expliquer les phénomènes observés.

Une explication possible peut être liée au développement de processus non linéaires qui peuvent limiter la croissance des ondes en enlevant des ondes linéairement instables de la région de résonance de l'espace des vitesses [Papadopoulos et al., 1974]. Ce processus réduit ainsi la contre-réaction des ondes sur les particules du faisceau. Dans le cadre de la théorie de la turbulence faible [Sagdeev and Galeev, 1969, Kaplan and Tsytovich, 1973] le processus de décroissance de l'onde de Langmuir en onde électrostatique secondaire et onde ionique-sonore peut jouer un rôle important sur la limitation de l'énergie des ondes résonantes. Dans ce scénario, l'onde de Langmuir secondaire est loin de vérifier la condition de résonance avec les particules du faisceau, et la densité d'énergie des ondes dans la région de résonance de l'espace des vitesses diminue de manière significative. Une autre étape consiste en un développement de la turbulence forte. La théorie est basée sur l'instabilité de modulation et pendant la phase nonlinéaire, sur l'effondrement d'onde [Zakharov, 1972, Papadopoulos et al., 1974, Galeev et al., 1977b]. La théorie de la turbulence forte assure une fuite encore plus rapide de l'énergie des ondes de la région d'interaction résonante. Les modèles semi-quantitatifs décrivant les émissions solaires radio de type III dans le vent solaire de 0.1 AU à 1 AU ont été développés en prenant en compte cet effet [Smith et al., 1976].

Dès les premières mesures à bord de satellites, il a été observé que les ondes de Langmuir ne sont pas réparties de manière homogène dans l'espace, mais elles ont plutôt tendance à s'agglutiner en épis avec des amplitudes de pics généralement de trois ordres de grandeur au-dessus du niveau moyen. [Gurnett et al., 1978]. Sime et Smith [1979] partant d'analyse des ondes de plasma dans la région source des émissions radio solaire de type III, sont arrivés à la conclusion qu'aucun élément dans les données ne permet d'avancer l'argument en faveur d'une présence de processus non- linéaires tels que l'effondrement de l'onde ou de la formation de solitons. Ils ont suggéré que le phénomène d'agglutination doit être associé à la présence de fluctuations irrégulières de densité dans le plasma. Ces irrégularités de densité peuvent causer des changements dans la vitesse de phase des ondes de Langmuir, et, par la suite, elles peuvent entraîner un effondrement rapide des conditions pour le développement de l'instabilité faisceau-plasma. Si les échelles caractéristiques spatiales des inhomogénéités sont comparables au taux de croissance spatiale, une onde peut donc passer d'une région où elle peut subir un accroissement vers une autre région où les conditions de résonance du type interaction onde-particule sont violées. Par conséquent, une forte amplification peut se produire seulement le long de certains trajets où les inhomogénéités successives satisfont aux conditions permettant une amplification significative de l'amplitude d'onde

[Muschietti et al., 1985, Melrose et al., 1986, Robinson, 1992].

Des observations des fluctuations de densité d'électrons dans le vent solaire ont été faites en utilisant les mesures de scintillations interplanétaires en visant une source extragalactique [Coles and Harmon, 1978]. Les résultats ont indiqué que pour des échelles de l'ordre de 100 km, les fluctuations peuvent atteindre un niveau moyen d'ordre de 10^{-3}. Les mesures in situ des spectres des variations de densité à bord des satellites ISEE 1 et 2 [Celnikier et al., 1983] ont révélé que les fluctuations observées dans le vent solaire peuvent atteindre un niveau moyen supérieur à 10^{-2}. La présence de fluctuations d'une telle amplitude peut avoir un impact important sur la propagation des ondes de Langmuir qui à son tour affecte la dynamique d'interaction entre le faisceau et le plasma [Bale et al., 1998, Kellogg et al., 1999, Malaspina and Ergun, 2008].

Dans le cadre de la théorie de la turbulence faible le mouvement des électrons issus du soleil traversant le vent solaire non homogène a été étudié par de nombreux auteurs [Kontar and Pécseli, 2002, Li et al., 2006, Krasnoselskikh et al., 2007, Kontar and Reid, 2009, Ziebell et al., 2011, Krafft et al., 2014]. Les simulations numériques récentes tiennent compte différents effets. On peut citer l'amortissement de Landau, l'effet de collisions, la réflexion des ondes par de forts gradients de densité, la diffusion angulaire, les processus non linéaires d'interactions d'ondes, l'expansion du champ magnétique solaire de la couronne vers l'espace interplanétaire, la génération d'émissions électromagnétiques, etc. [Reid and Kontar, 2010, Krafft et al., 2013, Ratcliffe et al., 2014, Reid and Kontar, 2015]. Ces études confirment le fait que les irrégularités de densité affectent fortement la dynamique et l'évolution des ondes. Pour un plasma admettant un profil de densité monotone décroissant similaire aux conditions héliosphèriques, les électrons éjectées par le Soleil perdent très progressivement leur énergie, ce qui permet au faisceau de s'étendre sur des distances beaucoup très grandes devant l'échelle relative au cas du plasma honogène. En outre, il a été prouvé que la relaxation est accompagnée d'une augmentation de la population de particules énergétiques. L'accélération de ces particules est associée à une diminution du niveau de l'énergie des ondes, ce qui implique le fait que les fluctuations de densité peuvent annihiler tout processus non-linéaire d'interaction d'ondes.

Récemment, Voshchepynets et al. [2015] ont proposé un modèle probabiliste autocohérent pouvant décrire l'instabilité faisceau-plasma dans un plasma subissant des fluctuations aléatoires de densité. Les fluctuations de densité ont été supposées suffisamment élevées pour produire une variation sur le vecteur k dans la direction de propagation de l'onde. En conséquence, la vitesse de phase de l'onde peut changer, permettant à cette dernière d'interagir avec les électrons du faisceau dans une très large gamme de vitesses. L'hypothèse selon laquelle la vitesse de phase est une grandeur aléatoire, qui obéit à une distribution prédéterminée, permet de décrire l'échange d'énergie entre les ondes et le faisceau en termes du taux moyen de croissance des ondes dans

l'espace des vitesses. La même hypothèse est prise afin de déterminer le coefficient moyen de diffusion de vitesses des électrons. Le taux moyen de croissance et le coefficient de diffusion dépendent de la forme de la fonction de distribution des vitesses de phase de l'onde qui, elle-même, est contrôlée par la fonction de distribution des fluctuations de densité. Nous avons proposé une technique d'évaluation de la fonction de distribution de densité en utilisant les variations des fluctuations de densité obtenues à partir des mesures à bord de satellites. Nous avons utilisé la technique de Pearson pour classer les différentes fonctions de distribution [Pearson, 1895]. Le but est alors de déterminer quel type de distribution aboutit au meilleur ajustement sur les variations de densité de plasma observées dans le vent solaire et de voir comment leur forme affecte le processus de relaxation du faisceau. En utilisant la distribution de Pearson de type II, celle qui se rapproche la plus des données, nous avons déterminé la fonction de distribution des vitesses de phase des ondes. La même distribution a été également appliqué à notre modèle d'interaction de faisceau avec un plasma. Appliqué à des conditions réalistes dans le vent solaire, le modèle nous a alorspermis d'étudier comment les paramètres clés du processus de relaxation, comme l'énergie des particules à la fin de la relaxation, le niveau de saturation de la densité d'énergie des ondes, le temps caractéristique de la relaxation, etc., dépendent du niveau de fluctuations de densité et de la vitesse initiale du faisceau. Il convient de noter que les résultats obtenus dans le modèle sont dans un bon accord avec ceux prédits par la théorie de la turbulence faible.

Le manuscrit est organisé comme suit. Le Chapitre 2 fournit une brève introduction à l'essentiel de la physique de l'interaction faisceau-plasma dans le plasma homogène ainsi que dans le plasma avec des irrégularités de densité à grande échelle. Certains sujets décrits dans ce Chapitre sont proposés dans différents manuels dédiés à la physique des plasmas [Artsimovich and Sagdeev, 1979, Akhiezer, 1975, Melrose, 1980b] et dans des articles originaux publiés dans des revues scientifiques [Breizman and Ryutov, 1970, Ryutov, 1969, Vedenov and Ryutov, 1975]. Dans le Chapitre 3 nous présentons le modèle probabiliste [Voshchepynets et al., 2015]) récemment publié d'interaction d'un faisceau avec un plasma comprenant des fluctuations de densité de relativement petite échelle spatiale ($10^2\lambda_D$-$10^5\lambda_D$). Appliqué à un plasma dont la distribution de probabilité des fluctuations de densité obéit à la loi normale, ce modèle nous a permis d'étudier comment les paramètres clés du processus de relaxation, tels que l'énergie des particules à la fin de la relaxation, le niveau de saturation de la densité d'énergie des ondes, le temps caractéristique de relaxation, etc., dépendent du niveau de fluctuations de la densité et de la vitesse initiale du faisceau. Dans le Chapitre 4 nous réalisons une étude statistique des fluctuations de la densité, et nous en déduisons la distribution probabiliste de fluctuations de densité à partir de mesures à bord des satellites explorant le vent solaire. Notre analyse indique que pour des fluctuations ayant des échelles spa-

tiales de l'ordre de $10^2\lambda_D$, la répartition dès les fluctuations obéit à une distribution de Pearson de type II. Les simulations numériques de l'interaction du faisceau d'électrons avec un plasma pour les deux distributions différentes, une distribution Gaussienne et une autre non Gaussienne n'ont pas montré de différence importante. Dans le Chapitre 5 nous présentons une analyse statistique préliminaire des résultats de simulations réalisées à l'aide des équations établies dans notre modèle probabiliste d'interaction du faisceau-plasma avec la distribution de probabilité de fluctuations de densité correspondante à celle observée dans le vent solaire. Les résultats que nous avons obtenus dans nos simulations sont des distributions statistiques d'intensités d'ondes pendant le développement et l'évolution de l'instabilité du faisceau dans un plasma homogène et non-homogène. Il a été montré que les caractéristiques statistiques des champs d'ondes dépendent fortement du niveau de fluctuations de densité.

Chapter 2

Quasi-linear theory of the beam-plasma instability

2.1 Introduction

For the sake of logical completeness we shall begin from a brief introduction to essentials of plasma physics necessary for the further presentation. The following chapter aims to provide a description of main variables, concepts and processes considered in our model. Part of this material can be found in various textbooks dedicated to plasma physics [Artsimovich and Sagdeev, 1979, Akhiezer, 1975, Melrose, 1980b].

The model we propose deals with the interaction of the weak electron beam with Langmuir waves, so we should use the kinetic description of the plasma. Thus, the description of plasma by Vlasov's system of equations, allowing to describe self-consistent electric fields in plasma is of special interest. Application of this self-consistent theory to the high frequency electrostatic oscillations allows one not only to obtain dispersion relations for this type of waves, in other words, to describe the propagation Langmuir wave within the plasma, but also to describe the processes of wave-particle interaction.

The propagation of waves in plasma perturbs the trajectories of all particles, but only some relatively small part of particles population, that satisfies certain resonance conditions is responsible for the processes of the amplification and damping of the waves. In the case of the Langmuir waves, the main contribution is provided by the electrons satisfying the Cherenkov resonance: velocities of the particles are close to the wave phase velocity. Wave-plasma resonant interaction of such type results in the wave growth/damping. The damping rate in homogeneous plasma is proportional to the derivative of the electron distribution function in the vicinity of the resonance. The natural feature of such relation consists in damping of Langmuir waves in the Maxwellian plasma (Landau damping) that corresponds to thermal equilibrium state.

If the wide spectrum of waves would be excited in the plasma out of equilibrium as a result of the development of some instability, the turbulent state of plasma oscillations can occur. The quasi-liner (QL) theory describing evolution of instabilities and

wave particle interactions in turbulent plasmas is based on important assumption that all waves have small amplitudes. This assumption allows one to neglect all types of non-linear wave-wave interactions, and the only nonlinear effects taken into account in the model are related to resonant interaction of the waves with particles. Beam-plasma instability is one of the first kinetic instabilities described using QL theory [Vedenov et al., 1962, Drummond and Pines, 1964]. In the case of homogeneous plasma, QL theory predicts a formation of the plateau on the electron velocity distribution function in the range of velocities smaller than the velocity of the beam. The process of "plateauing" is accompanied by the transfer of the free kinetic energy of the electrons to the potential energy of the Langmuir waves.

The presence of the density inhomogeneity in the plasma may causes several important effects that influence the developments of the beam-plasma instability. In the following chapter we consider only one of them, namely, the change in magnitude of the wave vector of the primarily generated Langmuir wave in the direction of its propagation. These changes, in their turn, lead to the changes in the wave phase velocity, and consequently, they may cause the shift of the Langmuir waves from the region of the velocity space where they were primarily generated [Breizman and Ryutov, 1970]. Monotonically decreasing profile of the plasma density results in the outflow of the wave energy toward lower velocities, while increasing density profile causes the shift of the wave phase velocities toward larger values. When there are many inhomogeneities in plasma, there can occur regions with humps and depletions of the density. These last can form plasma density cavities [Ryutov, 1969], and waves can be captured by this cavities, if their depth is sufficiently large. As a result the Langmuir wave may be trapped inside one of the density depletions, and it will oscillate between turning points where the wave vector of wave is equal to zero. The phase velocity will vary between its minimum value (in the vicinity of the bottom of density cavity) and infinity (in the vicinity of the turning point).

Below in the chapter, we present the results of computer simulation of the beam plasma interaction when the wave trapping dominates the dynamics of Langmuir waves. As a result of simulation we obtain estimations of the key parameters of the relaxation of the electron beam in inhomogeneous plasma, such as characteristic time and spatial scales of the relaxation, wave spectral density and electron distribution function during and at the end of the relaxation, etc, in a similar way as it was done in original papers [Breizman and Ryutov, 1970, Ryutov, 1969, Vedenov and Ryutov, 1975]. The results of the numerical simulations of the beam relaxation in the plasma with density cavities were obtained and published by Voshchepynets and Krasnoselskikh [2013].

2.2 Kinetic theory

Ideal plasma is described by kinetic equation for particle distribution function in the phase space. Full kinetic description requires distribution functions for each sort of particles in a plasma, such as electrons, protons, ions, etc. The distribution function, $f(x, y, z, v_x, v_y, v_z, t)$, determines the number of particles per unit volume of the phase space, that are in the vicinity of the coordinates x, y, z, and have velocities close to v_x, v_y, v_z at moment of time t. One can use vectors $\vec{r}(x, y, z)$ and $\vec{v}(v_x, v_y, v_z)$ instead of coordinates. Integration of the moments of the $f(\vec{r}, \vec{v}, t)$ over the velocity space provides different macroscopic moments of the distribution, such as density, particle flow vectors, second order and higher order moments, including plasma temperature, heat fluxes, at a given point of coordinate space.

Let us consider a simplest case when the changes in the distribution functions for each sort of particles in plasma are caused by macroscopic electric fields $\vec{E}(\vec{r}, t)$. It might be the external fields or fields produced by charge separation in some volume within the plasma. When we say, macroscopic, we mean that the spatial scales of the processes under consideration are much larger then the Debye length, λ_D. The Debye length characterizes the scale of the quasi-neutrality of the plasma. The sphere having the radius equal to Debye length is a sphere outside which any external charge is screened. Thus, at the scales larger than λ_D plasma can be considered as quasi-neutral.

For the considered macroscopic fields, one can apply the Liouville's theorem to describe an evolution of the distribution function under the reaction of the fields. This implies that the number of the particles in a volume of the phase space moving with this particles is constant in time. As a result, an equation describing evolution of the distribution function can be written as follows:

$$\frac{d}{dt} f(\vec{r}, \vec{v}, t) = \frac{\partial}{\partial t} f(\vec{r}, \vec{v}, t) + \frac{\partial \vec{r}}{\partial t} \frac{\partial}{\partial \vec{r}} f(\vec{r}, \vec{v}, t) + \frac{\partial \vec{v}}{\partial t} \frac{\partial}{\partial \vec{v}} f(\vec{r}, \vec{v}, t) = 0 \tag{2.1}$$

By making use of the equations of motion: $\partial \vec{r}/\partial t = \vec{v}$ and $\partial \vec{v}/\partial t = q\vec{E}(\vec{r}, t)/m$, where q and m are charge and mass of current sort of the particles, one can obtain equation 2.1 in following form:

$$\frac{\partial}{\partial t} f(\vec{r}, \vec{v}, t) + \vec{v} \frac{\partial}{\partial \vec{r}} f(\vec{r}, \vec{v}, t) + \frac{q\vec{E}(\vec{r}, t)}{m} \frac{\partial}{\partial \vec{v}} f(\vec{r}, \vec{v}, t) = 0 \tag{2.2}$$

Under the action of the electric fields on the plasma particles, the charge separation may occurs in some volume within the plasma. This, in turns, leads to the fact that the charged density of the volume becomes nonzero. Contribution of the charged density to the electric filed can be estimated by the Gauss's law as follows:

$$\nabla \vec{E}(\vec{r}, t) = 4\pi e \left(\int f_i dv - \int f_e dv \right) \tag{2.3}$$

where f_i and f_e are the distribution function of the ions and electrons, respectively. For this case, the electric field is called self-consistent, because interrelationship between the $\vec{E}(\vec{r},t)$ and $f(\vec{r},\vec{v},t)$ exists. It is worth noting that we neglect all collisional effects. Such an approximation is valid for the processes with characteristic times much larger than time of collision between the particles. The system of equations 2.2, 2.3 describes behavior of the collisionless plasma and is known as Vlasov equations.

2.2.1 Langmuir waves

One can use system of equations 2.2, 2.3 to describe propagation of different types of waves in the plasma. Let us consider propagation of the monochromatic electrostatic plane wave with frequency ω and wave vector k. For one dimensional case, the potential of the self-consistent electric field can be written as follows:

$$\psi = \tilde{\psi}\exp(ikx - i\omega t) \tag{2.4}$$

Assuming that the amplitude of the wave is small, one can use the perturbation theory to describe the behavior of particles distribution functions. This implies that the distribution function of k sort of particles (electrons or ions) can be written as follows:

$$f_k = f_{0k} + \delta f_k \tag{2.5}$$

where f_{0k} is unperturbed distribution function and δf_k is a small term related to the presence of the wave. By keeping terms up to the first order of accuracy, an equation 2.2 for ions can be rewritten as follow:

$$\frac{\partial \delta f_i}{\partial t} + v\frac{\partial \delta f_i}{\partial x} - \frac{e}{m_i}\frac{\partial \psi}{\partial x}\frac{\partial f_{0i}}{\partial v} = 0 \tag{2.6}$$

The term δf_i is dependent upon ψ, and thus one can expect that it will show similar dependence on time and space coordinate as ψ. By substituting δf_k in a form $\delta\tilde{f}_i\exp(ikx - i\omega t)$ to equation 2.6, one can obtain:

$$-i(\omega - kv)\delta\tilde{f}_i - \frac{e}{m_i}ik\tilde{\psi}\frac{\partial f_{0i}}{\partial v} = 0 \tag{2.7}$$

By making use of equation 2.7 an estimation of the perturbation in the ion density caused by the wave can be obtained:

$$\delta n_i = \int \delta\tilde{f}_i dv = -\frac{e}{m_i}k\tilde{\psi}\int \frac{\partial f_{0i}/\partial v}{\omega - kv}dv \tag{2.8}$$

In a similar way the perturbation in the electron density, δn_e, can be found. Assuming that $\partial/\partial x \sim ik$ and taking into account that $E \sim ik\psi$, one can rewrite equation 2.3 as follows:

$$k^2\tilde{\psi} = 4\pi k\tilde{\psi}(\delta n_i - \delta n_e) \tag{2.9}$$

By substituting δn_i and δn_e into equation 2.9 one can obtain following equation:

$$k^2 = -\frac{4\pi e^2}{m_i}k\left(\int \frac{\partial f_{i0}/\partial v}{\omega - kv}dv + \frac{m_i}{m_e}\int \frac{\partial f_{e0}/\partial v}{\omega - kv}dv\right) \tag{2.10}$$

Equation 2.10 contains in an implicit form the relation between wave vector and wave frequency and thus can provide the dispersion relation for such perturbation in a plasma. Let us consider fast oscillations of the electric field potential caused by oscillations of the electron density (Langmuir waves). For such a case, the first term in equation 2.10 can be neglected. Assuming the frequency of the oscillations to satisfy the condition: $\omega \gg kv_t$, where v_t is the thermal velocity of electrons, the denominator in the second term can be presented in the form of power series on (kv/ω), as follows:

$$\frac{1}{\omega - kv} = \frac{1}{\omega} + \frac{kv}{\omega^2} + \frac{k^2v^2}{\omega^3} + \frac{k^3v^3}{\omega^4} \tag{2.11}$$

The substitution 2.11 onto dispersion relation 2.10 allows one to perform integration explicitly. Assuming that the distribution of electrons is Maxwellian, $f_{e0}(v) = \exp -v^2/v_t^2$, and by performing integration by parts one can obtain the following result:

$$\frac{1}{\omega}\int \frac{\partial f_{e0}(v)}{\partial v}dv = f_{e0}(\infty) - f_{e0}(-\infty) = 0, \tag{2.12}$$

$$\frac{k}{\omega^2}\int v\frac{\partial f_{e0}(v)}{\partial v}dv = -\frac{k}{\omega^2}\int f_{e0}(v)dv = -(\frac{k}{\omega^2})n_e, \tag{2.13}$$

$$\frac{k^2}{\omega^3}\int v^2\frac{\partial f_{e0}(v)}{\partial v}dv = -\frac{k^2}{\omega^3}\int v^3 f_{e0}(v)dv = 0, \tag{2.14}$$

(since integrant is odd function) and

$$\frac{k^3}{\omega^4}\int v^3\frac{\partial f_{e0}(v)}{\partial v}dv = -3\frac{k^3}{\omega^4}\int v^2\frac{\partial f_{e0}(v)}{\partial v}dv = -3\frac{k^3}{\omega^4}n_e v_t^2. \tag{2.15}$$

Finally, by making use of these results, one can find from equation 2.10 the well known Bohm-Gross dispersion relation as follows:

$$\omega^2 = \omega_p^2(1 + 3k^2\lambda_D^2) \tag{2.16}$$

where $\omega_p = 4\pi e^2 n_e/m_e$ is a plasma frequency and $\lambda_D = v_t\omega_p$ is the Debye length.

2.2.2 Landau damping

Now let us consider an interaction of the monochromatic Langmuir wave with the electrons. Under action of the electric field of the wave, the velocity of the major part of the electrons will oscillate in time with a frequency ω. The magnitude of the oscillation is approximately of the order of $(Ee)/(m\omega)$, and taking into account that the frequency of oscillations is large, the magnitude of the velocity of these electrons can be considered as a constant. However, for those electrons, that have a velocity, v, close to the phase velocity of the wave, $V = \omega/k$, the situation is quite different. This phenomenon determines the criterium for the Cherenkov resonance.

To consider an interaction of wave with such electrons it is convenient to use coordinate system that is moving with velocity equal to a phase velocity of the wave. It allows one to treat these electrons in terms of trapped inside the potential well created by the Languir wave. Figure 2.1 provides a schematic illustration of the motion of the electrons with velocity $v \sim V$ under the action of the electric field potential. The width of the resonance in the velocity space can be obtained by comparing the kinetic energy of the electrons in the moving coordinate system with the potential energy of the well. Namely, the electrons with velocities that satisfy condition $|v - V| < (e\psi/m_e)^{1/2}$ can be considered as trapped. The motion of such an electron in the velocity space can be described as oscillations between the turning points. During the reflection from the borders of the well around the turning points electrons can exchange energy with the wave.

Depending of the initial velocity, two species of resonant electrons can be distinguished: with velocities larger than V and velocities lower then V. Point P_1 in Figure 2.1 corresponds to the first class of the electrons while point P_2- to the second. As a result of the reflection the velocity of the both types of the electrons in the moving coordinate system change its sign. However, for the first type, the velocity after reflection, $v_1 = V - v + V$ is less than the velocity before the reflection. As a result the electron transfers part of its kinetic energy to the wave. For the second type of the electrons the situation is opposite. As a result of the reflection kinetic energy of the electron increases. The increase is accompanied by decreasing of the potential energy of the wave. For the Maxwellian plasma, the number of the electrons of the second type is always larger than the number of electrons corresponding to the first type, and thus, the Langmuir waves should damp in such a plasma. Damping of the Langmuir waves as a result of resonant interaction with electrons is well known effect called the Landau damping.

To estimate characteristic time of the damping one can use Liouville equation for the wave energy density, W:

$$\frac{dW}{dt} = 2\gamma W \tag{2.17}$$

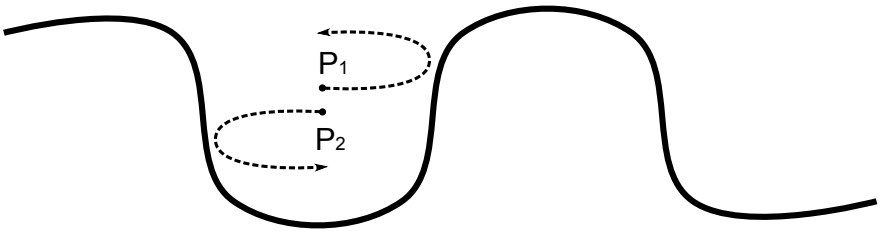

Figure 2.1: Schematic illustration of the resonant interaction of Langmuir wave with electrons. Solid line represents potential well of the wave electric field. Dashed lines correspond to the trajectories of the resonant electrons [adapted from Artsimovich and Sagdeev, 1979].

where γ characterizes the growth/damping rate of the Langmuir wave energy density.

It is not difficult to calculate the energy losses of one electron of the first type after single reflection from the border of the potential well:

$$\Delta W_1 = m_e \frac{v^2}{2} - m_e \frac{(2\omega/k - v)^2}{2} = 2m \left(v - \frac{\omega}{k}\right) \frac{\omega}{k} \tag{2.18}$$

The number of the reflections per second can be estimated from the velocity of the electron in the moving coordinate system and the width of the potential well, determined by wave length, λ, as follows: $(v - \omega/k)/\lambda$. Thus, the energy transferred from the electron to Langmuir wave per time unit may be evaluated as:

$$\frac{\Delta W_1}{\Delta t} = 2m \frac{\omega}{k\lambda} \left(v - \frac{\omega}{k}\right)^2 \tag{2.19}$$

The change in the kinetic energy of the electron of the second type is described by the same equation. To evaluate total gain/damping of the wave energy density one should sum the contributions from all electrons that are in the resonance with the wave. This procedure can be performed as follows:

$$\frac{dW}{dt} = \frac{2m_e}{k\lambda} \left(\int_{\omega/k}^{\omega/k+((2eE_{e0})/(km_e))^{1/2}} (v - \omega/k)^2 f_{e0}(v) dv \right) - \frac{2m_e}{k\lambda} \left(\int_{\omega/k-((2eE_{e0})/(km_e))^{1/2}}^{\omega/k} (v - \omega/k)^2 f_{e0}(v) dv \right) \tag{2.20}$$

where, E_0 is an amplitude of the Langmuir wave, and f_{e0} is unperturbed electron velocity distribution function. The first therm in equation 2.20 corresponds to the gain of the wave energy density, as a result of interaction with the electrons of the first type, while the second therm describes the damping of the wave energy, caused by acceleration of the electrons of the second type. We also took into account that the half-width of the resonance in the velocity space is $((2eE_{e0})/(km_e))^{1/2}$. Regarding

that the amplitude of the wave is small, the velocities of the resonant electrons are oscillating in time in the vicinity of the wave phase velocity, V. As a result one can write f_{e0} in a form of Taylor series around the V, as follows:

$$f_{e0} = f_{e0}(\omega/k) + \frac{\partial f_{e0}(v)}{\partial v}|_{v=\omega/k} \left(v - \frac{\omega}{k}\right) \tag{2.21}$$

By substituting f_{e0} from equation above into equation 2.20 one can obtain Liouville's equation in following form:

$$\frac{dW}{dt} = \frac{2e^2}{\pi m_e} \frac{\omega}{k^2} E_0^2 \frac{\partial f(v)}{\partial v}|_{v=\omega/k} \tag{2.22}$$

By taking into account that wave energy density related to the wave amplitude as: $W = E^2/(8\pi)$, equation 2.22 can be used to estimate wave growth/damping rate, γ, as follows:

$$\gamma \sim \frac{\omega_p^2}{\pi n} \frac{\omega}{k^2} \frac{\partial f(v)}{\partial v}|_{v=\omega/k} \tag{2.23}$$

As one can notice, γ is proportional to the derivative of the electron velocity distribution function, in the direction of the wave propagation. Now it is clearly seen that for the case of Maxwellian plasma Langmuir waves damp in the all ranges of phase velocities, since the $\partial f_{e0}/\partial v \sim -(v/v_t^2) f_{e0}$ is always negative. More over, the damping of Langmuir waves appears in any sort of plasmas, if the velocity distribution function of the electrons decreases with increase of the $|v|$. However, it is worth noting that for waves with phase velocities $V \gg 3v_t$ the damping is rather weak, because the number of the electrons that satisfies the resonant conditions is small.

However, in a plasma with several populations of electrons, for instance, the core plasma electrons, and fast electron beam with beam velocity much larger then v_t the situation is quite different. For such a case the velocity distribution function has a positive slope in some range of the velocities, and thus the beam can generate waves with phase velocities in this range.

2.3 Quasi-linear theory: homogeneous plasma

It is convenient to consider an interaction of the resonant particle with Langmuir waves in a framework of quasi-linear approximation. QL theory suggests that the Langmuir waves are distributed in some range of the phase velocities, $(\omega/k)_{max} < V < (\omega/k)_{min}$ in such a way, that the borders of the intervals for trapped particles for the neighbor waves overlap. The condition required for overlapping of the interval of resonant interaction can be written as follow:

$$\delta(\omega/k) < \left((e/mk)(E_k^2 \delta_k)^{1/2}\right)^{1/2} \tag{2.24}$$

where $\delta(\omega/k)$ and δk are difference between two neighbors harmonics in phase velocity and wave vectors, respectively, and E_k^2 is spectral energy density. Factor $(E_k^2\delta k)k$ corresponds to the energy density of the wave in the interval δk. The criteria 2.24 can be interpreted also as overlapping of borders of the potential wells created by neighbor Langmuir waves.

QL theory also deals with additional important assumption, namely, the amplitudes of the Langmuir waves are supposed to be low. This assumptions allows one to neglect all non-linear effects related to wave-wave interactions. Thus the resonance interaction of Langmuir waves with electrons is the only non-linear effect considered in the model. For this case electron distribution function can be divided into two parts: slowly changing part, $\overline{f(v,t)}$, and fast oscillating part $\delta f(x,v,t)$. Let us assume that averaged functions $\overline{f(v,t)}$ and $\delta f(v,t)$ satisfy conditions $\langle\overline{f(v,t)}\rangle = f_e(v,t)$ and $\langle\delta f(x,v,t)\rangle = 0$. By averaging here is meant a spatial averaging over large scales, much larger then the wavelength of the Langmuir waves. Equation for $\overline{f(v,t)}$ can be obtain from the kinetic equation 2.2 by making use the procedure of averaging, as follows:

$$\frac{\partial\overline{f(v,t)}}{\partial t} = \frac{e}{m}\langle E(x,t)\frac{\partial\delta f(x,v,t)}{\partial v}\rangle \tag{2.25}$$

Equation 2.25 describes slow temporal evolution of the electron velocity distribution function caused by the averaged contribution of the fast oscillations of the $\delta f(t,v)$ and $E(t)$. It is convenient to present the electric field and related oscillating part of the distribution function in the form of the Fourier series, as follows:

$$E(x,t) = \sum_k E_k(t)\exp i(kx) \tag{2.26}$$

$$\delta f(x,v,t) = \sum_k \delta f_k(v,t)\exp i(kx) \tag{2.27}$$

By substitution $\delta f(x,v,t)$ and $E(x,t)$ to equation for $\overline{f(v,t)}$ and taking into account that components with $E_k(t)$ and $E_{-k}(t)$, as well as $\delta f_k(v,t)$ and $\delta f_{-k}(v,t)$ are complex conjugate, the equation 2.25 can be rewritten as follows:

$$\frac{\partial\overline{f(v,t)}}{\partial t} = \frac{e}{m}\sum_k (E_k(t)\delta f_k^*(t,v) + E_k^*(t)\delta f_k(v,t)) \tag{2.28}$$

where asterisk indicates complex conjugate. By subtracting equation 2.28 from the original kinetic equation 2.2 one can obtain following equation for each component $\delta f_k(v,t)$ (keeping only terms up to the second order on E):

$$\frac{\partial\delta f_k(v,t)}{\partial t} + ikv\delta f_k(v,t) = \frac{eE_k(t)}{m}\frac{\partial\overline{f(v,t)}}{\partial v} \tag{2.29}$$

Now let us define $\delta f_k(v,t)$ and $E_k(t)$ as $\delta f^{'}(t)\exp(-ikvt)$ and $E_k^{'}(t)exp(-i\omega_k t)$, where $\delta f^{'}(t)$ and $E_k^{'}(t)$ are slowly varying function of time, and frequencies ω_k are

related to the wave vectors k by dispersion relation 2.16. By making substitution $\delta f_k(v,t)$ and $E_k(t)$ into equation 2.29 and integrating the equation over time, $\delta f^{'}(t)$ can be obtained as follows:

$$\delta f_k^{'}(t) = \int_0^t \frac{e}{m} E_k^{'}(t) \frac{\partial \overline{f(v,t^{'})}}{\partial v} \exp i(kv - \omega_k) t^{'} dt^{'} \tag{2.30}$$

Complex conjugate component $\delta f_k^{'*}(t)$ can be estimated from the equation 2.30 after substitution $k = -k$ and $\omega_{-k} = -\omega_k$ as follows:

$$\delta f_k^{'*}(t) = \int_0^t \frac{e}{m} E_k^{'*}(t) \frac{\partial \overline{f(v,t^{'})}}{\partial v} \exp -i(kv - \omega_k) t^{'} dt^{'} \tag{2.31}$$

Now, by making use of $\delta f_k(v,t)$ and $\delta f_k^*(v,t)$, one can obtain the equation for the slowly varying part of electron velocity distribution function as follows:

$$\frac{\partial \overline{f(v,t)}}{\partial t} = \frac{e^2}{m^2} \sum_k \left(\frac{\partial}{\partial v} E_k^{'}(t) E_k^{'*}(t) \int_0^t \exp i(kv - \omega_k)(t - t^{'}) dt^{'} \frac{\partial \overline{f(v,t)}}{\partial v} + c.c. \right) \tag{2.32}$$

(here we also used that fact that $E_k^{'}(t)$ and $\overline{f(v,t)}$ are slowly varying in time, and thus they can be moved outside the integral). Finally, taking into account that the integral in the equation 2.32 is a Dirac delta-function:

$$2\pi\delta(vk - \omega_k) = \int_0^t \exp i(kv - \omega_k)(t - t^{'}) dt^{'} + c.c. \tag{2.33}$$

one can rewrite the equation 2.32 in following form:

$$\frac{\partial \overline{f(v,t)}}{\partial t} = \frac{2\pi e^2}{m^2} \frac{\partial}{\partial v} \left(\sum_k \left| E_k^{'}(t) \right|^2 \delta(kv - \omega_k) \frac{\partial \overline{f(v,t)}}{\partial v} \right) \tag{2.34}$$

Equation 2.34 describes diffusion of the electron velocity distribution function in the velocity space, caused by the interaction of particles with the set of the Langmuir waves. The diffusion results in the uniform distribution in the velocity space for the electrons in the range of velocities where the interaction occurs, i.e., in the range of velocities of the wave spectrum: $(\omega/k)_{max} < V < (\omega/k)_{min}$. To describe temporal evolution of the electric field component $E_k^{'}(t)$ one can use the set of equations similar to the equation 2.23:

$$\frac{\partial E_k^{'2}(t)}{\partial t} = \frac{\pi}{N_0} \omega_k \left(v^2 \frac{\partial \overline{f(v,t)}}{\partial v} \right)_{v=\omega_k/k} E_k^{'2}(t) \tag{2.35}$$

The resonant nature of the interactions can be affected by any physical mechanism which is able to destroy coherence resulting in broadening of the resonance. To take into account these effects the Dirac delta-function in equation 2.34 should be replaced by so called resonance function $R(\omega - kv, \Delta\omega)$:

$$\pi\delta(vk - \omega_k) = R(vk - \omega_k, \Delta\omega), \tag{2.36}$$

where $\Delta\omega$ is the lifetime of the wave in the resonance. Both, $R(vk - \omega_k, \Delta\omega)$ and $\Delta\omega$, depend on the appropriate mechanism that provides resonance broadening. For instance, recently this framework was applied to take into account effects of scattering Langmuir waves in fluctuating plasmas on the wave-particle interaction [Bian et al., 2014].

2.3.1 Relaxation of the electron beam

The system of equations 2.34 and 2.35 can be used to describe the interaction of the weak electron beam with wide spectrum of the Langmuir waves. However, it is convenient to make slight modification in the equations. First, the sum, $\sum k$ in the equation 2.34 can be replaced by the integration over k: $\sum_k = (1/\pi)\int_{k>0} dk$. Second, one can use wave spectral energy density, $W_s(k)$, instead of term $\left|E'_k(t)\right|^2$. For particular case of Langmuir waves it can be written as follows: $W_s(k) = \left|E'_k(t)\right|^2/(8\pi)$. It is worth noting that $W_s(k)dk$ is the wave energy density concentrated in the part of the spectrum from k to $k + dk$. Third, integration over wave vector, k, can be replaced by the integration over wave phase velocity, V, by making use of relation $k = \omega_k/V$, and thus $dk \sim (\omega_k/V^2)dV$.

As we already seen, the typical electron beams in the interplanetary space and in the vicinity of collisionless shocks have densities, n_b, much smaller than the background plasma density and they propagate along the magnetic field lines. This justifies an assumption that the problem can be considered as one-dimensional. Assuming that the condition of the overlapping of the resonances is satisfied, the equations for the beam electrons velocity distribution function and waves spectral energy density can be obtain from equations 2.34 and 2.35 as follows:

$$\frac{\partial f(v,t)}{\partial t} = \frac{\partial}{\partial v} D(v,t) \frac{\partial f(v,t)}{\partial v} \tag{2.37}$$

$$\frac{\partial W_s(V,t)}{\partial t} = 2\gamma(v,t) W_s(V,t) \tag{2.38}$$

here, D is the velocity diffusion coefficient, determined as follows:

$$D(v,t) = \frac{8\pi^2 e^2}{m^2} \left(\frac{W(V,t)}{V}\right)_{V=v} \tag{2.39}$$

and $\gamma(v,t)$ is the waves growth rate:

$$\gamma(v,t) = \frac{\pi}{2}\omega_p \frac{n_b}{N_0}\left(v^2 \frac{\partial f(v,t)}{\partial v}\right)_{V=v} \tag{2.40}$$

where beam electron velocity distribution function, $f(v,t)$, is normalized to one: $\int_0^\infty f(v,t) = 1$.

As one can see from the dependence of γ upon electron distribution function the waves start growing from initial thermal noise level only in the region of the velocity space where $\partial f(v,t)/\partial v > 0$. Namely, this mean that the electron beam propagating in the plasma, generates only the Langmuir waves with phase velocities, V, less than the beam velocity v_b. This waves will determine a backward reaction on the beam. It is worth noting that the contribution of waves with $V > v_b$ can be neglected. This implies that the diffusion coefficient $D(v,t)$ is close to 0 in the range of velocities $v > v_b$. Thus, in this approximation the process of the relaxation will run only toward lower velocities.

The saturation of the beam instability occurs when the wave growth rate became close to 0 or negative for all phase velocities. This implies that the stable equilibrium state for the electron velocity distribution function in the range of phase velocities of waves is a plateau, since this distribution leads to vanishing derivative of $f(v,t)$ and as a result to $\gamma = 0$. Thus the relaxation process consists of plateau formation of the velocity distribution function in the range of velocities less than v_b (solid line at Figure2.2). One can find that in the end of the relaxation $f(v,t)$ can be described as follows:

$$n_b f_{end} = \begin{cases} \frac{n_b}{v_b} & \text{for } v < v_b \\ 0 & \text{for } v > v_b \end{cases} \tag{2.41}$$

It is worth noting that during the relaxation process described by the of equations 2.37 and 2.38 a system of waves and particles conserves its total energy. Moreover the system has addition specific quasi-linear constant of motion:

$$\frac{\partial}{\partial t}\left[n_b f(v,t) - \frac{2\omega_p}{m}\frac{\partial}{\partial v}\left(\frac{W(V,t)}{V^3}\right)_{V=v}\right] = 0. \tag{2.42}$$

If we consider the Langmuir waves as an ensemble of the quasi-particles with energy distribution $W(V)/V$, the equation 2.42 can be interpreted as a conservation of the total number of particles and quasi-particles in the system. By making substitution of f_{end} into equation 2.42 one can obtain the spectrum of the waves energy density in the end of relaxation:

$$W_{end}(V) = \begin{cases} \frac{m n_b V^4}{2\omega_p v_b} & \text{for } V < v_b \\ 0 & \text{for } V > v_b \end{cases} \tag{2.43}$$

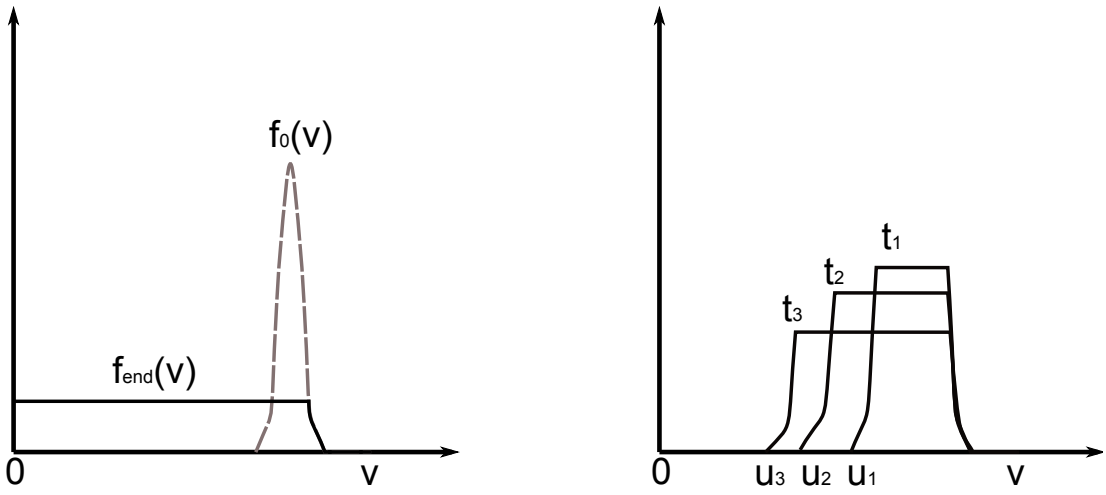

Figure 2.2: Left panel: forms of the electron distribution function at the beginning (dashed line) and in the end of the relaxation process (solid line). Right panel: snapshots of the electron velocity distribution function in the consequent moments of time: $t_1 < t_2 < t_3$. The core distribution, that corresponds to the cold electrons of background plasma has not been considered [adapted from Vedenov and Ryutov, 1975].

The asymptotic solutions $f_{end}(v)$ and $W_{end}(V)$ represent a well known result for monochromatic electron beam relaxation in homogeneous plasma: the beam preserves only third part of its initial free energy, while two-thirds of the particles energy is transferred to the Langmuir waves.

2.3.2 Characteristic scales of the relaxation

As one can notice from the equation 2.38, the gain of the wave energy density, ΔW, is proportional to the wave energy density W itself. The substantial gain of the waves energy occurs in some regions of the velocity space where the growth rate is high enough to ensure sufficient amplification. Namely, the left border of this region, u, is determined by the initial thermal width of the beam, Δv_b. Since the initial spectral energy density of the wave is very low, $W_{in}/W_{end} \ll 1$, at the beginning of the relaxation the waves with phase velocities V that satisfy condition $u < V < v_b$ will grow, while the waves with phase velocities less than u will be maintained on a level about W_{in}. Thus, one can expect that the backward reaction of the waves on the beam, will plateau the velocity distribution function in the range of velocities from u to v_b. Subsequently, the left border $u(t)$ of the plateau will move toward the lower velocities (right panel of Figure 2.2), and the temporal evolution of the $f(v,t)$ can be roughly described as follows:

$$n_b f(v,t) = \begin{cases} 0 & \text{for } v < u(t) \\ \frac{n_b}{v_b - u(t)} & \text{for } u(t) < v < v_b \\ 0 & \text{for } v > v_b \end{cases} \tag{2.44}$$

The function $u(t)$ can be found from equation 2.38 by substituting solution $f(v,t)$

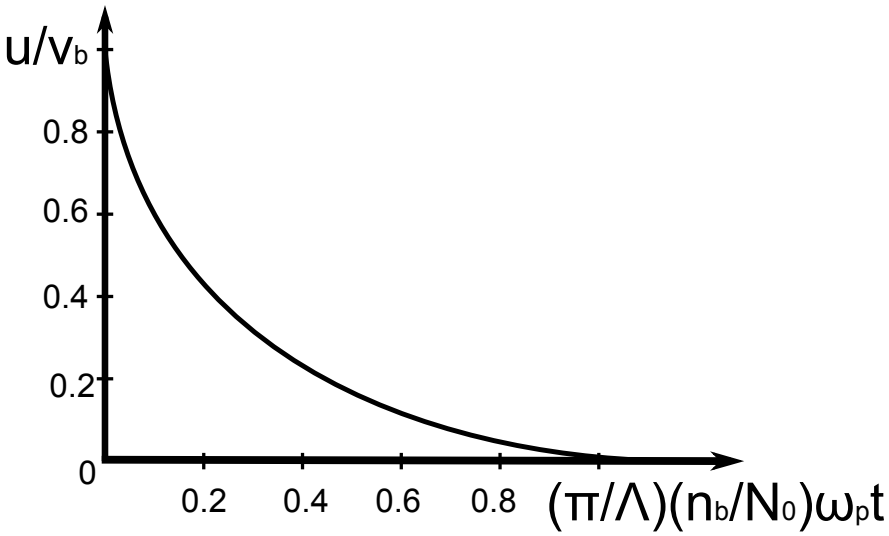

Figure 2.3: Position of the left border of the distribution function as a function of the time [adapted from Vedenov and Ryutov, 1975].

defined be equation 2.44 and integration over V. This procedure allows one to write equation for $u(t)$ as follows:

$$\frac{du(t)}{dt} = -\frac{\pi}{\Lambda}\omega_p \frac{n_b}{N_0} \cdot \frac{u^2(t)}{v_b - u(t)} \tag{2.45}$$

here Λ is well known Coulomb logarithm. Figure 2.3 shows a solution of the equation 2.45. The relaxation stops, when the velocity distribution function of the beam electrons reaches a region of the velocity space occupied by the background plasma. As one can notice, the characteristic time of the relaxation, t_t, can be estimated as follows:

$$t_r \sim \frac{\Lambda}{\pi}\frac{1}{\omega_p}\frac{N_0}{n_b}. \tag{2.46}$$

In the simple manner, an estimate of a characteristic spatial scale of the relaxation, r_s, can be obtained by multiplying t_r by a initial beam velocity, v_b

$$r_s \sim \frac{\Lambda}{\pi}\frac{v_b}{\omega_p}\frac{N_0}{n_b}. \tag{2.47}$$

2.4 Plasma with monotonically decreasing density profile

Let us consider a propagation of the Langmuir wave packet generated by the beam in a plasma with monotonically decreasing density along the wave's path. Decreasing of the density results in the decreasing of the plasma frequency and thus the propagation in such a plasma differs from the case of homogeneous plasma. The effect related to the density inhomogeneity should be included in the dispersion relation for the Langmuir wave. If the spatial change of the density is slow, the $k(x)$ vector of wave will change in

such a way that the dispersion relation should be satisfied with the condition that the wave frequency remains constant while plasma frequency varies according to variation of the density. The changes of the k vector, in their turn, result in the changes of the wave phase velocity. Suggesting that the condition above is satisfied, equation 2.16 can be rewritten:

$$\omega = \omega_p(x)\left(1 + \frac{3}{2}\frac{v_t^2}{V^2(x)}\right). \tag{2.48}$$

By making use of equation 2.48 one can estimate the variation of the phase velocity of the wave, ΔV, after passing the distance Δx. Using the condition that the frequency of the wave, ω remains constant along the trajectory, the equation 2.48 leads to following:

$$(1 + \frac{3}{2}\frac{v_t^2}{V^2})\frac{d\omega_p}{dx}\Delta x - 3\omega_p\frac{v_t^2}{V^2}\frac{\Delta V}{V} = 0. \tag{2.49}$$

As one can notice, a decrease of the plasma frequency results in a decrease of the phase velocity of the wave. As a result, in the plasma with monotonically decreasing density profile, the Langmuir waves are shifted from the region of the velocity space, where they were generated by the beam instability, toward lower phase velocities. Thus, such inhomogeneity do not cause an appearance of the waves with phase velocities larger than v_b and the asymptotic solution for the electron distribution function $f_{end}(v)$ is the same as for homogeneous plasma. Assuming that phase velocities of the waves are close to the velocity of the beam, $V \sim v_b$ and that $d\omega_p/dx \sim \omega_p/L_{un}$, where L_{un} is a characteristic scale of the density inhomogeneity, ΔV can be obtained from equation 2.49 as follows:

$$\Delta V \sim v_b\frac{\Delta x}{L_{un}}\frac{v_b^2}{v_t^2}. \tag{2.50}$$

As we have already seen in the previous section, the effective gain of the waves energy occurs in the range of the phase velocities from $v_b - \Delta v_b$ to v_b. Due to the shift of the phase velocity, the wave leaves this region and the amplification of wave amplitude stops. This happens on a characteristic spatial scale Δx_c that can be obtained from equation 2.50 as follows:

$$\Delta x_c \sim L_{un}\frac{\Delta v_b}{v_b}\frac{v_t^2}{v_b^2}. \tag{2.51}$$

A characteristic time scale of the shift of the waves from the region of effective growth, t_c, can be estimated taking into account that the wave packet propagates with the group velocity $v_g = v_t^2/v_b$. Thus:

$$t_c \sim \frac{L_{un}}{v_b}\frac{\Delta v_b}{v_b}. \tag{2.52}$$

To obtain the growth of waves during the time t_c up to a level significantly larger than noise level the following condition should be satisfied:

$$\gamma t_c \geq \Lambda \tag{2.53}$$

To estimate the gain of the wave one can use the simplified form of the equation 2.40, as follows:

$$\gamma \sim \pi \omega_p \frac{n_b}{N_0} \frac{v_b^2}{\Delta v_b^2} \tag{2.54}$$

By substituting γ from equation 2.54 and t_c from equation 2.52, one can rewrite inequality 2.53 as follows:

$$\frac{n_b}{N_0} \frac{\pi \omega_p L_{un}}{v_b} \frac{v_b}{\Delta v_b} \geq \Lambda \tag{2.55}$$

As one can notice the left side of the inequality 2.55 decreases as Δv increases. When the beam is wide enough and the condition 2.55 is not satisfied anymore, the relaxation stops, because the gain of the wave is very low, namely about the thermal noise level. Corresponding Δv_b can be estimated as follows:

$$\frac{\Delta v_b}{v_b} \sim L_{un} \frac{\pi}{\Lambda} \frac{n_b}{N_0} \frac{\omega_p}{v_b} \tag{2.56}$$

Equation 2.56 can be used to illustrate a peculiarity of the beam relaxation process in the plasma with decreasing density profile. Let us assume that the characteristic spatial scale of the density inhomogeneity is about the distance that the Langmuir waves are able to pass during the time of the relaxation in homogeneous plasma, t_r. By substituting $L = v_g t_r$ into equation 2.56 one can obtain:

$$\frac{\Delta v_b}{v_b} \sim \frac{v_t^2}{v_b^2}. \tag{2.57}$$

This lead to the conclusion that in the inhomogeneous plasma, the process of the relaxation is much slower. During a period of time t_r the electron velocity distribution function in homogeneous plasma relaxes to the form of the plateau, while according to equation 2.57 in the inhomogeneous plasma $f(v,t)$ after time t_r has only a small dispersion about $v_t^2/v_b^2 \ll 1$. Thus, the outflow of the wave energy from the resonance region of the velocity space, caused by decrease of the background density of the plasma, slows down the relaxation, however the velocity distribution of the electrons in the end of the relaxation is the same as in homogenous plasma.

2.5 Plasma with monotonically increasing density profile

Relaxation of the electron beam in a plasma with monotonically increasing density profile has a characteristic peculiarity that differs this case from the two considered

before. An increase of the plasma density along the path of the waves propagation leads to decrease of the k vectors of waves, and thus to increase of the waves phase velocities. As a result, the waves generated by a beam instability are shifted to the region of the velocity space, where $\partial f(v)/\partial v < 0$ and the growth rate of the wave is negative. Process of decrease of the wave energy is accompanied by the transfer of wave's energy to the particles. Such energy transfer from the electrons with velocities, $v < v_b$, to the electrons with velocities $v > v_b$ via generation and reabsorption of the Langmuir waves leads to the formation of the tail of the energetic particles on the velocity distribution function in the end of the relaxation process.

For a sake of simplicity let us consider an electron beam with small initial thermal dispersion $\Delta v_b/v_b \ll 1$ propagating within the plasma with a very slow spatial density gradient. In this case, two characteristic spatial scales could be noticed: the scale of the relaxation in the homogeneous plasma, r_s, and the scale of the change of the phase velocity of the Langmuir waves, r_{shift}. A rough estimate of r_{shift} can by done by making use of equation 2.51:

$$r_{shift} = L_{un}\frac{v_t^2}{v_b^2}. \tag{2.58}$$

Above mentioned condition implies that $r_s/r_{shift} \ll 1$. This inequality allows one to describe the process of the relaxation of the beam in a two steps. At the first step, with characteristic scale x_r relaxation runs as in homogeneous plasma, namely runs toward lower velocities and ends with a plateau formation of the electron velocity distribution function in the rage of velocities $0 < v < v_b$. Spectral energy density of the waves in the end of the first stage corresponds to $W_{end}(V)$ obtained by making use of equation 2.43. At the second step, with much larger scale r_{shift}, the waves generated at the first stage propagate within a plasma until decay due to the Landau damping on the electrons with $v > v_b$. Reabsorption of the wave by the particles leads to the shift of a right border of the electron distribution function toward larger velocities. In the end of the relaxation the distribution function can be described as follows:

$$n_b f_{end} = \begin{cases} \frac{n_b}{v_b} & \text{for } v < v_{end} \\ 0 & \text{for } v > v_{end} \end{cases} \tag{2.59}$$

where v_{end} is new position of the right border of the velocity distribution function and $v_{end} > v_b$.

To estimate v_{end} one can use the energy conservation law. If the all energy of the waves is reabsorbed by the electrons, than total energy of the electrons in the end of relaxation should be equal to the initial energy of the beams. This implies following equation:

$$\frac{1}{2}mn_b \int_0^{v_{end}} v^2 f_{end} dv = \frac{1}{2}mn_b v_b^2 \tag{2.60}$$

By substituting f_{end} determined by equation 2.59 into equation 2.60 one can obtain that $v_{end} = \sqrt{2}v_b$. Now one can use obtained v_{end} to estimate an energy of the accelerated particles in the end of the relaxation, E_a, as follows:

$$E_a = \frac{1}{2}mn_b \int_{v_b}^{v_{end}} v^2 f_{end} dv \tag{2.61}$$

In a case of the initially thin beam E_a is about 65% of the initial energy of the beam. The estimation is rather high. In more realistic cases it can be much smaller if take into account several additional physical processes, such as, collision losses, decay of primary Langmuir waves on secondary Langmuir waves and ion-sound waves, the generation of electromagnetic emissions.

2.6 Plasma with random density cavities

In this section, we describe the effects of background plasma random density fluctuations on the relaxation of electron beams. For this end, we assume that the level of fluctuations is so high that the majority of Langmuir waves generated as a result of beam-plasma instability are trapped inside density depletions. The k vector of waves undergoes oscillations from zero (in the reflection points) to some maximum value (in the point with minimal density). An appropriate approach to such a problem consists in consideration of the problem in terms of spatial averaged wave growth rate, $\overline{\gamma}$, and electron velocity diffusion coefficient , $\overline{D}$.

2.6.1 Procedure of averaging

For the problem under consideration we assumed that the initial velocity of the beam, v_b, significantly exceeded the plasma thermal velocity, v_t. The second assumption is that the initial width (variance) of the velocity, Δv, of the beam is small as compared to the beam velocity, v_b. The density of a plasma is supposed to depend on the coordinates as follows: $n(x) = N_0 + \Delta n(x)$, where $\Delta n(x)$ describes small deviations from N_0. An important additional condition is that the spatial scale of inhomogeneities, a, is supposed to be much larger than the wavelength of the Langmuir waves generated by the beam: $a\omega_p/v_b \gg 1$. For such a case the dispersion relation of the Langmuir wave can be modified as follows:

$$\omega(k,x) = \omega_{p0}\left(1 + \frac{1}{2}\frac{\Delta n(x)}{N_0}\right) + \frac{3}{2}\frac{k^2 v_t^2}{\omega_p 0} \tag{2.62}$$

where ω_{p0} is unperturbed plasma frequency. It is worth noting, that the change of the wave spectral energy density, at the timescale of one period of oscillation between turning points, a/v_{gr}, is small, and thus one can use averaged over this period waves growth rate. Let us begin from Liouville equation for $W_s(x,k,t)$:

$$\frac{\partial W_s(x,k,t)}{\partial t} + \frac{\partial \omega}{\partial k}\frac{\partial W_s(x,k,t)}{\partial x} - \frac{\partial \omega}{\partial x}\frac{\partial W_s(x,k,t)}{\partial k} = 2\gamma W_s(x,k,t) \tag{2.63}$$

(equation 2.63 can be obtained from equation 2.22 by taking into account that $d/dt = \partial/\partial t + (\partial x/\partial t)(\partial/\partial x) + (\partial k/\partial t)(\partial/\partial k)$ and by making use of Hamiltonian equations for the Langmuir waves: $\partial x/\partial t = \partial\omega/\partial k$ and $\partial k/\partial t = -\partial\omega/\partial x$). Equation 2.63 can be simplify by substitution of wave energy spectral density as a function of the ω instead of k (relation between ω and k is determined by dispersion relation 2.62), as follows:

$$\frac{\partial W_s(x,\omega,t)}{\partial t} + \frac{\partial \omega}{\partial k}\frac{\partial W_s(x,\omega,t)}{\partial x} = 2\gamma W_s(x,\omega,t) \tag{2.64}$$

In order to find the solution of the equations above, one can use the perturbation theory $W_s = W_{s0} + \gamma W_{s1}$ and taking into account that $\frac{\partial W_{s0}}{\partial t} \sim 2\gamma W_{s0}$ one can obtain in the first order approximation:

$$\frac{\partial W_1}{\partial x} = \frac{2\gamma W_0 - \partial W_0/\partial t}{\partial\omega/\partial k}. \tag{2.65}$$

Integrating equation 2.65 over close trajectories of the Langmuir waves between their turning points, and taking into account that W_{s0} does not depend on x, one cane obtain the following equation:

$$\frac{\partial W_{s0}(\omega,t)}{\partial t} = 2\overline{\gamma} W_{s0}(\omega,t), \tag{2.66}$$

where $\overline{\gamma}$ is averaged wave growth rate

$$\overline{\gamma} = \left(\oint \gamma / \frac{\partial\omega}{\partial k} dx\right) / \left(\oint dx (\frac{\partial\omega}{\partial k})^{-1}\right), \tag{2.67}$$

If the level of fluctuations is sufficiently high, main wave activity is localized in the vicinity of the bottom of the density well with coordinate, x_0. For this case the density profile can be assumed to be similar to parabolic:

$$\Delta n(x) = \Delta n_0 + \frac{1}{2}|\Delta n|\frac{(x-x_0)^2}{a_0^2}, \tag{2.68}$$

where $\Delta n_0 = \Delta n(x_0)$ and

$$\frac{1}{a_0^2} = \frac{1}{|\Delta n_0|}\frac{\partial^2 \Delta n}{\partial x^2} \tag{2.69}$$

Then the dispersion relation of the Langmuir waves reads:

$$\omega = \omega_p \frac{|\Delta n|}{2n_0} \frac{(x-x_0)^2}{a_0^2} + \frac{3}{2}\frac{k^2 v_t^2}{\omega_p}. \tag{2.70}$$

The term $\partial\omega/\partial k$ in the equation 2.67 is a group velocity of the Langmuir waves and thus: $\partial\omega/\partial k = 3v_t^2/v$. Also it is convenient to determine the term $(x-x_0)^2$ from the dispersion relation 2.70 as follows:

$$(x-x_0)^2 = \frac{a_0^2 v_t^2}{\varepsilon}\left(\frac{1}{u^2} - \frac{1}{v^2}\right), \frac{\partial\omega}{\partial k} = 3\frac{v_t^2}{v}, \tag{2.71}$$

where $u = \omega_p/k(x_0)$ is a phase velocity of the wave in the bottom of the density well. By making substation $\partial\omega/\partial k$ and $(x-x_0)^2$ into equation 2.67 and by making use of the new variable of integration $V = \omega/k(x)$ (can be defined from condition $\omega(x,k) = const$), one can obtain averaged growth rate of the wave as follows:

$$\overline{\gamma}(u,t) = \int_u^\infty \frac{\partial f(V,t)}{\partial v}\left(\frac{1}{u^2} - \frac{1}{V^2}\right)^{-\frac{1}{2}} dV. \tag{2.72}$$

In a similar way, the equation describing evolution of the electron velocity distribution function can be obtained from the corresponding QL equation 2.37 by making spatial integration over the closed trajectories of the waves. By taking into account that the oscillations in each single cavity are independent on those in the other cavities, one can derive the averaged diffusion coefficient as follows:

$$\overline{D} = \frac{8\pi^2 e^2}{m^2} v_t \int_0^v \frac{\overline{W}(u,t)}{u^2\sqrt{v^2-u^2}} du, \tag{2.73}$$

where

$$\overline{W}(u,t) = \lim_{L\to\infty} \frac{1}{L}\sqrt{\frac{3}{2}\frac{N_0}{\Delta n_0}} a_0 W_0. \tag{2.74}$$

2.6.2 Evolution of the beam velocity distribution function and wave spectral energy density

The complete system of equations that describes relaxation of the electron beam in the plasmas with random density cavities in a quasi-linear approximation is

$$\frac{\partial\overline{f}}{\partial t} = \frac{\partial}{\partial v}\overline{D}\frac{\partial\overline{f}}{\partial v} \tag{2.75}$$

where

$$\overline{D} = \frac{8\pi^2 e^2}{m^2} v_t \int_0^v \frac{\overline{W}}{u^2\sqrt{v^2-u^2}} du, \tag{2.76}$$

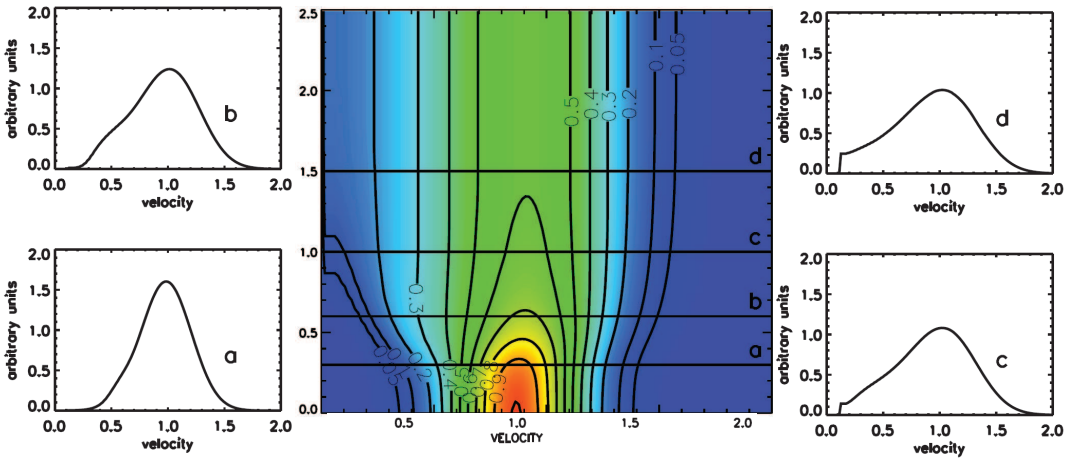

Figure 2.4: The dynamics of the electron distribution function obtained from the numerical simulation (shown in the central panel). The small panels provide snapshots of the distribution function. The values of the distribution function and the velocity are provided in arbitrary units. The width of the initial Gaussian is $\Delta v = 0.2 v_b$ [from Voshchepynets and Krasnoselskikh, 2013].

and

$$\frac{\partial \overline{W}}{\partial t} = 2\overline{\gamma}\overline{W}, \tag{2.77}$$

where $\overline{\gamma}$ is

$$\overline{\gamma} = \frac{1}{2}\omega_p \frac{n_b}{N_0} u \int_u^\infty \frac{v \partial \overline{f}/\partial v}{\sqrt{v^2 - u^2}} dv. \tag{2.78}$$

It is worth noting that velocity diffusion coefficient and waves growth rate in the plasma with density cavities (defined by 2.76 and 2.78) differ strongly from the corresponding coefficients in homogeneous plasma (defined by 2.39 and 2.40).

After substitution of variables $\overline{f} \to \frac{\overline{f}}{v_b}$, $\overline{W} \to \frac{n_b m v_b^4}{\pi \omega_p v_t}\overline{W}$, $t \to \frac{n_b}{N_0 \omega_p} t$, $v = v_b v$, $u = v_b u$ one can notice that the system conserves its total energy:

$$\frac{d}{dt}\left[\frac{1}{2}\int_0^\infty v^2 \overline{f} dv + \int_0^\infty \frac{\overline{W}}{u^3} du\right] = 0. \tag{2.79}$$

The first term corresponds to the particle kinetic energy ϵ_k, the second - to the wave energy ϵ_w.

The dynamic of $\overline{f}$ obtained from the numerical simulation based on the system above is shown in Figure 2.4. On the right and left panels one can see the snapshots of $\overline{f}$ for different moments of time. In a homogeneous plasma, relaxation stops when within the entire range of velocities the distribution satisfies the condition $\partial \overline{f}/\partial v \leq 0$ corresponding to the absence of instability. The time of relaxation in dimensionless units is on the order of $\tau \approx 1$. As it is shown in Figure 2.4, at the end of the period of beam evolution the relaxed beam distribution, $\overline{f}$, in our case still has a positive

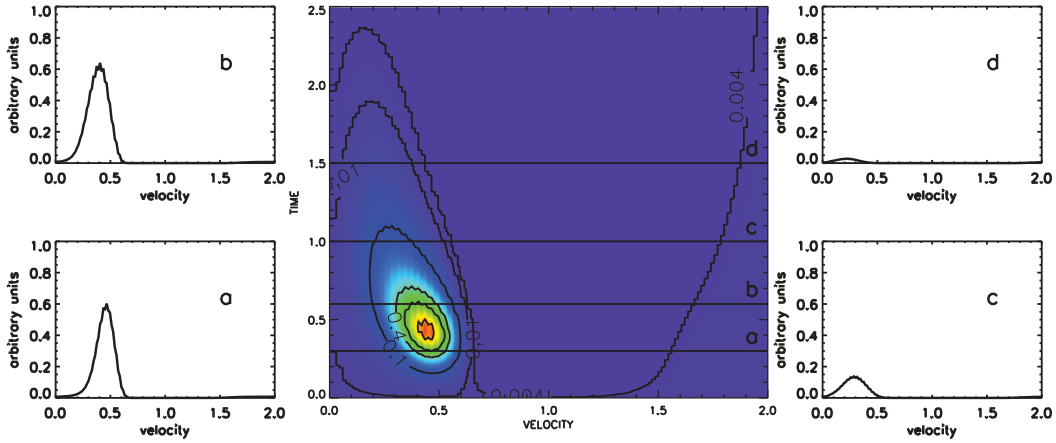

Figure 2.5: The dynamics of the averaged wave spectral power obtained using the numerical simulation, as shown in the central panel. Small panels provide snapshots of the wave spectral power. The values of the wave spectral power and the velocity are provided in arbitrary units [from Voshchepynets and Krasnoselskikh, 2013].

slope. The dynamics of $\overline{W}$ obtained in the simulation is shown in Figure 2.5. The maximum value of $\overline{W}$ obtained in simulation was $\overline{W}_{max} = 0,15$ in dimensionless units determined above. We normalized $\overline{W}$ to $\overline{W}_{max}$ in Figure 2.5. By comparing the dynamics of $\overline{f}$ and the wave energy ϵ_w one can notice that the process of the positive slope decrease corresponding to conventional formation of the plateau of the electron distribution ("plateauing") continues to operate while ϵ_w continues to grow (in Figure 2.4 and Figure 2.5 it corresponds to time interval $t = 0.0$, $t = 0.5$). After this time, ϵ_w begins to decay but particle diffusion is still at work for some time. For the conditions of simulation as presented in the Figure 2.4 the relaxation process ends after $\tau \approx 1.4$.

2.6.3 Waves growth rate

In Figure 2.6 the dependencies of the distribution function and the growth rate on velocity are presented for two moments of time. As one can see, the impact of wave trapping in randomly inhomogeneous plasma as described by the averaged $\overline{\gamma}$ results in significant reduction of the range of phase velocities u where waves can be generated. Very important difference between beam plasma interaction in homogeneous and inhomogeneous plasmas consists in the direct relation of the slope of distribution with

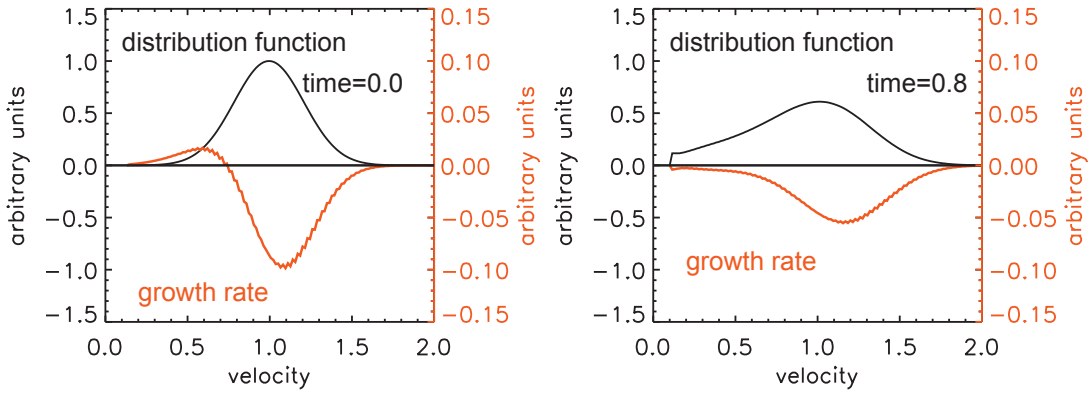

Figure 2.6: The electron distribution function $\overline{f}$ (black) and the related Langmuir wave growth rate $\overline{\gamma}$ (red) (the X and Y axis are same as in Figure 2.4) [from Voshchepynets and Krasnoselskikh, 2013].

the positiveness of growth rate in homogeneous plasma and absence of such relation in inhomogeneous. Indeed the waves can damp in the areas of the velocity space where the distribution function has positive slope. The effect appears due to the variation of the wave's phase velocity in inhomogeneous plasma. The majority of waves that are trapped pass a significantly longer time in areas where they are damped than in areas where they can grow. Therefore, the effect of averaging along the wave's trajectory explains the change in the relationship between the slope of the velocity distribution and wave growth/damping. The process of plateau formation can take place only if the wave intensity in the corresponding region is strong. Thus, relaxation of the beam significantly slows down due to the shrinking of the region where waves grow $\gamma > 0$. The region becomes narrower with time and from the moment shown in the left panel in Figure 2.6, we have $\gamma < 0$ for all waves. After $\tau = 0.8$ the waves could only be damped and the formation of the plateau eventually is stopped, electrons begin to reabsorb the energy of Langmuir waves allowing the diffusion process to be supported until the wave energy is completely reabsorbed.

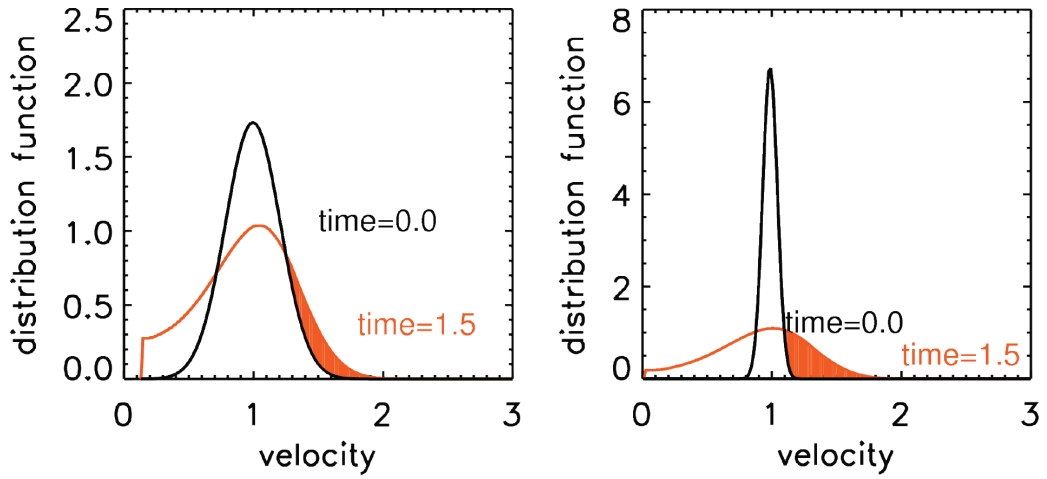

Figure 2.7: $\overline{f}$ for different moments of time (in arbitrary units). The initial electron beam distribution, $\overline{f}$, is plotted in black and the final distribution, $\overline{f}$, is plotted in brown. The right and left panels correspond to the different width of the beam Δv ($\Delta v = 0.2v_b$ and $\Delta v = 0.08v_b$) [from Voshchepynets and Krasnoselskikh, 2013]

2.6.4 Acceleration of the electrons

As seen from equation 2.76, all the waves with phase velocities $u < v$ were involved in the acceleration of particles with a velocity v. Therefore, acceleration was basically provided by waves that were grown in a region with a positive growth rate. Wave propagation in plasma with density fluctuations suggests that part of the time waves pass in the region where their phase velocity is larger than the phase velocity of primarily generated waves, resulting in an interaction with particles having velocities higher than the velocity of particles of the beam that transfers part of their energy to waves.

Such an action allows the transfer of part of the wave energy to energetic particles forming the tail of the distribution with energies larger than the beam energy. We used this process to describe the diffusion process toward higher energies. From Figure 2.7 one can see that the population of fast electrons within the tail of the distribution function grows during beam relaxation (the filled areas). Therefore, electrons could be efficiently accelerated. Calculations with different initial conditions indicated that the energy of energetic particles depend on the initial Δv.

For $\Delta v < 0.1v_b$, more than 50% of the initial ϵ_k might be transferred to a higher energy tail due to the wave energy absorption by particles having energies higher than the energy of the beam.

2.7 Conclusions

Relaxation of the electron beam in the plasma with density inhomogeneities differs from the relaxation in the homogenous plasma. In this chapter we considered the

effects produced by the changes in magnitude of the wave vector of the Langmuir waves, generated by the beam instability, in the direction of the wave propagation. The changes in the wave vector lead to changes in the wave phase velocity, and cause the outflow of the wave spectral energy density from the resonant region in velocity space.

For the case of monotonically decreasing density profile in the direction of the beam propagation, the outflow of the wave energy going toward lower phase velocities. As a result, the wave energy in the volume of the velocity space resonant with electron of the beam is reduced. This in turn, reduces the back reaction of the wave on the electron distribution function, and the relaxation is slowed down in comparison to relaxation in the homogeneous plasma. On the spatial scale, on which in homogeneous plasma the electron velocity distribution function already takes form of the plateau, in the plasma with decreasing density, the beam electrons are characterized by a small spread of the velocities on the order of v_t/v_b. However, asymptotical solution are the same as in homogeneous plasma.

In a plasma with monotonically increasing density profile, the wave phase velocity is shifted toward larger velocities. Thus, the waves generated with phase velocities around beam velocity consistently enter to the region of the velocity space where, $\partial f(v,t)/\partial v < 0$ where the increment of the instability is negative. As a result of interaction with electrons, the wave energy decreases with time, while the kinetic energy of this electrons increases. For the case of small density gradient, the relaxation of the beam in such inhomogeneous plasma can be separated into two stages. On the first stage, relatively short in time, the electron velocity distribution function takes a form of the plateau, and significant part of the kinetic energy of the electrons transfers to the energy of the wave. At the second stage, the waves slowly move in the velocity space toward region with $\gamma < 0$ and decay. Relaxation stops when all energy of the waves is absorbed by the fast electrons, that form the energetic tail on the electron distribution function.

If the plasma contains random density cavities with sufficiently large depth, the overwhelming majority of the generated waves are trapped by density depletions. Under these conditions the growth rate can be averaged along the wave path in the vicinity of the bottom of density wells. Two important features were observed during the relaxation of the beam that were different from the beam-plasma interaction in a homogeneous plasma. The relaxation process stops prior to the formation of a plateau-like distribution function because wave growth stops even when the slope of the distribution function remains positive locally in the velocity space. The relaxation process causes a transfer of a portion of the energy of waves to the high energy part of the electron velocity distribution. For the narrow beam ($\Delta v < 0.1 v_b$) the energy of accelerated electrons can reach up to 50% of the total initial energy of the beam. However, the presence of

wave damping by the background distribution in the plasma, as well as a number of other effects, such as, decay of primary Langmuir wave on secondary Langmuir wave and the ion-sound wave, the generation of electromagnetic emissions, and others, may also have an important impact on availability of wave energy that can be reabsorbed by the higher energy electrons.

2.8 Resume in French

Nous allons commencer par une brève introduction de physique des plasmas. Ces points seront nécessaires pour la compréhension du manuscrit et de la logique de la présentation. Dans ce chapitre nous allons définir les principales variables du problème, décrire les concepts et les processus mis en jeu dans notre modèle. Une partie assez importante de cette description peut être trouvée dans des différents ouvrages dédiés à la physique des plasmas [Artsimovich and Sagdeev, 1979, Akhiezer, 1975, Melrose, 1980b].

Le modèle que nous proposons a pour objet de décrire l'interaction de faisceau d'électrons de faible densité avec des ondes de Langmuir, donc nous devrions à cet effet utiliser la description cinétique du plasma. La description du plasma par le système d'équations de Vlasov nous permet de déterminer les champs électriques qui y règnent de façon auto-consistante. L'application de cette théorie auto-consistante aux oscillations électrostatiques de hautes fréquences nous fournira non seulement les relations de dispersion pour ce type d'ondes, en d'autres termes, la description de la propagation des ondes de Langmuir dans le plasma, mais aussi plus de compréhension sur les processus d'interaction onde-particule.

La propagation des ondes dans un plasma perturbe les trajectoires de toutes ses particules, toutefois une population relativement petite de ces particules, notamment celle qui satisfait la condition de résonance est responsable de phénomènes d'amplification et d'amortissement des ondes. Dans le cas des ondes de Langmuir, la principale contribution à ces phénomènes est fournie par les électrons répondant à la résonance Cherenkov: les vitesses des particules sont proches de la vitesse de phase de l'onde. L'interaction résonante onde-plasma de ce type permet d'expliquer la croissance et l'amortissement de l'onde. Dans un plasma homogène, le taux d'amortissement/croissance est proportionnel à la dérivée de la fonction de distribution électronique aux voisinages de la résonance. La caractéristique naturelle d'une telle relation consiste à produire toujours l'amortissement des ondes de Langmuir dans les plasmas Maxwellien (grâce à l'amortissement de Landau) qui correspond à l'état de l'équilibre thermique.

Suite à des instabilités, si un spectre d'ondes de large bande est excité dans le plasma hors l'équilibre, un état turbulent des oscillations de plasma peut se produire. La théorie quasi linéaire (QL) décrivant l'évolution des instabilités et de l'interaction des particules avec les ondes dans des plasmas turbulents est basée sur une hypothèse importante:

celle que toutes les ondes ont de faibles amplitudes. Cette hypothèse conduit à négliger tous les types d'interactions onde -onde non linéaires. Le seul effet non linéaire pris en compte dans ce modèle se rapporte à l'interaction résonante des ondes avec des particules. L'instabilité faisceau-plasma est l'une des premières instabilités cinétiques étudiée par l'utilisation la théorie QL [Vedenov et al., 1962, Drummond and Pines, 1964]. Dans le cas du plasma homogène, la théorie QL prédit la formation de plateau de la fonction de distribution des vitesses d'électrons dans la plage de vitesses inférieures à la vitesse du faisceau. Le processus de formation de plateau est accompagné par le transfert d'une partie de l'énergie cinétique des électrons en une énergie potentielle des ondes de Langmuir.

La relaxation du faisceau d'électrons dans un plasma de densité électronique non-homogène se développe d'une manière différente comparée à celle d'un plasma homogène [Breizman and Ryutov, 1970, Ryutov, 1969, Vedenov and Ryutov, 1975]. Dans ce chapitre, nous avons examiné les effets liés aux changements de la magnitude du vecteur d'onde des ondes de Langmuir, générées par l'instabilité de faisceau, dans la direction de propagation de l'onde. Une variation du vecteur d'onde a comme conséquence une variation de la vitesse de phase de l'one ceci engendre alors une diminution de la densité spectrale d'énergie de l'onde de la région résonante dans l'espace des vitesses. Cette dernière est due à des pertes d'energie à partir du domain de génération.

Lorsque le profil de densité décroît de manière monotone dans la direction de propagation du faisceau, le flux d'énergie des ondes se dirige vers des vitesses de phase inférieures. En conséquence, l'énergie des ondes dans le volume de l'espace des vitesses résonantes avec électron du faisceau diminue. Ceci, à son tour, réduit la contre-réaction de l'onde sur la fonction de distribution des électrons, et la relaxation se trouve atténuée, c'est-à-dire, le temps de relaxation est plus long par rapport à celui du plasma homogène. En ce qui concerne l'échelle spatiale, on considère la distance sur laquelle dans le plasma homogène d'une part,la fonction de distribution de vitesse des électrons commence à prendre la forme de plateau, et dans le plasma ayant le profil de la densité décroissante d'autre part, la fonction de distribution des électrons présente une variation traduisant un petit effet de diffusion dans l'espace des vitesses de l'ordre de v_t/v_b. Dans les deux cas, toutefois, les solutions tendent vers la même forme asymptotique.

Dans un plasma avec le profil de la densité monotone et croissant, la vitesse de phase de l'onde augmente et dépasse la vitesse du faisceau. Ainsi, les ondes générées avec des vitesses de phase voisines de la vitesse du faisceau se déplace systématiquement dans la région de l'espace des vitesses où $\partial f(v,t)/\partial v < 0$, l'onde se trouve alors amortie. Suite à l'interaction avec les électrons, l'énergie des ondes diminue avec le temps, tandis que l'énergie cinétique des électrons énergétiques augmente. En présence de petit gradient de densité, la relaxation du faisceau dans un tel plasma non-homogène peut être séparée en deux phases. Dans une première phase, relativement bref dans le temps, la fonction

de distribution des vitesses des électrons prend une forme dotée de plateau, et une partie significative de l'énergie cinétique des électrons est transférée vers de l'onde. Au cours de la deuxième phase, les ondes se déplacent lentement dans l'espace des vitesses vers la région $v > v_b$ ou $\gamma < 0$ et leur énergie est absorbée par les particules. La relaxation s'arrête quand toute l'énergie des ondes est absorbée par les des électrons rapides. Ce processus aboutit à la formation de queue de la fonction de distribution, du côté des électrons énergétiques.

Si le plasma renferme des cavités suffisamment profondes de densité, réparties de manière aléatoire, l'écrasante majorité des ondes générées sont piégées dans ces cavités de densité. Dans ces conditions le taux de croissance peut être évalué comme une moyenne sur le trajet de l'onde oscillant au voisinage de fond de puit de densité. Deux caractéristiques importantes du processus de relaxation de faisceau différentes de celles de l'interaction faisceau-plasma dans un plasma homogène ont étaient trouvées dans ce cas. Premièrement, le processus de relaxation peut s'arrêter avant la formation d'un plateau la raison en est que la croissance d'onde s'arrête alors que la pente de la fonction de distribution reste encore positive localement dans l'espace des vitesses. Deuxièmement, le processus de relaxation est accompagné d'un transfert d'une partie de l'énergie d'ondes aux particules de plus haute énergie et de la formation de queue dans la distribution de vitesses des électrons. Pour un faisceau étroit ($\Delta v < 0.1 v_b$) l'énergie des électrons accélérés peut atteindre jusqu'à 50% de l'énergie totale initiale du faisceau.

Chapter 3

Probabilistic model of beam-plasma interaction in randomly inhomogeneous plasma.

3.1 Introduction

In this chapter we present recently published model for beam plasma interaction in a randomly inhomogeneous plasma [Voshchepynets et al., 2015]. We replace the continuous spatial interval by discrete one of finite (but very large) length and divide it into a set of finite equally sized sub-intervals of size a. Such discretization allows one to apply in a simpler way the probabilistic approach. The scale a is stated to be much less than the characteristic scale of changes for the electron distribution function, L_c. We consider an interaction of a coherent small amplitude wave with a particle on such a small interval by assuming that the density profile on this interval is linear. However, it is supposed that it is sufficiently larger than the wave's wavelength. Our assumptions allow one to describe the action of the field of a wave with a known frequency on a particle using a necessary degree of accuracy to calculate the effect of wave particle interaction on any particular interval with chosen densities at the ends. The key point of our description is that, on each interval, we assume that the values for the density in the center of the interval are random and independent, and they are described by a predetermined known statistical distribution. The density profile is continuous without discontinuities being skewed at the ends of neighboring intervals. The distribution can be chosen either by taking it to correspond to real observations or choosing a model distribution that allows calculations to be performed in a simpler manner. Based on this knowledge, the statistical distribution for the phase velocities of waves can be derived for any given frequency. The last distribution is uniquely determined by the distribution of the density fluctuations. This probability allows one to calculate the average energy exchange between particles with a given velocity and a wave with a given frequency. While calculating particle motion under the action of a chosen wave, we

consider its phase to be determined, although, afterwards, we shall perform statistical averaging over the phases by assuming that they are random and uniformly distributed in the interval from 0 to 2π. We also assume that the wave particle interaction at each interval is independent of wave particle interactions at previous intervals. Using such assumptions, we calculate the probability that a particle having at initial time t_0 velocity v_0 after Q interactions that occur during a time interval $(t - t_0)$ will have a velocity v, where the number of steps, Q, should be large enough to justify statistical averaging. We replace time averaging by averaging over an ensemble with a given probability distribution. Such an assumption allows one to determine an averaging procedure over a predetermined distribution that is related to the statistical distribution of the density fluctuations, suggesting the number of steps, Q, to be large. An assumption of random and independent interactions corresponding to an uncorrelated Marcovian process leads to a description of the evolution of the particle distribution function based on an equation of diffusion similar to the Fokker-Planck equation in the velocity space. Under such assumptions, the diffusion coefficient so determined is dependent on the probability distribution of the density fluctuations. To calculate the growth rate of a wave, we use the energy change of particles energy and take into account the fact that on a small interval with a linear profile of density, the gain/loss of energy by the particle is equal to the energy loss/gain by the wave. Local conservation of energy occurs on small intervals and allows one to calculate an average energy change for wave energy density and the increment of instability or damping for a wave having given frequency.

3.2 Lungmuir waves in the plasma with density fluctuations

Here, we consider a one dimensional problem where the Langmuir wave packet generated by the beam propagates in an inhomogeneous plasma. The density inhomogeneities of the background plasma with density N_0 are stated to have a relatively small amplitude, $\delta n \ll N_0$ and their characteristic scales, L, (even the smallest) are much larger than the wavelength, λ, of the waves generated by the beam and propagating in a plasma: $L \gg \lambda$. Our goal is to describe the process of beam-plasma interaction in inhomogeneous plasma with density fluctuations described by the probability density distribution, $P(\delta n)$. Assuming the conditions above are satisfied, the propagation, amplification, and damping of waves can be described either using Zakharov's equation [Zakharov, 1972] for the envelope of an electric field or by means of a Liouville description for the spectral energy density, $W_s(k, x, t)$. For our purposes, these two descriptions are equivalent. Let us begin with the Zakharov's equation

$$2i\frac{\partial E}{\partial t} + 3\omega_p \frac{\partial^2 E}{\partial x^2} = \omega_p \frac{\delta n}{n_0} E + \widehat{\gamma} E, \tag{3.1}$$

where $E(k,x,t)$ is the electric field amplitude, ω_p is the average plasma frequency, λ_D is the Debye length, δn indicates density fluctuations, and $\widehat{\gamma}$ is an operator describing the local growth/damping rate of waves. The first two terms on the left-hand side of the equation (3.1) describe a propagating wave having some frequency and a wave-vector in a homogeneous plasma. The two terms on the right-hand side of the equation (3.1) are dependent on random density fluctuations. The equation (3.1) provides an appropriate dynamic description for wave field evolution and propagation on relatively small scales, smaller or comparable to the characteristic scale of variations in density fluctuations. The first term on the right-hand side of the equation (3.1) describes variations in the wave vector due to variations in the density. The second term on the right-hand side of the equation (3.1) describes wave-particle interactions that vary along the wave path due to changes in the wave phase velocity.

By considering a simplified model when inhomogeneities can be presented in the form of localized regions where the density is different from an "averaged background", the presence of the following characteristic scales can be identified for our problem: 1) a characteristic scale for the localized inhomogeneity, which we denote with L, and 2) a sufficiently larger characteristic scale, L_c, where the electric field of the wave can be considered as "statistically averaged" over a long path with many inhomogeneities. It should include multiple interactions of wave with different groups of particles having velocities equal to the local phase velocity of wave. In each localized region, the phase velocity of the wave undergoes relatively small variations. Thus, characterization using a local phase velocity is justified and locally determines the growth/damping rate. The evolution of the averaged wave amplitude can be characterized by some averaged growth/damping rate when the wave traverses many localized regions. The short time scale is related to wave dynamics in the localized region corresponding to the characteristic scale L. On this scale, the evolution of the wave can be described using a quite precise description with quite accurate precision. The evolution of the wave is determined by variations of the wave vector and a change in the wave amplitude due to the presence of an instability or dissipation provided by wave particle interaction. The approach is similar to the SGT proposed by Robinson Robinson et al. [1993]. However, the SGT does not address the question how wave energy is dissipated by particles and how it affects the distribution function of beam generating waves. The SGT only defines the asymptotic characteristics of wave amplitudes that are independent of the statistics of density fluctuations. Here, we refine the SGT by taking into account the statistical properties of density fluctuations that we characterized using the probability density distribution. The second important goal of our study is the description of the relaxation of the beam particles. In other words, here, we describe how wave particle interactions influence the beam and how the process of relaxation depends on the characteristics of the beam and the statistical characteristics of density fluctuations.

3.3 Characteristic scales of the density fluctuations

Several important scales are known from studies of beam plasma interaction in homogeneous plasma and plasma with monotonically changing density as compared with density inhomogeneity scale.

Characteristic scales of the beam plasma interaction depend on the characteristic growth rate γ. To obtain the growth of waves up to a level significantly larger than noise level one should satisfy the following condition:

$$\gamma \frac{L}{v_g} \gg \Lambda. \tag{3.2}$$

Here L is the characteristic scale of the density inhomogeneities; $v_g \sim v_t^2/v_b$ is the group velocity of the Langmure wave; v_t is the thermal velocity of the background plasma; and v_b is the velocity of the beam; Λ is the so called Coulomb logarithm and $\Lambda = \ln N_0 \lambda_D^3$, where λ_D is the characteristic Debye length. If L is smaller than $(v_g/\gamma)\Lambda$, the growth of the waves is stopped on such a level that nonlinear phenomena such as wave particle interactions can be neglected. The linear growth rate of the beam plasma instability reads:

$$\gamma \simeq \omega_p \left(\frac{n_b}{N_0}\right) \left(\frac{v_b}{\Delta v_b}\right)^2,$$

where ω_p is the characteristic plasma frequency, Δv_b is the characteristic beam width in the velocity space, and n_b is the density of the beam electrons. Then the condition above can be presented as follows:

$$L_{min} = \left(\frac{\Delta v_b}{v_b}\right)^2 \frac{N_0}{n_b} \frac{v_t}{v_b} \Lambda \lambda_D.$$

For parameters relevant to solar Type III electron beam and background plasma at 1 AU, the following parameters are applicable [Ergun et al., 1998] : $N_0 \approx 5 \times 10^6 m^{-3}$; $\omega_p/2\pi \approx 20kHz$; $n_b/N_0 \approx 10^{-5}$; $\lambda_D \approx 15m$; $\Delta v/v_b \approx 0.05$; $v_b \approx 15 v_t$ and $\Lambda \approx 15$; L_{min} results in $250\lambda_D$ or $3750m$.

Density fluctuations having very large spatial scales, larger than the beam relaxation length in homogeneous plasma, can not significantly influence the process of the beam plasma interaction. Relaxation stops with a plateau formation when $\Delta v/v_b \sim 1$. Then, L_{max} can be estimated, as follows:

$$L_{max} = \frac{N_0}{n_b} \frac{v_t}{v_b} \Lambda \lambda_D.$$

For the parameters mentioned above, L_{max} results in $10^5 \lambda_D$ or $1.5 \times 10^6 m$.

For the case of a quiet solar wind with $v_{SW} = 450kms^{-1}$, L_{min} and L_{max} can yield two characteristic frequencies in a frame of spacecraft $f_h = 120Hz$ and $f_l = 0.3Hz$. Herein, we consider density fluctuations with characteristic spatial scales, L, that satisfy conditions: $L_{min} < L < L_{max}$.

3.4 Procedure of discretization. Separation of scales

To apply the statistical approach to our system, below we describe our continuous system, making use of the procedure of discretization. To this end, we divide the continuous spatial interval on a set of equally sized subintervals of a length a. The size a is supposed to be match smaller than the characteristic scale of the change of electron distribution function. Moreover, it is supposed to be smaller than the characteristic scale of the density gradient but sufficiently larger than the wavelength of Langmuir waves generated by the election beam:

$$\lambda \ll a \ll L.$$

Another important limitation for a can be obtained by considering velocity change on an interval with an inhomogeneity having linear profile: $N(x) = N_0 + \Delta n x/L$. The dispersion relationship for the Langmuir wave can be written as follows: $\omega = \omega_p(x)(1+(3/2)(v_t^2/V^2))$. Here ω and V are the frequency and the phase velocity of the wave. Assuming that the frequency of the wave and the thermal velocity of particles are constant, the following equation can obtained:

$$\Delta\omega = \left(1 + \frac{3}{2}\frac{v_t^2}{V^2}\right)\frac{d\omega_p(x)}{dx}\Delta x - 3\omega_p\frac{v_t^2}{V^2}\frac{\Delta V}{V} = 0,$$

where ΔV is the deviation of the phase velocity on the scale Δx caused by a density gradient. Since

$$\frac{1}{\omega_p}\frac{d\omega_p(x)}{dx} = \frac{1}{2}\frac{d}{dx}\left(\frac{x}{L}\frac{\Delta n}{N_0}\right) = \frac{1}{2L}\frac{\Delta n}{N_0},$$

and taking into account the fact that $V \sim v_b \gg v_t$, ΔV can be estimated as follows:

$$|\Delta V| \sim v_b\frac{\Delta x}{L}\frac{|\Delta n|}{N_0}\frac{v_b}{v_t}.$$

Langmuir waves can grow or decay due to the interaction with the electron beam, while the phase velocity, V, remains in the interval $v_b - \Delta v_b < V < v_b + \Delta v_b$. The interaction will stop when $\Delta V \sim \Delta v_b$ and when the resonant conditions are not satisfied anymore for beam particles. Such deviation of phase velocity occurs on the following spatial scale:

$$\Delta x_c = L \frac{N_0}{\Delta n} \frac{\Delta v_b}{v_b} \frac{v_t^2}{v_b^2}.$$

For the condition mentioned before ($\Delta v_b / v_b = 0.05$, $v_b = 15 v_t$) and $\Delta n / N_0 = 0.01$, waves escape from resonance on the scale $\Delta x_c \sim 0.02L$. In our model, the change of velocity on one single interval should be much smaller than a velocity variation that would lead to a violation of the resonant condition. This implies that the characteristic scale for subinterval a is sufficiently smaller than Δx_c. In this case a wave can be considered to remain in resonance with the electron beam on a single interval without a loss of coherence.

3.5 Evaluation of the contribution from the angular diffusion

Two major physical effects are caused by density fluctuations, lead to changes in the wave phase velocity. Both result in changing of the conditions of resonance and consequently shift wave-particle interaction in another part of the phase space. Thus, the wave with frequency ω and unperturbed wave vector k_0 will interact with particles, that have velocities different from ω / k_0.

The first effect consists in angular diffusion of the direction of wave propagation and the angular deviation of the wave vector from its supposed trajectory in a homogeneous plasma. The process becomes extremely important, for density fluctuations with a spatial scales, l, that are small compared to v_g / γ, and with amplitudes, that are not to large $|\Delta n / N_0| \ll v_t^2 / v_b^2$. The first of inequalities implies that the angular deflection on each scattering event is much smaller than unity, so that process can be described by angular diffusion. The second of inequalities states that the k vector magnitude of the Langmuir waves is conserved (see Nishikawa and Ryutov [1976] and Krasnoselskikh et al. [2007] for additional details).

The second effect consists of a change in magnitude of k in the direction of wave propagation. Density fluctuations should have amplitudes that satisfy condition $|\Delta n / N_0| \geq v_t^2 / v_b^2$ to be involved in this process. As shown earlier, the most important impact on beam relaxation is provided by fluctuations with spatial scales, L, that lie within the range $L_{min} < L < L_{max}$. It is worth noting that inequality (3.2) leads to conclusion that L is much larger than, the spatial scale, l, of the fluctuations that are the most important for the process of angular diffusion.

Thereby, the process of angular diffusion is dominant, when density fluctuations have relatively "small" scales and amplitudes, while the effect of a change of k magnitude prevails for the fluctuations with larger scales and amplitudes. Our goal hereafter is to study the role of the density fluctuations of the second type in the beam plasma interactions.

Let us evaluate contribution from the angular diffusion of the scale Δx_c. These effect is described by the diffusion equation [Nishikawa and Ryutov, 1976, Krasnoselskikh et al., 2007] , and the corresponding process is characterized by a diffusion coefficient that can be estimated to be of the order of:

$$D \sim \omega_p \frac{1}{lk} \frac{1}{(k^2\lambda_D^2)} \left| \frac{\Delta n_{ad}}{N_0} \right|^2 .$$

Here k is the characteristic wave vector of the primary Langmuir wave generated due to beam-plasma interaction, Δn_{ad} and l, amplitude and spatial scale of an inhomogeneity involved in the process of the angular diffusion. To significantly reduce the instability growth the wave vector should deviate from its initial direction to the angle θ, as determined by the following condition:

$$1 - \cos\theta = \frac{\Delta v_b}{v_b}.$$

If $\Delta v_b / v_b \ll 1$ then $\theta \sim (\Delta v_b / v_b)^{1/2}$. Thus, the characteristic time of angular diffusion in the velocity space can be estimated as follows:

$$D\tau_{ad} \sim \frac{\Delta v_b}{v_b},$$

and

$$\tau_{ad} \simeq \frac{1}{D}\left(\frac{\Delta v_b}{v_b}\right) = \omega_p^{-1} \frac{(k^2\lambda_D^2)}{\left|\frac{\Delta n_{ad}}{N_0}\right|^2} kl \left(\frac{\Delta v_b}{v_b}\right).$$

Now one can compare the time of the angular diffusion, τ_{ad}, and the time of a propagation, $\tau_{pr}(\Delta x_c)$, of a Langmuir wave through the interval Δx_c:

$$\frac{\tau_{ad}}{\tau_{pr}(\Delta x_c)} = \frac{l}{L}\left(\frac{\Delta n}{\Delta n_{ad}}\right)^2 k^2\lambda_D^2 \frac{N_0}{\Delta n}\frac{v_b k}{\omega_p}$$

Taking into account that $v_b k/\omega_p \sim 1$, $l/L \leq 1/\Lambda$, $\Delta n/\Delta n_{ad} \gg 1$, and $\Delta n/N_0 \geq k^2\lambda_D^2$ one can find: $\tau_{ad}/\tau_{pr}(\Delta x_c) \gg 1$. Thereby, the effect of the angular diffusion is too 'slow' to make significant influence on the wave-particle interactions on the subinterval, $a \ll \Delta x_c$. Observations of the Langmuir waves in the solar wind show that most Langmuir waves have angles with background magnetic field smaller than 20° [Ergun et al., 2008, Malaspina and Ergun, 2008, Krasnoselskikh et al., 2011], that gives additional argument validating the weakness of angular diffusion of waves.

3.6 Probabilistic model of the beam plasma interaction in plasma with density fluctuations

Let us assume that a change in the density, $\Delta n = \delta n(x_{in} + a) - \delta n(x_{in})$, for each subinterval satisfies the condition $\Delta n/N_0 \ll 1$. Now we can consider the problem of

wave particle interaction on the interval with the density profile so determined. We shall consider the interaction of a small amplitude coherent wave, with a known frequency ω and an amplitude E_ω, with a particle with known velocity v_e on such an interval. These assumptions allow one to calculate changes in the particle velocity, Δv and in the wave amplitude, ΔE_ω, with necessary degree of accuracy.

We now consider deviations of the plasma density, δn, from N_0 at the ends of the subintervals as random and independent with a predetermined statistical distribution, $P_{\delta n}(\delta n)$. This last distribution uniquely determines the distribution of the wave phase velocity $P_\omega(V)$. Efficient variations for Δv and ΔE_ω only occur if the condition of exact resonance, $V = v_e$, is satisfied inside the selected interval. Change in the velocity of an electron depends on E_ω, a phase difference between an electron and a wave, ϕ, and the wave phase velocity on the selected subinterval. Without loss of generality, the initial phase ϕ can be suggested to be a random variable with a uniform distribution. Thus, variations in both Δv and ΔE_ω on ensemble of subintervals are determined by the random variables with the known probability distributions. An important additional assumption that allowed us to solve the statistical problem is an assumption that wave particle interactions on each subinterval are independent of wave particle interactions on the previous interval. The result indicates that the process can be considered to be a series of random and independent interactions, which allows one to describe the process of beam relaxation in terms of the uncorrelated Marcovian process. Another simplification that we used is based on the smallness of the changes in electron velocity: $\Delta v/v_e \ll 1$.

Under such conditions, one can define the probability density function, $U(v, t|v_0, t_0)$, that determines the probability $U(v, t|v_0, t_0)dv$ that a particle having a velocity v_0 at a moment of time t_0 will have a velocity v after Q interactions that occur during the time interval $t - t_0$. By suggesting that the number of steps, Q, be large enough to justify statistical averaging, the Fokker-Planck equation can be used to describe the evolution of $U(v, t|v_0, t_0)$, as follows:

$$\frac{\partial U(v,t|v_0,t_0)}{\partial t} = -\frac{\partial}{\partial v}A(v)U(v,t|v_0,t_0) + \frac{\partial^2}{\partial v^2}B(v)U(v,t|v_0,t_0), \tag{3.3}$$

where $A(v)$ and $B(v)$ are drift and diffusion coefficients that indicate the averaged characteristics for variations in the velocity and its dispersion:

$$A(v) = \frac{<\Delta v>}{\Delta t}, B(v) = \frac{1}{2}\frac{<\Delta v^2>}{\Delta t}.$$

To obtain the drift and diffusion coefficients, the change in velocity that an electron undergoes within subinterval a should be estimated, as described above. Time averaging should then be replaced by the average over the ensemble, which allows calculation of

the averaged characteristic variation, $\langle \Delta v \rangle$ and the dispersion $\langle \Delta v^2 \rangle$ of the particle's velocity. The averaging means averaging over phase ϕ and over phase velocity of the wave, that are supposed to be the random variables with the known distributions $P_\phi(\phi)$ and $P_\omega(V)$, respectively. As discussed before, it is reasonable to assume that ϕ is uniformly distributed within the interval $[0, 2\pi]$, while $P_\omega(V)$ can be determined using the distribution of the density fluctuations. To obtain an equation describing an evolution of an electron distribution function, $f(v,t)$, one should integrate $U(v,t|v_0,t_0)$ multiplied on $f(v_0,t_0)$ over v_0, where $f(v_0,t_0)$ is the electron distribution function at a moment t_0.

Following substitution of $\langle \Delta v \rangle$ and $\langle \Delta v^2 \rangle$, equation (3.4) can be written as follows (for more details see Appendix A.2):

$$\frac{\partial f}{\partial t} = \frac{2\pi^2 e^2 W}{m^2 \omega} \frac{\partial}{\partial v} v P_\omega(v) \frac{\partial f}{\partial v}, \tag{3.4}$$

where $W = E_\omega^2/(8\pi)$ is the wave energy density, and $f(v,t)$ is normalized to one. The next step consists of considering a spectrum of waves with different frequencies. For the sake of simplicity and without losing generality in the description, we considered it to be comprised of a set of discretized equidistant frequencies, ω_i. To describe the interaction of the beam with several monochromatic waves with frequencies, ω_i, and energy densities, W_i, the contribution of each wave in equation (3.4) should be summed.

To study the evolution of wave energy density, one can use the fact that on each subinterval, a, the change in wave energy density for any wave, W_i, is equal to a change in the total energy density of the electrons involved in a resonant wave-particle interaction taken with an opposite sign. By assuming that the change in W_i after passing one subinterval is small, $\Delta W_i / W_i \ll 1$, one can use $\langle \Delta v \rangle$ and $\langle \Delta v^2 \rangle$ in order to characterize the averaged change in particle energy (for more details see Appendix A.1). Using this approach allows one to derive an equation for the variation of W_i over a larger (statistical) scale:

$$\frac{dW_i}{dt} = \pi \omega_{p0} \frac{n_b}{N_0} W_i \int_0^\infty V^2 \frac{\partial f}{\partial V} P_{\omega_i}(V) dV, \tag{3.5}$$

where n_b is the density of the electron beam. For a homogenous plasma, there are no variations in the wave phase velocity and $P_\omega(V)$ may be replaced by the Dirac delta function. For such a case, equation (3.5) takes a form similar to the corresponding equation in QL theory [Vedenov et al., 1962]. The wave's growth rate, γ, only depends on the value of the derivative of the electron distribution function at a single point within the velocity space. The presence of density fluctuations leads to variations in the wave's phase velocity, and, as a result, the wave can interact with different parts of the electron distribution function on different subintervals. Integration into equation (3.5) corresponds to the procedure of averaging the local growth rate γ.

Equations (3.4) and (3.5) allows one to describe beam-plasma interactions in the presence of random density fluctuations. Here, the reader should note that the system conserves the total energy of particles and waves (Appendix A.3). Key parameters of the model are the probability distribution function of the wave phase velocity, $P_{\omega_i}(V)$, derived from the probability distributions of the density fluctuations, $P_{\delta n}(\delta n)$.

3.7 Probability distribution function of the wave phase velocity

Considering density variations to be linear on scale a, a linear approximation can be said to be valid for an electron plasma frequency with the same degree of accuracy, causing changes in the wave phase velocity. Using the dispersion relationship for Langmuir waves, one can obtain a relationship between the plasma frequency and the corresponding phase velocity, as follows: $\omega_p^2(n) = \omega^2(1 - 3v_t^2/V^2)$, where $\omega_p(n)$ depends on the density fluctuations.

Knowledge of the distribution function for density fluctuations at the edges of subinterval a allows one to find the distribution function of the corresponding plasma frequencies, $f_{\omega_p}(\omega_p)$. To evaluate the probability that resonant conditions for wave particle interactions are satisfied on any selected interval having a known density, the common probability that the wave phase velocity on one of the subinterval is larger than the particle velocity and smaller on the other end should be calculated. The probability can be found by making use of the following expression:

$$P_\omega(V) = P(u_{i1} < V) \cdot P(u_{i2} > V),$$

Here, $P(u_{i1} < V)$ is the probability that the phase velocity u_{i1} on one end of the interval is less than the given value of the wave phase velocity, V, as follows: $P(u_{i1} < V) = \int_0^{\omega_p(V)} f_{\omega_p}(\omega_p)d\omega_p$. In a similar manner, $P(u_{i2} > V)$ is the probability that on the other end of the subinterval the phase velocity u_{i2} is larger than V, and can be calculated as follows: $P(u_{i2} > V) = \int_{\omega_p(V)}^{\infty} f_{\omega_p}(\omega_p)d\omega_p$. We consider that a change in phase velocity on an interval caused by the inhomogeneity is much less than its magnitude $\Delta V(\Delta n)/V \ll 1$. After normalizing $P_\omega(V)$ to 1, $P_\omega(V)dV$ can be interpreted as the ratio of a number of subintervals a on the characteristic scale $L_c \gg L$ to the total number of subintervals where a wave with constant frequency ω has a phase velocity V.

Another important effect to be taken into account is the probability that a wave can be reflected from a region where the plasma frequency becomes equal to the wave frequency. The result can occur one or many times. For the sake of simplicity we calculate the total probability that the wave is reflected, including all multiple possible reflections. In terms of the probability, the probability of the single reflection can

be written as follows: $P_r(\omega) = \int_{\omega}^{\infty} f_{\omega_p}(\omega_p) d\omega_p$. The generated wave maintains its initial direction if there are no reflections at all, or if the reflections compensate for one another. In the limit $L_c/a \to \infty$ the total probability that the wave keeps its initial direction after multiple reflections can be estimated as follows: $P_{ret}(\omega) = 1 - P_r(\omega) + P_r^2(\omega)(1 - P_r(\omega)) + P_r^4(\omega)(1 - P_r(\omega)) + ... = 1/(1 + P_r(\omega))$. The probability that the wave moves in the opposite direction is $P_{opp}(\omega) = P_r(\omega)/(1 + P_r(\omega))$.

To derive a complete description in terms of the probability distributions, an assumption should be made regarding the statistics of the density fluctuations. For the sake of simplicity, hereafter, we use the Gaussian distribution for the magnitudes of plasma frequency at the ends of subintervals $f_{\omega_p}(\omega_p) = \exp -(\omega_p - \omega_{p0})^2/\Omega^2$, where ω_{p0} is the plasma frequency of the unperturbed plasma and Ω is the dispersion of the distribution. A ratio Ω/ω_{p0} can easily be rewritten as $(1/2)((\langle \delta n^2 \rangle)^{1/2}/N_0)$, where $(\langle \delta n^2 \rangle)^{1/2}$ is the dispersion of the density fluctuations. Obviously, the probability distribution function that corresponds to observed spectrum of density fluctuations [Celnikier et al., 1987, Kellogg and Horbury, 2005, Chen et al., 2012] is non-Gaussian. However, it seems to be reasonable to use Gaussian distribution as a first step approximation. A detailed study of effects related to a deviation from Gaussian statistic is beyond the scope of the present chapter. Here, it is worth mentioning, that rare, large-amplitude fluctuations (that correspond to non-Gaussian 'wings' of the distribution function) can be included into the proposed model, because spatial scale of subinterval is still small enough to ensure that Langmuir wave remain in resonance with a beam on subinterval. Figure 3.1 provides examples of $P_\omega(V)$ for a wave with a ratio of $\omega/k_0 = 7v_t$, where k_0 corresponds to the wave vector of the resonant Langmuir wave in a plasma without density fluctuations having an average density of N_0 for a various levels of density fluctuations.

An increase in the magnitudes of the density fluctuations results in a broadening of the probability distribution function in the velocity space. Density fluctuations with larger magnitudes should change the plasma frequency stronger, leading to larger variations of the wave vector and, hence, resulting in an increase in the dispersion of the phase velocity of the wave. In the case of $(\langle \delta n^2 \rangle)^{1/2}/N_0 \to 0$, the probability function $P_\omega(V)$ tends toward the Dirac delta function, corresponding to a homogeneous plasma where the wave can have only a fixed phase velocity, $V = \omega/k_0$.

3.8 The growth rate of the wave

To evaluate the effects of density fluctuations on the wave generation, we compare wave growth rates obtained in the framework of different approaches. In QL theory, the growth rate can be written as follows:

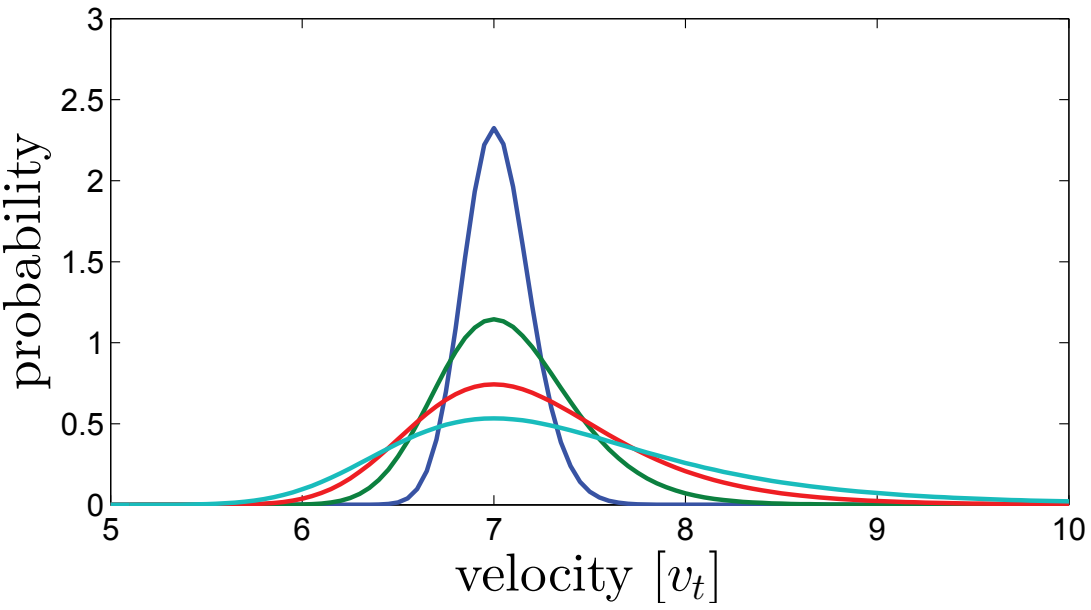

Figure 3.1: Examples of the probability distribution functions, $P_\omega(V)$, for the various fluctuation levels. $P_\omega(V)dV$ is the probability that a wave with a ratio of $\omega/k_0 = 7v_t$ will have a phase velocity V at a given interval. P_ω was normalized to 1 using: $\int_0^\infty P_\omega(V)dV = 1$. Colors correspond to various fluctuation levels, as follows: $(\langle\delta n^2\rangle)^{1/2}/N_0 = 0.005$, blue; $(\langle\delta n^2\rangle)^{1/2}/N_0 = 0.01$, green; $(\langle\delta n^2\rangle)^{1/2}/N_0 = 0.015$, red; $(\langle\delta n^2\rangle)^{1/2}/N_0 = 0.02$, cyan.

$$\gamma = \pi \frac{n_b}{N_0} \left(v^2 \frac{\partial f(v)}{\partial v} \right)_{v=\omega/k}. \tag{3.6}$$

QL theory considers only resonant interaction between waves and particles. As a result, waves grow in region of the phase space where $f(v)$ has a positive slope and decay in region where the derivative of the electron distribution function is negative.

Using the probability distribution function of the wave phase velocity, the averaged growth rate of a wave can be calculated as follows:

$$\langle\gamma(\omega_i)\rangle = \pi \frac{n_b}{N_0} \int_0^\infty V^2 \frac{\partial f}{\partial V} P_{\omega_i}(V) dV. \tag{3.7}$$

Averaging is used to account for the effects of density inhomogeneities in the plasma on wave evolution. In a homogeneous plasma, waves with a frequency, ω_i, will have a uniquely determined phase velocity, $V_i = \omega_i/k_i$ and $P_{\omega_i} = \delta(V - V_i)$, where δ is the Dirac delta function. Density fluctuations cause variations of k along the path of wave propagation. As a result, the phase velocity of a wave changes following changes in the plasma density. Waves can interact with different parts of the electron distribution function and the growth rate at some points in the velocity space can be negative (which is really damping), despite the fact that the slope of the distribution function

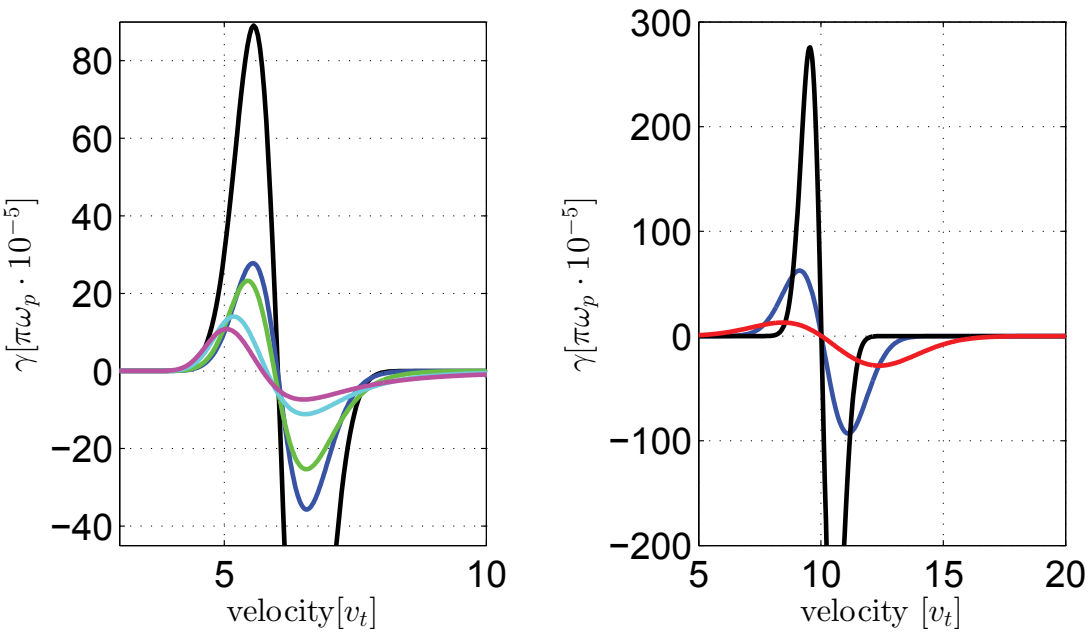

Figure 3.2: Left panel: Examples of the growth rate of waves for the various fluctuation levels. Different colors correspond to the different levels, as follows: $(\langle\delta n^2\rangle)^{1/2}/N_0 = 0.005$, blue; $(\langle\delta n^2\rangle)^{1/2}/N_0 = 0.01$, green; $(\langle\delta n^2\rangle)^{1/2}/N_0 = 0.02$, cyan; $(\langle\delta n^2\rangle)^{1/2}/N_0 = 0.04$, magenta. Black line corresponds to the growth rate obtained in the QL approximation for a case of a homogeneous plasma. The driven beam has a Gaussian velocity distribution with $v_b = 6v_t$ and $\Delta v_b = 0.5v_t$. Right panel: The growth rate of waves in the QL approximation obtained for the different thermal velocities of the beam. The black line corresponds to $\Delta v_b = 0.5v_t$, the blue line to $\Delta v_b = 1v_t$, the red line to $\Delta v_b = 2v_t$. For all cases $v_b = 10v_t$. All results are provided for a ratio of $n_b/N_0 = 10^{-5}$.

is positive.

In our simulations, we use a set of 2000 waves with uniformly distributed phase velocities, V_i, in the range from $3v_t$ to $40v_t$, in order to construct $\langle\gamma(\omega_i)\rangle$ as a function of the wave frequency. The left panel of Figure 3.2 provides examples of $\langle\gamma(\omega_i)\rangle$ for various levels of the density fluctuations, obtained by making use equation (3.7). The black curve corresponds to the wave growth rate obtained from the QL approximation using equation (3.6). To this end, we use a Gaussian distribution with beam velocity $v_b = 6v_t$ and beam thermal velocity $\Delta v_b = 0.5v_t$ as the initial velocity distribution function for beam electrons.

An increase in the level of density fluctuations, $(\langle\delta n^2\rangle)^{1/2}/N_0$, leads to a decrease in the maximum wave growth rate. Even fluctuations with a small amplitude, $\left(\langle\delta n^2\rangle\right)^{1/2} = 0.005N_0$, (blue curve in Figure 3.2) result in a substantial reduction in $\langle\gamma(\omega_i)\rangle$. Thus, one should expect that the characteristic time of the growth of a wave significantly increases in a plasma with random density fluctuations. Another notable effect is a shift in the maximum growth rate in the velocity space toward lower phase velocities.

The shift is accompanied by a decrease of the region where the growth rate is positive. As a result, an increase in the level of density fluctuations reduces the volume of the velocity space where waves could grow efficiently.

Another important parameter that causes a change in the growth rate is the beam thermal dispersion, Δv_b, or the width of the electron velocity distribution function. The right panel of Figure 3.2 provides the examples of γ obtained from the QL approximation for beams with the same v_b for different values of the thermal dispersion, Δv_b. As expected, an increase in the thermal dispersion of the beam results in a decrease in the maximum growth rate. From equation (3.6), for the case of a Gaussian distribution of electrons, the simple relationship between γ and Δv_b could be determined. The well-known relationship for kinetic beams, $\gamma \sim (v_b/\Delta v_b)^2$, remains valid for our case. Here, it is worth noting, that a change in the thermal dispersion of a beam does not lead to a change in the region of the velocity space where waves can grow.

To evaluate, which quantity, $\Delta v_b/v_b$ or $(\langle \delta n^2 \rangle)^{1/2}/N_0$, is more important for the process of the generation, we calculated growth rate of the waves for different values of $\Delta v_b/v_b$ and $(\langle \delta n^2 \rangle)^{1/2}/N_0$. Results shown at left panel of Figure 3.3 was obtained for a beam with beam velocity $v_b = 6v_t$ and different Δv_b (shown with various colors). For most of cases, the ratio $\Delta v_b/v_b$ is larger than $(\langle \delta n^2 \rangle)^{1/2}/N_0$, except the case of $\Delta v_b = 0.5v_t$ (shown with black color). As one can see, for this cases, an increase in the level of the density fluctuation does not change the growth rate significantly. From the other hand, an increase in Δv_b result in substantial decrease in γ. Thus, one may conclude, that for the slow and wide beams, presence of the density fluctuations has no substantival influence on the generation of the Langmuir wave.

Middle panel of Figure 3.3 shows results for a beam with beam velocity $v_b = 12v_t$. As previously, an increase in $(\langle \delta n^2 \rangle)^{1/2}/N_0$ results in decrease of wave growth rate. As one can notice, for the cases of $\Delta v_b/v_b \leq (\langle \delta n^2 \rangle)^{1/2}/N_0$ an increase in Δv_b leads to increase in γ. For instance, starting with $(\langle \delta n^2 \rangle)^{1/2}/N_0 > 0.2$, beam with $\Delta v_b = 2v_t$ (blue line) has maximum in γ larger than beams with $\Delta v_b = 0.5v_t$ and $\Delta v_b = v_t$ (shown with black and red colors respectively). Thus, the thermal dispersion of the beam, reduces efficiency of the effects related to the density fluctuations.

Right panel of Figure 3.3 provides results for a beam with $v_b = 16v_t$. It is clearly seen that there is no significant difference in a waves growth rates, that correspond to different Δv_b. At the same time, changes in $(\langle \delta n^2 \rangle)^{1/2}/N_0$, result in substantial reduce of γ. For instance, an increase of the level of density fluctuations from 1% to 2%, reduces the maximum of the growth rate more than in 10 times. For the fast beams, with beam velocities higher that $15v_t$, the process of growth and decay of the Langmuir waves is completely determined by the density fluctuations.

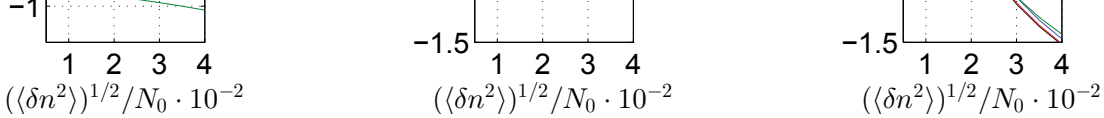

Figure 3.3: Logarithm of the maximum in the averaged growth rate as a function of the level of density fluctuations. The driven beam has a Gaussian velocity distribution with different beam velocities: $v_b = 6v_b$, left panel; $v_b = 12v_b$, middle panel; $v_b = 16v_b$, right panel. Colors correspond to the various thermal velocities of the beam, as follows: $\Delta v_b = 0.5v_t$, black; $\Delta v_b = v_t$, red; $\Delta v_b = 2v_t$, blue; $\Delta v_b = 4v_t$, green.

3.9 Relaxation of the electron beam in the plasma with density fluctuations

To consider the interaction of the beam with several monochromatic waves with energy densities, W_i, and frequencies ω_i the contributions from each wave in Equation (3.4) should be summed. For this case, the system of equations can be written, as follows:

$$\frac{\partial f}{\partial t} = \frac{\partial}{\partial v} v \sum_{i=1}^{K} W_i P_{\omega i}(v) \frac{\partial f}{\partial v}, \tag{3.8}$$

and

$$\frac{dW_i}{dt} = \int_0^\infty W_i V^2 \frac{\partial f}{\partial V} P_{\omega_i}(V) dV. \tag{3.9}$$

To better adapt equations (3.8) and (3.9) for the numerical simulations it is worth introducing the dimensionless variables, as follows: $\tilde{t} = (1/(\pi\omega_{p0}))(N_0/n_b)t$, $\tilde{v} = v_t v$, $\tilde{f} = f/v_t$, $\tilde{P}_\omega(V) = P_\omega(V)/v_t$, and $\tilde{W} = 2n_b m v_t^2 W$. We omitted the tildes to simplify form of the equations.

The system conserves the total energy, as follows:

$$\frac{d}{dt}\left(\frac{1}{2}\int_0^\infty v^2 f(v) dv + \sum_{i=1}^{K} W_i\right) = 0. \tag{3.10}$$

The first term in equation (3.10) corresponds to the electron energy. The second term corresponds to the total energy of the waves (for details see Appendix A.3).

For this study we performed numerical simulations of the system using equations (3.8) and (3.9) and present results in the next section. We used a set of $1:2000$ waves, with ω/k_0 uniformly distributed in the range from $2v_t$ to $38v_t$. To solve the system we applied a Leapfrog method. We used Simpson's rule in order to obtain the integration in equation (3.9).

Results of the numerical simulation for $(\langle\delta n^2\rangle)^{1/2}/N_0 = 0.02$ are presented in Figure 3.4. We use Gaussian distribution by employing the beam velocity $v_b = 10v_t$ and the dispersion $\Delta v_b = 0.5v_t$ as the initial condition for the electron distribution function. The case presented corresponds to the condition $(1/2)((\langle\delta n^2\rangle)^{1/2}/N_0) = v_t^2/v_b^2$, when density fluctuations play a significant role in the relaxation process. As can be seen, beam relaxation results in plateau formation in the velocity range of $v < v_b$, as for a homogeneous plasma. One can expect such a result, since for Langmuir waves with large k vector (and correspondingly small phase velocity) that satisfy condition $v_t^2/V^2 \gg (1/2)((\langle\delta n^2\rangle)^{1/2}/N_0)$ the influence of the density fluctuations on beam relaxation is negligible. However, the number of particles with velocities $v > v_b$ grows during the relaxation process. The energy transfer to energetic particles is possible because fluctuations of plasma density change the wave phase velocity and the resonant condition for wave-particle interactions. Thus, a wave generated with a phase velocity of V_0 can be reabsorbed by electrons with velocities $v_e > V_0$ and even $v_e \gg V_0$. The reabsorption of generated waves also leads to an increase in the relaxation time.

Figure 3.5 provides the initial electron distribution function, $f_{in}(v)$, and the distribution function, $f_{end}(v)$, at the end of the relaxation process. To consider the influence of density fluctuations on the acceleration of particles, we selected particles with velocities larger than $v_b + 3\Delta v_b$. Thus, the number of accelerated electrons was determined as a difference between the integrals $\int_{v_b+3\Delta v_b}^{\infty} f_{end}(v)dv$ and $\int_{v_b+3\Delta v_b}^{\infty} f_{in}(v)dv$. In a similar manner, the energy of the accelerated particles can be found from $\frac{1}{2}[\int_{v_b+3\Delta v_b}^{\infty} v^2 f_{end}(v)dv - \int_{v_b+3\Delta v_b}^{\infty} v^2 f_{in}(v)dv]$.

The left panel of Figure 3.6 provides the ratio for the energy of accelerated particles, E_a, to the initial energy of the beam, E_{b0}, for beams with different beam velocities and different levels of density fluctuations. The right panel of the Figure 3.6 provides the relative numbers, n_a/n_b, of accelerated electrons. For instance, for the beam velocity $v_b = 6v_t$ and density fluctuation level 0.005, the energy of accelerated particles is less than 0.1% from the initial energy of the beam. For the same level of fluctuations but for a beam with $v_b = 12v_t$ the ratio of the energy of accelerated particles increases to 29%. An increase in the beam velocity leads to an inequality $(1/2)((\langle\delta n^2\rangle)^{1/2}/N_0) \gg v_t^2/v_b^2$ and, thus, results in a more effective acceleration of the particles. Similar results can be obtained by increasing the level of the density fluctuations. For instance, for a beam with $v_b = 8v_t$ the number of accelerated particles for $(\langle\delta n^2\rangle)^{1/2}/N_0 = 0.01$ is $7\%n_b$, and $30\%n_b$ for a case with $(\langle\delta n^2\rangle)^{1/2}/N_0 = 0.035$. Therefore, all cases can be separated

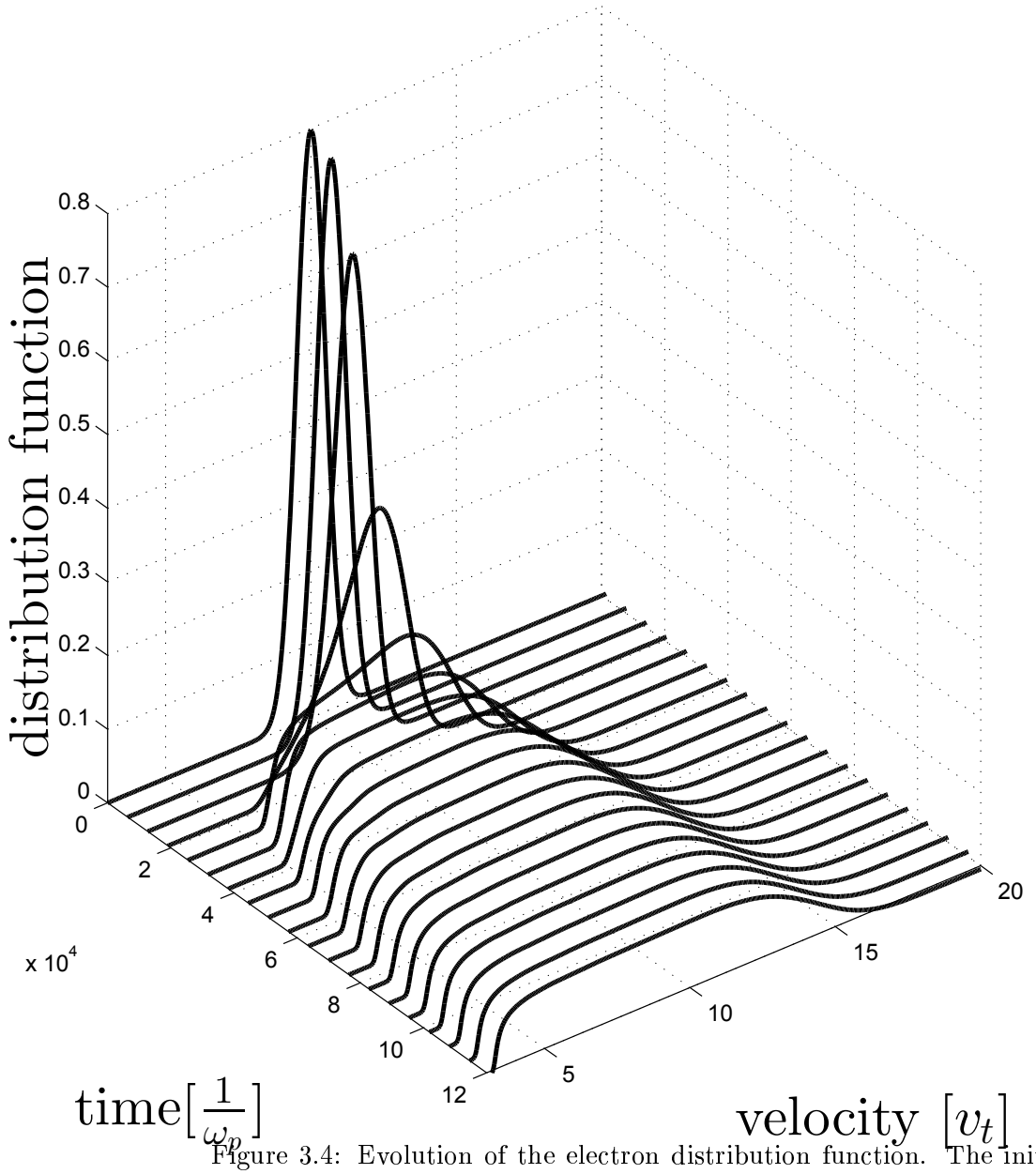

Figure 3.4: Evolution of the electron distribution function. The initial condition for beam electrons is the Gaussian distribution with a beam velocity of $v_b = 10v_t$ and a velocity dispersion of $\Delta v_b = 0.5v_t$. The core distribution, that corresponds to the cold electrons, has not been considered. The dimensionless electron distribution function was normalized to 1. Axes: velocities normalized to the thermal velocity of the background plasma v_t; the time normalized to the backward plasma frequency $(1/\omega_p)$. The beam density $n_b/N_0 = 2.5 \times 10^{-5}$. The level of fluctuations is $(\langle \delta n^2 \rangle)^{1/2}/N_0 = 0.02$ [from Voshchepynets et al., 2015].

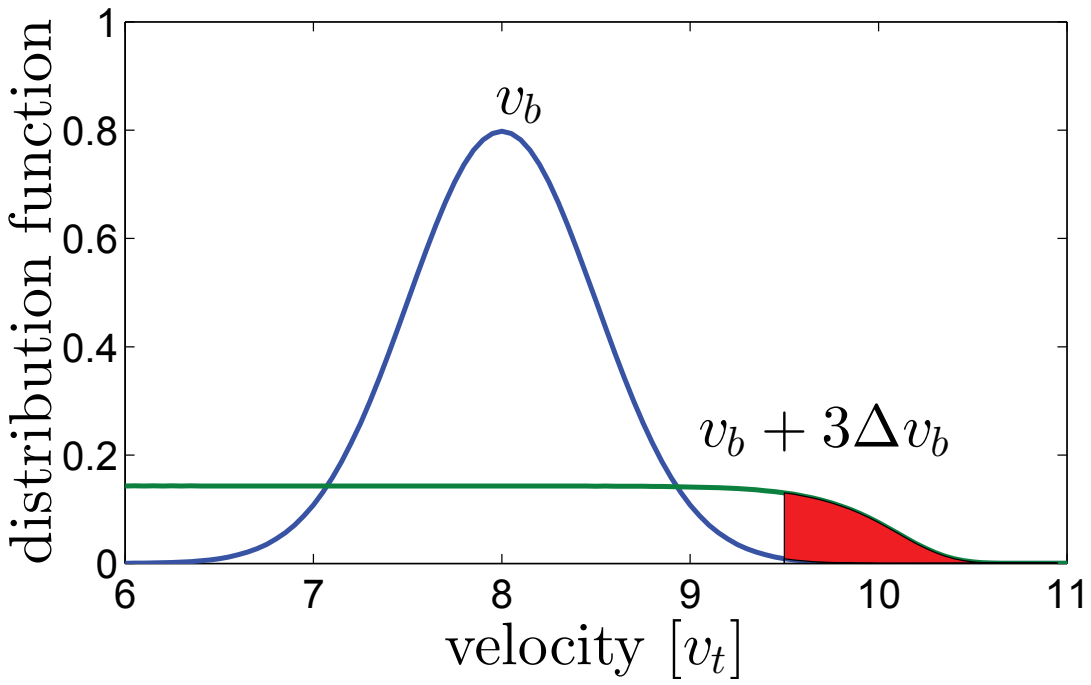

Figure 3.5: The electron distribution function at the beginning of relaxation (blue line) and at the end (green line). The level of fluctuation is 1%. The beam velocity $v_b = 8v_t$, and the thermal velocity of the beam is $0.5v_t$; $n_b/N_0 = 2.5 \times 10^{-5}$. The filled area corresponds to accelerated particles [from Voshchepynets et al., 2015].

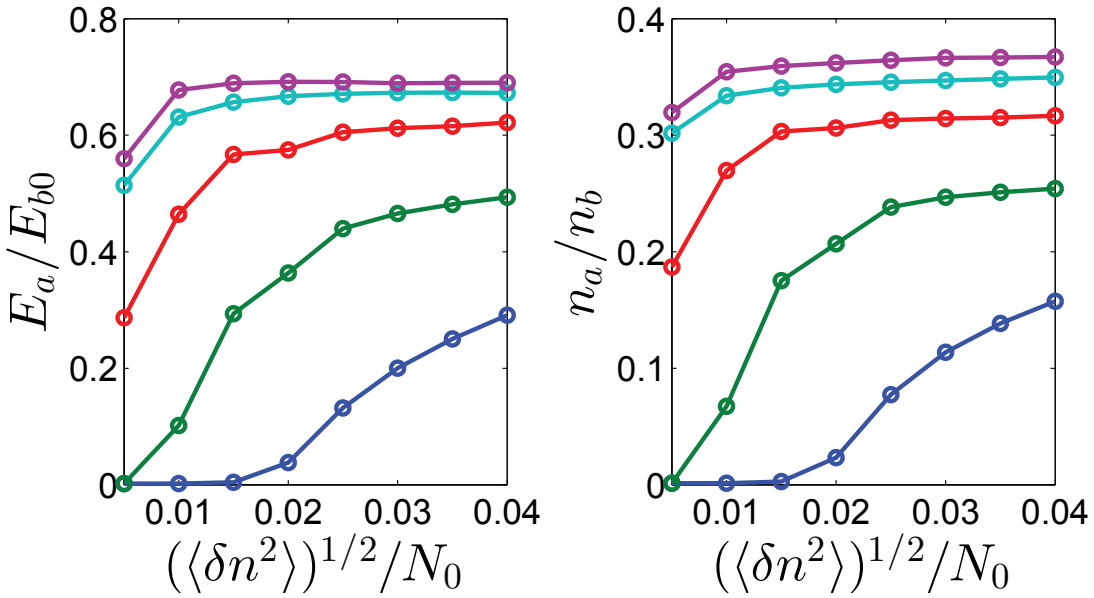

Figure 3.6: The energy, E_a, (left panel) and the number, n_a, (right panel) of accelerated particles as a function of the density fluctuation level. E_{b0} and n_b are the initial energy of the beam and the density of the beam electrons. Colors correspond to the various velocities of the beam, as follows: $v_b = 6v_t$, blue; $v_b = 8v_t$, green; $v_b = 12v_t$, red; $v_b = 16v_t$, cyan; and $v_b = 20v_t$, magenta. The thermal velocity of all beams $\Delta v_b = 0.5v_t$ [from Voshchepynets et al., 2015].

into the following three classes: (1) $(1/2)((\langle\delta n^2\rangle)^{1/2}/N_0) \ll v_t^2/v_b^2$- corresponding to homogeneous plasma, fluctuations too small to influence the relaxation process; (2) $(1/2)((\langle\delta n^2\rangle)^{1/2}/N_0) \sim v_t^2/v_b^2$- an intermediate regime, characterized by a presence but containing a small quantity of accelerated particles; and (3) $((1/2)((\langle\delta n^2\rangle)^{1/2}/N_0) \gg v_t^2/v_b^2$- fluctuations resulting in an effective energy transfer to both cold and energetic particles where the energy of the accelerated electrons can reach up to 70% of the initial beam energy. Both quantities, n_a/n_b and E_a/E_{b0}, manifest the same tendency with increasing fluctuation levels. For cases of the third class a simple relationship can be determined, as follows: $n_a/n_b, E_a/E_{b0} \sim \sqrt{(\langle\delta n^2\rangle)^{1/2}/N_0}$.

Figure 3.7 provides the evolution of the total energy of waves for the case of $v_b = 8v_t$ and various fluctuation levels. The blue line corresponds to $(\langle\delta n^2\rangle)^{1/2}/N_0 = 0.005$ and for this case we have $(1/2)(\langle\delta n^2\rangle)^{1/2}/N_0 \ll v_t^2/v_b^2$. As for a homogeneous plasma, the energy of the waves grows in time until a plateau formation is obtained. An increase in the level of density fluctuations results in larger dispersion of the phase velocities, and makes the absorbtion of generated waves more effective. Such can be seen in the case of $(\langle\delta n^2\rangle)^{1/2}/N_0 = 0.04$ (the red line shown in Figure 3.7). Following a period of growth, waves begin to decay, corresponding to a phase of electron acceleration.

Ratios for the total energy of waves, E_w, to the initial beam energy as a function of the fluctuations are provided in the left panel of Figure 3.8. Colors correspond to the various beam velocities. As one can see, in the limit of a homogeneous plasma ($v_b = 6v_t$ and $(\langle\delta n^2\rangle)^{1/2}/N_0 = 0.005$) a ratio of 30% is in good agreement with QL approximation. An increase in the magnitude of the density fluctuations leads to a decrease in the wave energy. For instance, for the same beam, but for a case of $(\langle\delta n^2\rangle)^{1/2}/N_0 = 0.04$, the ratio E_a/E_{b0} is two times less than for the previously mentioned case. For cases with $(1/2)((\langle\delta n^2\rangle)^{1/2}/N_0) \gg v_t^2/v_b^2$ (the right bottom portion of the plot) the energy of the waves is less than 10% of the initial beam energy. The results are consistent with values for energy transferred to beam accelerated particles, as estimated above. Thus, density fluctuations can result in an "inverse" energy flux. Energy can be transferred from "slow" electrons to "fast" electrons through the generation and absorption of Langmuir waves.

To estimate the characteristic time of wave energy growth, t_r, we consider the difference in time between the moment when the total wave energy reaches 1% of the initial energy of the beam and the another moment of time when the wave energy for different levels of fluctuations reaches some energy level the same for all simulation set that we choose to be equal to $min(E_{max}((\langle\delta n^2\rangle)^{1/2}))$. We define this $min(E_{max}((\langle\delta n^2\rangle)^{1/2}))$ as the smallest level of all of the maximum energies of waves achieved in the set of simulations with the same v_b and different levels of fluctuation (for instance, see the Figure 3.7). The right panel of Figure 3.8 displays t_r as a function of $(\langle\delta n^2\rangle)^{1/2}/N_0$ for different values of the beam velocity. As can be seen from the figure,

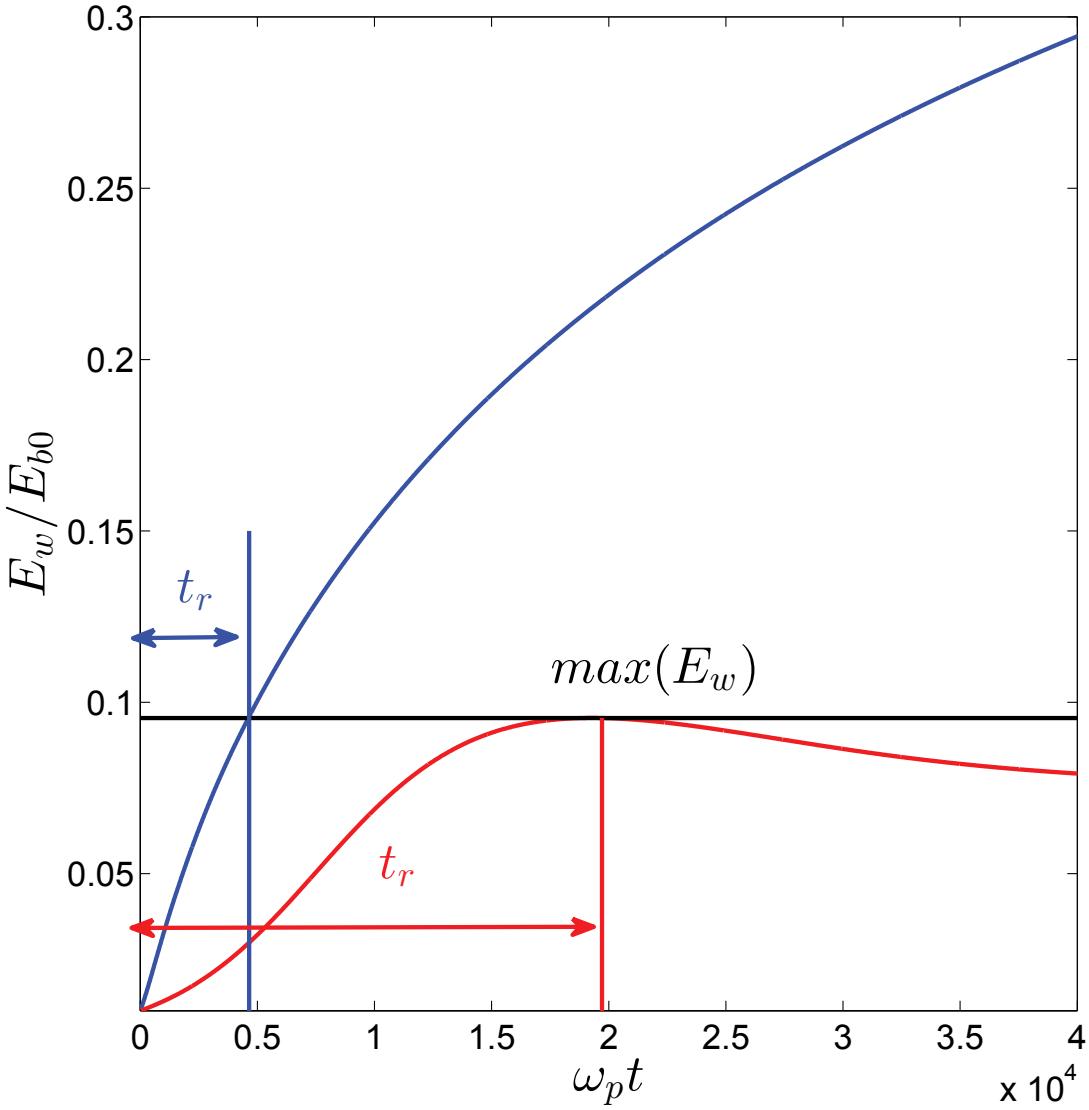

Figure 3.7: The evolution of the total energy of waves, E_w, for different levels of fluctuations ($(\langle \delta n^2 \rangle)^{1/2}/N_0 = 0.005$, the blue line; $(\langle \delta n^2 \rangle)^{1/2}/N_0 = 0.04$, the red line). The beam velocity $v_b = 8v_t$; $\Delta v_b = 0.5v_t$; and $n_b/N_0 = 2.5 \times 10^{-5}$ [from Voshchepynets et al., 2015].

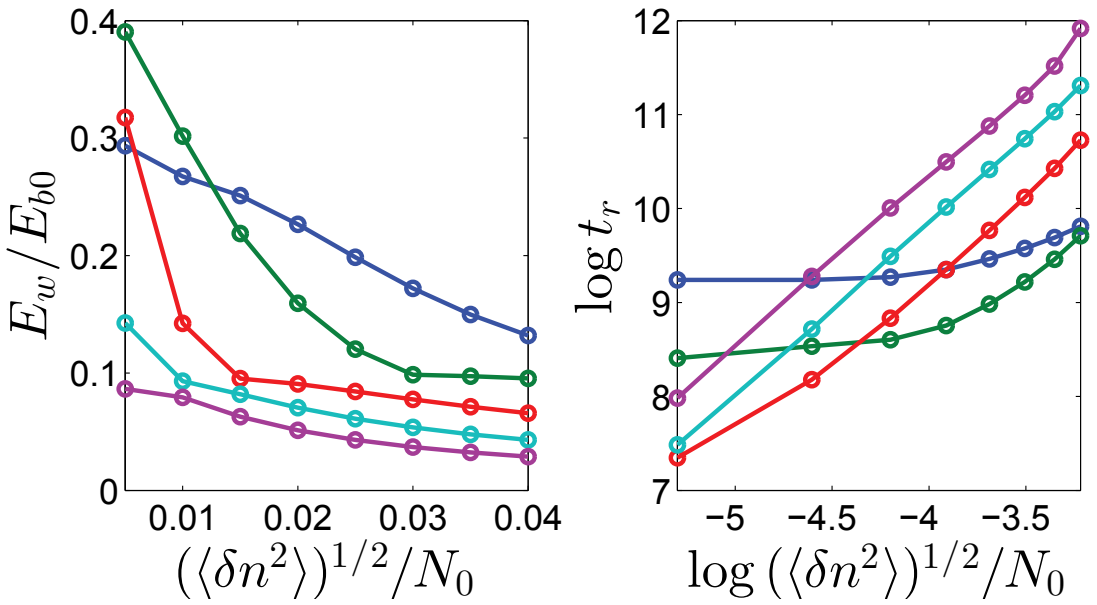

Figure 3.8: The maximum of the total energy of the waves, E_w, (left panel) reached in the relaxation process as a function of the density fluctuation level. E_{b0} is the initial energy of the beam. Different colors correspond to the different velocities of the beams (the same as in Figure 3.6). Right panel: The time of growth, t_r, normalized to $1/\omega_p$ as a function of $(\langle\delta n^2\rangle)^{1/2}/N_0$ on the log-log scale. Colors correspond to different v_b. The beam density $n_b/N_0 = 2.5 \times 10^{-5}$ [from Voshchepynets et al., 2015]

for cases with $(1/2)((\langle\delta n^2\rangle)^{1/2}/N_0) \leq v_t^2/v_b^2$ (the blue line in Figure 3.8), an increase in the fluctuation level results in a slight increase in the characteristic time of growth. However, for cases with $(1/2)((\langle\delta n^2\rangle)^{1/2}/N_0) \geq v_t^2/v_b^2$, t_r increases significantly with an increase in $(\langle\delta n^2\rangle)^{1/2}/N_0$. When fluctuations strongly affect the relaxation process $(1/2)(\langle\delta n\rangle/N_0) \gg v_t^2/v_b^2$ a simple approximation for t_r can be found, as follows: $t_r \sim ((\langle\delta n^2\rangle)^{1/2}/N_0)^2$.

All the results provided above were obtained for the same value of the velocity dispersion of the beam, $\Delta v_b/v_t = 0.5$. Now let us consider the role of the initial thermal velocity of the beam. The left panel of Figure 3.9 provides a ratio of the energy of accelerated particles to the initial energy of the beam for different initial beam velocities and different initial thermal velocities of the beam particles. The energy of the accelerated particles displays typical behavior- an increase in the density fluctuation level and/or the initial velocity of the beam resulting in an increase in the energy of accelerated particles. However, an increase in the initial thermal velocity of beam electrons leads to a decrease in E_a. For instance, for the case with $v_b = 10v_t$ and an initial thermal velocity of $\Delta v_b = 0.5v_t$ (the red solid line in Figure 3.9), the ratio E_a/E_{b0} at the end of the relaxation is equal to 58% for $\langle\delta n\rangle/N_0 = 0.04$. An increase in the beam thermal velocity to v_t results in a decrease of E_a/E_{b0} to 43% (the red dashed line in Figure 3.9). For a beam with the same v_b and for the thermal velocity, $\Delta v_b = 2v_t$,

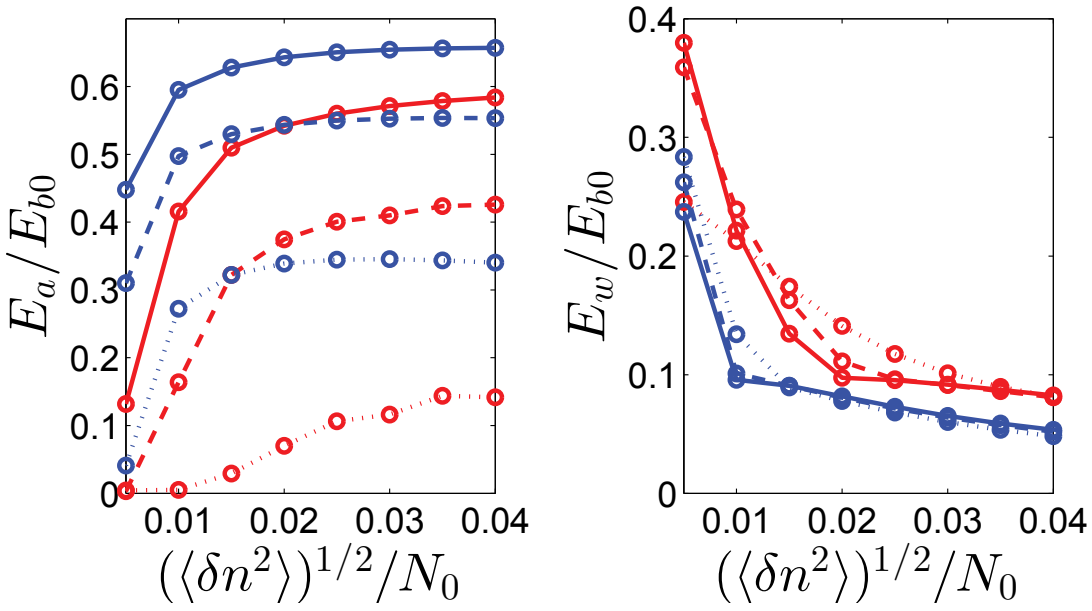

Figure 3.9: The energy of the accelerated particles, E_a, (left panel) and maximum of the total energy of the waves, E_w, (right panel) reached during relaxation as a function of the level of the density fluctuations. Colors correspond to the different initial velocities of the beam, as follows: red color, $v_b = 10v_t$; and blue color, $v_b = 14v_t$. Line styles correspond to the different initial thermal velocities of the beam, as follows: solid line, $\Delta v_b = 0.5v_t$; dashed line, $\Delta v_b = 1v_t$; and dotted line, $\Delta v_b = 2v_t$ [from Voshchepynets et al., 2015].

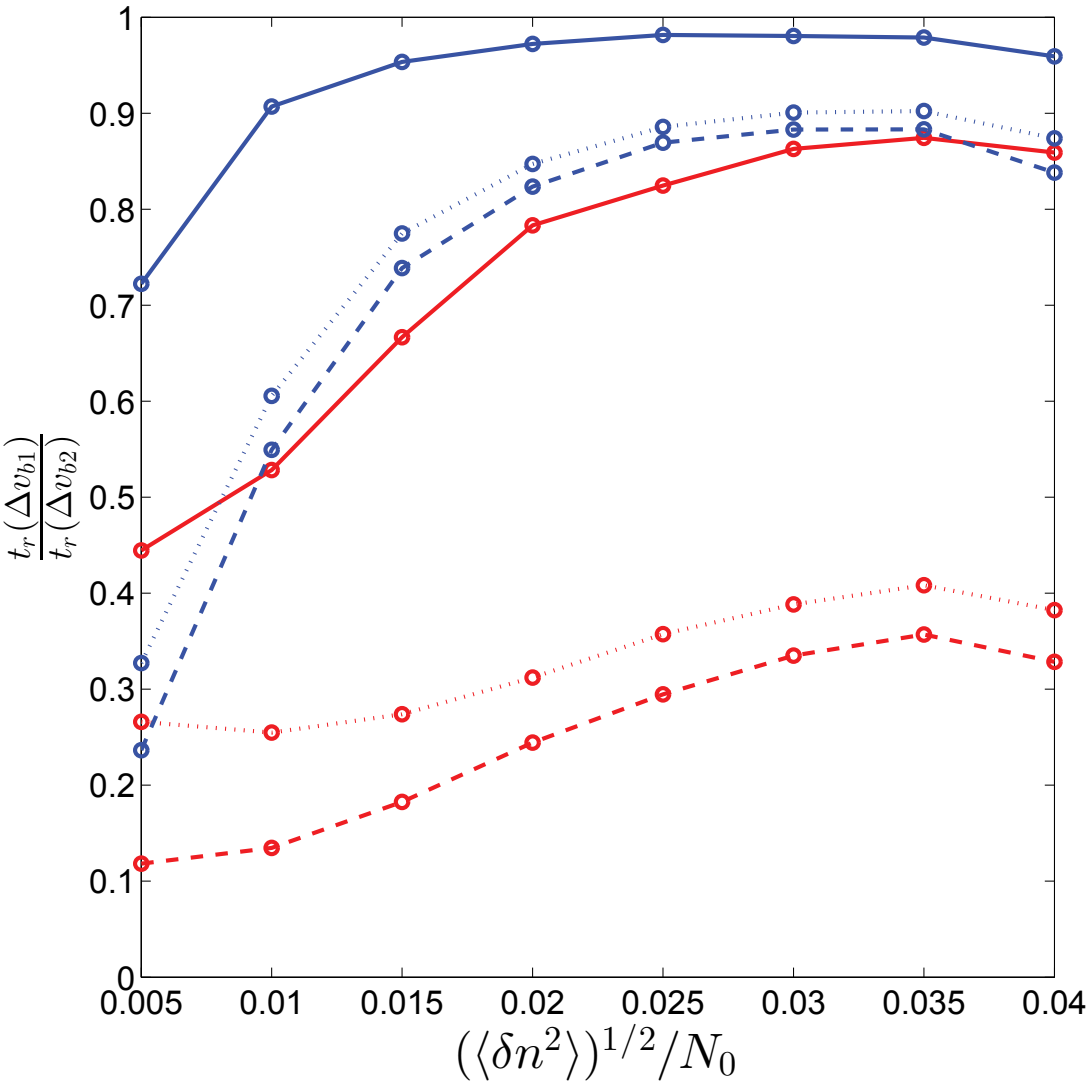

.

Figure 3.10: The ratio of times t_r for various thermal velocities of the beam as a function of the level of density fluctuations. Colors correspond to the various initial velocities of the beam, as follows: red color, $v_b = 10v_t$; and blue color, $v_b = 14v_t$. Line styles correspond to the various initial thermal velocities of the beam, as follows: solid line, $t_r(\Delta v_b = 0.5v_t)/t_r(\Delta v_b = 1v_t)$; dashed line, $t_r(\Delta v_b = 0.5v_t)/t_r(\Delta v_b = 2v_t)$; and dotted line, $t_r(\Delta v_b = 1v_t)/t_r(\Delta v_b = 2v_t)$ [from Voshchepynets et al., 2015].

the energy of accelerated particles decreases to a value of only 15% from the initial energy of the beam (the red dotted line in Figure 3.9). The result is expected, since we defined the accelerated particles as particles with velocities larger than $v_b + 3\Delta v_b$. According to this definition, for beams with $v_b = 14v_t$ and $\Delta v_b = 0.5v_t$, only particles with velocities larger $15.5v_t$ may be considered as accelerated. At the same time, for a case with $v_b = 14v_t$ and $\Delta v_b = 2v_t$, electrons considered as accelerated should have velocities larger than $20v_t$. For both cases, the energy of particles with velocities larger than $18v_t$ differs slightly.

The right panel of Figure 3.9 provides the maximum for total wave energy reached during the relaxation process as a function of the level of density fluctuations for beams with a different initial v_b and a different thermal velocity, Δv_b. The growth rate of waves depends on the derivative of the distribution function. Thus, a change in the initial thermal velocity of the beam should cause changes in the region of the phase space where waves can grow effectively. On the other hand, the presence of density fluctuations results in a broadening of the resonant conditions of the wave-particle interactions and a modification of the region where waves can be generated. As a result, two parameters that determine the efficiency of wave growth during relaxation (for the same initial velocity of the beam) are provided. The red lines in Figure 3.9 correspond to relaxation of a beam with $v_b = 10v_t$. As can be seen, while $(1/2)((\langle \delta n^2 \rangle)^{1/2}/N_0) \leq v_t^2/v_b^2$ ($(\langle \delta n^2 \rangle)^{1/2}/N_0 \leq 0.025$ for the present beam), changes in the initial thermal velocity of the beam lead to significant changes in the rate of wave generation. For instance, for a beam with $\Delta v_b = 2v_t$ (the red dotted line in Figure 3.9) and $(\langle \delta n^2 \rangle)^{1/2}/N_0 = 0.02$, the maximum for total wave energy is equal to 15% of the initial energy of the beam. A decrease of Δv_b to $0.5v_t$ results in a decrease in E_w to 10%. However, an increase in the density fluctuation level reduces the role of the initial thermal dispersion of the beam. For a beam with $v_b = 14v_t$ (the blue lines in Figure 3.9), beginning with level of density fluctuation equal to 0.015, there is no significant difference in the E_w for cases with a different initial Δv_b. Thus, for fluctuation levels corresponding to condition $(1/2)((\langle \delta n^2 \rangle)^{1/2}/N_0) \gg v_t^2/v_b^2$, resonance broadening plays a major role in the process of wave generation.

In a homogeneous plasma, the time of wave growth can be written in the following form:

$$t_r = \frac{W_{end}}{W_{init}} \frac{1}{\omega_{p0}} \frac{N_0}{n_b} \frac{\Delta v_b^2}{v_b^2},$$

where W_{end} and W_{init} are the energies of the waves at the end and beginning, respectively, of the relaxation process. One can note that an increase in the initial thermal velocity of the beam should lead to an increase in the time of growth. For two beams with thermal velocities Δv_{b1} and Δv_{b2} and the same v_b, the ratio of t_{r1} and t_{r2} is, as

follows:

$$\frac{t_{r1}}{t_{r2}} = \left(\frac{\Delta v_{b1}}{\Delta v_{b2}}\right)^2.$$

Figure 3.10 provides the ratio of the times of wave growth for beams with different v_b and Δv_b as a function of the level of density fluctuations. As can be seen, when the level of fluctuations is high enough, $((1/2)((\langle \delta n^2 \rangle)^{1/2}/N_0) \gg v_t^2/v_b^2)$, the change in the initial velocity of the beam does not strongly affect the time of wave growth.

3.10 Conclusions

Here, we propose a statistical model that describes the relaxation of an electron beam in a plasma with relatively small scale ($10^2\lambda_D$-$10^5\lambda_D$) density fluctuations. Using the model, we describe the evolution of the electron distribution function and the energy of Langmuir waves. The suggested $1D$ numerical scheme is applicable for physical parameters of the solar wind plasma at different distances from the Sun (e.g. ~ 1 AU). Thus, we can use our computations to describe Type III solar bursts, as well as beam plasma interactions, within the vicinity of the heliosphere and planetary shocks.

Using the model, computations require much less computer resources than PIC simulations or the Zakharov technique. However, the proposed numerical scheme is $1D$ and, thus, the effects of the angular diffusion of Langmuir waves on density fluctuations were ignored. At this stage the model does not include the effects of collision losses, ion-sound waves, and the generation of electromagnetic emissions. For this reason, the system conserves the total energy that can be transferred from the beam to waves and backward during the relaxation process. The relationships between energy or the number of accelerated particles and the levels of the density fluctuations, $n_a/n_b, E_a/E_{b0} \sim \sqrt{(\langle \delta n^2 \rangle)^{1/2}/N_0}$, are quite simple for cases with $(1/2)((\langle \delta n^2 \rangle)^{1/2}/N_0) \gg v_t^2/v_b^2$. The goal of the present work is to show the importance of small scale density fluctuations and to propose a self-consistent and closed description of the beam relaxation process.

In the study, numerical simulations indicated that there are three key parameters that influence the relaxation process- the ratio of the initial beam velocity v_b to the thermal velocity v_t of a background plasma, the level of the density fluctuations $(\langle \delta n^2 \rangle)^{1/2}/N_0$, and width of the beam in velocity space. Depending on the values of v_b^2/v_t^2 and $(\langle \delta n^2 \rangle)^{1/2}/N_0$ three different scenarios for the beam relaxation can be noticed.

1) $(1/2)((\langle \delta n^2 \rangle)^{1/2}/N_0) \ll v_t^2/v_b^2$- the wave excitation process is very similar to the one taking place in the homogeneous plasma. Relaxation results in plateau formation of the electron distribution function without a significant increase in the population of energetic particles. The total energy of waves at the end of the relaxation equals 30%.

2) $(1/2)((\langle \delta n^2 \rangle)^{1/2}/N_0) \sim v_t^2/v_b^2$- corresponds to the intermediate regime. Density fluctuations can affect the phase velocity of waves. Thus, reabsorption of a portion of the wave energy by energetic electrons occurs but the number of accelerated particles is still relatively low.

3) Under the condition $(1/2)((\langle \delta n^2 \rangle)^{1/2}/N_0) \gg v_t^2/v_b^2$ the process of beam relaxation is totally determined by the density fluctuations. The resonance broadening caused by density fluctuations allows the wave to interact with particles over a wide range of velocities. There is very efficient energy transfer from electrons with velocities of $v < v_b$ to higher energy electrons with $v > v_b$ via the generation and reabsorption of Langmuir waves. The case is characterized by a low level of total wave energy at the end of the relaxation process. In contrast, the energy of accelerated electrons can reach up to 70% of the initial energy of the beam for cases of a small initial spread for a beam in the velocity space. However, as in a homogeneous plasma, relaxation runs mainly toward low velocities and finishes with the formation of a plateau.

An increase in the density fluctuation level results in an increase in the time characterizing wave energy growth, t_r. The average growth rate of the waves, γ, and the diffusion coefficient, D, strongly depend on the magnitude of the fluctuations. High amplitude fluctuations can strongly impact the resonant condition of the wave-particle interaction that leads to broadening of the resonance in the phase space and the wave damping. This, in turn, significantly slows down the relaxation. In the case of the Gaussian distribution for the fluctuation magnitudes and for high level of density fluctuations, a simple relationship between t_r and $(\langle \delta n^2 \rangle)^{1/2}$ was found, as follows: $t_r((\langle \delta n^2 \rangle)^{1/2}) \sim \langle \delta n^2 \rangle$.

3.11 Resume in French

Dans ce chapitre, nous présentons un modèle récemment publié décrivant l'interaction d'un faisceau avec un plasma renferme des inhomogénéités aléatoires. Nous remplaçons l'intervalle spatial continu par un intervalle de grande longueur, fini et discret, et nous le séparons en un ensemble de sous-intervalles de tailles égales et d'échelle a. Cette discrétisation permet d'appliquer de façon plus simple une approche probabiliste. L'échelle, a, est supposée être beaucoup plus petite que l'échelle caractéristique de variation de la fonction de distribution électronique, L_c, et suffisamment plus grande que la longueur d'onde de l'onde de Langmuir générée par le faisceau. Nous considérons l'interaction d'une onde cohérente de petite amplitude avec une particule qui traverse cet intervalle en supposant que le profil de la densité est linéaire sur cet intervalle. Nos hypothèses permettent de décrire l'action du champ d'une onde ayant une fréquence connue sur une particule en utilisant le degré de précision nécessaire pour évaluer l'effet de l'interaction des particules avec une onde sur un intervalle particulier avec des densités fixées aux extrémités.

Le point-clé de notre description est que, sur chaque intervalle, nous supposons que les valeurs de la densité au centre de l'intervalle sont aléatoires et indépendantes, et elles sont décrites par une distribution statistique connue. Le profil de la densité est continu. La distribution peut être choisie soit de façon à correspondre à des observations réelles, soit choisie comme une distribution artificielle de façon à faire des calculs simplifiés. Ainsi, la distribution statistique des vitesses de phase des ondes peut être obtenue quelque soit la fréquence. Cette probabilité permet d'effectuer des calculs de caractéristiques moyennes, tels que l'échange d'énergie entre les particules à une vitesse donnée et l'onde à une fréquence donnée. En faisant le calcul du mouvement des particules sous l'action d'une onde choisie, nous considérons que la phase d'onde est déterminée au départ. Ensuite, nous évaluons la moyenne statistique en supposant que les phases sont aléatoires et uniformément répartie dans l'intervalle entre 0 et 2π. Nous supposons également que l'interaction des particules avec une onde à chaque intervalle est indépendante des interactions des particules avec l'onde aux intervalles précédents.

En utilisant ces hypothèses, nous calculons la probabilité qu'une particule ayant au temps initial t_0 une vitesse v_0 aura une vitesse v après Q interactions qui se produisent pendant un intervalle de temps $(t-t_0)$. Le nombre d'étapes d'interactions, Q, doit être suffisamment grand pour justifier la statistique et la procédure de calcul de moyenne. L'hypothèse que des interactions sont aléatoires et indépendantes correspond à un processus Marcovian non corrélé. Ceci permet d'aboutir à une description de l'évolution de la fonction de distribution des particules basées sur une équation de diffusion similaire à l'équation de Fokker-Planck dans l'espace des vitesses. Dans le cadre de ces hypothèses, le coefficient de diffusion déterminé de cette façon dépend de la distribution de probabilité des fluctuations de la densité. Pour calculer le taux de croissance d'une onde, on utilise le fait que sur un petit intervalle le gain/perte d'énergie par la particule est égal au gain/perte d'énergie par l'onde. La conservation locale de l'énergie se produit sur de petits intervalles et permet de calculer un changement d'énergie moyenne de la densité d'énergie des ondes.

En utilisant notre modèle, nous décrivons l'évolution de la fonction de distribution des électrons et d'énergie des ondes de Langmuir. Le schéma 1D suggérée est applicable pour des paramètres physiques de plasma du vent solaire à différentes distances du Soleil (par exemple à $\sim$ 1 AU). Ainsi, nous pouvons utiliser nos calculs pour décrire des émissions solaires de Type III, ainsi que les interactions de faisceau avec le plasma, à des distances d'une Unité Astronomique du Soleil dans l'héliosphère et au voisinage des chocs planétaires.

En utilisant ce modèle, les calculs nécessitent des ressources informatiques beaucoup plus faibles que des simulations avec des codes PIC ou la technique de Zakharov. Toutefois, dans le cadre du schéma numérique 1D proposé, les effets de la diffusion angulaire des ondes de Langmuir sur les fluctuations de la densité ont été ignorés. À

cette étape le modèle n'inclut pas non plus les effets des pertes dues aux collisions, les ondes ioniques et la génération d'émissions électromagnétiques. Pour cette raison, le système conserve l'énergie totale qui peut être transférée du faisceau aux ondes, ainsi qu'aux particules plus rapides pendant le processus de relaxation. Les relations entre la quantité d'énergie transférée aux particules énergétiques, ou le nombre de particules accélérées, et le niveau des fluctuations de densité, $n_a/n_b, E_a/E_{b0} \sim \sqrt{(\langle \delta n^2 \rangle)^{1/2}/N_0}$, sont assez simples pour les cas où $(1/2)((\langle \delta n^2 \rangle)^{1/2}/N_0) \gg v_t^2/v_b^2$. Le but de ce travail est de montrer le rôle et l'importance des fluctuations de densité de petites échelles et de proposer une description auto-consistante du processus de relaxation du faisceau.

Dans notre étude, des simulations numériques ont démontré qu'il existe trois paramètres clés qui déterminent les caractéristiques de processus de relaxation: 1)v_t^2/v_b^2, où v_b est la vitesse initiale du faisceau, et v_t la vitesse thermique de plasma thermique; 2) le niveau des fluctuations de densité $(\langle \delta n^2 \rangle)^{1/2}/N_0$; 3) la dispersion de vitesses des particules du faisceau dans l'espace des vitesse Δv_b. En fonction de rapport entre les valeurs de v_b^2/v_t^2 et $(\langle \delta n^2 \rangle)^{1/2}/N_0$ trois scénarios diffésrents peuvent être réalisés pour le processus de relaxation du faisceau.

1) $(1/2)((\langle \delta n^2 \rangle)^{1/2}/N_0) \ll v_t^2/v_b^2$ - le processus d'excitation d'onde est très semblable à celui qui a lieu dans un plasma homogène. La relaxation résulte de l'évolution de la fonction de distribution des électrons vers un plateau à des vitesses plus faibles que la vitesse de faisceau, sans une augmentation significative de la population de particules énergiques. L'énergie totale des ondes à la fin de la relaxation est égale à 30% de l'énergie initiale du faisceau.

2)$(1/2)((\langle \delta n^2 \rangle)^{1/2}/N_0) \sim v_t^2/v_b^2$- correspond au régime intermédiaire. Les fluctuations de densité peuvent affecter assez fortement les variations de la vitesse de phase des ondes. Ainsi, la réabsorption d'une partie de l'énergie des ondes par les électrons énergétiques se produit mais le nombre de particules accélérées est encore relativement faible.

3) Si la condition $(1/2)((\langle \delta n^2 \rangle)^{1/2}/N_0) \gg v_t^2/v_b^2$ est satisfaite le processus de relaxation est déterminé par les fluctuations de densité. Chaque onde interagit avec des particules distribuées dans un large domaine de l'espace de phases grâce à l'élargissement de la résonance dû aux fluctuations. La relaxation se developpe d'abord vers le domaine de vitesses plus petites que la vitesse de faisceau et elle s'arrête quand en espace de vitesse un plateau est formé. Cependant, un autre processus se developpe, notamment, une absorption d'énergie d'ondes par des électrons ayant des vitesses plus élevés $v > v_b$. En effet, ce dernier assure un transfert d'énergie d'électrons moins énergétiques vers des électrons plus énergétiques. L'énergie des électrons accélérés peut ainsi atteindre jusqu'à 70% de l'énergie initiale du faisceau pour les cas d'une faible dispersion de vitesses de faisceau Δv_b. Cependant, comme dans un plasma homogène, la relaxation se développe principalement vers des vitesses plus basses et elle s'arrête avec la formation

d'un plateau.

Une augmentation du niveau de fluctuations de densité aboutit à une augmentation du temps caractéristique d'une croissance d'énergie des ondes, t_r. Le taux de croissance moyen des ondes, γ, et le coefficient de diffusion, D, dépendent fortement de l'amplitude des fluctuations. Les fluctuations de grande amplitude peuvent fortement modifier la condition de résonance des interactions onde-particule. Ceci amène un élargissement de la résonance dans l'espace de phase et à l'atténuation de l'onde. Dans le cas d'une distribution Gaussienne des amplitudes de fluctuations et pour de forts niveaux de fluctuations de densité, une relation simple entre t_r et $(\langle \delta n^2 \rangle)^{1/2}$ a été trouvée: $t_r((\langle \delta n^2 \rangle)^{1/2}) \sim \langle \delta n^2 \rangle$.

Appendix A

Appendices

A.1 Equation for the Wave

Here, we begin with a consideration of the interaction of a single electron with a monochromatic wave. In a $1D$ case the equation of motion can be written as follows:

$$\frac{dv}{dt} = -\frac{eE}{m}\cos(kx - \omega t + \tilde{\phi}),$$

where v is the electron velocity, E is the wave amplitude, and $\tilde{\phi}$ is the initial phase of the wave.

Using perturbation theory for the velocity, $v = v_0 + v_1 + v_2$, where v_0 is the unperturbed velocity of the particle, one can write equations for the first two terms, as follows:

$$\frac{dv_1}{dt} = -\frac{eE}{m}\cos((kv_0 - \omega)t + \phi), \tag{A.1}$$

and

$$\frac{dv_2}{dt} = -\frac{eE}{m}[\cos((kv_0 - \omega)t + k\int_0^t v_1 dt + \phi) - \cos((kv_0 - \omega)t + \phi)],$$

where $\phi = \tilde{\phi} + kx_0$.

Taking into account that the $\cos(k\int_0^t v_1 dt) \approx 1$ and $\sin(k\int_0^t v_1 dt) \approx k\int_0^t v_1 dt$ one can re-write the second term as follows:

$$\frac{dv_2}{dt} = \frac{eE}{m}k\int_0^t v_1 dt \sin((kv_0 - \omega)t + \phi). \tag{A.2}$$

Following integration in (A.1) over a small time interval $t \to 0$, the first term can be rewritten, as follows:

$$v_1 = -\frac{eE}{m}\frac{1}{(kv_0-\omega)}[\sin((kv_0-\omega)t+\phi)-\sin(\phi)]. \tag{A.3}$$

Now, it is easy to find:

$$\int_0^t v_1 dt = \frac{eE}{m}\frac{1}{(kv_0-\omega)^2}[\cos((kv_0-\omega)t+\phi)-\cos(\phi)] + \frac{eE}{m}\frac{t}{(kv_0-\omega)}\sin(\phi).$$

Following substitution of $\int_0^t v_1 dt$ in (A.2) one can obtain

$$\frac{dv_2}{dt} = \frac{e^2E^2}{m^2}\frac{k}{(kv_0-\omega)^2}[\cos((kv_0-\omega)t+\phi)-\cos(\phi)]\sin((kv_0-\omega)t+\phi) + \frac{e^2E^2}{m^2}\frac{kt}{(kv_0-\omega)}\sin(\phi)\sin((kv_0-\omega)t+\phi). \tag{A.4}$$

By keeping the terms to a second order of accuracy, the equation for changes in the electron energy can be written as follows:

$$\frac{d\epsilon}{dt} = mv_1\frac{dv_1}{dt} + mv_0\frac{dv_2}{dt}. \tag{A.5}$$

Substituting v_1, dv_1/dt and dv_2/dt in to (A.5) one can find:

$$\frac{d\epsilon}{dt} = \frac{e^2E^2}{m}\frac{1}{(kv_0-\omega)}[\sin((kv_0-\omega)t+\phi)-\sin(\phi)]\cos((kv_0-\omega)t+\phi) + \frac{e^2E^2}{m}\frac{vk}{(kv_0-\omega)^2}[\cos((kv_0-\omega)t+\phi)-\cos(\phi)]\sin((kv_0-\omega)t+\phi) + \frac{e^2E^2}{m}\frac{vkt}{(kv_0-\omega)}\sin(\phi)\sin((kv_0-\omega)t+\phi). \tag{A.6}$$

By taking into account that ϕ is a random variable with a uniform distribution, it is necessary to average (A.6) over ϕ, as follows:

$$\left\langle\frac{d\epsilon}{dt}\right\rangle_\phi = \frac{e^2E^2}{2m^2}\frac{1}{(kv_0-\omega)}\sin((kv_0-\omega)t) - \frac{e^2E^2}{2m^2}\frac{v_0k}{(kv_0-\omega)^2}\sin((kv_0-\omega)t) + \frac{e^2E^2}{2m^2}\frac{vkt}{(kv_0-\omega)}\cos((kv_0-\omega)t). \tag{A.7}$$

Due to fluctuations of the plasma density, the phase velocity of the wave can have various values at different intervals. With a probability distribution function $P_\omega(V)$, one can average (A.7) over V, as follows:

$$\left\langle \frac{d\epsilon}{dt} \right\rangle_{\phi V} = \frac{e^2E^2}{2m} \int_0^\infty [\frac{1}{k(v-V)} \sin(k(v-V)t) - \frac{v}{k(v-V)^2} \sin(k(v-V)t) + \frac{vt}{(v-V)} \cos(k(v-V)t)] P_\omega(V) dV. \quad \text{(A.8)}$$

Here we consider the particle ensemble with a given distribution function, $f(v)$. The change in the energy of a wave over time t is equal to the total change of the particle energy at a volume taken with am opposite sign, as follows:

$$\frac{dW}{dt} = -n_b \int_{-\infty}^{\infty} \left\langle \frac{d\epsilon}{dt} \right\rangle_{\phi V} f(v) dv. \quad \text{(A.9)}$$

Changing the order of the integration in (A.9) and making a Taylor series expansion for $f(v)$, Equation (A.9) can be rewritten, as follows:

$$\frac{dW}{dt} = \frac{e^2E^2}{2m} n_b \int_0^\infty [\frac{V^2}{\omega} f(V) \int_{-\infty}^{\infty} \frac{\sin((v-V)kt)}{(v-V)^2} dv + \frac{V^2}{\omega} \frac{\partial f(v)}{\partial v}|_{v=V} \int_{-\infty}^{\infty} \frac{\sin(k(v-V)t)}{v-V} dv] P_\omega(V) dV. \quad \text{(A.10)}$$

The remaining terms in the expansion are proportional to t and do not make any contribution to the integrals. The first term in Equation (A.10) is equal to zero because the integrand is an odd function. After simple calculations, the second term can be written as $\int_{-\infty}^{\infty} (\sin(x)/x) dx = \pi$. By taking into account the fact that $W = E^2/(8\pi)$ and $\omega_{p0} = 4\pi e^2 N_0/m$, following equation can be obtained:

$$\frac{dW}{dt} = \pi \omega_{p0} \frac{n_b}{N_0} W \int_0^\infty V^2 \frac{\partial f}{\partial V} P_\omega(V) dV. \quad \text{(A.11)}$$

A.2 The equation for the electron distribution function

Here, we introduce a probability density function $U(v, t|v_0, t_0)$ for the electron velocity. The function provides the probability that a particle with a velocity v_0 in the moment of time t_0 will have a velocity v at time t and satisfies the following Fokker-Planck equation:

$$\frac{\partial U(v, t|v_0, t_0)}{\partial t} = -\frac{\partial}{\partial v} A(v) U(v, t|v_0, t_0) + \frac{\partial^2}{\partial v^2} B(v) U(v, t|v_0, t_0), \quad \text{(A.12)}$$

Here, functions $A(V)$ and $B(v)$ represent the averaged characteristics for variations in the velocity and its dispersion, as follows:

$$A(v) = \frac{\langle v_2 \rangle_{\phi V}}{t},$$

$$B(v) = \frac{1}{2}\frac{\langle v_1^2 \rangle_{\phi V}}{t}.$$

where the brackets indicate averaging over ϕ and V.

To define an equation for the electron distribution function it is necessary to multiply (A.12) by $f(v_0, t_0)$ and integrate it over v_0, as follows:

$$\frac{\partial f(v,t)}{\partial t} = -\frac{\partial}{\partial v}A(v)f(v,t) + \frac{\partial^2}{\partial v^2}B(v)f(v,t). \tag{A.13}$$

Subsequent to integration in (A.2), one can write v_2, as follows:

$$v_2(v,\phi) = \frac{e^2E^2}{2m^2}\frac{k}{(kv_0-\omega)^3}(\sin^2((kv_0-\omega)t+\phi) - \sin^2(\phi) + 2\cos(\phi)\cos((kv_0-\omega)t+\phi) + 2\sin(\phi)\sin((kv_0-\omega)t+\phi) - 2) - \frac{e^2E^2}{m^2}\frac{kt}{(kv_0-\omega)^2}\sin(\phi)\cos((kv_0-\omega)t+\phi).$$

Now, it is easy to determine $\langle v_1^2 \rangle_\phi$ and $\langle v_2 \rangle_\phi$, as follows:

$$\langle v_2 \rangle_\phi = \frac{e^2E^2}{m^2}\frac{k}{(kv_0-\omega)^3}(\cos((kv_0-\omega)t) - 1) + \frac{e^2E^2}{2m^2}\frac{kt}{(kv_0-\omega)^2}\sin((kv_0-\omega)t),$$

$$\langle v_1^2 \rangle_\phi = \frac{e^2E^2}{m^2}\frac{1}{(kv-\omega)^2}(1-\cos((kv-\omega)t)).$$

By taking into account that $t = a/v$, $A(v)$ and $B(v)$ can be written as follows:

$$A(v) = \frac{e^2E^2}{m^2}\int_0^\infty [\frac{v}{ak^2(v-V)^3}(\cos((v-V)kt) - 1) + \frac{1}{2k(v-V)^2}\sin((v-V)kt)]P_\omega(V)dV,$$

$$B(v) = \frac{e^2E^2}{2m^2}\int_0^\infty \frac{v}{ak^2(v-V)^2}(1-\cos((v-V)kt))P_\omega(V)dV.$$

Here, it is also worth writing the following equation for $\partial B(v)/\partial v$:

$$\frac{\partial B(v)}{\partial v} = \frac{e^2E^2}{2m^2}\int_0^\infty (\frac{V+v}{ak^2(v-V)^3}(\cos((v-V)kt)-1) + \frac{V}{kv(v-V)^2}\sin((v-V)kt))P_\omega(V)dV.$$

By taking the first derivative of the second term of Equation (A.13) and substituting $A(v)$, $B(v)$, and $\partial B(v)/\partial v$, one can obtain an equation for the electron distribution function in the following form:

$$\frac{\partial f}{\partial t} = -\frac{e^2E^2}{2m^2}\frac{\partial}{\partial v}[\int_0^\infty \frac{1}{ak^2(v-V)^2}(\cos((v-V)kt)-1)P_\omega(V)dVf(v) + \int_0^\infty \frac{1}{kv(v-V)}\sin((v-V)kt)P_\omega(V)dVf(v) - \int_0^\infty \frac{1}{tk^2(v-V)^2}(1-\cos((v-V)kt))P_\omega(V)dV\frac{\partial f}{\partial v}]. \quad (A.14)$$

Through a Taylor series expansion of $P_\omega(V)$ at $V = v$, one can integrate the terms in (A.14), as follows:

$$\int_0^\infty \frac{1}{ak^2(v-V)^2}(\cos((V-v)kt)-1)P_\omega(V)dVf(v) =$$

$$-P_\omega(v)\frac{2}{\omega}\int_0^\infty \frac{1}{kt(V-v)^2}\sin^2((V-v)\frac{kt}{2})dVf(v) = -P_\omega(v)\frac{\pi}{2\omega}f(v),$$

$$\int_0^\infty \frac{1}{kv(v-V)}\sin((v-V)kt)P_\omega(V)dVf(v) =$$

$$P_\omega(v)\frac{1}{\omega}\int_0^\infty \frac{1}{(V-v)}\sin((V-v)kt)dVf(v) = P_\omega(v)\frac{\pi}{2\omega}f(v),$$

$$\int_0^\infty \frac{1}{tk^2(v-V)^2}(1-\cos((v-V)kt))P_\omega(V)dV\frac{\partial f}{\partial v} =$$

$$P_\omega(v)\frac{2v}{\omega}\int_0^\infty \frac{1}{tk(V-v)^2}\sin^2((V-v)\frac{kt}{2})dV\frac{\partial f}{\partial v} = \frac{\pi}{2}\frac{v}{\omega}P_\omega(v)\frac{\partial f}{\partial v}.$$

After substitution of the results to (A.14), one can find the final equation for the $f(v,t)$ function, as follows:

$$\frac{\partial f}{\partial t} = \frac{2\pi^2e^2W}{m^2\omega}\frac{\partial}{\partial v}vP_\omega(v)\frac{\partial f}{\partial v}, \quad (A.15)$$

where $W = E^2/(8\pi)$.

A.3 Conservation law

Equations (A.11) and (A.15) constitute the basic system of equations for our model. To make this system more convenient for numerical simulation, here, we introduce the following dimensionless variables: $\tilde{t} = (1/(\pi\omega_{p0}))(N_0/n_b)t$, $\tilde{v} = v_t v$, $\tilde{f} = f/v_t$, $\tilde{P}_\omega(V) = P_\omega(V)/v_t$, and $\tilde{W} = 2n_b m v_t^2 W$. We omit tildes to simply the form of the equations. The system takes the following form:

$$\frac{\partial f}{\partial t} = \frac{\partial}{\partial v} v W P_\omega(v) \frac{\partial f}{\partial v}, \tag{A.16}$$

$$\frac{dW}{dt} = \int_0^\infty W V^2 \frac{\partial f}{\partial V} P_\omega(V) dV. \tag{A.17}$$

One can easily determine that the system has a conservation law for total energy, as follows:

$$\begin{aligned}
&\frac{\partial}{\partial t}[\frac{1}{2}\int_0^\infty v^2 f(v)dv + W] = \frac{1}{2}\int_0^\infty v^2 \frac{\partial f(v)}{\partial t} dv + \frac{\partial W}{\partial t} = \\
&\frac{1}{2}\int_0^\infty v^2 \frac{\partial}{\partial v} v W P_\omega(v) \frac{\partial f}{\partial v} dv + \int_0^\infty W V^2 \frac{\partial f}{\partial V} P_\omega(V) dV = \\
&\quad -\int_0^\infty W v^2 P_\omega(v) \frac{\partial f}{\partial v} dv + \int_0^\infty W V^2 \frac{\partial f}{\partial V} P_\omega(V) dV = 0.
\end{aligned} \tag{A.18}$$

Chapter 4

Probabilistic model of beam-plasma interaction in randomly inhomogeneous solar wind.

4.1 Introduction

In the previous chapter we proposed a self-consistent probabilistic model that describes beam-plasma instability in a plasma with random density fluctuations. In contrast to the model proposed by Nishikawa and Ryutov [1976], density fluctuations were supposed to be high enough to cause significant changes in the k magnitude in the direction of wave propagation. As a result, the wave phase velocity undergo changes, allowing the wave to resonantly interact with beam electrons that have different velocities within a quite large range. An assumption that the phase velocity is a random quantity that obeys a predetermined distribution allows one to describe the energy exchange between the waves and the beam in terms of an averaged in the velocity space growth rate of the waves, $\langle\gamma\rangle_V$, and similarly averaged electron velocity diffusion coefficient, $\langle D\rangle_V$. The $\langle\gamma\rangle_V$ and $\langle D\rangle_V$ depend on the distribution function for the wave phase velocity that is determined by the distribution function of the density fluctuations. The model was initially applied for a case with a normal distribution for the density fluctuations. This allowed us to investigate how key parameters of the relaxation process depend on the level of density fluctuations and on the initial velocity of the beam. It is worth noting that the results obtained in the model are in a good agreement with weak turbulence theory. The goal of the present chapter is to determine what type of distribution represents the best fit for observed density variations in the solar wind plasma and how it's form affects the beam relaxation process. We shall also compare the results obtained with those for the normally distributed density fluctuations.

In the present chapter we propose a technique for evaluating the distribution func-

tion of density fluctuations using density fluctuations obtained from measurements onboard satellites. We use the Pearson technique for classifying different distributions [Pearson, 1895] in order to define the type of distribution corresponding to the observations. The Pearson classification allows one to obtain an analytical form for the distribution function of density fluctuations for observed distributions depending on four statistical parameters, namely, the mean value, the variance, the skewness, and the kurtosis. Using the Pearson distribution type, we determine the distribution function of wave phase velocities and apply this distribution in our model for beam plasma interaction. Finally we obtain the results of the numerical simulations of the relaxation of the electron beams having different beam velocities, thermal spread and at different levels of the density fluctuations in the plasma under conditions similar to those in the solar wind.

4.2 Density fluctuations in the solar wind

Spectrum of the density fluctuations in the solar wind have been obtained from the in situ spacecraft measurements [Neugebauer, 1975] and phase scintillations of the signals transmitted from satellite to Earth [Woo and Armstrong, 1979] already in 70-ties. Celnikier et al. [1983] analyzed data from ISEE propagation experiments and reported that the spectral density of fluctuations, W_k, can be presented in the form of a double-power law. In the low frequency (long wavelengths) part of the spectrum, it can be approximated quite well using the Kolmogorov power law, as follows:

$$W_k \sim \left(\frac{\Delta n}{N_0}\right)^2 \sim k^{-5/3}.$$

In the higher frequency range (shorter wavelengths) the power law was evaluated to have different spectral index, as follows:

$$W_k \sim k^{-\nu}, \nu \simeq 0.64 \pm 0.01.$$

Here N_0 is the background plasma density and Δn is the amplitude of the fluctuations. The transition occurs at a frequency around $6 \times 10^{-2}\ Hz$. Here, it is worth mentioning that in this frequency range the wave dispersion is still negligible and that the relationship between frequencies and wavelengths can be established by assuming the Taylor hypothesis. The result was obtained by Celnikier et al. [1983], making use the technique of active sounding between two satellites. Noteworthy, spectral indices depend on an angle between solar wind and a background magnetic field [Forman et al., 2011]. In some cases the low frequency part of the density fluctuations spectrum is measured to be steeper than $-5/3$ [Celnikier et al., 1987]. Recently, a similar spectrum was determined onboard Cluster [Kellogg and Horbury, 2005], Artemis [Chen et al., 2012] and Spektr-R [Šafránková et al., 2015].

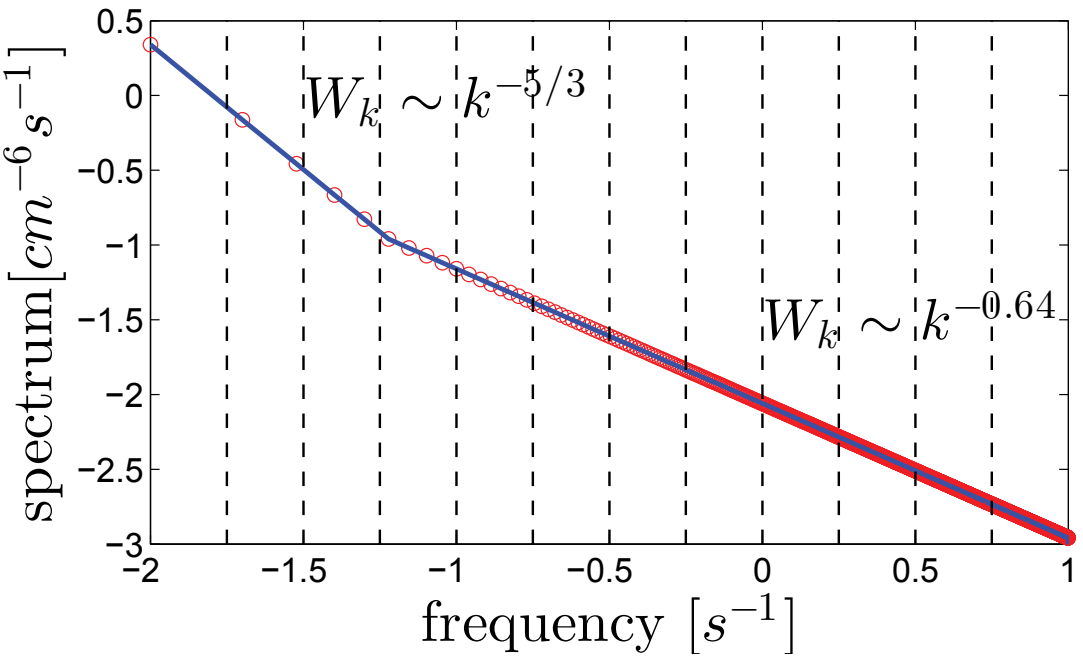

Figure 4.1: A power spectrum of the density fluctuations in $log - log$ scale. The blue line corresponds to the spectrum of the density fluctuation observed in the solar wind. The red circles- spectrum of the density fluctuations calculated from syntectic time series of the density perturbations.

To obtain a probability distribution for density fluctuations, the time series should be constructed that have the same statistical properties as data collected by satellites. For this purpose, we divided the spectrum into 10^4 equally sized intervals and calculated the series in which the coefficients were equal to the square root of the power spectrum multiplied by the width of the interval: $A_i = \sqrt{W(f_i) \cdot \Delta f}$. We used the spectrum obtained by Celnikier et al. [1983] over a frequency range of 10^{-2} Hz to 10^2 Hz (shown with blue line in Figure 4.1). For conditions of a quiet solar wind, the lowest frequency corresponds to density variations with a spatial scale of approximately $3 \cdot 10^6 \lambda_D$, which is comparable to the length of relaxation for an electron beam in homogeneous plasma. The highest frequency corresponds to density variations with a spatial scale of approximately $300\lambda_D$. At such scale, the gain of the wave energy produced by resonant interaction with a typical electron beam is approximately about the noise level. To obtain the growth of waves up to a level significantly larger than the noise level, one should consider density fluctuations with larger spatial scales. To exclude small scale fluctuations, we set all coefficients that corresponded to the spectrum within the frequency domain above 10 Hz to be equal to zero.

These procedures were used to obtain synthetic density profiles corresponding to these spectra, the above described series may be used as follows: $n(t) = \sum_i A_i \cos(2\pi f_i t + \phi_i)$, where ϕ_i is a random phase with a uniform distribution from 0 to 2π. Averaged spec-

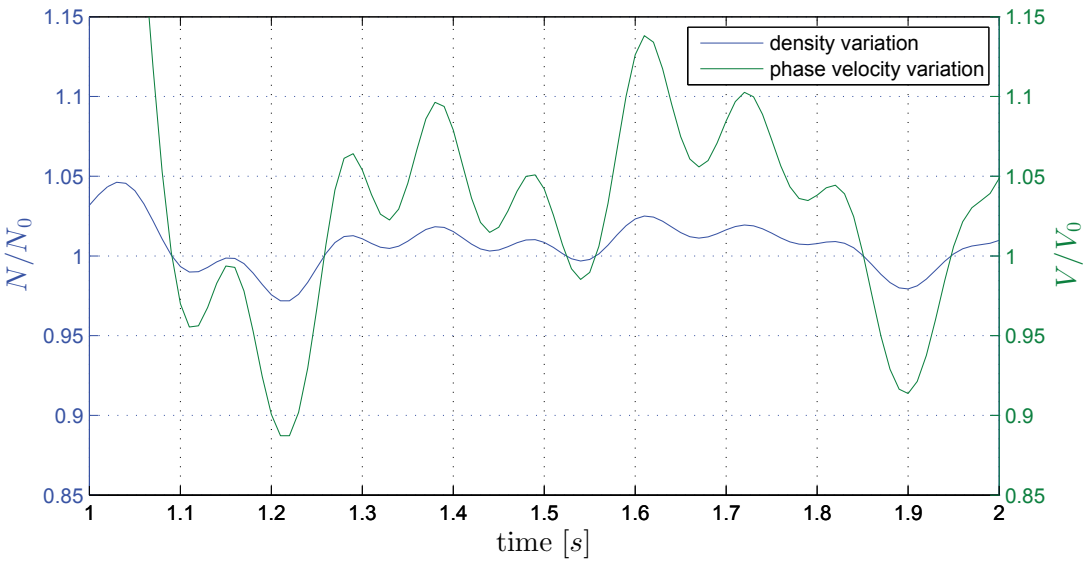

Figure 4.2: A synthetic time series of density fluctuations reconstructed from the spectrum shown in Figure 4.1 (the blue curve) and a corresponding variations of the wave phase velocity of the wave (the green curve) [from Voshchepynets and Krasnoselskikh, 2015].

trum of density fluctuations obtained from the synthetic time series is shown with red circles in Figure 4.1. In Figure 4.2, the reconstructed time series for the density fluctuations are shown. As a Langmuir wave propagates through a plasma with a varying density, the frequency of the wave remains approximately constant. If spatial variations for the density fluctuations [see also Kellogg et al., 1999], the conservation of the frequency implies that the k vector of the wave will change by satisfying the dispersion relationship. Changes in the k vector result in variations in the phase velocity of the wave (the green line in Figure 4.2). As one can notice, even small variations in the plasma density may lead to significant changes in the wave phase velocity.

4.3 Pearson curves for approximation of statistical distributions

Due to the central limit theorem, Gaussian distributions are often found in The Nature. In the previous chapter we considered electron beam relaxation in a plasma with density fluctuations that obey normal distribution. The purpose of present chapter is to define the distribution that describes density fluctuations in the solar wind as precisely as possible. To this end we suggest to use a powerful method proposed by K.Pearson to study the distribution obtain from the synthetic time series. Pearson [1895] proposed a classification of the distributions according to their first four moments, each class corresponding to the well known distributions.

Here we perform a brief description of the Pearson's curves family (more detailed

information can be found in various textbooks[for instance Kendall and Stuart, 1977, Tikhonov, 1982]. The Pearson distributions are defined by the differential equation:

$$\frac{dp(x)}{dx} = \frac{x-a}{b_0 + b_1 x + b_2 x^2} p(x), \tag{4.1}$$

where a and b_i are constant parameters of the distribution. Depending on the values of this parameters, 12 types of curves can be obtained, including famous distributions such as normal, log-normal, χ^2, and others. As it was shown in [Pearson, 1895], the parameters in equation 4.1 could be expressed in terms of the first four moments, μ_1-μ_4, of the distribution $p(x)$ as follows:

$$\begin{aligned} a &= b_1 \\ b_0 &= \frac{\mu_2(4\mu_2\mu_4 - 3\mu_3^2)}{10\mu_2\mu_2 - 18\mu_2^3 - 12\mu_3^2} \\ b_1 &= \frac{-\mu_3(\mu_4 + 3\mu_2^2)}{10\mu_2\mu_2 - 18\mu_2^3 - 12\mu_3^2} \\ b_2 &= \frac{-2\mu_2\mu_4 + 6\mu_2^3 + 3\mu_3^2}{10\mu_2\mu_2 - 18\mu_2^3 - 12\mu_3^2} \end{aligned} \tag{4.2}$$

Analytical solution of equation 4.1 for the case of centered distribution can be obtained as follows:

$$p(x) = C \exp\left(\phi(x)\right) \tag{4.3}$$

where

$$\phi(x) = \int_0^x \frac{y - b_1}{b_0 + b_1 y + b_2} dy \tag{4.4}$$

As can be seen, the features of the $\phi(x)$ strongly depend on the roots of quadratic equation: $b_0 + b_1 y + b_2 y^2 = 0$.

Since Pearson curves are determined by first four moments, and centered distributions are concerned, the Pearson's classification can done in the terms of Pearson's betas, β_1 and β_2 (shown in a form of diagram in Figure 4.3), defined as follows:

$$\beta_1 = \frac{\mu_3^2}{\mu_2^2}, \beta_2 = \frac{\mu_4}{\mu_2^2}$$

Certain distributions are represented by a single point, for instance, the normal distribution (corresponds to type VIII) and the exponential distribution (corresponds to type X). It is worth noting that β distribution corresponds to type I, while the γ distributions corresponds to type III. However, certain distribution can not be represented at the diagram, if at least one of the moments does not exist.

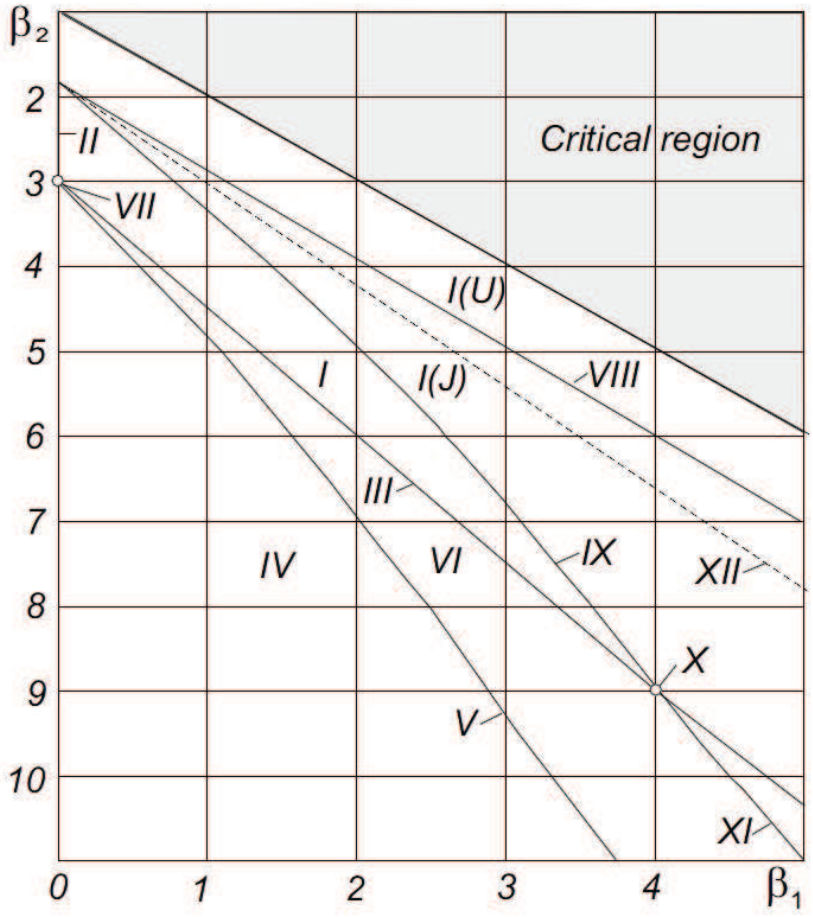

Figure 4.3: The diagram of different distribution of Pearson curves family. Axis: β_1 - skewness, β_2 -kurtosis+3 [from Podladchikova et al., 2003].

4.4 The probability distribution function of density fluctuations

To obtain a probability distribution function for density fluctuations, we used $K_s = 3500$ synthetic data samples, each 100 seconds in duration. For each sample, we used 6400 equidistant points corresponding to a sampling frequency of approximately 60 Hz. This frequency corresponds to a spatial resolution of approximately $500\lambda_D$. At such scales, variations in the phase velocity are negligible in comparison to the initial phase velocity. On the other hand, the spatial intervals are large enough to provide sufficient energy exchange between waves and beam electrons.

Following normalization for all the data samples using standard deviations, σ, we built a set of histograms for the density fluctuations using K_b - 50 bins spaced between -5σ to 5σ. A histogram, averaged over all the K_s ensembles, is provided in Figure 4.4 (blue curve). The obtained distribution was characterized using an averaged $\beta_1 = 2 \cdot 10^{-6}$ and $\beta_2 = 2.86$. According to the Pearson classification [Pearson 1895], the distribution corresponded to a Type II Pearson distribution. This distribution is described by a symmetric β function and depends on the following three parameters: the mean, the standard deviation, and the kurtosis. Analytical form of the type II Pearson distribution can be obtained by integrating equation 4.4 and substituting the result in the equation 4.3 as follows:

$$p(x) = A_c \left|1 - x^2 a_b\right|^{m_b}$$

where

$$a_b = 2\left(\frac{\mu_4}{\mu_2}\right) / \left(3 - \frac{\mu_4}{\mu_2^2}\right), m_b = \left(\frac{5\mu_4}{\mu_2^2 - 9}\right) / \left(2\frac{3 - \mu_4}{\mu_2^2}\right),$$

and factor A_c can be estimated from the normalization of $p(x)$ to one. It is worth noting that, this distribution is very close to the normal distribution which is characterized by $\beta_1 = 0$ and $\beta_2 = 3$ [Tikhonov, 1982, Podladchikova et al., 2003].

To evaluate the goodness of fit for each distribution we used the χ^2 squared statical test [Bendat and Piersol, 2000, Krasnoselskikh et al., 2007]. The χ^2 test basically consists of an assumption that if the data is distributed according to a predicted distribution function, $f(x)$, the normalized error of fit, X^2:

$$X^2 = \sum_{i=1}^{K_b} \frac{(Nf(x_i) - h_i)^2}{Nf(x_i)} \tag{4.5}$$

is a random variable that follows a χ^2_ν distribution with $\nu = K_b - K_f - 1$, where ν is the number of free parameters in the χ^2_ν distribution and K_f is the number of free parameters in the fitted function. In equation 4.5 x_i is the center of each bin, h_i is

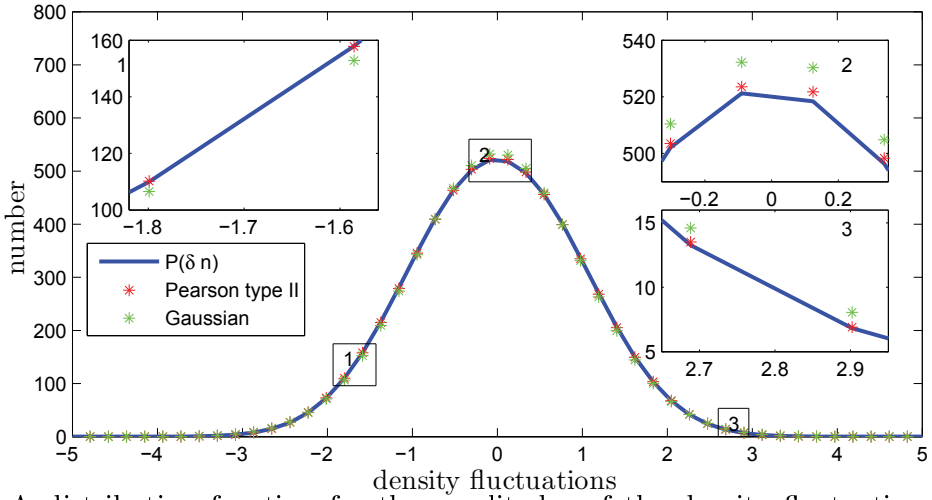

Figure 4.4: A distribution function for the amplitudes of the density fluctuations. The blue line corresponds to the averaged distribution function obtained from the synthetic time series of the density variation. All of the time series was normalized to its standard deviation. Red and green asterisks correspond to the distribution functions obtained from the Pearson type II and the normal probability distribution functions, respectively. Parameters of the fitting probability distribution functions were calculated from synthetic data.

a number of observations in each bin, and $N = \sum h_i$. Thus, one can use the χ^2 test to validate a hypothesis that the data under consideration follows a given distribution function based on a comparison of the value of X^2 with the percentage, $\chi^2_{\nu,\alpha}$, for the chi squared distribution, χ^2_ν, for a chosen significance level, α [Bendat and Piersol, 2000].

To obtain the required parameters for the Pearson type II distribution, we calculated the first four moments of the time series. Figure 4.4 provides a comparison of a distribution obtained using synthetic data with the Pearson type II distribution (green asterisks) and the normal distribution (red asterisks). It was shown that the distribution for the density fluctuations is close to the normal distribution but some deviations occur and are clearly identifiable. For a distribution function of $K_b = 10$, the normalized error of the fit X^2 for the normal distribution case is equal to 2.98. Thus, a hypothesis that the density fluctuations distribution obeys a normal distribution cannot be rejected at a significance level of 95%. On the other hand, for the Pearson Type II distribution case, $X^2 = 0.14$, indicating that the hypothesis that distribution of density fluctuations follows this distribution cannot be rejected at a level of significance above 99.99%. Therefore, one can conclude that the distribution indeed corresponds to a type II Pearson distribution.

4.5 The probability distribution function of wave phase velocities

Using obtained probability distribution function of the density fluctuations, $P_{\delta n}(\delta n)$, one can reconstruct a probability distribution function for the phase velocities of the Langmuir waves on the borders of the subintervals, $P_V(V)dV$. For this aim, we use the following single value functional dependence for the plasma frequency on plasma density: $\omega_p^2(\delta n) = 4\pi e^2(N_0 + \delta n)/m$. Thus, a distribution function for the plasma frequencies $P_{\omega_p}(\omega_p)$ could be found using a unique relationship: the probability to find plasma frequency less than $\omega_p(N_0 + \delta n)$ is equivalent to probability to find the density fluctuation less than δn:

$$P_{\omega_p}(\omega_p)d\omega_p = P_{\delta n}(\delta n(\omega_p))d\delta n = P_{\delta n}(\delta n(\omega_p))\frac{\partial \delta n}{\partial \omega_p}d\omega_p.$$

Then, using the dispersion relationship for Langmuir waves, one can obtain the relationship between the local plasma frequency and the wave phase velocity, as follows: $\omega^2 = \omega_p^2(\delta n)(1 + 3v_t^2/V^2)$. By taking into account that the frequency of the wave is constant, the probability distribution function of the phase velocities $P_V(V)$ may be determined in a similar manner, as was done for $P_{\omega_p}(\omega_p)$:

$$P_V(V)dV = P_{\omega_p}(\omega_p(V))\frac{\partial \omega_p}{\partial V}dV.$$

It is worth reminding that $P_V(V)dV$ is the probability of finding a wave with a phase velocity equal to V at one of the edges of the subinterval. The probability of finding a wave with a phase velocity equal to some value, V_i, in some point inside subinterval, $P_\omega(V_i)$, can be obtained by making use of the procedure described in the previous chapter.

Figure 4.5 provides examples of $P_\omega(V)$ for a wave with $V = 7v_t$ (in homogeneous plasma), where v_t is the thermal velocity of the background plasma, for cases with different levels of density fluctuations, $(\langle \delta n^2 \rangle)^{1/2}/N_0$ (shown with colors). Solid lines correspond to the $P_\omega(V)$ obtained from the Pearson type II distribution of the density fluctuations, while dashed lines correspond to $P_\omega(V)$ calculated from the normal distribution. As indicated, both types of $P_{\delta n}(\delta n)$ result in a similar form for the probability distribution function of the wave phase velocities. In both cases, $P_\omega(V)$ shows a similar behavior with an increasing level of density fluctuations. An increase in the magnitude of the density fluctuations causes wider broadening in the probability distribution function within the velocity space. A deviation in distribution of density fluctuations from the normal distribution mainly consists in the presence of a higher amount of fluctuations with amplitudes within the range of $0.3\sigma < |\delta n| < 2.5\sigma$. These fluctuations cause significant changes in the wave phase velocity. As a result, $P_\omega(V)$, for a case of density fluctuations with the non-Gaussian distribution, is characterized by wider broadening

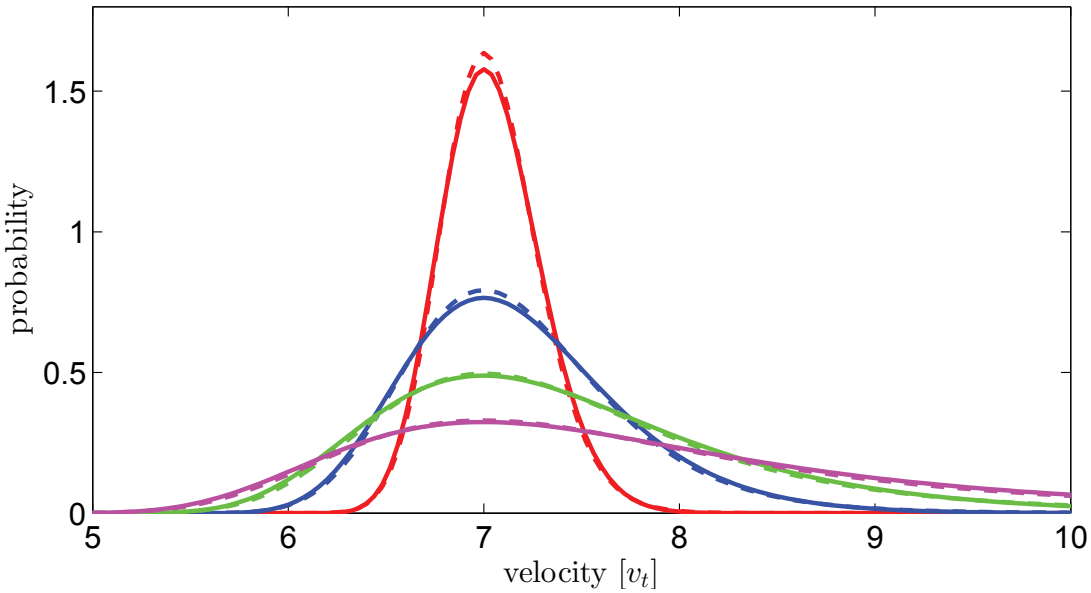

Figure 4.5: Examples of the probability distribution functions, $P_\omega(V)$, for various fluctuation levels. $P_\omega(V)dV$ is the probability that a wave with a ratio of $\omega/k_0 = 7v_t$ will have a phase velocity V at a given interval. P_ω was normalized to one using: $\int_0^\infty P_\omega(V)dV = 1$. Colors correspond to the various fluctuation levels, as follows: $(\langle\delta n^2\rangle)^{1/2}/N_0 = 0.005$, red; $(\langle\delta n^2\rangle)^{1/2}/N_0 = 0.01$, blue; $(\langle\delta n^2\rangle)^{1/2}/N_0 = 0.015$, green; $(\langle\delta n^2\rangle)^{1/2}/N_0 = 0.02$, magenta. Solid lines correspond to density fluctuations obtained using the Pearson type II distribution and the dashed line to density fluctuations obtained using the normal distribution.

of the region of resonance. Thus, for this case, the effects of density inhomogeneities in the plasma on the electron beam relaxation process will be more important. However, the difference between $P_\omega(V)$, corresponding to the Gaussian and non-Gaussian distributions of the density fluctuations, decrease with an increase in the level of the density fluctuations, $(\langle\delta n^2\rangle)^{1/2}/N_0$. When it reaches a level of approximately 1.5% or is larger than this level (the green and magenta lines in Figure 4.5), no significant difference occurred between the probability distribution functions of phase velocity for normal and more realistic (for solar wind conditions) distributions of density fluctuations.

4.6 The evolution of Langmuir waves

To evaluate the importance of the non-Gaussian form for a distribution of density fluctuations on the generation of Langmuir waves, we compare results obtained from stimulations with non-Gaussian distribution of the density fluctuations with those obtained using normal distribution. The left panel in Figure 4.6 provides the evolution of the total energy density of waves, $W_t = \sum W_i$, generated by an electron beam with an initial Gaussian velocity distribution function for $v_b = 6v_t$ and $\Delta v_b = v_t$. The level of the density fluctuations $(\langle\delta n^2\rangle)^{1/2}/N_0$ was chosen to be 0.005. The energy density

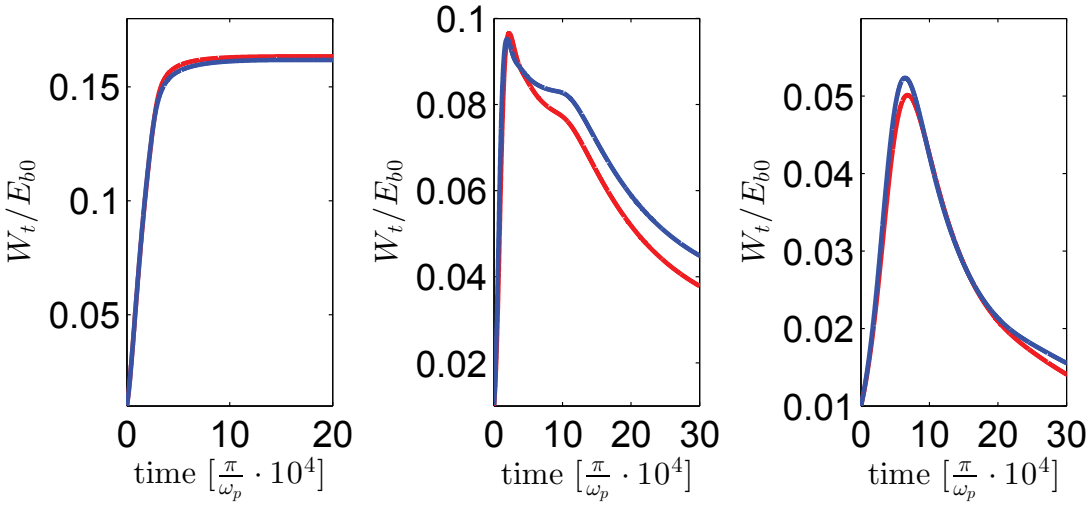

Figure 4.6: Evolution for the total energy density of waves, W_t, for different levels of density fluctuations and different parameters for the driven beams. Blue lines correspond to density fluctuations with a normal distribution for the density fluctuations while red lines correspond to fluctuations that obey the Pearson type II distribution. Left panel: $(1/2)(\langle\delta n^2\rangle)^{1/2}/N_0 = 0.005$, $v_b = 6v_t$, $\Delta v_b = v_t$. Middle panel: $(1/2)(\langle\delta n^2\rangle)^{1/2}/N_0 = 0.02$, $v_b = 10v_t$, $\Delta v_b = v_t$. Right panel: $(1/2)(\langle\delta n^2\rangle)^{1/2}/N_0 = 0.03$, $v_b = 16v_t$, $\Delta v_b = v_t$. All of the panels provide the wave energy density with respect to the corresponding initial energy density of the beam, E_{b0}.

obtained for the Gaussian density fluctuations distribution is shown in blue, while the energy density for the Pearson type II distribution is shown in red. For this study, the term $(3/2)(v_t/v_b)^2$ that corresponds to the thermal effects in the non-linear dispersion relationship for Langmuir waves [Krafft et al., 2013] is significantly larger than the term, $(1/2)(\langle\delta n^2\rangle)^{1/2}/N_0$, related to density fluctuations. Thus, one can expect that the influence of the density fluctuations on the process of wave generation will be rather low. For both cases, W_t shows dynamics similar to those for a homogeneous plasma, namely, the energy density of the waves increases with time, until it reaches a plateau. However, the presence of even small amplitude fluctuations reduces the saturation level of the waves. In stimulations, saturation occurs when the total energy of the waves approximately reaches 15% of the initial energy of the beam, while conventional QL theory predicts saturation at a level of approximately 67%.

The results, obtained for a beam with $v_b = 10v_t$ and $\Delta v_b = v_t$, and a density fluctuations level $(\langle\delta n^2\rangle)^{1/2}/N_0 = 0.02$, are presented in the middle panel of Figure 4.6. For this case, the term proportional to $(3/2)(v_t/v_b)^2$ is slightly above the term $(1/2)(\langle\delta n^2\rangle)^{1/2}/N_0$. Thus, the presence of density fluctuations should have a more significant effect on the evolution of waves. As for a previous study, the energy density of waves initially increases with time until it reaches a maximum. After that, the wave energy density, W_t, begins to decrease. A decay in wave energy can be explained in terms of resonant broadening [Bian 2014]. Since density fluctuations lead to variations

in the phase velocity of a waves, the very same wave can resonantly interact with different parts of the electron distribution function. If a wave spends more time in the region of the velocity space where the velocity distribution function has a negative slope, it will provide more energy to particles than it can gain by being in a region where the derivative of $f(v)$ is positive. As a result, the decay of wave energy density is associated with the acceleration of some parts of the electrons. In this study, we observed quite unusual dynamics of the system. After a short intensive decrease in the wave energy density, the system achieved a state of relatively marginal stability. During this period, W_t decays very slowly. The period of stability is followed by another period of intensive decay. For the case of a Gaussian distribution of density fluctuations, the wave energy density initially grows faster. At the same time, for the case of non-Gaussian distribution, the waves loose their energy more rapidly.

The right panel of Figure 4.6 provides the results for a beam with $v_b = 16v_t$ and $\Delta v_b = v_t$. The level of the density fluctuations is 3%. This regime corresponds to a situation where the term $(1/2)(\langle \delta n^2 \rangle)^{1/2}/N_0$ is sufficiently larger than $(3/2)(v_t/v_b)^2$. Under such conditions, the processes of growth and decay are completely determined by density irregularities. The wave energy density increases in the beginning, however, the stage of the waves growth takes longer time and the absorption of wave energy by electrons is significantly stronger. Making use of the non-Gaussian distribution of the density fluctuations leads to a slight increase in the time of wave energy growth and to a decrease of the time of the decay. Also it leads to a decrease in maximum of the energy density of waves attained during the growth phase and the level of energy density obtained at the end of relaxation.

The maximum level of Langmuir wave's energy generated by the electron beams depends on the level of density fluctuations. The right panel of Figure 4.7 presents the dependence of maximum in total wave energy density that was reached during the relaxation process, W_{max}, as a function of $(\langle \delta n^2 \rangle)^{1/2}/N_0$. Here, we show the results of simulations for beams with different beam velocities (shown with various colors) and different beam thermal dispersions (shown with various symbols). An important feature to be noted for all the cases is that an increase in the level of density fluctuations leads to a decrease in W_{max}. However, the initial thermal dispersion of the beam reduces effects related to the density fluctuations. For a case with slow and wide beams ($v_b < 10v_t$ and $\Delta v_b > v_t$), the presence of density fluctuations in a plasma does not cause any notable effects. For fast beams with velocities larger than $10v_t$, the change in the initial thermal beam dispersion does not lead to any substantial change in the results. For all cases, an increase in $(\langle \delta n^2 \rangle)^{1/2}/N_0$ results in a significant decrease in the maximum total energy density of the Langmuir waves.

To estimate the dependence of the wave growth efficiency on the level of density fluctuations and the parameters of the driven beam, we introduced the following quantity

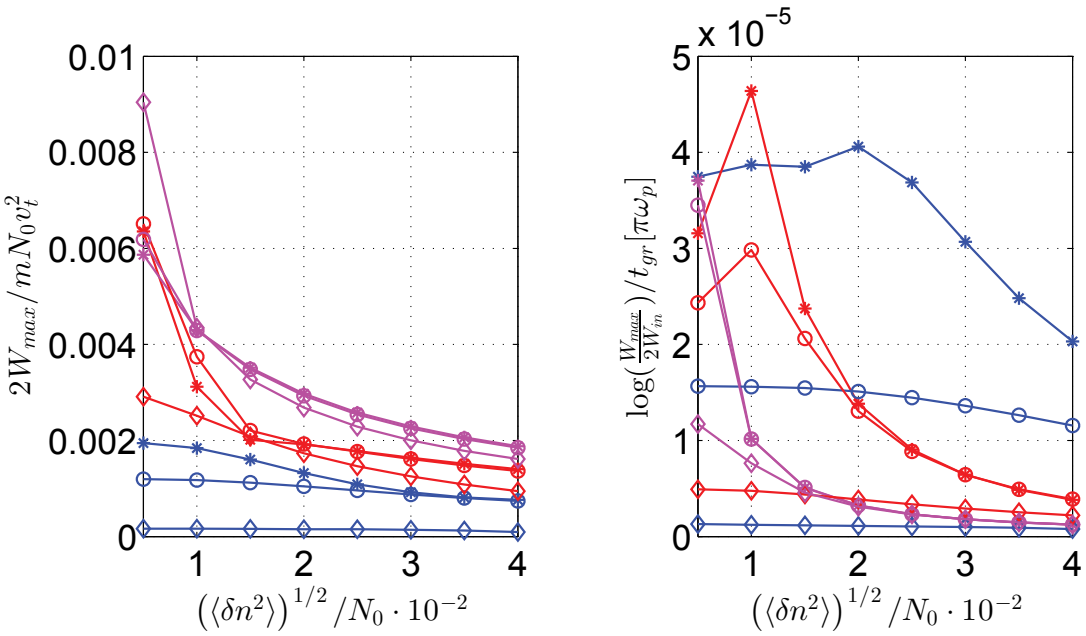

Figure 4.7: The maximum for wave total energy density, W_{max}, reached during the relaxation process (left panel) and the effective growth rate of waves (right panel) as a function of the level of density fluctuations. W_{max} is provided with respect to the energy density of the background plasma. W_{in} and t_{gr} in the right panel represent the initial total energy density of waves and the period of time, over which the wave energy density has grown from W_{in} to W_{max}, respectively. Results are provided for various parameters of the beam. Colors correspond to the various velocities of the beam, as follows: $v_b = 6v_t$, blue; $v_b = 10v_t$, red; $v_b = 16v_t$, magenta. Different marks correspond to various thermal dispersions of the beam, as follows: $\Delta v_b = 0.5v_t$- asterisk; $\Delta v_b = v_t$- circle; $\Delta v_b = 3v_t$- diamond.

that characterizes the average time for the growth of waves: $\gamma_{ef} = \log(W_{max}/W_{in})/t_{gr}$ where W_{in} and W_{max} indicate the initial and maximum values of the total wave energy density, respectively, and t_{gr} is the time during which the energy density of waves grows from W_{in} to W_{max}. The right panel of Figure 4.7 shows γ_{ef} as a function of $(\langle \delta n^2 \rangle)^{1/2}/N_0$ obtained in simulations for beams with different v_b and Δv_b. As seen in Figure 4.7, beams with a large initial thermal dispersion $\Delta v_b \geq 3v_t$ generate waves less efficiently than narrow beams (with $\Delta v_b \leq v_t$). A decrease in γ_{ef}, was obtained using an increase in the level of the density fluctuations. However, the increase in thermal dispersion for the beam reduces effects related to the density fluctuations. On the other hand, when the level of the density fluctuations is quite high, $(\langle \delta n^2 \rangle)^{1/2}/N_0 \gg \Delta v_b/v_b$, there is no notable difference in γ_{ef} corresponded to beams with a different Δv_b. For these cases, the efficiency of wave growth is significantly reduced by effects caused by density fluctuations.

The left panel of Figure 4.8 provides the time of growth for the wave energy, t_{gr}, as a function of the level of density fluctuations. The results are for simulations with electrons beams having beam velocities in the range of $10v_t$ to $20v_t$, and the initial thermal beam velocities in the range of $0.5v_t$ to $3v_t$. For all of these beams $(v_t/v_b)^2 \leq (\langle \delta n^2 \rangle)^{1/2}/(3N_0)$. One can clearly see that the presence of density fluctuations plays a crucial role in the process of wave generation. For all considered cases, an increase in the $(\langle \delta n^2 \rangle)^{1/2}/N_0$ leads to an increase in t_{gr}. The results were expected since we already knew that an increase in the density fluctuation level leads to a decrease in the effective growth rate. Under a condition of $(\langle \delta n^2 \rangle)^{1/2}/N_0 \gg \Delta v_b/v_b$, t_{gr} linearly depends on changes in $(\langle \delta n^2 \rangle)^{1/2}/(N_0)$ with a coefficient of approximately one.

We indicated that the density fluctuations may cause a decay in the energy density of waves. The process becomes important when $(\langle \delta n^2 \rangle)^{1/2}/(N_0)$ is large enough to strongly affect the non-linear dispersion relationship for Langmuir waves. Characteristic times for the decay of the wave energy density, t_{dec}, are shown in the right panel of Figure 4.8. We designate t_{dec} as the time interval between the moment in time when W_t achieves its maximum, and the moment in time when W_t decreases to a level of $W_{max}/2$. As can be seen, all the results can be separated into the following two classes: (1) While the initial thermal dispersion of an electron beam is relatively large $\Delta v_b/v_b \geq (\langle \delta n^2 \rangle)^{1/2}/N_0$, an increase in the level of density fluctuations leads to a decrease in the time of decay. This result indicates that an increase in $(\langle \delta n^2 \rangle)^{1/2}/N_0$ makes the process of the absorption of waves by electrons from the tail of the distribution more efficient. (2) The inequality $\Delta v_b/v_b \ll (\langle \delta n^2 \rangle)^{1/2}/N_0$ indicates that the region in the phase space, where waves can effectively interact with beam electrons, is almost completely determined by the level of density fluctuations. For this case, an increase in the $(\langle \delta n^2 \rangle)^{1/2}/N_0$ results in the linear growth of the t_{dec}.

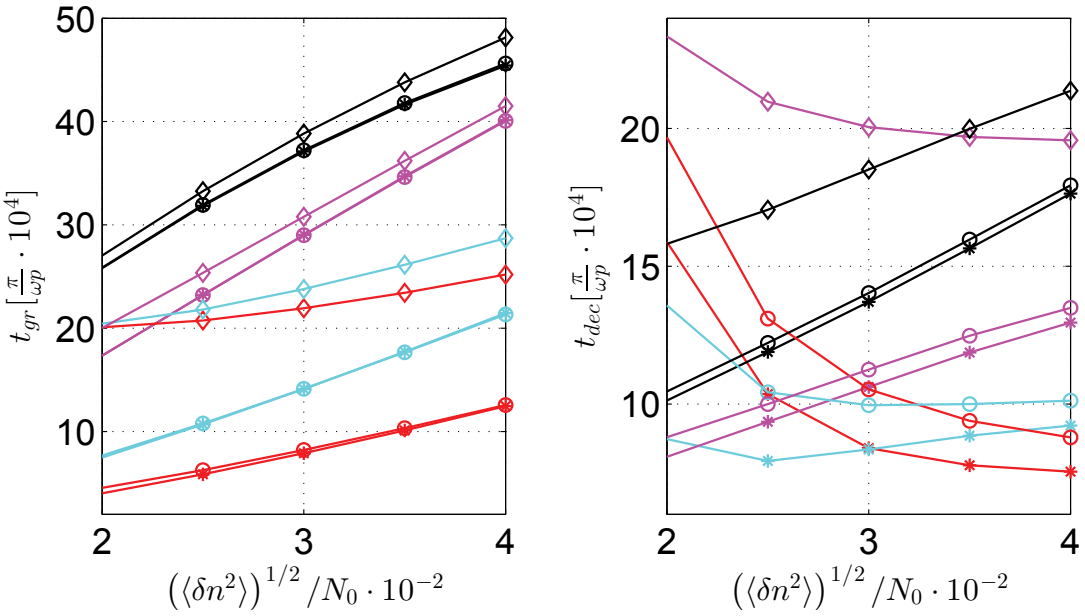

Figure 4.8: A characteristic time for growth, t_{gr}, and a characteristic time for decay, t_{dec}, for the total energy density of waves as a function of the level of the density fluctuation. Different colors correspond to different beam velocities, as follows: $v_b = 10v_t$, red; $v_b = 12v_t$, cyan; $v_b = 16v_t$, magenta; and $v_b = 20v_t$, black. Different marks correspond to various initial thermal dispersions of the beam (the same as for Figure 4.7)

4.7 Evolution of the electron velocity distribution function

In the following section we consider the influence of density fluctuations on dynamics and the evolution of the electron velocity distribution function. First, we compare the process of relaxation for cases with different distributions of the density fluctuations. Figure 4.9 provides snapshots of the electron distribution function, $f(v)$, at different moments of time. Blue curves indicate simulations with density fluctuations described by a Gaussian distribution. Electron distribution functions obtained from simulations employing a non-Gaussian distribution for density irregularities are shown in red.

The top panels of Figure 4.9 provide the results for the relaxation of beams with a beam velocity $v_b = 6v_t$ and an initial thermal dispersion $\Delta v_b = v_t$. The level of density fluctuations is 0.005. The evolution for the total energy density of waves corresponding to this study is presented in the left panel of Figure 4.6. The distribution function shows a behavior typical for a homogeneous plasma: relaxation runs towards lower velocities and stops with plateau formation. Accelerated particles are not observed. As shown, for both the Gaussian and non-Gaussian density fluctuations distributions, the results are very similar.

The middle panels of Figure 4.9 provides the results obtained for beams with a $v_b = 10v_t$, a $\Delta v_b = v_t$, and $(\langle \delta n^2 \rangle)^{1/2}/N_0 = 0.02$. As stated previously, relaxation

mainly evolves toward lower velocities. However, the process of relaxation is slowed as compared to a case with a smaller $(\langle \delta n^2 \rangle)^{1/2}/N_0$. Moreover, the number of particles with velocities larger than the initial v_b significantly increased during the process of relaxation. Energy transfer to energetic particles is possible, due to resonance broadening. In the case with the Gaussian distribution of the density fluctuations the relaxation runs faster than in the case with non-Gaussian distribution. However, at the end of relaxation no substantial difference between the two cases was determined.

Results provided in the bottom panels of Figure 4.9 correspond to simulations with beams having an initial beam velocity $16v_t$ and a thermal velocity v_t. The level of density fluctuations is $(\langle \delta n^2 \rangle)^{1/2}/N_0 = 0.03$. Under such initial conditions, density fluctuations play a very important role in the process of relaxation. Here, two aspects should be emphasized: 1) Even after passing a time above $80 \cdot 10^4 \pi \omega_p^{-1}$, the electron velocity distribution function still contains a region with a small but positive slope. 2) The efficiency of the acceleration mechanism significantly increased: particles with velocities larger than $30v_t$ are seen in the distribution function. As previously mentioned, relaxation runs faster when the Gaussian distribution is used for density fluctuations.

To evaluate the efficiency of the acceleration process, we calculated the energy of accelerated particles, i.e. particles with velocities higher than $v_b + 3\Delta v_b$, at the end of the relaxation process. The left panel of Figure 4.10 provides the ratio of the energy of accelerated electrons, E_a, to the initial energy of the beam, E_{b0}, as a function of the level of density fluctuations. Here, we present results obtained from simulations for beams having different initial beam velocities ($v_b = 6v_t$, $v_b = 10v_t$, and $v_b = 16v_t$) and different thermal dispersions ($\Delta v_b = 0.5v_t$, $\Delta v_b = v_t$, and $\Delta v_b = 3v_t$). An increase in the level of the density fluctuations leads to an increase in the energy of accelerated particles. Under a condition of $(v_t/v_b)^2 \leq (\langle \delta n^2 \rangle)^{1/2}/(3N_0)$, even density fluctuations with a small amplitude cause a significant acceleration for electrons. For instance, for the case of a beam with a beam velocity $v_b = 16v_t$ (shown with magenta curves), the energy of accelerated particles reached a level of approximately 60% of E_{b0}, even for cases for which the level of density fluctuations is quite small (e.g. 0.005). It is worth noting that the increase in initial thermal dispersion of the beam noticeably reduces the efficiency of the acceleration mechanism.

The left panel of Figure 4.10 provides the thermal dispersion, $\langle (v_b - v)^2 \rangle^{1/2}$, of the electron velocity distribution function over the range of velocities $v > v_b$ at the end of relaxation as a function of the level of density fluctuations. As previously mentioned, for slow and wide beams (with $v_b < 10v_t$ and $\Delta v_b > v_t$) the effect of density fluctuations on the acceleration of particles is negligible. For fast beams with beam velocities larger than $10v_t$, the presence of density fluctuations in the plasma results in a significant increase in thermal dispersion at the end of the relaxation process. For instance, a beam that initially has a $\Delta v_b = 0.5v_t$ and a $v_b = 16v_t$ (the magenta line marked with

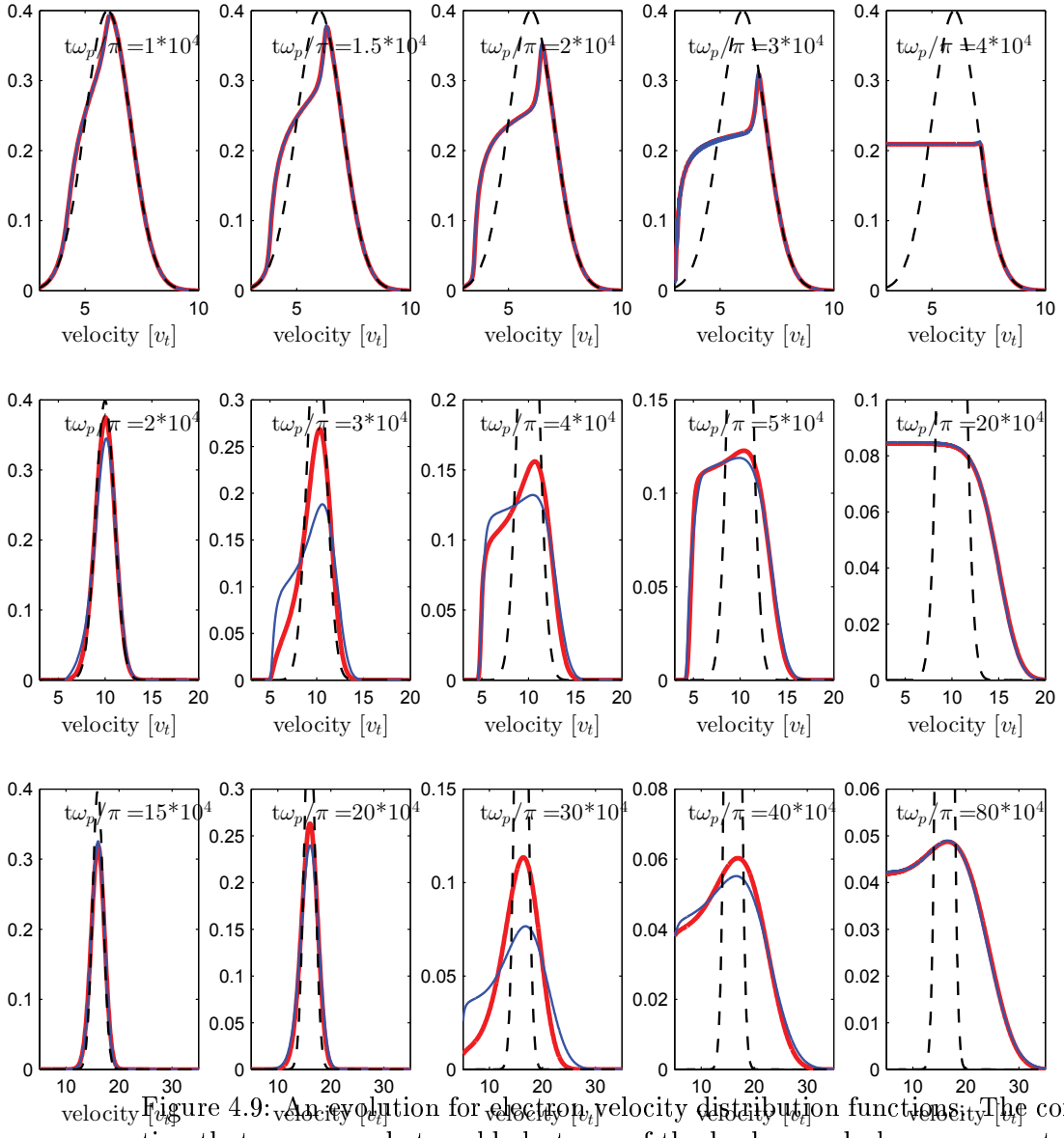

Figure 4.9: An evolution for electron velocity distribution functions. The core distribution that corresponds to cold electrons of the background plasma was not considered. The dimensionless electron distribution function was normalized to one. Each plot provides a snapshot of the electron distribution function at different moments of time. Colors correspond to simulations with various distributions for the density fluctuations, as follows: blue, the Normal distribution and red, the Pearson type II distribution. Results were obtained for various parameters of the beam and levels of the density fluctuation. Up panel: $(\langle \delta n^2 \rangle)^{1/2}/N_0 = 0.005$; $v_b = 6v_t$; and $\Delta v_b = v_t$. Middle panel: $(\langle \delta n^2 \rangle)^{1/2}/N_0 = 0.02$; $v_b = 10v_t$; and $\Delta v_b = v_t$. Bottom panel: $(\langle \delta n^2 \rangle)^{1/2}/N_0 = 0.03$; $v_b = 16v_t$; and $\Delta v_b = v_t$

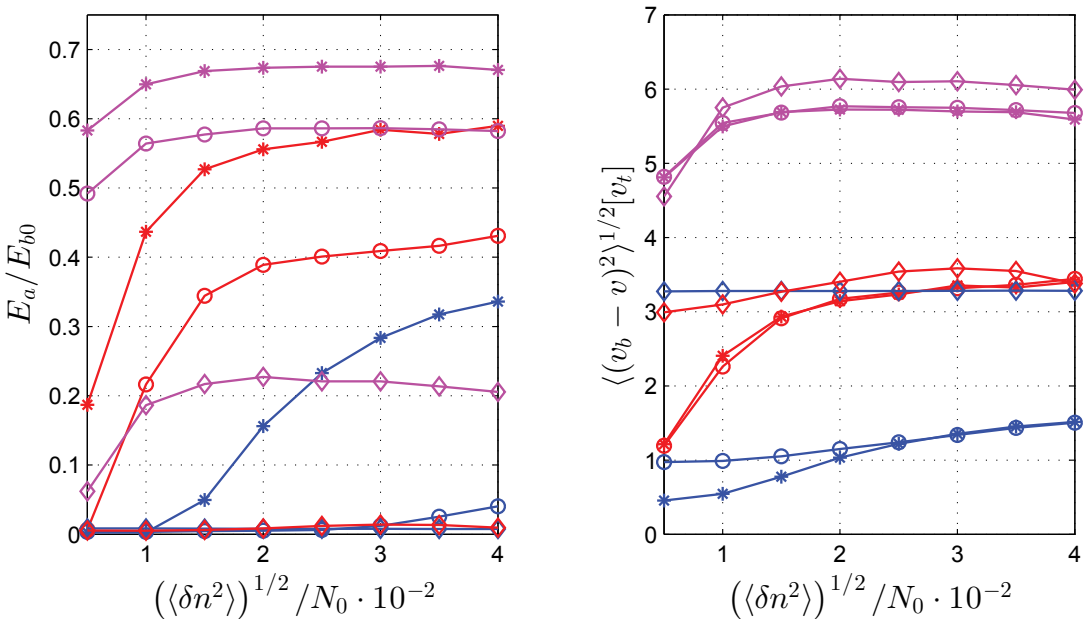

Figure 4.10: The energy, E_a, (left panel) for accelerated particles and the thermal dispersion of the beam at the end of relaxation, $\langle(v_b-v)^2\rangle$, (right panel), as a function of the density fluctuation level. E_{b0} is the initial energy of the beam and the density of the beam electrons. Colors and marks correspond to the various initial beam velocities and the thermal dispersions of the beam (the same as in Figure 4.7).

asterisks) has a thermal dispersion above $5v_t$ once relaxation stopped. As shown, for a condition of $\Delta v_b/v_b \ll (\langle\delta n^2\rangle)^{1/2}/N_0$, no substantial difference was determined in simulations with beams having different initial Δv_b.

4.8 Two stage relaxation

As previously discussed, when the level of density fluctuations is high enough to strongly affect the non-linear dispersion relationship of Langmuir waves, the electron velocity distribution function can preserve a region in velocity space with a positive slope during a period of time above $80\cdot 10^4\pi/\omega_p$. The right panel of Figure 4.11 provides the distribution function at two different moments of time, $t_1 = 10^6\pi/\omega_p$ (marked in blue) and $t_2 = 50\cdot 10^8\pi/\omega_p$ (marked in red). The beam initially had a velocity $v_b = 20v_t$ and a thermal dispersion $\Delta v_b = v_t$. The level of density fluctuations is 0.04. As shown, following the major phase of the relaxation process, instability still occurs at some marginal level and relaxation becoming very slow. As the distribution function evolves to form a plateau, the number of energetic particles increases. However, relaxation occurs very slowly, hundreds of times slower than during the major phase of relaxation. Based on a rough estimate of the growth rate for this "marginal" instability, we concluded that the distribution function is able to maintain a region with a positive gradient even for a time period above $10^{10}\pi/\omega_p$.

After analyzing the data obtained in the simulations using different values of v_b, Δv_b, and $\langle(\langle\delta n^2\rangle)^{1/2}/N_0$, we determined a simple criteria that indicates the end of the active stage: the maximum growth rate of waves $\langle\gamma\rangle$ becomes smaller than $25\cdot 10^{-9}\pi\omega_p$. Therefore, a significant increase in the amplitude of waves in this stage requires a very long time interval (above $\langle\gamma\rangle^{-1}$). It is evident from our results that an important criteria for the applicability of a conventional QL-type relaxation: $\gamma L_c/v_b \gg \Lambda$, where Λ is Coulomb logarithm, is not applicable in this case. As a result, it is difficult to determine whether or not this stage of relaxation can be correctly described by any model because small external factors that we did not take into account could completely change our interpretation.

The left panel of Figure 4.11 provides two examples of distribution functions that satisfy these criteria $\langle\gamma\rangle \leq 25\cdot 10^{-9}\pi\omega_p$. Both results were obtained for a beam with $v_b = 16v_t$ and $\Delta v_b = v_t$. The blue curve indicates the electron velocity distribution function at $t = 40\cdot 10^4\pi/\omega_p$ for a case of $(\langle\delta n^2\rangle)^{1/2}/N_0 = 0.01$. One can see that under a condition of $v_t^2/v_b^2 \geq (\langle\delta n^2\rangle)^{1/2}/(3N_0)$, the first stage of relaxation results in the formation of a plateau in the range of velocities less than v_b. The red curve is $f(v)$ for a case of $(\langle\delta n^2\rangle)^{1/2}/N_0 = 0.04$ at a moment in time of approximately $10^6\pi/\omega_p$. Despite the fact that for both cases the maximum $\langle\gamma\rangle$ is equal, for a case with $(\langle\delta n^2\rangle)^{1/2}/N_0 = 0.04$, the positive slope for $f(v)$ is still clearly seen.

Hereafter, we refer to the time for the major phase of relaxation, namely t_r, as the characteristic time for the active stage of the relaxation process. The left panel of Figure 4.12 provides t_r for beams with different initial v_b and Δv_b as a function of the level of density fluctuations. As shown, beams with a relatively large thermal dispersion, $\Delta v_b/v_b > (\langle\delta n^2\rangle)^{1/2}/N_0$, have a time of relaxation that is longer than more narrow beams. For all of these beams, the characteristic time of relaxation decreases with an increase in $(\langle\delta n^2\rangle)^{1/2}/N_0$. In contrast, for beams that satisfy the condition $\Delta v_b/v_b < (\langle\delta n^2\rangle)^{1/2}/N_0$, t_r is longer in a plasma with a higher level of density fluctuations.

The characteristic often used to describe beam plasma interaction is the length of beam relaxation. To evaluate a characteristic spatial scale for the relaxation process r_s, we first calculate the averaged velocity of the beam, $\langle v(t)\rangle = \langle vf(v,t)\rangle$, as a function of time. We then estimate r_s by integrating the corresponding function $\langle v(t)\rangle$ over t from 0 to t_r. Our results are provided in the right panel of Figure 4.12. As clearly seen, the relaxation scale in the presence of density fluctuations is much larger than for the case of a homogeneous plasma. Even for a relatively slow beam with a $v_b = 10v_t$, the r_s is above $10^6\lambda_D$. For faster beams, with beam velocities larger than $15v_t$, the relaxation scale can reach values of approximately $10^7\lambda_D$ for cases of $(\langle\delta n^2\rangle)^{1/2}/N_0 > 0.02$. However, for all of the cases we considered, the first stage of relaxation finishes on the scale of the order of the Solar radius.

One should note that the second slow stage of the beam relaxation evolved in quite

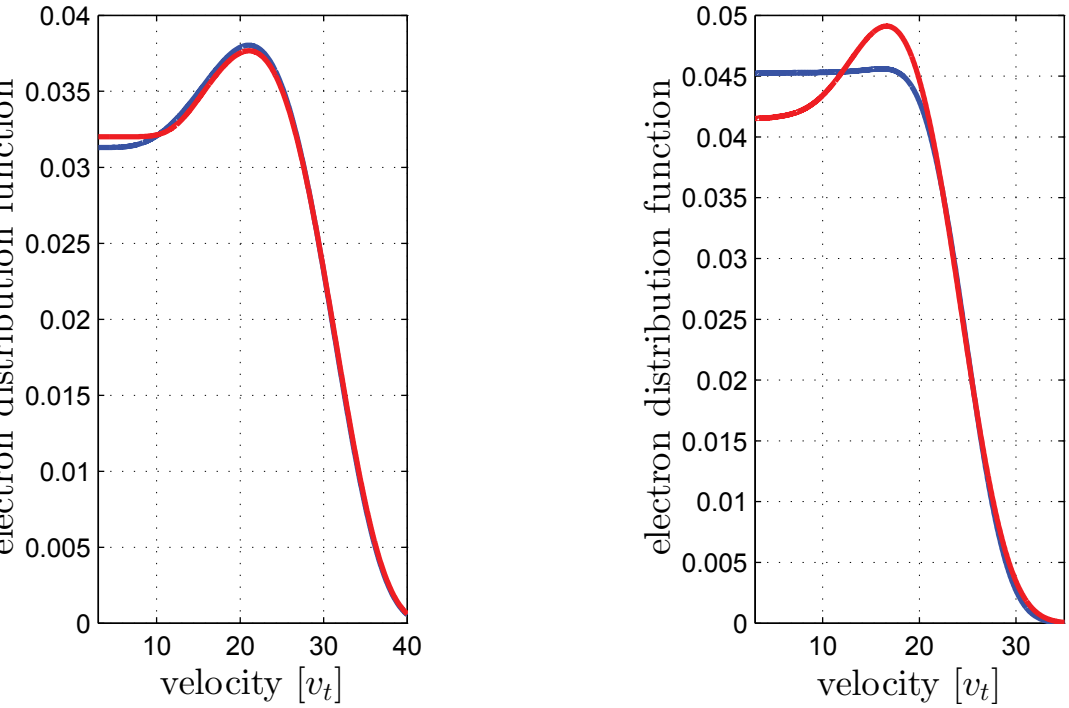

Figure 4.11: Left panel: The results of a simulation with a beam with $v_b = 20v_t$ and $\Delta v_b = v_t$. The level of the density fluctuation, 0.04. The red line indicates the form of the electron distribution function at time $t_1 = 20 \cdot 10^6 \pi/\omega_p$ and the blue line at $t_2 = 50 \cdot 10^9 \pi/\omega_p$. Right panel: Examples of the electron velocity distribution functions at the end of the first stage of the relaxation process. For both $f(v)$ maximum of the $\langle\gamma\rangle$ is approximately $25 \cdot 10^{-9}\omega/\pi$. Initially, the beams have a $v_b = 16v_t$ and a $\Delta v_b = 1v_t$. The blue line corresponds to a simulation with a level of density fluctuations of 0.01; the red line corresponds to a simulation with a $(\langle \delta n^2 \rangle)^{1/2}/N_0 = 0.04$.

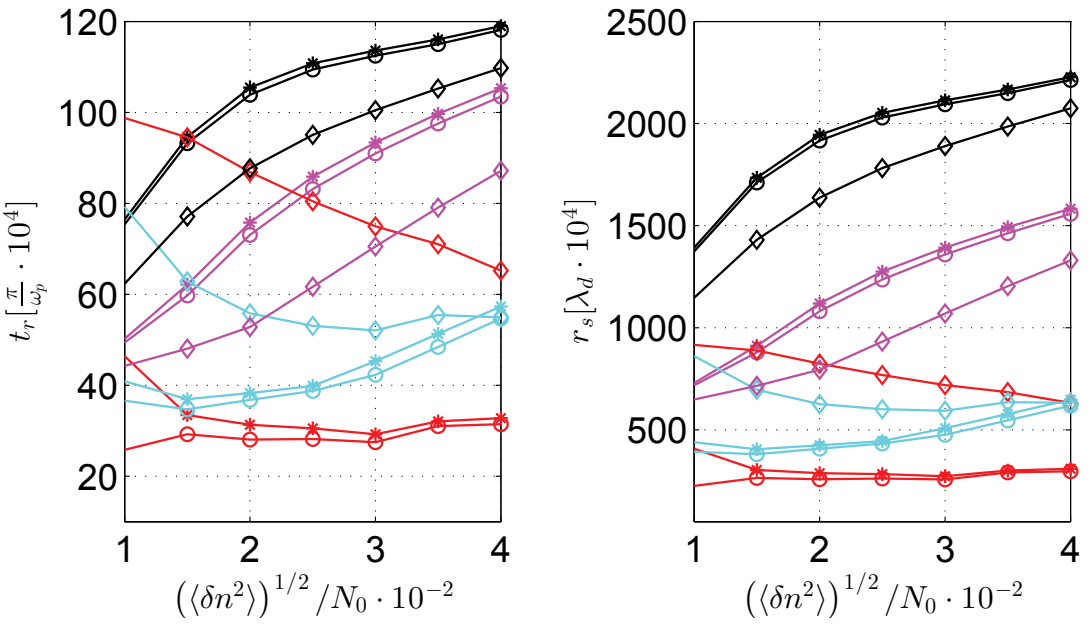

Figure 4.12: A characteristic time for the relaxation, t_r, and a characteristic spatial scale for the relaxation, r_s, as a function of the level of the density fluctuation. Colors and marks correspond to the various initial beam velocities and the thermal dispersions of the beam (the same as in Figure 4.7).

a similar manner to the evolution of beams, as suggested by the SGT. The distribution functions obtained at this stage of the beam plasma interaction are very similar to those observed in the solar wind at large distances from the Sun. One can assume that the complete solution for the famous Sturrock paradox should account for this two-stage process.

4.9 Conclusions

We presented a self-consistent probabilistic model for describing the relaxation of an electron beam in a solar wind with random density irregularities having the same spectral properties as measured onboard satellites and by means of other techniques. We suppose that, the system has several characteristic scales related to the characteristic scale of density fluctuations. On a scale lower than the characteristic scale of density fluctuations, wave-particle interaction can be precisely determined for waves with known parameters: phase, frequency and amplitude. However, on scales sufficiently larger than the characteristic scale of density irregularities, wave and particle dynamics are described by their characteristics averaged over the velocity space, namely, by the growth/damping rate and by the particle diffusion coefficient. The procedure of averaging requires the knowledge of the probability distribution function of wave phase velocities that can be determined from the probability distribution of density fluctuations. To this end, we performed a statistical study of density fluctuations, deduced

from measurements onboard satellites when they were in the solar wind. Our analysis indicates that on spatial scales of approximately $10^2\lambda_D$, the distribution of the fluctuations obeys a Pearson type II distribution. However, deviations from the normal distribution are rather small. The closeness of the density fluctuation distributions results in quite similar probability distribution functions for wave phase velocities. Numerical simulations for the electron beam plasma interaction for both cases of the Gaussian and non-Gaussian distribution does not lead to substantial difference. Thus, one can conclude that the normal distribution of density fluctuations may be used as a good approximation for studies of the beam relaxation in the solar wind.

Applying a model to the system having parameters relevant to typical solar type III events, we determined that depending on v_b^2/v_t^2 and $(\langle\delta n^2\rangle)^{1/2}/N_0$, three different scenarios for the relaxation process can take place:

(1) When the level of density fluctuations is sufficiently low, $(\langle\delta n^2\rangle)^{1/2}/(3N_0) \ll v_t^2/v_b^2$, the beam relaxation and the excitation of Langmuir waves are developed in a manner similar to that of a homogeneous plasma. Relaxation only runs toward lower velocities and after plateau formation there is no energy transfer to accelerated particles. The energy of the waves increases in time until it reaches the saturation level, which is typically above several tens of percent from the initial energy of the beam.

(2) $(\langle\delta n^2\rangle)^{1/2}/N_0 \sim v_t^2/v_b^2$- corresponding to the intermediate regime. The density fluctuations are high enough to impact the non-linear dispersion relationship of Langmuir waves and to cause absorption of the waves by particles from the tail of the electron velocity distribution function. As a result, the energy of waves decays after reaching a maximum value. The wave decrease is accompanied by an increase in the number of energetic particles.

(3) $(\langle\delta n^2\rangle)^{1/2}/N_0 \gg v_t^2/v_b^2$ - the presence of density fluctuations strongly slows down beam relaxation. Resonant broadening allows a wave generated with a phase velocity, V, to interact resonantly with particles having velocities v_p smaller and larger than V, even with particles having much larger velocities. As a result, the saturation level of the wave energy is significantly reduced. The energy of waves at the end of relaxation can be five times less than the maximum value achieved during the relaxation process. The energy transfer from slow particles with velocities $v < v_b$ to energetic particles with velocities larger than v_b is very effective. The energy transferred to accelerated particles can reach levels up to 60% of the initial energy of the beam.

Thus, we conclude that even small amplitude density irregularities with spatial scales in the range of $10^3\lambda_D - 10^4\lambda_D$ play an important role in the process of the relaxation of solar energetic beams with beam velocities larger than $15v_t$. The results are in a good agreement with results obtained using computer simulations in the framework of a Hamiltonian description for beam-plasma interaction in the presence of random density fluctuations [Krafft et al., 2013].

Our study revealed very important characteristics for the beam plasma interaction for very energetic beams with beam velocities above $15v_t$. For these beams, the relaxation takes place in two stages process. The first stage has a relatively short duration, with characteristic time, t_r, typically below $10^7\pi/\omega_p$. This stage is characterized by an effective energy exchange between Langmuir waves and beam electrons. At the end of the first stage the system achieves a quasi-stable state. Despite the fact that the electron distribution function preserves a region with a positive gradient, the averaged growth rate for waves is close to zero, however, it keeps a small positive value over a very long time period. Even for very fast beams with beam velocities of approximately $20v_t$, the characteristic spatial scale of the first stage of relaxation is approximately $20 \cdot 10^7\lambda_D$, indicating that this stage takes place in the solar corona. However, as shown in our simulations, the second stage of relaxation is at least 500 times longer. Thus, one can expect that the electron distribution function will have a positive slope at distances up to several AU. This two stage process can explain the Sturrock paradox, observations of weak beams and, associated with them, wave activity at distances from the Sun up to 5 AU. This result also indicates that beams can only be registered by very capable particle instruments, and provides an explanation as to why there are so few direct observations of the positive slope of the electron distribution function onboard satellites [Anderson et al., 1981, Lin et al., 1981, Fuselier et al., 1985].

4.10 Resume in French

Nous avons présenté un modèle probabiliste auto cohérent pour décrire là relaxation d'un faisceau d'électrons dans un vent solaire rempli par les fluctuations aléatoires de la densité ayant les mêmes propriétés spectrales, que celles mesurées à bord de satellites et en utilisant d'autres techniques. On suppose que, le système possède plusieurs échelles caractéristiques liées à l'échelle caractéristique des fluctuations de la densité. En échelle inférieure à l'échelle caractéristique des fluctuations de la densité, l'interaction onde- particule peut être décrite avec une précision si des paramètres d'onde sont connus: notamment, la phase, la fréquence et l'amplitude. Cependant, sur des échelles suffisamment plus grandes que l'échelle caractéristique des irrégularités de la densité, l'interaction des ondes et de particules ne peut être déterminé que par leurs caractéristiques moyennes dans l'espace des vitesses, à savoir, par le taux de croissance/ amortissement et par le coefficient de diffusion des particules. La procédure d'évaluation de moyenne nécessite la connaissance de la fonction de distribution de densité de probabilité de vitesses de phase d'ondes de qui peut être déterminée à partir de la distribution de la densité de probabilité des fluctuations de densité électronique. À cette fin, nous avons réalisé une étude statistique des fluctuations de densité, déduite de mesures à bord des satellites quand ils étaient dans le vent solaire. Notre analyse indique que sur les échelles spatiale d'environ $10^2\lambda_D$, la distribution des fluctuations obéit à la distribution

de Pearson de type II. Cependant, les écarts entre cette distribution et la distribution normale sont plutôt assez petits. La proximité de deux distributions de fluctuations de la densité électronique se traduit en similarité assez proche de fonctions de distribution de probabilités des vitesses de phase d'ondes. Des simulations numériques décrivant l'interaction d'un faisceau d'électrons avec un plasma pour les deux cas, celui d'une distribution Gaussienne et celui d'une distribution non-Gaussienne, ne démontrent pas de différence importante. Ainsi, on peut conclure que la distribution normale des fluctuations de la densité électronique peut être utilisée comme une bonne approximation pour l'étude de la relaxation de faisceau dans le vent solaire.

En appliquant un modèle utilisant des paramètres semblables à ceux des domaines de sources des émissions radio solaires de Type III, nous avons déterminé que selon le rapport entre v_b^2/v_t^2 et $(\langle \delta n^2 \rangle)^{1/2}/N_0$ trois scénarios différents pour le processus de relaxation peuvent avoir lieu:

(1) $(\langle \delta n^2 \rangle)^{1/2}/(3N_0) \ll v_t^2/v_b^2$ - lorsque le niveau des fluctuations de densité est suffisamment faible, la relaxation du faisceau et l'excitation des ondes de Langmuir se développent de façon très semblable au cas d'un plasma homogène. La relaxation et formation du plateau se développent seulement pour des vitesses inférieures à la vitesse du faisceau; après la formation du plateau, il n'y à plus d'énergie transférée aux particules accélérées. L'énergie des ondes augmente jusqu'à atteindre le niveau de saturation, qui est typiquement de l'ordre de quelques dizaines de pourcent de l'énergie initiale du faisceau.

(2) $(\langle \delta n^2 \rangle)^{1/2}/N_0 \sim v_t^2/v_b^2$- corresponde au régime intermédiaire. Les fluctuations de densité sont suffisamment élevées pour avoir une influence sur la relation de dispersion non linéaire des ondes de Langmuir. Ceci provoque l'absorption des ondes par des particules appartenant à la queue de la distribution de vitesses électroniques. En conséquence, l'énergie des ondes décroît après avoir atteint une valeur maximale. La baisse de l'énergie d'ondes est accompagnée par une augmentation de nombre de particules énergétiques.

(3) $(\langle \delta n^2 \rangle)^{1/2}/N_0 \gg v_t^2/v_b^2$ - la présence des fluctuations de densité ralentit fortement le processus de relaxation du faisceau. L'élargissement du domaine de résonance permet à une onde générée avec une vitesse de phase, V, d'entrer en résonance avec des particules possédant des vitesses $v_p \leq V$ aussi bien qu'avec des particules beaucoup plus rapides. En conséquence, le niveau de saturation de l'énergie des ondes est réduit de manière très significative. L'énergie des ondes à la fin de la relaxation peut être cinq fois inférieure à la valeur maximale atteinte pendant le processus de relaxation. Le transfert d'énergie à partir de particules lentes possédant des vitesses $v < v_b$ vers les particules énergétiques de vitesse $v \gg v_b$ est très efficace. L'énergie transférée aux particules accélérées peut atteindre des niveaux allant jusqu'à 60% de l'énergie initiale du faisceau.

Ainsi, nous concluons que même des irrégularités de densité de faible amplitude à des échelles spatiales comprises entre $10^3\lambda_D$ et $10^4\lambda_D$, jouent un rôle très important dans le processus de relaxation des faisceaux de particules énergétiques solaires ayant des vitesses supérieures à $15v_t$. Ces résultats sont en bon accord avec les résultats obtenus en utilisant des simulations numériques utilisant une description Hamiltonienne de l'interaction d'un faisceau avec un plasma en présence des fluctuations de densité aléatoire [Krafft et al., 2013].

Notre étude a révélé les caractéristiques d'interaction d'un faisceau avec un plasma pour des faisceaux très énergétiques ayant des vitesses supérieures à $15v_t$. Pour ces faisceaux, la relaxation se développe en deux étapes. La première étape a une durée relativement courte, avec un temps caractéristique, t_r, typiquement inférieur à $10^7\pi/\omega_p$. Cette phase est caractérisée par un échange d'énergie très efficace entre les ondes de Langmuir et les électrons du faisceau. À la fin de la première étape, le système atteint un état quasi stable. La fonction de distribution des électrons conserve malgré tout une région possédant un gradient positif dans l'espace des vitesses, mais le taux de croissance moyen pour les ondes est assez proche de zéro. Cette petite valeur positive est cependant gardée pendant une période de temps très longue. Même pour des faisceaux très rapides avec des vitesses de l'ordre de $20v_t$, l'échelle spatiale caractéristique de la première étape de relaxation est environ de $20 \cdot 10^7\lambda_D$, ce qui indique que cette étape a plutôt lieu dans la couronne solaire. Cependant, comme les simulations l'indiquent, la seconde étape de relaxation est au moins 500 fois plus longue. Ainsi, on peut s'attendre à ce que la fonction de distribution des électrons ait une pente positive à des distances allant jusqu'à plusieurs AU. Ce processus en deux étapes peut expliquer le paradoxe de Sturrock, c'est à dire, l'observation de faibles faisceaux d'électrons et d'activité des ondes associées jusqu'à des distances d'environ 5 AU. Ce résultat indique également que les pentes positives de la fonction de distribution des électrons ne peuvent être mesurées que par des instruments assez sensible. Ceci explique pourquoi il y a peu d'observations directes de la pente positive de la fonction de distribution des électrons à bord de satellites [Anderson et al., 1981, Lin et al., 1981, Fuselier et al., 1985].

Chapter 5

Langmuir waves in the fluctuating solar wind

5.1 Introduction

The Langmuir waves have been the object of intensive studies in the solar wind, within the Earth's electron foreshock, and in the vicinity of other planetary shocks over the last 6 decades. From the very beginning it was pointed out that plasma waves are clumped into spikes with peak amplitudes typically three orders of magnitude above the mean. Smith and Sime [1979] proposed the explanation of the clumping phenomenon based on the idea that the plasma is inhomogeneous, and in most regions where the beam could excite the waves the characteristic scale of the inhomogeneity is comparable with the spatial growth rate. Based on this idea Robinson [1992], proposed the model that describes interaction of the electron beam with Langmuir waves in such inhomogeneous plasma. The beam propagates alternately through the regions where the wave growth rate is alternately positive and negative, and as a result of interaction of the beam with the waves, the slope of the electron distribution function oscillates close to the level of marginal stability. In turns, the resulting wave's growth rate has a form of the random walk in logarithm of the wave energy density with an upper boundary approximately equal to kinetic energy density of the beam. The proposed model allowed to explain observed clumping phenomenon as well as made prediction regarding the probability distribution of the magnitudes of the clumps. Due to the central limit theorem, the Stochastic Growth theory predicts the log-normal distribution of the amplitudes of the electric field of the Langmuir wave envelopes obeys the log-normal distribution.

Event studies using different experimental data registered onboard various spacecraft and in laboratory plasma [Cairns and Robinson, 1999, Cairns and Menietti, 2001, Austin et al., 2007] found the distribution of the amplitudes close to the log-normal. However, different non-linear physical process, such as electrostatic decay of the Langmuir waves, or other, result in deviation of the distribution from the log-norma. Recently, Krasnoselskikh et al. [2007], proposed the model that describes the linear in-

teraction of Langmuir wave packets with an electron beam and takes into account two important effects caused by the density irregularities, namely the angular diffusion of the wave vector due to wave scattering on small-amplitude density fluctuations, and suppression of the instability caused by the removal of the wave from the resonance with particles during crossing density perturbations of relatively large amplitude. The authors showed that distributions for the logarithm of wave intensity can belong to Pearson type IV rather than normal under some circumstances. The main reason for deviations of distributions from the normal is that the effective number of regions where the waves grow is not very large and, as a consequence, the central limit theorem fails to be true.

The aim of the following chapter is to study the properties of the Langmuir waves in the fluctuating solar wind by making use the numerical model based on the Hamiltonian description of the beam-plasma interaction. The Hamiltonian models describing the self-consistent wave-particle and wave-wave interactions in homogeneous or inhomogeneous magnetized plasmas. Various physical problems could be efficiently studied by such methods, concerning nonlinear and turbulent stages of different instabilities of electron or ion distributions, wave-particle interactions at multiple resonances, quasi-linear diffusion processes of particles on waves due to wave particle interaction, wave turbulence in randomly inhomogeneous plasmas, wave focusing, scattering, reflection and decay [Krafft et al., 2015]. Recently, [Volokitin et al., 2013, Krafft et al., 2013, 2014, 2015] the self-consistent model was used for the problem of the resonant interaction of an electron beam with Langmuir wave packets in plasma with density fluctuations under conditions close to the typical solar type III bursts region. Comparison of the wave-form of the Langmuir obtained in the simulations with recent measurements by the STEREO and WIND satellites shows that their characteristic features are very similar [Krafft et al., 2014]. In the following chapter we perform the study of the distributions of the amplitudes of the Langmuir obtained from our probabilistic model and from the Hamiltonian model as well.

5.2 Stochastic growth theory

The Stochastic Growth theory (SGT) was developed to describe origin of the clumping of the Lungmuir waves in the source region of the type III solar radio bursts. An important consequence of the SGT is prediction of the statistical distribution of the amplitudes of the electric field in the clumps. The predicted log-normal distribution was found in different experimental data registered onboard various spacecraft and in laboratory plasma. In the following section we present a brief description of the basics of SGT following the original papers [Robinson, 1992, Robinson et al., 1993, Robinson, 1995, Cairns and Robinson, 1999].

Initial problem treated in the model was related to the scattering of the Langmuir

waves by the density fluctuations. The fluctuations in the solar wind have been inferred to scatter the beam-driven Langmuir waves out of the resonance with the beam at the typical rate of $\leq 10s^{-1}$, while the largest growth rate for observed beams are approximately of the order of $\leq 1s^{-1}$. Thus, for these reasons the waves cannot grow uniformly in the space. The authors showed that the observed time-averaged growth rates can overcome $10s^{-1}$ in localized clumps with spatial scale of approximately 100km. The authors argued that at least in the regions where scattering is not too large, the beam-driven growth rate can overcome the refraction of waves out from the growth region in the velocity space.

The stochastic-growth model considers the beam propagating in the state close to the marginal stability, predicted by QL theory. The beam passing through the type III source releases part of it's free energy to the energy of the Langmuir waves due to the beam plasma instability, that results in plateau formation on the electron distribution function within some range of the velocities. However, between the interactions with intensive clumps, the positive slope can be recovered because of the advection, which transforms spatial gradients into velocity gradients as the electrons propagate [Grognard, 1982, Melrose and Goldman, 1987, Robinson et al., 1993].

The presence of the density fluctuations affects the waves, allowing them to grow effectively only in the certain clumps, while other clumps of waves corresponding to unfavorable density fluctuations are damped. This, in turn, results in perturbation of the beam (in the sense of spatial inhomogeneities in the electrons distribution function) about its averaged state of the marginal stability on the time scales determined by the characteristic time scales of the change of density fluctuations. These inhomogeneities provide the fluctuations of the growth rate of the Langmuir waves, while the averaged growth rate is close to zero. Under such consideration the growth rate of the waves in a given clump (with characteristic spatial scale of the order of characteristic scales of the density fluctuations) undergo a random walk until either the waves leave the clump or the wave growth rate saturates via non-linear processes. The characteristic time of the interaction, t_g, can be obtained as l/v_g, where l is the clump size and v_g is the group velocity of the Langmuir waves (in the terms of the thermal velocity of the background electrons, v_t, and beam velocity, v_b, $v_g = 3v_t^2/v_b$). During a time t_g, the beam propagating at velocity v_b can propagate over a distance up to $v_b t_g$ and traverse $v_b t_g/\langle l \rangle$ clumps in transit, where $\langle l \rangle$ is a mean clump size. The authors assume that the ion-sound waves responsible for the density inhomogeneities in the solar wind, and thus the characteristic lifetime of the clumps can be estimated as $t_s = \langle l \rangle / c_s$, where c_s is the typical ion-sound speed. This estimation indicates that a typical clump forms and disperses $\langle t_g \rangle / t_s$ times near a particular location during time t_g. Each formation and dispersal of clump results in appearance of a corresponding inhomogeneities in the part of the beam that interacts with given clump during t_g. The total number of

inhomogeneities on the electron distribution function was obtained as:

$$n_g(l) = \frac{v_g t_g}{\langle l \rangle} \frac{\langle t_g \rangle}{t_s} = \frac{v_b c_s l}{\langle l \rangle v_g^2} \tag{5.1}$$

It is worth noting that for the typical solar wind conditions, $n_g \gg 1$. During the time $t < t_g$ the total number if inhomogeneities that pass trough the clump can be estimated as:

$$n_i(t) = \frac{n_g t}{t_g} = \frac{t}{t_i} \tag{5.2}$$

where t_i is $(\langle l \rangle v_g)/(c_s v_b)$.

The solution of the Liouville equation for the spectral energy density of the Langmuir waves packet, W_s, can be obtained as follows:

$$W_s(t) = W_s(t_0) \exp(G) \tag{5.3}$$

where $W_s(t)$ and $W_s(t_0)$ are the spectral energy density at the moments of time t and t_0, respectively, and G is the total growth of the wave during the time $t - t_0$. The total growth of a given group of Langmuir waves is a sum over individual increments $\Delta G_i = \gamma_i t_i$ as the waves are encountered by each inhomogeneity of the beam

$$G = \sum_i \Delta G_i \tag{5.4}$$

where γ_i is the growth rate provided by single inhomogeneity and varies between inhomogeneities. The mean and variance of G are thus related to corresponding quantities of ΔG as:

$$\langle G \rangle = \langle \Delta G \rangle n_i(t) = \langle \gamma \rangle t, \tag{5.5}$$

$$\sigma^2(G) = \sigma^2(\Delta G) n_i(t) = \sigma^2(\gamma) t_i t, \tag{5.6}$$

for time $t < t_g$ and:

$$\langle G \rangle = \langle \Delta G \rangle n_g = \frac{\langle \gamma \rangle l}{v_g}, \tag{5.7}$$

$$\sigma^2(G) = \sigma^2(\Delta G) n_g = \frac{\sigma^2(\gamma) l^2}{v_b v_g}, \tag{5.8}$$

for $t = t_g$.

In the terms of $\langle G \rangle$ and $\sigma(G)$, the spatially averaged probability distribution function of G can approximately defined as follows:

$$P(G) = \frac{1}{\sqrt{2\pi\sigma^2(G)}} \exp\left(-\frac{(G - \langle G \rangle)^2}{2\sigma^2(G)}\right), \tag{5.9}$$

via central limit theorem (since $n_g \gg 1$). Thus, by making use of solution 5.3 and equations 5.5 and 5.6 one can obtain following equation:

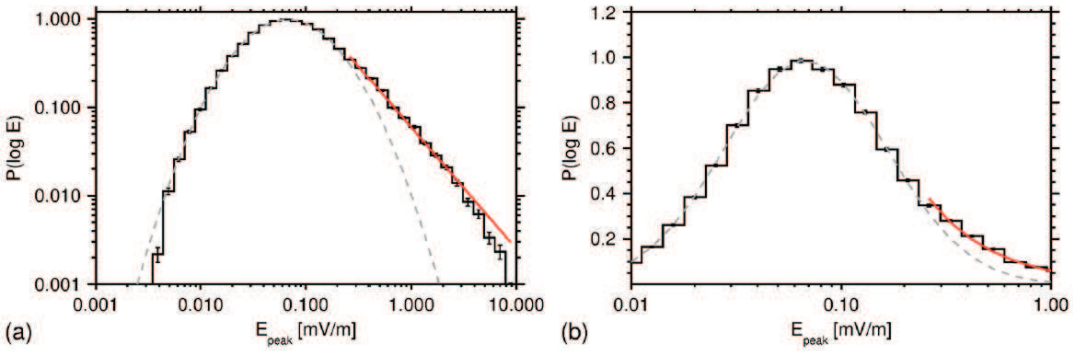

Figure 5.1: Probability distribution of wave amplitude for the electric field of the selected waveform observed by Cassini WBR (Wideband Receiver). The gray dashed line represent a fit of log-normal distributions. The red line shows the high amplitude fit (from 0.25 to $1mV/m$) with a power low exponent. a) Overall amplitude distribution using log-log scale. b) Detail of distribution function for amplitudes between 0.001 and $0.1mV/v$ using a linear scale [from Píša et al., 2015].

$$\langle W(t)\rangle = exp([\langle\gamma\rangle + \frac{1}{2}\sigma^2(\gamma)t_i]t) \tag{5.10}$$

for $t < t_g$ [Robinson, 1992]. The effective growth rate of the waves, Γ_{eff}, was defined by the authors as:

$$\Gamma_{eff} = \langle\gamma\rangle + \frac{1}{2}\sigma^2(\gamma)t_i \tag{5.11}$$

This result allows one to resolve the paradox of wave growth despite that the mean growth rate $\langle\gamma\rangle$ is negative because the Γ_{eff} can be positive even for $\langle\gamma\rangle < 0$. Another important result was obtained by taking into account that solution 5.3 leads to following relation between G and amplitude of the waves electric filed: $G = 2\ln(E/E_0)$ and thus the distribution of the waves amplitudes should obeys the log-normal distribution:

$$P\left[\ln\left(\frac{E}{E_0}\right)\right] = \frac{1}{\sqrt{2\pi\sigma(G)}}\exp\left(-\frac{[2\ln(E/E_0) - \langle G\rangle]^2}{2\sigma^2(G)}\right) \tag{5.12}$$

Therefore the SGT predicts a parabolic profile for $\ln P(\ln E)$ when it plotted as function of $\ln E$. This theoretical prediction is in the good agreement with observations of the Lagmuir waves amplitudes in the Earth's foreshock [Cairns and Robinson, 1999] and polar cap region [Cairns and Menietti, 2001]. For instance, Figure 5.1 provides the evidence of the log-normal observed inside the Saturn's foreshock by the Cassini spacecraft [from Píša et al., 2015]. One can see that deviation of the distribution from the log-normal for amplitudes $> 0.25mV/m$ are rather large. The power low exponent distribution at the high amplitudes was explained by aggregated distribution, as a result of a combination of many log-normal distributions for spatially limited regions [Boshuizen et al., 2001].

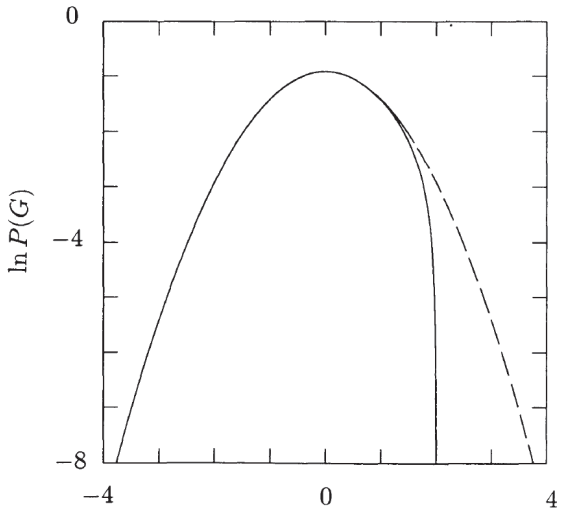

Figure 5.2: Theoretical distribution $P(G)$ with and without the presence of a three-wave decay threshold as given by equations 5.9 and 5.14, solid and dashed curves respectively [from Robinson et al., 1993].

The SGT was refined to take into account the non-linear wave-wave interaction [Lin et al., 1986, Robinson et al., 1993]. If the highest wave levels saturate via three-wave decay (or via some other non-linear process) the distribution of G will fall rapidly beyond the point G_c corresponding to the the threshold magnitude of the electric field E_c for decay. Dynamically, the energy density of the waves that reached the threshold rapidly decreases as product waves are generated, falling to an asymptotic level that is exponentially decreasing function of the extent to which the threshold was exceeded. The authors approximated the threshold as an absorbing boundary and solved the the diffusion problem in G for the half-interval $G < G_c$ in order to calculate $P(G)$. After normalization to unit the probability function $P(G)$ was obtained as follows:

$$P(G) = \left[\sqrt{2\pi\sigma^2(G)}Erf\left(\frac{G_c - \langle G\rangle}{\sqrt{2}\sigma(G)}\right)\right]^{-1} \times \left[\exp\left(-\frac{(G-\langle G\rangle)^2}{2\sigma^2(G)}\right) - \exp\left(-\frac{(2G_c - \langle G\rangle - G)^2}{2\sigma^2(G)}\right)\right] \tag{5.13}$$

for $G < G_c$ and $P(G) = 0$ for $G > G_c$. Figure 5.2 shows the distributions 5.9 and 5.14 and illustrates the effect of the three-wave decay process.

5.3 Statistical properties of the small-amplitude Langmuir waves in the plasma with density fluctuations.

Recently, the model that describes the linear interaction of Langmuir wave packets with the electron beam and takes into account the angular diffusion of the wave vector

due to the wave scattering on the small-amplitude density fluctuations, as well as a suppression of the instability caused by the removal of the wave from the resonance with particles during crossing density fluctuations with large amplitudes was proposed by Krasnoselskikh et al. [2007]. The authors used the Pearson technique to classify the distributions of the wave spectral energy density obtained from the numerical modeling. They argued that under certain circumstances the effective number of the of the regions where the waves can grow effectively is not very large, and thus the central limit theorem fails to be true. For this cases the distribution of the logarithm of the wave energy density corresponds rather to Pearson type IV distributions rather than normal. In the following section we briefly describe main ideas and results of the original paper [Krasnoselskikh et al., 2007].

The model considers to effects related to the density inhomogeneity on the interaction of the electron beam with Langmuir waves, namely: the angular diffusion of the waves and removal the wave from the resonance with the beam. Depending on their magnitude the fluctuations are involved in one of these processes. The first process is caused by a small-amplitude fluctuations, with amplitudes, Δn, that satisfy conditions:

$$\Delta n/N_0 \ll 3kT/(m\omega_{pe}^2), \tag{5.14}$$

where T is electron temperature and k is Boltzmann constant. The second effect is provided by the large-amplitude fluctuations, with amplitudes, ΔN, that satisfy inequality:

$$\Delta N/N_0 \leq 3kT/(m\omega_{pe}^2), \tag{5.15}$$

In other words the wave vector can be changed significantly during crossing of such inhomogeneities but the inhomogeneities are not large enough to reflect the packet backward.

If the typical wave numbers q and Q, corresponding to the fluctuations of the first and the second type, respectively, are relatively large as compared with wavelength of the Langmuir waves:

$$Q < \Gamma/v_g \ll q \ll k \tag{5.16}$$

where Γ is the growth rate, v_g is the group velocity of the wave packet, and k is a typical wave number of Langmuir waves, the waves spectral energy density, W_s, can be performed as averaged in time and space on the characteristic intervals Δt and Δr that satisfy the conditions:

$$1/(qv_g) \ll \Delta t \ll 1/\Gamma, 1/(Qv_g) \tag{5.17}$$

and

$$1/q \ll \Delta r \ll v_g/\Gamma, 1/(Q) \tag{5.18}$$

For this case, the evolution of the averaged wave spectral energy density can be describe by the Fokker-Plank equations, where the diffusion process due to the small-amplitude fluctuations is considered as a stochastic process, while the interaction of the wave packet with each large-amplitude density disturbances is considered in deterministic approach. As it was shown in [Krasnoselskikh et al., 2007] the equations can be written as follows:

$$\frac{\partial W_s}{\partial t} + (\vec{v_g} \cdot \nabla) W_s = \Delta D W_s + \Gamma W_s. \tag{5.19}$$

It is worth noting that when the effect of the diffusion is negligible and some inhomogeneities are large enough to provide reflection of the wave packet backward, the amplitude of the waves can also change due to the variations of the group velocity. Such a picture corresponds to a WKB solution that can be written as:

$$W_s(t, \vec{r}) = \frac{W_0}{\sqrt{k_n}} \exp\left(-i\omega t + i \int \vec{k} d\vec{r}\right), \tag{5.20}$$

where $\vec{k}$ is a complex wave vector describing variations in both the wave phase and amplitude, and k_n is a component of the wave vector perpendicular to the surface of the inhomogeneity.

The simplified stationary state problem was considered by Krasnoselskikh et al. [2007], when the Langmuir waves enter the half space $x > 0$ occupied by unstable nonuniform plasmas, and both the plasma parameters and the solutions of equation 5.19 depend only on the coordinate, x, and do not depend on time. The spatial evolution of the wave packet can be described by following equation:

$$v_g \cos(\theta) \frac{\partial W_s}{\partial x} = \frac{1}{\sin(\theta)} \frac{\partial}{\partial \theta} \left(D \sin(\theta) \frac{\partial W_s}{\partial \theta} \right) + \Gamma W_s, \tag{5.21}$$

where $\Gamma(x, k, \theta)$ is effective growth/damping rate, θ is an angle between the axis x and wave vector, and $D(x, k, \theta)$ is a diffusion coefficient that describes the effect of the small-amplitude fluctuations.

To study the effects of different types of fluctuations on the behavior of the wave packet it is convenient to introduce dimensionless quantities $\delta_1 = \Gamma/D$ and $\delta_2 = \Gamma \Delta x / v_g$, where Δx is a characteristic length. The second quantity describes the spatial growth rate for the case when the effect of angular diffusion is negligible. For $\theta = 0$, the spatial growth rate $\Gamma(x, 0)$ stays approximately constant over the distance Δx, and the wave spectral energy density at the points x_1 and x_2 spaced apart by Δx, differs by a factor of δ_2, i.e.,

$$\delta_2 = \Delta x \frac{\Delta \ln W_s}{\Delta x}|_{D=0}. \tag{5.22}$$

Thus to evaluate the relative contribution of the growth/daping rate with respect to diffusion it is convenient to consider a ratio

$$R = \Delta x \frac{\Delta \ln W_s}{\Delta x} \Big/ \delta_2 \tag{5.23}$$

which can be introduced both for the spectral energy density $W_s(x, \theta)$ and for the total wave energy density,

$$W_{tot} = 2\pi \int_0^\pi W_s(x, \theta) \sin\theta d\theta, \tag{5.24}$$

if the dependencies of $W_s(x, \theta)$ and $W_{tot}(x)$ on the distance Δx are approximately exponential. For this case the growth rate depends only on θ and can be describe for instance as follows [Krassnoselskikh et all 2007]:

$$\frac{\Gamma(x, \theta)}{\Gamma_{max}} = -0.1 + 1.1 \exp\left[-\frac{1}{2}\left(\frac{\theta}{\Delta\theta}\right)^2\right]. \tag{5.25}$$

The result of numerical solutions of the equation 5.21 with the growth rate profile 5.25 obtained by Krasnoselskikh et al. [2007] are shown in Figure 5.3 for the case of $\Delta\theta = \pi/10$. From the top panel it is clearly seen that when diffusion process dominates (small ratios of Γ_{max}/D), the growth rate does not depend on θ, and thus the spectra should be isotropic. However, the anisotropy of the spectra becomes apparent as ratio Γ_{max}/D increases. When it reached a threshold value, the regions of k space with the positive growth rate appear and the instability develops. It is worth noting that even for large value of the ratio Γ_{max}/D (20 for instance) the growth rate of the instability is sufficiently smaller than that without diffusion. To illustrate the dependence of the isotropy of the spectra on the ration Γ_{max}/D the authors defined the angular half width of the spectra, $\Delta\theta_{fin}$, at the end of the simulation box, $x = x_{max}$. The results are presented at the right panel of Figure 5.3. As already mentioned, the spectra is quasi-isotopic for the small ratios Γ_{max}/D and becomes more narrowed for larger values of this ratio.

The large-amplitude fluctuations in the plasma result in change in the direction of the wave vector of the wave packet and in it's absolute value. For this case the equation 5.21 should be replaced by a more general one. However, as it was shown in [Krasnoselskikh et al., 2007], some qualitative aspects of the problem could be studied by making use of the equation 5.21, for the case when the spatial variation of the growth rate are incorporated to take into account the effects of removing of the waves out from the resonance with the driven beam as a result of crossing the inhomogeneity:

$$\frac{\Gamma(x, \theta)}{\Gamma_{max}} = -0.1 + 1.1 \exp - \left[\frac{1}{2}\left(\frac{\theta}{\Delta\theta}\right)^2\right] \exp - \left[\frac{1}{2}\left(\frac{x - x_0}{\Delta x}\right)^2\right], \tag{5.26}$$

where Δx is a characteristic scale of the inhomogeneity. The results obtained from the numerical simulation of the equation 5.21 with the growth rate given by 5.26 are shown in Figure 5.4. By comparing the panels (a) and (b) the authors concluded that the

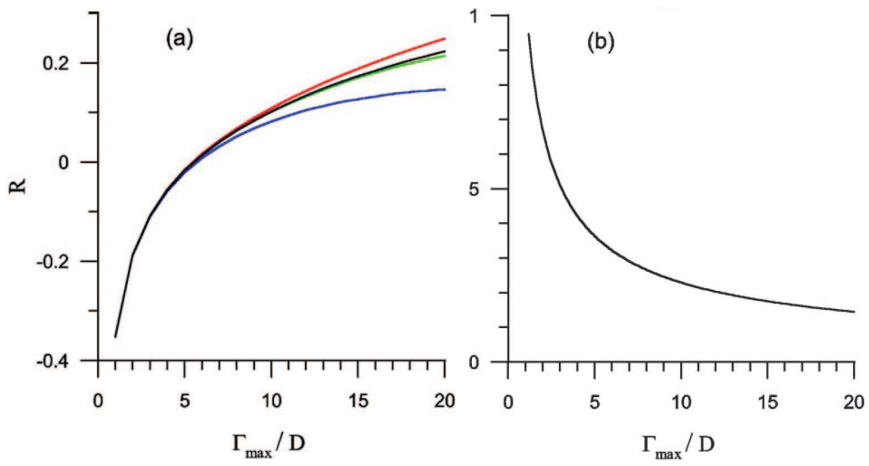

Figure 5.3: a) The dependencies of normalized effective growth rates R (defined by 5.23) on the ratio Γ_{max}/D for the Gaussian profile of $\Gamma(\theta)$ given be 5.25 with $\Delta\theta = \pi/10$. The black line shows the results for the total energy density W_{tot} (defined by 5.24). Red, green and blue lines show represent the data derived for the spectral energy density $W_s(x,\theta)$m where $\theta = 0$, $\pi/2$ and π respectively. b) The dependence of the final angle half-width of the wave spectra on the ratio Γ_{max}/D [from Krasnoselskikh et al., 2007].

spatial widths of the wave packets are more narrow than that of the growth rate and that the relative position of the maximum in wave energy density depends on the ratio Γ_{max}/D. Despite the fact that the spatial distribution of the wave energy density for the cases of different ratios Γ_{max}/D look similar some substantial differences could be noticed. Panel (c) in Figure 5.4 shows the profiles after shifts such that the maximum in the profiles coincide. It is clearly seen that for the small values of the Γ_{max}/D the packets are asymmetrical with respect to the maximum, while the increase in Γ_{max}/D results in the vanishing of the asymmetry.

To study statistical properties of small amplitude Lanfmuir waves in the plasma with

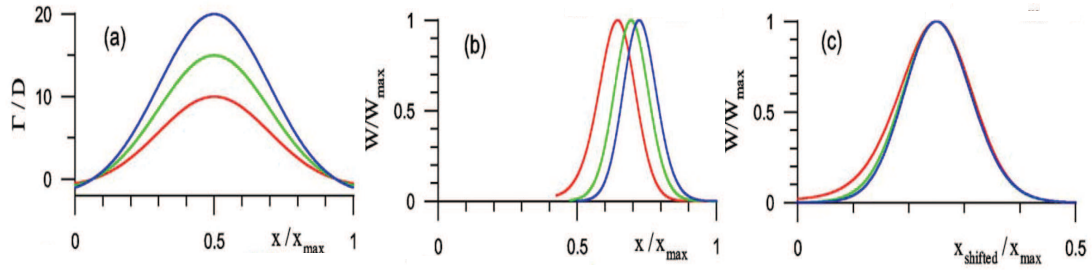

Figure 5.4: The result of the numerical simulations of instability with a single large-scale inhomogeneity. a) Spatial profile of the ratio Γ/D for $\theta = 0$ and different values of Γ_{max}/D. b) Spatial dependencies of normalized wave energy densities obtained for $\Gamma_{max}/D = 10$ (red line), 15 (green line) and 20 (blue line) c) The profiles shown in panel (b) after spatial shifts such that the maximums of the curves coincide [from Krasnoselskikh et al., 2007].

density fluctuations, the authors considered the following boundary value problem for equation 5.21 under assumption that all non-linear effects are negligible:

$$W_s|_{x=0} = W_s(\theta) \quad for \quad 0 \leq \theta \leq \pi/2, \qquad (5.27)$$
$$W_s|_{x=x_{max}} = 0 \quad for \quad \pi/2 < \theta \leq \pi.$$

Second condition indicates that for the large x the instability stops and the Langmuir waves damp. For the numerical simulations, the authors used a growth rate $\Gamma(x, \theta)$ as a superposition of the shot-noise-like functions of the coordinates with random position. The mean number of the of the impulses was chosen to be equal to 50, but the exact number was a random quantity that obeys the Poisson distribution. The impulses was defined by equation 5.26 but had different amplitudes uniformly distributed between zero and maximum value corresponding to $\Gamma_{max}/D = 15$. The characteristic scales of the inhomogeneities, Δx, were chosen to be equal to the ratio of the total width of the interval to the mean number of the impulses, 50. As a result, for any given point there were only two overlapping impulses.

The results deduced from the numerical simulations are shown in Figure 5.5. The diagram represents the statistical properties of the distribution of the logarithm of the normalized wave energy density $\log_{10} W$ obtained in the simulations in β_1, β_2 plane. Parameters β_1 and β_2 are Pearson parameters defined as $\beta_1 = \mu_3^2/\mu_2^3$ and $\beta_2 = \mu_4/\mu_2^2$, where μ_2, μ_3, μ_4 are second, third, and fourth moments of the distributions of $\log_{10} W$. Different data points correspond to the different distances from the boundary $x = 0$, and as a consequence to a different number of the growth rate impulses, N_{imp}. As it can be seen, for the chosen profile of the growth rate, the distribution of $\log_{10} W$ almost everywhere differs significantly from the normal distribution (represented as a black cross in the both panels). According to the Pearson classification the distribution rather corresponds to the Pearson type IV distribution than to log-normal. However, as N_{imp} increases, the data points approach the point representing the normal distribution, in accordance to the central limit theorem. For the N_{imp} as large as $45-50$ the differences from the normal distribution are insignificant. The authors argued that the conditions for the applicability of the limiting form of the pure SGT could be rather severe, at least in the Earth's foreshock where an estimate for a typical value of the number of growth rate fluctuations is slightly higher than 10 [Cairns and Robinson, 1999].

5.4 Hamiltonian description of the beam-plasma interaction in randomly inhomogeneous plasma.

The kinetic theory of plasmas, based on Vlasov-Poisson system of equations, considered in Chapter 2, can effectively solve only some aspects of the extremely large panel of

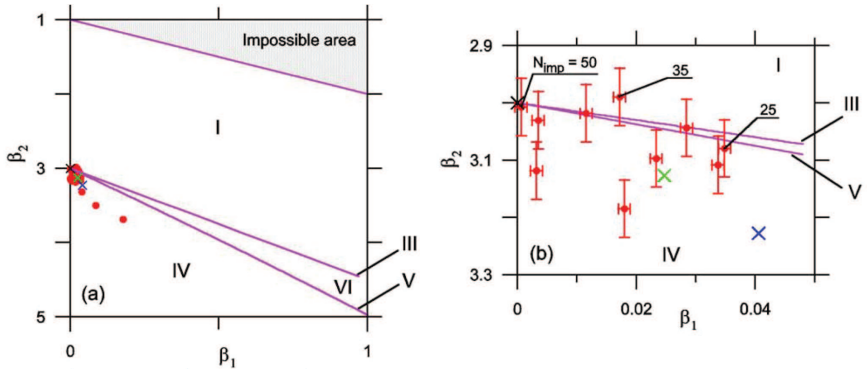

Figure 5.5: a) The diagram of the various types of Pearson distributions, together with the results of the numerical simulations (red circles). The regions corresponding to different distribution classes are denote by a roman numbers. A black cross corresponds to the normal distribution. b) A small part of previous diagram. For several points shown also are effective numbers of regions with positive growth rate, N_{imp} [from Krasnoselskikh et al., 2007].

problems involving wave-particle and wave-wave interaction processes in plasma. The Hamiltonian approach allows to describe the dynamics of charged particles and waves in self-consistent manner, and can be used as alternative to Vlasov-Poisson system of equations when considering the wave-wave and wave-particle interaction in magnetized or inhomogeneous plasma. This approach was successfully applied to study non-linear stage of the interaction of the electron beam with an electrostatic waves [Onishchenko et al., 1970, O'Neil et al., 1971]. Recently, the generalized model for the magnetized plasma, that involves $3D$ geometry, wave-wave interactions, effects related to inhomogeneity of plasma was proposed in [Krafft and Volokitin, 2006, 2004, Zaslavsky et al., 2008]. The authors derived the set of equations describing the wave-particle and wave-wave interactions using Hamiltonian description and obtained the system of equations allowing to study the Langmuir turbulence in the presence of particle fluxes streaming in the plasma with density fluctuations [Volokitin et al., 2013, Krafft et al., 2013]. The present Hamiltonian model allowed to recover many characteristic features of the observations performed by various satellites in the solar wind, concerning notably the Langmuir waveforms generated in the source regions of type III solar bursts and emitted by energetic electron beams accelerated in the solar corona during flares [Krafft et al., 2014]. As a next step, in the present section we perform statistical analysis of the distributions of the wave amplitudes obtained from the model under the conditions relevant to source region of solar type III radio bursts. The basic ideas behind Hamiltonian model are described in numerous original papers [Krafft et al., 2013, 2014, 2015]. However, for the sake of logical completeness, here, we present a brief explanation of the model.

5.4.1 Hamiltonian model

The derivation of self-consistent equations for wave-particle systems can be performed starting from Maxwell and Vlasov equations, under assumption that two types of the particles can be selected and described separately by the velocity distributions, namely, the the core of non-resonant particles forming the background plasma and the resonant particles which interact strongly with the waves and whose density n_{res} is much smaller than that of the background plasma, i.e. $n_{res} \ll N_0$. The first sort of the particles is responsible for the wave propagation, while the second type is related to process of the waves growth and damping. This approach allows to study linear, nonlinear and turbulent processes involving wave-particle and wave-wave interactions, for various particle distributions and types of waves, in magnetized homogeneous or inhomogeneous plasmas. For the case of electrostatic waves in homogeneous plasma the equations that describe Fourier component of the wave electric field potential, $\psi_k(k, \omega_k)$, can be written as follows (similarly to equation 2.9):

$$\frac{\partial \psi_k}{\partial t} = \frac{8i\pi e}{k^2 \epsilon_k^{'}} \frac{n_{res}}{Z} \sum_p^Z \exp -i(\omega_k t - \vec{k} \cdot \vec{r}_p), \tag{5.28}$$

where $Z = n_{res}V$, V is a volume occupied by wave-particle system, $\vec{r}_p$ is position of the particle p, ϵ_k is the plasma dielectric function and $\epsilon_k^{'} = \partial \epsilon_k / \partial \omega_k$. The electrons are moving in the wave's electric field according to the Newton equations:

$$\frac{\partial \vec{v_p}}{\partial t} + \frac{e}{mc} \vec{v_p} \times \vec{B_0} = \frac{e}{m} Re \sum_k \vec{k} \psi_k \exp i(\vec{k} \cdot \vec{r}_p - \omega_k t), \tag{5.29}$$

where $\vec{B_0}$ is background magnetic field chosen to be directed along the axis z, c is a speed of light, and $\vec{v_p}$ is a velocity of the particle. The equation 5.29 can be presented as the Hamiltonian equations as

$$\frac{d\vec{P_p}}{dt} = -\frac{\partial \mathcal{H}_{w-p}}{\partial \vec{r}_p} \tag{5.30}$$

and

$$\frac{d\vec{r}_p}{dt} = \frac{\partial \mathcal{H}_{w-p}}{\partial \vec{P_p}} = \vec{v_p}, \tag{5.31}$$

where $P_p = m\vec{v_p} - e\vec{A}(\vec{r}_p)/c$ is the generalized particle moment, $\vec{A}(\vec{r}_p) = (\vec{B_0} \times \vec{r}_p)/2$ is the vector potential, and $\mathcal{H}_{w-p}$ is the Hamiltonian of the wave-particle system. For the case of absence of wave-wave interaction, the Hamiltonian is given as:

$$\mathcal{H}_{w-p} = \sum_{p}^{Z} \left(\frac{(\vec{P}_p + e\vec{A}(\vec{r}_p))^2}{2m} - eRe \sum_{k} \psi_l \exp i(\vec{k} \cdot \vec{r}_p - \omega_p k) \right) + V \sum_{k} \omega_k \epsilon_k^{'} \frac{\left| \vec{k}\psi_k \right|^2}{16\pi} \tag{5.32}$$

where two first terms represent the kinetic particle energy and the wave-particle interaction energy, respectively; the last term corresponds to the wave energy $\sum_k \omega_k |C_k|^2$ expressed through the normal wave amplitudes $C_k = \alpha\psi_k \exp -i(\omega_k t)$ as

$$\sum_{k} \omega_k |C_k|^2 = V \sum_{k} W_k = V \sum_{k} \omega_k \epsilon_k^{'} \frac{\left| \vec{k}\psi_k \right|^2}{16\pi}, \tag{5.33}$$

where $\alpha = k\sqrt{(V\epsilon_k^{'})/(16\pi)}$. It is worth noting that equation 5.28 describing temporal changes in wave's potential can be obtained in the framework of Hamiltonian description as follows:

$$\frac{\partial C_k}{\partial t} = -i\frac{\partial \mathcal{H}_{w-p}}{\partial C_k^*} = -i\omega_k C_k + i\frac{e}{2}\frac{\partial \psi_k^*}{\partial C_k^*} \sum_{p}^{Z} \exp i(\omega_k t - \vec{k} \cdot \vec{r}_p) \tag{5.34}$$

To consider the non-linear effects related to wave-wave interaction, an appropriate Hamiltonian, describing interaction between waves, could be added to the $\mathcal{H}_{w-p}$. For the case of three-wave resonance process with matching and resonance conditions $\vec{k} = \vec{k}' + \vec{k}''$ and $\omega_k = \omega_{k'} + \omega_{k''}$ the Hamiltonian can be written as follows:

$$\mathcal{H}_{w-w} = \frac{1}{\sqrt{V}} \sum_{k,k',k''} V_{k,k',k''} C_k^* C_{k'} C_{k''} + c.c \tag{5.35}$$

where $V_{k,k',k''}$ is the wave-wave interaction matrix element. Thus, the total Hamiltonian of the system, $\mathcal{H}_{tot} = \mathcal{H}_{w-p} + \mathcal{H}_{w-w}$, can be written in following form:

$$\mathcal{H}_{tot} = \sum_{p}^{Z} \left(\frac{mv_p^2}{2} - Re \sum_{k} e\psi_k \exp i(\vec{k}\vec{r}_p) \right) V \left(\sum_{k} \frac{\left| \vec{k}\psi_k \right|^2}{8\pi} + \sum_{k,k',k''} \frac{kk'k''}{(16\pi)^{3/2}} \sqrt{\epsilon_{k'}^{'} \epsilon_{k''}^{'} \epsilon_k^{*'}} V_{kk'k''} \psi_k^* \psi_{k'} \psi_{k''} \exp i(\omega_k - \omega_{k'} - \omega_{k''}) + c.c \right) \tag{5.36}$$

The equation 5.34 describing the temporal evolution of the normal wave amplitudes C_k for the case of three-wave process takes following form:

$$\frac{\partial C_k}{\partial t} = -i\frac{\partial\left(\mathcal{H}_{w-p} + \mathcal{H}_{w-w}\right)}{\partial C_k^*} \tag{5.37}$$

The Hamiltonian description based on the equations 5.37 and 5.37 allows developing the numerical code that involves symplectic method. From the numerical point of view, the use of such method provides several advantages compared to the kinetic Vlasov-Poisson approach, namely, it allows to calculate the dynamics of waves and particles during very long time periods, to study the interaction of small relative density particle distributions with waves and to collect large numbers of particles trajectories that can be analyzed further using statistical algorithms. Moreover, it can be used to investigate physical processes connected with the dynamics of individual particles (as, for instance, the slow growth of wave energy density with time in the saturation stage of the wave-particle interaction). Compared to Particle-In-Cell (PIC) codes, the number of particles used in the simulations is drastically reduced, so that long time computations in 3D magnetized plasmas can be carried out. Moreover, as the system of equations involving wave-particle as well as wave-wave interactions terms have a Hamiltonian form, symplectic integrators give the possibility to use larger time steps and to accelerate strongly the calculations.

5.4.2 Model of plasmas with external density inhomogeneities

The appropriate model describing the interaction of the an electron beam with Langmuir waves packet in a plasma with density fluctuations was derived from the Zakharov's equations. The equations for the electric field $\vec{E}$ and low frequency density variations δn can be written in following form:

$$i\frac{\partial \vec{E}}{\partial t} + \frac{3\lambda_D^2}{2}\omega_p \nabla(\nabla \cdot \vec{E}) = \frac{\omega_p}{2}\frac{\delta n}{N_0}\vec{E}, \tag{5.38}$$

$$\frac{\partial v_i}{\partial t} = \nabla\frac{\partial \Phi}{\partial t} = -\nabla\left(c_s^2\frac{\delta n}{N_0} + \frac{\left|\vec{E}\right|^2}{16\pi m_i N_0}\right). \tag{5.39}$$

where $\vec{E} = Re\sum_k \vec{E}_k \exp i(\vec{k}\cdot\vec{r} - \omega t)$ is electric field of the wave packet, δn describes the ion density fluctuations, m_i is ion mass, and Φ is the hydrodynamic flux potential. The right hand side term of equation 5.38 describes the non-linear effect of density perturbation that causes refraction of the Langmuir waves into low density plasma region. The last therm in equation 5.39 corresponds to the ponderomotive force that expels particles out of regions of larger wave energy density. In the $1D$ geometry the continuity equation for ions reads:

$$\frac{\partial}{\partial t}\frac{\delta n}{N_0} = -\frac{\partial v_i}{\partial z} = -\frac{\partial^2 \Phi}{\partial z^2} \tag{5.40}$$

where z is a coordinate along the magnetic field line. By making use of equation 5.40, equation 5.39 one can derive:

$$\left(\frac{\partial^2}{\partial t^2} - c_s^2 \frac{\partial^2}{\partial z^2}\right) \frac{\delta n}{N_0} = \frac{\partial^2}{\partial z^2} \frac{|E|^2}{16\pi m_i N_0}, \tag{5.41}$$

Equations 5.38 and 5.41 can be derived from the Hamiltonian

$$\mathcal{H} = \int_L dz \left(\frac{\delta n}{2N_0} \frac{|E|^2}{8\pi} + \frac{3\lambda_D^2}{16\pi} \left| \frac{\partial E}{\partial z} \right|^2 \right. \tag{5.42}$$
$$\left. + \frac{N_0 m_i}{2} \left[c_s^2 \left(\frac{\delta n}{N_0} \right)^2 + \left(\frac{\partial \Phi}{\partial z} \right)^2 \right] \right) = const,$$

where the integration on z is performed over the length of the system L. It is worth noting that the system has other time invariants, the total number of quanta of high-frequency field

$$\mathcal{I}_1 = \int_L \frac{|E|^2}{8\pi} dz = const \tag{5.43}$$

and the total momentum $\mathcal{P}$

$$\mathcal{P} = \int_L dz \left(N_0 m_i \frac{\delta n}{N_0} \frac{\partial}{\partial t} \frac{\partial \Phi}{\partial z} + \frac{i}{16\pi\omega_p} \left(E \frac{\partial E^*}{\partial z} - E^* \frac{\partial E}{\partial z} \right) \right) \tag{5.44}$$

Then $E/\sqrt{8\pi\omega_p}$ and $E^*/\sqrt{8\pi\omega_p}$, as well as $\delta n/N_0$ and $-N_0 m_i \Phi$ are canonically conjugated variables of hamiltonian $\mathcal{H}$. Thus equations 5.38 and 5.39 could be recovered by making use of Hamilton equations:

$$\frac{1}{8\pi\omega_p} \frac{\partial E}{\partial t} = -i \frac{\delta \mathcal{H}}{\delta E^*}, \quad N_0 m_i \frac{\partial \Phi}{\partial t} = -\frac{\delta \mathcal{H}}{\delta \left(\frac{\delta n}{N_0} \right)} \tag{5.45}$$

where δ is functional derivative.

The interaction of the beam electrons with the Langmuir waves in an inhomogeneous plasma can be described by a total Hamiltonian $\mathcal{H}_t = \mathcal{H} + \mathcal{H}_{w-p}$, where $\mathcal{H}_{w-p}$ is defined by 5.33. Thus, the motion of the beam electrons is described by the Hamilton equations 5.30 and 5.31. The total Hamiltonian of the system, $\mathcal{H}_t$, reads [Krafft et al., 2013]:

$$\mathcal{H}_t = \mathcal{H} + L n_b \left(\frac{1}{Z} \sum_p \frac{m v_p^2}{2} - eRe \sum_k i \frac{E_k}{k} J_k^* \right) = const \tag{5.46}$$

where n_b is density of the beam, $Z = L n_b$ is the number of the electrons in the beam, and

$$J_k = \frac{1}{Z} \sum_p \exp i(\omega_p t - k z_p). \tag{5.47}$$

Applying the equations 5.45 to the Hamiltonian $\mathcal{H}_t$ (5.46), the equation of Langmuir turbulence driven by an electron beam was derived in [Krafft et al., 2013] as follows:

$$i\frac{\partial E}{\partial t}+\frac{3\lambda_D^2}{2}\omega_p\frac{\partial^2 E}{\partial z^2}-\omega_p\frac{\delta n}{2N_0}E=4\pi i e n_b\sum_k\frac{\omega_p}{k}J_k\exp\left(ikz\right) \tag{5.48}$$

In the k space the equation 5.48 reads:

$$i\left(\frac{\partial}{\partial t}-\gamma_k^{(e)}\right)E_k=\frac{3}{2}\omega_p k^2\lambda_D^2 E_k+\frac{\omega_p}{2}(\rho E)_k+i\frac{4\pi e\omega_p n_b}{k}J_k \tag{5.49}$$

where $\rho=\delta n/N_0$, $\gamma_k^{(e)}=-Im\epsilon_k^e/(\partial Re\epsilon_k^e/\partial\omega_k)$ is a damping factor and ϵ_k^2 is the electronic part of the dielectric constant ϵ_k, which gives the possibility to include the damping effects of Langmuir waves due to their Landau resonance with the thermal electrons. Equation 5.49 can be used to obtain a nonlinear dispersion relation of Langmuir waves as follows:

$$\omega_k\simeq\omega_p+\frac{3}{2}\omega_p k^2\lambda_D^2+\omega_p\frac{\delta n}{2N_0}+i\gamma_k^{(e)} \tag{5.50}$$

Introducing the dimensionless plasma velocity $u=v_i/c_s$, the Fourier transforms of equation 5.38, keeping the second order terms, and equation 5.39 can be written as follows,

$$\frac{\partial}{\partial}\rho_k=ikc_s(u_k+(\rho u)_k), \tag{5.51}$$

$$\frac{\partial u_k}{\partial t}-2\gamma_k^{(i)}u_k=ikc_s\left(\rho_k+\frac{\left(|E|^2\right)_k}{16\pi m_i N_0 c_s^2}\right). \tag{5.52}$$

where damping effect due to the ions is introduced through the damping rate rate $\gamma_k^{(i)}=-Im\epsilon_k^{(i)}/(\partial Re\epsilon_k^{(i)}/\partial\omega_k$. Equations 5.48, 5.51, and 5.52 together with equations 5.29 5.30, and 5.31 form the complete set of equations of the model. In the subsection presenting the numerical simulation's results, we are using normalized values described in detail in the Appendix B.1 [see also Krafft et al., 2013].

5.4.3 Numerical simulations' results

Here we present results of the simulations for a range of parameters relevant to solar type III electron beams and plasma observed at 1 AU [Ergun et al., 1998]: $T_e=10eV$, $N_0=5\cdot10^6$, $\lambda_D=15m$, $\omega_p/(2\pi)=20kHz$, and $v_{sw}=450km/s$. At first we consider a case of small density fluctuations. Figure 5.6 shows the spatial profile of the energy density $|E|^2$ superposed to the electric field envelope $Re(E)$ and the density fluctuations $\delta n/N_0$ as well as the electron distribution function for the three moments of time. The level of the density fluctuations is chosen to be 0.001 and the driven beam has beam velocity, $v_b=14v_t$, beam thermal velocity $\Delta v_b=v_t$, and density $n_b=5\cdot10^{-5}N_0$. The electron distribution function shows behavior very close to predicted by QL theory for the homogeneous plasma. At the beginning, the relaxation

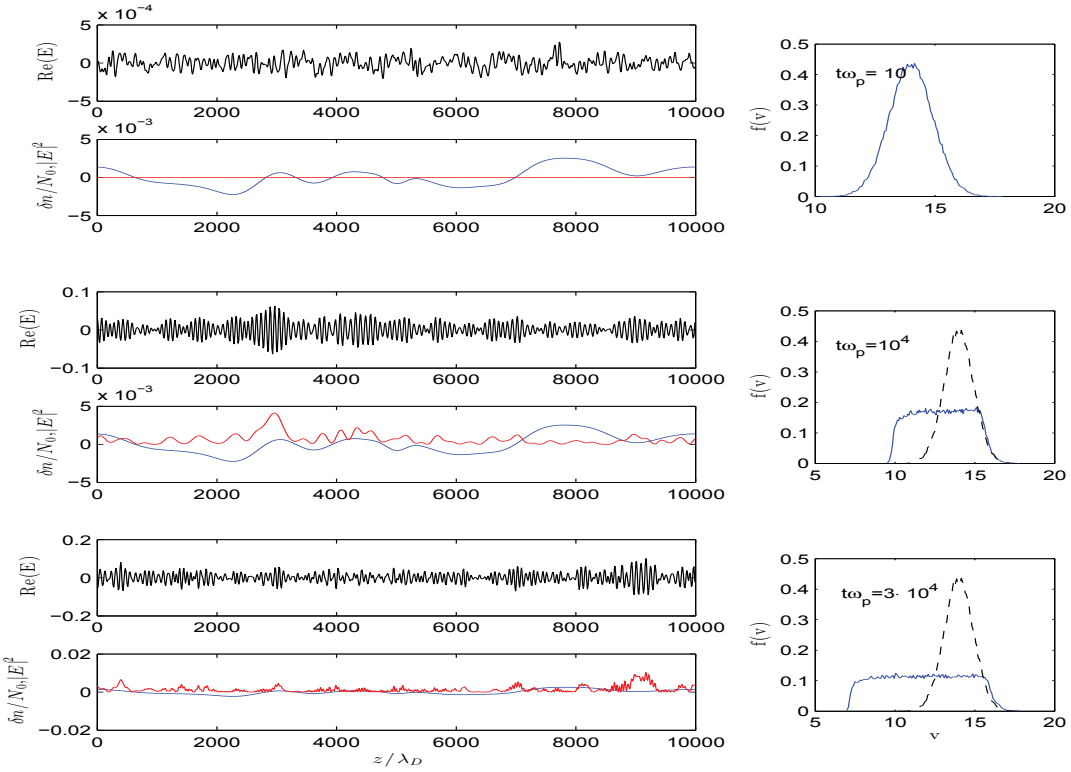

Figure 5.6: Beam's dynamics and the wave packet's evolution at three moments of time:$t\omega_p = 10{,}10^4$, and $3 \cdot 10^4$ (from upper to lower panels). The left panels: spatial profile of the electric field envelope $Re(E)$ (upper panels) and the wave energy density $|E|^2$ (shown with red), superposed to density fluctuations $\delta n/N_0$ (shown with blue) (lower panels). Right panels: electron velocity distribution function $f(v)$ (shown with blue). Dashed curves correspond to the initial electron distribution function. Main parameters: $v_b = 14v_t$, $\Delta v_b = v_t$, $\left(\langle \delta n^2 \rangle\right)^{1/2}/N_0 = 0.001$, $L = 10000\lambda_D$, $n_b/N_0 = 5 \cdot 10^{-5}$.

results in the plateau formation in the most unstable region of the velocity space, namely in the range of velocities $v_b - 3\Delta v_b < v < v_b$ (see for instance right middle plot in Figure 5.6). Subsequently, the left border of the distribution function moves toward lower velocities, until reaches the region occupied by plasma of the solar wind. The number of the energetic electrons with velocities larger than $v_b + 3\Delta v_b$ at the end of the relaxation is very low. The amplitudes of the Langmuir waves increase with time. As one can notice, the $|E|^2$ is mostly uniformly distributed in space, however some peaks can be seen in the vicinity of the density gradients. This peaks with the magnitude several times above the mean can indicate that even weak density fluctuations may lead to observed clumping phenomena.

Figure 5.7 shows the evolution of the Langmuir wave energy density $W = \sum_k E_k^2$ (left panel) and the total energy of the beam electrons superposed with the energy of the energetic particles (right panel). The wave energy density monotonically increases with time. At a moment of time of approximately $t\omega_p = 4 \cdot 10^4$ the wave energy density

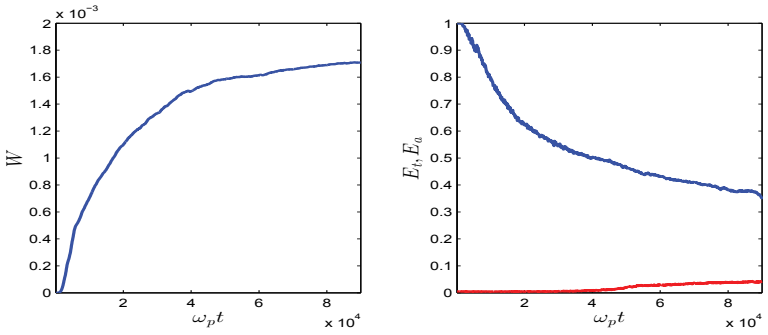

Figure 5.7: Left panel: evolution of the wave energy density, $W = \sum_k E_k^2$. Right panel: evolution of the total kinetic energy of the beam, E_t, (shown with blue), and energy of the energetic electrons, E_a, (shown with red). Main parameters are the same as in Figure5.6.

reaches the saturation level, and the subsequent changes go very slow. At the contrast, the total energy of the electrons decreases with time. It is worth noting that the at the end of the relaxation the beam reveals of approximately 2/3 of it's initial energy, that is in good agreement with the predictions of the QL theory. The energy of the accelerated particles at the end of the relaxation is less than 5% of the initial energy of the beam.

To study the distribution of the electric field of the Langmuir waves we confined ourselves by the time period when the wave energy density maintained approximately constant. Namely we consider all the envelops obtained in the simulation after the time $t\omega_p = 4 \cdot 10^4$. The distribution of the electric field, $P(E)$, is shown in Figure 5.8 (left panel). To obtain, $P(E)$, with used $K_b = 128$ bins spaced between -1.25 and 1.25. It is worth noting that the wave electric field is normalized according to $|E|^2/(4\pi N_0 T_e)$. To classify $P(E)$ we calculated corresponding Person's β parameters. The obtained distribution is characterized by $\beta_1 = 10^{-4}$ and $\beta_2 = 3.005$ and according to Pearson classification it corresponds to the normal distribution. The curve shown with red circles represent fit of the function $P(E)$ by normal distribution with zero mean and dispersion, $\sigma = 0.0286$. It can be clearly seen that the distribution of the electric field of the Langmuir wave packet of the present case obeys the normal distribution.

At the next step we selected from all the data only the values of the electric field, E_p, that correspond to the local maxima in $|E|^2$. The logarithm of the distribution of the $\ln(E_p^2)$ is shown at the right panel in Figure 5.8. It seems that obtained distribution resembles the distribution predicted by SGT (for instance see Figure 5.2). The logarithm of the distribution below it's maximum behaves as parabola, that in fact indicates that the distribution obeys log-normal distribution. The fit of the small amplitude part of the distribution by the log-normal distribution with parameters $\langle \ln(E_p^2) \rangle = -8$ and $\sigma^2 = 0.66$ is presented. A deviation from the log-normal normal distribution for the higher E_p can be caused by decay process. Large amplitude waves are limited by three-

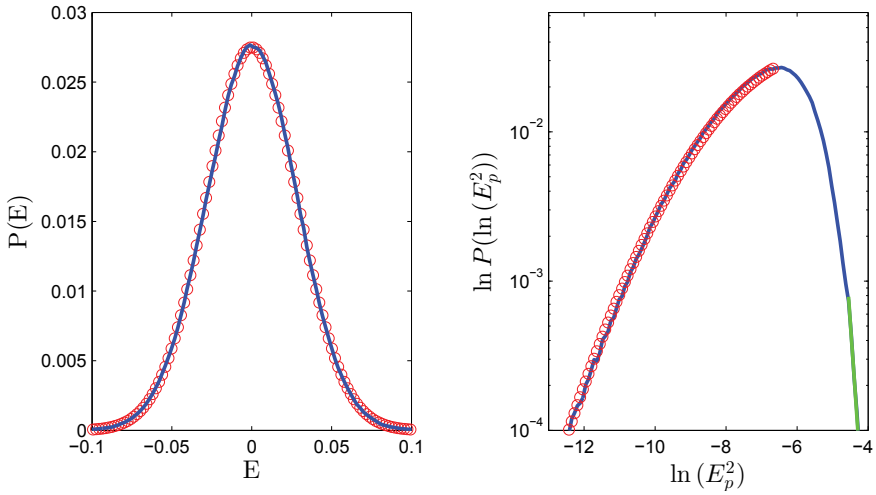

Figure 5.8: Left panel: Distribution of the electric filed of Langmuir wave envelop obtained in the numerical simulation (shown with blue). The distribution is normalized to one. The fit of the obtained distribution with the normal distribution is shown with red circles. Right panel: logarithm of the distribution of the logarithm of the magnitudes of the electric field peaks (shown with blue). The red circles represent the fit of the logarithm of distribution below the maximum with parabola. The approximation of the large magnitude part of the distribution with exponentially decreasing function $P(\ln(E_p^2)) = \exp(-a \ln E_p^2 - b)$, where $a = -7.9$ and $b = 42.8$ is shown with green.

wave decay process, the electric fields with magnitudes larger then the threshold for the nonlinear process, E_c, are rarely seen in the data. Due to this fact, the distribution of $\ln(E_p^2)$ falls rapidly beyond the point $\ln E_c^2$. The distribution at the higher E_p can be approximated by an exponentially decreasing function (shown with green line).

Now let us consider a case when the density fluctuations play substantial role in the processes of wave generation and propagation. Figure 5.9 shows spatial distributions of the $Re(E)$, $|E|^2$, and $\delta n/N_0$ at three moments of time. The right panels in Figure 5.9 complement consideration by electron velocity distribution function at the same moments of time. In the contrast to previous study, the level of the density fluctuations is chosen to be 0.03. For this case the term in the non-linear dispersion relation for Langmuir waves 5.50 related to density irregularities exceeds the term $(3/2)(v_t^2/v_b^2)$. As one can see, the wave energy density profile shows the peaks that significantly exceed the averaged level. The electric field of the Langmuir waves in the vicinity of the peaks resemble corresponding clumping features, which are similar to waveforms observed by STEREO and WIND satellites [Ergun et al., 2008]. This phenomenon can be explained as the superposition of two non-linear effects: 1) the resonance interaction of the waves with the beam electrons 2) the effects of the propagation of the wave in strongly inhomogeneous medium. It is worth noting that the maxima of $|E|^2$ are not localized at the bottom of the density wells. In the contrast, the positions of the peaks are frequently observed in the vicinity of the maxima of the positive gradient of

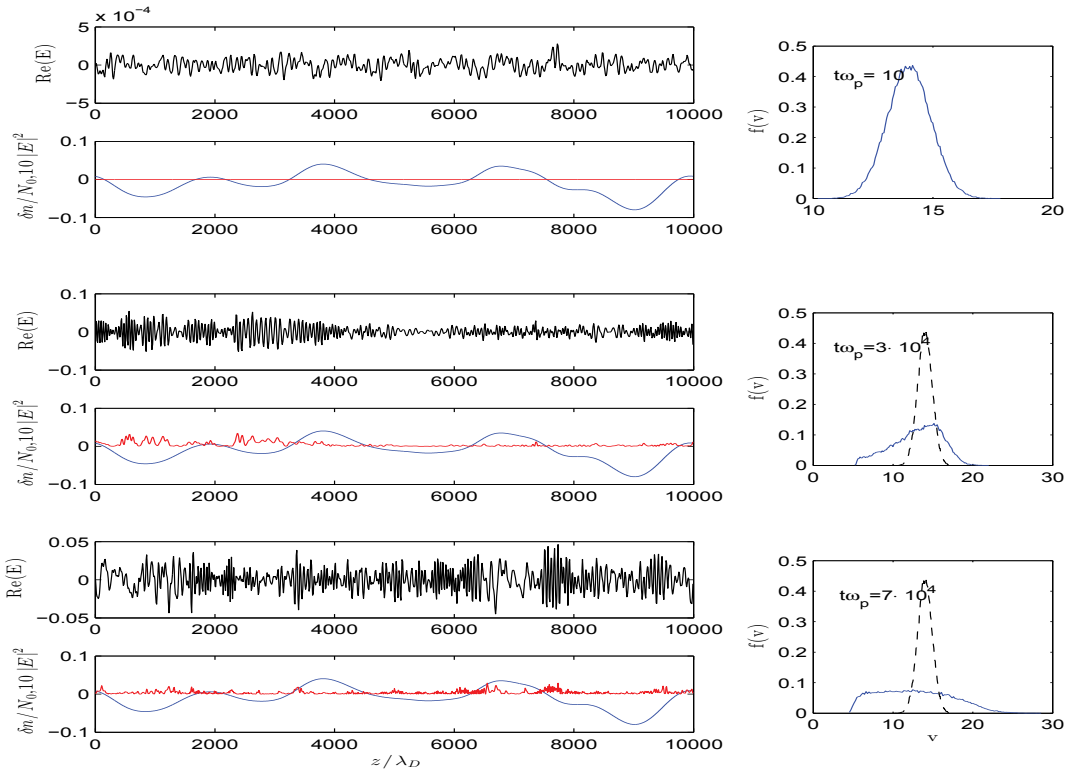

Figure 5.9: Beam's dynamics and the wave packet's evolution at three moments of time:$t\omega_p = 10{,}3 \cdot 10^4$, and $7 \cdot 10^4$ (from upper to lower panels). The left panels: spatial profile of the electric field envelope $Re(E)$ (upper panels) and the wave energy density $10\,|\cdot E|^2$ (shown with red), superposed to density fluctuations $\delta n/N_0$ (shown with blue) (lower panels). Right panels: electron velocity distribution function $f(v)$ (shown with blue). Dashed curves correspond to the initial electron distribution function. Main parameters: $v_b = 14v_t$, $\Delta v_b = v_t$, $\left(\langle \delta n^2 \rangle\right)^{1/2}/N_0 = 0.03$, $L = 10000\lambda_D$, $n_b/N_0 = 5 \cdot 10^{-5}$.

the density cavities. This points correspond to the conditions of wave reflection and frequency shift below the averaged plasma frequency. The effect of self focusing of the wave packet in the plasma with density cavities appears due to the coupling between E and δn described by non-linear term in equation 5.38. As a result the wave energy density is focused spatially. Regarding the beam evolution, two moments should be emphasized: 1) the relaxation runs slower than in the previous study, the positive slope on the electron distribution function is clearly seen at the moment of time $3 \cdot 10^4 \omega_p t$; 2) Presence of the high amplitude density fluctuations results in the acceleration of the energetic electrons to velocities much larger that their initial velocity. The tail of accelerated particles in clearly seen at the moment of time $7 \cdot 10^4 \omega_p t$

The left panel in Figure 5.10 presents the temporal evolution of the wave energy density. In contrast to the case of small density fluctuations, in the present study, the wave energy density decreases with time after it reached its maxima at the moment of time of approximately $4 \cdot 10^4 \omega_p t$. The decrease in W is accompanied by the increase of

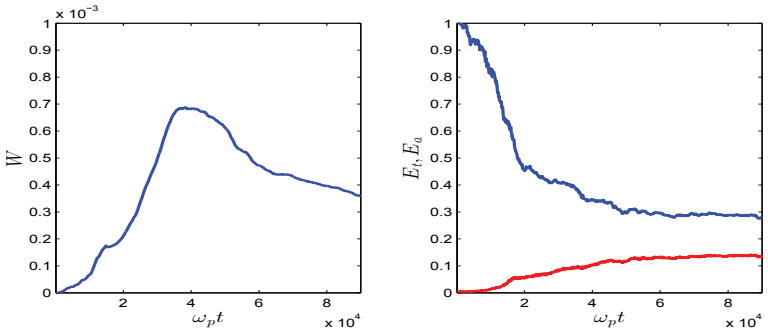

Figure 5.10: Left panel: evolution of the wave energy density, $W = \sum_k E_k^2$. Right panel: evolution of the total kinetic energy of the beam, E_t, (shown with blue), and energy of the energetic electrons, E_a, (shown with red). Main parameters are the same as in Figure5.9.

the energy of the energetic particles (red curve in right panel in Figure 5.10). Asymptotically, the accelerated particles carried up to 20% of the initial kinetic energy of the beam. The mechanism of the acceleration was already discussed in terms of the resonance broadening: being decelerated, the beam looses energy that is transferred to the waves with phase velocities smaller than v_b, than those waves can resonantly interact with particles with velocities $> v_b$ and transfer energy to them, if the magnitudes of the density irregularities are large enough to provide the necessary change in the waves phase velocity.

As previously, to study the statistical distributions of the electric field we chose time period when the the energy density of the Languir waves remains approximately constant. In the present study this period corresponds to the time interval starting from $6 \cdot 10^4 \omega_p t$. The distribution function of the electric field envelops of the Langmuir waves obtained in the simulation is shown in the left panel of the Figure 5.11. In the contrast to the previous study with small level of the density fluctuations, the obtained distribution shows significant deviation from the normal distribution. The corresponding Pearson's parameters are: $\beta_1 = 2 \cdot 10^{-3}$ and $\beta_2 = 3.8$. This indicates that according to the Pearson classification, the distribution corresponds to the Pearson type IV distribution. The fit of the $P(E)$ by the Pearson type IV distribution is shown with red circles. As one can see the obtained distribution obeys the predicted distribution with a high order of accuracy. The distribution of the logarithm of the peak magnitude of the electric field is shown in the right panel of the Figure 5.11. Despite that fact that the $P(E)$ is not normal, the $P(\ln(E_p^2))$ is still very close to the log-normal distribution (fit of the obtained distribution by the log-normal distribution is shown with red circles). It is worth noting that in the present study the $\langle \ln(E_p^2) \rangle$ is shifted toward the lower amplitudes comparing to the pervious case. This shift occurs due to the decrease in the wave energy density because of the effective reabsorption of the wave energy by the energetic electrons. Thus in the plasma the with higher density

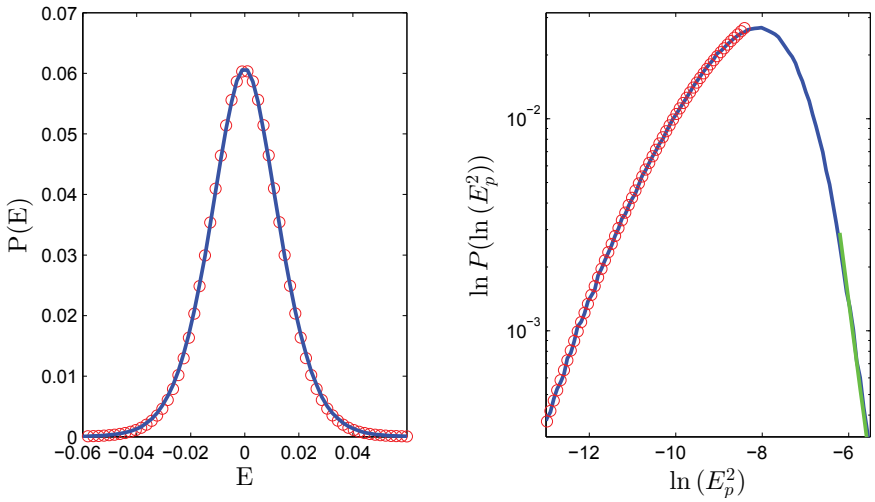

Figure 5.11: Left panel: Distribution of the electric filed of Langmuir wave envelop obtained in the numerical simulation (shown with blue). The distribution is normalized to one. The fit of the obtained distribution with Pearson type IV distribution is shown with red circles. Right panel: logarithm of the distribution of the logarithm of the magnitudes of the electric field peaks (shown with blue). The red circles represent the fit of the logarithm of distribution below the maximum with parabola. The approximation of the large magnitude part of the distribution with exponentially decreasing function is shown with green.

fluctuations the averaged level of the energy of the Langmuir waves is lower compared to the homogeneous plasma. However, is is still large enough to reach the threshold of the non-linear decay process. As one can see, the distribution $P(\ln(E_p^2))$ falls rapidly above its maxima and can be approximated by exponentially decreasing function for the large E_p^2 (shown with green line).

5.5 Probabilistic model

A pure probabilistic model described in Chapter 3 doesn't provide any information regarding spatial distributions of electric field of Langmuir waves. Hoverer it contains information about the energy density of the waves. Thus, by making use WKB approximation the propagation of the Langmuir waves within the plasma can be considered. The equation 5.20 for the monochromatic Langnuir wave with frequency ω_i and wave vector k_i reads:

$$E_i(t,x) = \frac{\sqrt{8\pi W_i(t)}}{k_i(x)} \exp\left(-i\omega_i t + ik_i(x)x\right) \tag{5.53}$$

where $W_i(t)$ is the wave energy density obtained from the simulations, $k_i(x)$ is the wave vector that satisfies dispersion relation for the Langmuir waves with plasma frequency that changes spatially due to the density fluctuations. The equation 5.53 takes into account an effect that the wave amplitude of the wave can also change during the

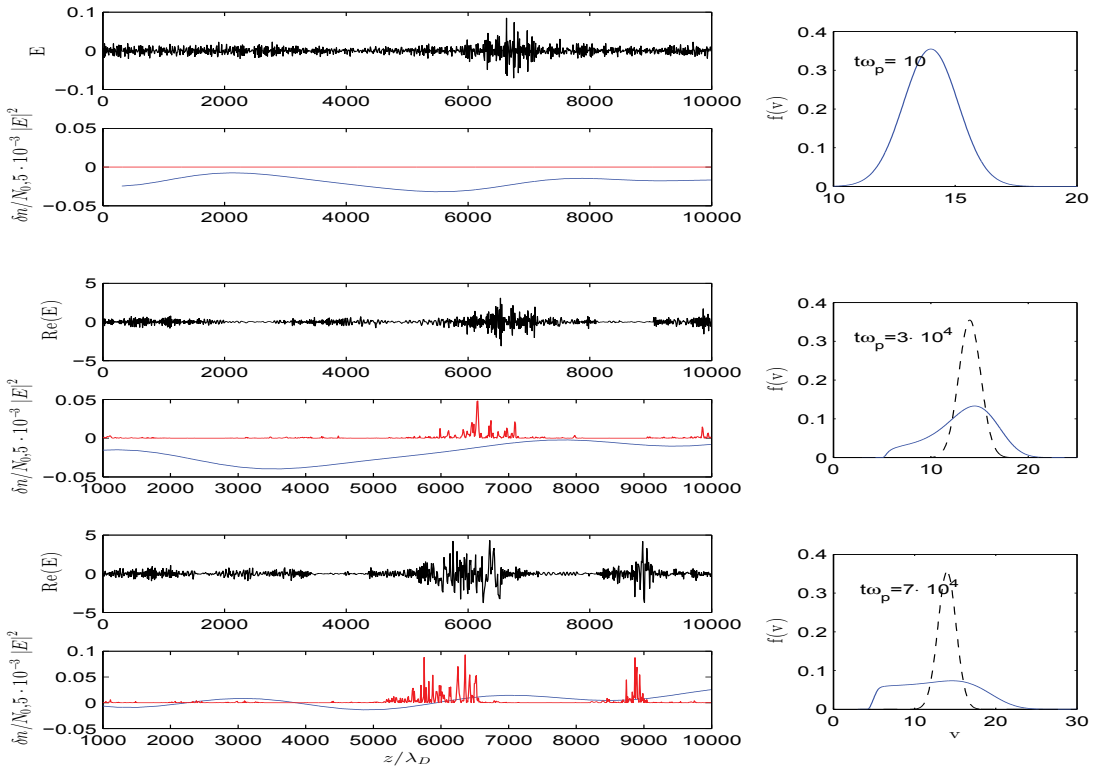

Figure 5.12: Beam's dynamics and the wave packet's evolution at three moments of time:$t\omega_p = 10{,}3\cdot 10^4$, and $7\cdot 10^4$ (from upper to lower panels). The left panels: spatial profile of the electric field envelope $\sum E_i$) (upper panels) and the wave energy density $5\cdot 10^{-3}\,|E|^2$ (shown with red), superposed to density fluctuations $\delta n/N_0$ (shown with blue) (lower panels). Right panels: electron velocity distribution function $f(v)$ (shown with blue). Dashed curves correspond to the initial electron distribution function. Main parameters: $v_b = 14v_t$, $\Delta v_b = v_t$, $\left(\langle \delta n^2\rangle\right)^{1/2}/N_0 = 0.003$, $L = 10000\lambda_D$, $n_b/N_0 = 5\cdot 10^{-5}$.

propagation because of the changes of group velocity. The spatial distribution of $k_i(x)$ is determined by the spatial distribution of the density irregularities. To obtain spatial profile of $k_i(x)$ we used syntectic time series of the density fluctuations that correspond to the density fluctuations in solar wind. The time series ware reconstructed from the spectrum of the density fluctuations observed in the solar wind by making use of the procedure described in Chapter 4. After we have the spatial profile of $\delta n/N_0$, function $k_i(x)$ was obtained by solution of the corresponding dispersion relation.

Figure 5.12 shows the reconstruction of the spatial distributions of the electric field of the of the Langmuir waves E, together with spatial distributions of the wave energy density $|E|^2$, density fluctuations $\delta n/N_0$ and electron velocity distribution function at three moment of time. To compare these results with those obtained in the Hamiltonian description we used a box with the same size, $L = 10000\lambda_D$. The spatial profile of the electric field was obtained as superposition of the 2000 waves with phase velocities uniformly distributed in the range from $3v_t$ to $40v_t$, i.e. $E(x) = \sum_i E_i(x)$. As one can

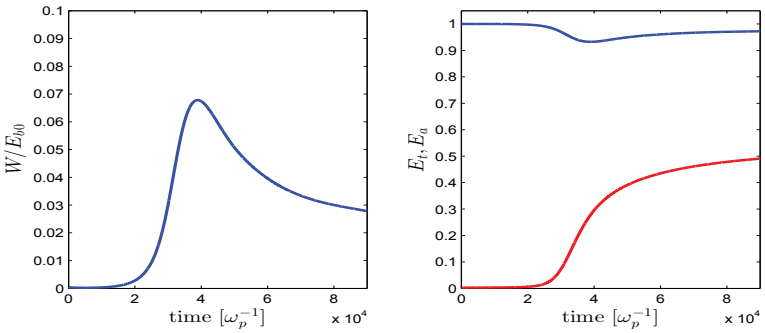

Figure 5.13: Left panel: evolution of the wave energy density, W. Right panel: evolution of the total kinetic energy of the beam, E_t, (shown with blue), and energy of the energetic electrons, E_a, (shown with red). Main parameters are the same as in Figure5.6.

see, the electric field of the envelope shows behavior that is very close to what we have already seen in the results of the simulations based on the Hamiltonian description. The maxima of $|E|^2$ are localized near the maxima of the positive density gradients. Since the probabilistic model is operated by the averaged waves growth rate, γ, the gain of the wave energy takes place on the spatial scales much larger than the scale of the single density irregularities. It can not describe the significant amplification of $|E|^2$ on scales that correspond to the characteristic scales of the clumps. From this fact we conclude, that observed clumping structures appear due to the effects related to the propagation of the Langmuir waves in the inhomogeneous plasma rather than because of the resonance interaction with beam electrons. It is worth noting that the temporal evolution of the electron velocity distribution function obtained with probabilistic approach is in a good agreement with the results obtained by making use of Hamiltonian description. The characteristic times of the relaxation are about the same in the both models.

The temporal evolution of the wave energy density, W, the total kinetic energy of the electrons E_t, and the energy of energetic particles E_a are shown in Figure 5.13. As in the Hamiltonian model, the wave energy density increases with time during time interval $t\omega_p < 4 \cdot 10^4$. After this moment of time, the W decreases at least twice. In the contrast to W, the total kinetic energy of the electrons shows different behavior. After some period of decrease, the E_t starts to increase. The energy of the energetic particles is twice higher than in the Hamiltonian model. Both these results can be explained by that fact, that the probabilistic model considers only one mechanism of the decrease in the W, namely, the absorbtion of the wave energy by the energetic electrons that occupy region of the velocity space where waves growth rate is negative. Non-linear decay of the Langmuir or another non-linear wave-wave process provides an outflow of the wave energy from the resonance region, and leads to the decrease in both, the energy of the accelerated particles and total kinetic energy of the beam particles.

Distribution of the electric field reconstructed from the numerical simulation based

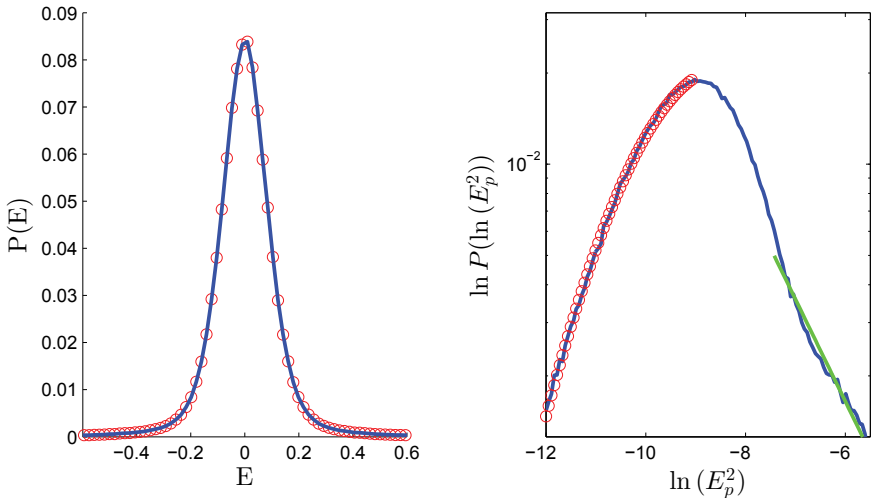

Figure 5.14: Left panel: Distribution of the electric filed of Langmuir wave envelop obtained in the numerical simulation (shown with blue). The distribution is normalized to one. The fit of the obtained distribution with Pearson type IV distribution is shown with red circles. Right panel: logarithm of the distribution of the logarithm of the magnitudes of the electric field peaks (shown with blue). The red circles represent the fit of the logarithm of distribution below the maximum with parabola. The approximation of the large magnitude part of the distribution with exponentially decreasing function $P(\ln(E_p^2)) = \exp(-a \ln E_p^2 - b)$, where $a = -7.9$ and $b = 42.8$ is shown with green.

on the probabilistic model is shown in the left panel in Figure 5.14. As in previous study the level of the density fluctuations is chosen to be 0.03. The obtained distribution is characterized by a Pearson parameters $\beta_1 = 0.05$ and $\beta_2 = 10.02$ and corresponds to Pearson type IV distribution according to Pearson classification. Thus, both models predict the same, non-normal distribution for the electric filed of the Langmuir waves envelope in a plasma with high level of the density fluctuations. We suppose that this fact can be used in future as an evaluation criteria of the level of inhomogeneity of the plasma. Right panel in Figure 5.14 represents the logarithm of the $P(\ln(E_p^2))$. As one can see, the distribution can be considered as log-normal (the fit by log-normal distribution is shown with red circles). In the contrast to the Hamiltonian model, the probabilistic model doesn't include the decay process, and as a result, the rapid decrease in $P(\ln(E_p^2))$ above its maxima is not observed. The deviation of the obtained distribution from the log-normal for large values of E_p^2 rather resembles the deviation observed by satellites in the planetary foreshocks (see also Figure 5.1). This power law exponent distribution can be explained as a consequence of combination of many log-normal distributions. Different log-normal distributions correspond to different spatial profiles of the density fluctuations that we have used during the reconstruction of electric fields of the Langmuir waves.

5.6 Conclusions

We have performed preliminary statistical analysis of the results of simulations carried out using equations derived in the probabilistic model of beam plasma interaction with probability distribution of density fluctuations corresponding to observed in solar wind. The results we obtain in simulations are statistical distributions of the wave intensities in the process of development and evolution of the beam plasma instability in inhomogeneous plasma. We do not calculate wave phases and their spatial distribution in the system. To carry out the analysis of the statistical distribution of wave fields we created an artificial data set taking pre-selected density profile having power spectrum similar to that of the solar wind. To reconstruct the spatial distributions of the electric field, on the scales smaller than the typical scales of the beam relaxation, we used the WKB approximation. To take into account the influence of the density irregularities we calculated spatial distributions of the wave vector from the spatial distributions of the density fluctuations. On the next step we have chosen the wave phases to be uniformly distributed on the interval [0,2π] and then constructed spatio-temporal series representing wave-fields. This was done by making use of non-linear dispersion relation of the Langmuir wave, under assumption that the frequency of the wave stays constant during the wave propagation. Slow temporal changes in E were taken from the numerical simulation based of probabilistic model. So constructed data sets were used for the data analysis.

The statistical analysis aiming to determine statistical characteristics of wavefields for different levels of density fluctuations was performed for two levels of density fluctuations, low level $\left(\langle \delta n^2 \rangle\right)^{1/2} \sim 0.001 N_0$ and $\left(\langle \delta n^2 \rangle\right)^{1/2} \sim 0.03 N_0$. The statistical analysis of the distribution of the peaks in the electric field showed that in the case of small density fluctuations (with averaged level of approximately $0.001 N_0$) the distribution of the $P(E_p^2)$ is rather similar to log-normal distribution, corresponding to Gaussian statistics for the increment as is supposed in the framework of SGT.

The distribution similar to log-normal was also observed in the case of large amplitude density fluctuations ($\left(\langle \delta n^2 \rangle\right)^{1/2} / N_0 = 0.03$). An increase in level of the density fluctuations results in the shift of the peak of the distribution toward lower values. The shift occurs because the large amplitude density fluctuations can suppress the beam instability, and thus, the amount of the energy gained by the waves is less in the plasma with higher level of fluctuations.

In the contrast to the distribution of the E_p^2 the distribution of the electric field of the Langmuir waves undergone essential changes with increase in $\left(\langle \delta n^2 \rangle\right)^{1/2} / N_0$. For the case of the low amplitude density fluctuation, the $P(Re(E))$ obeys the normal distribution with the high level of accuracy. For the case of the plasma with higher level of density fluctuations the obtained distribution is closer to the Pearson type IV distribution.

We carried out the very same analysis with the data of simulations carried out in the framework of Hamiltonian approach obtained by Krafft et al. [2015]. The results of the analysis for small amplitudes are very similar to those for probabilistic model, however for larger amplitudes to begin from some critical electric field E_c the distribution rapidly falls in range of amplitudes large than E_c. The simulations of Krafft et al. [2015] are carried out with very low Landau damping for low frequency density fluctuations, this allowed to observe additional physical phenomenon, decay instability of primary Langmuir wave on secondary Langmuir wave and ion sound wave. This leads to restriction of the wave amplitude, the waves having amplitudes larger than the threshold for decay instability decay. This effect explains the rapid cutoff of the distribution for amplitudes larger than E_c. For the data obtained in the same modeling with larger level of density fluctuations ($\left(\langle \delta n^2 \rangle\right)^{1/2}/N_0 = 0.03$) the distribution was found to be also similar to log-normal for small amplitudes and with a cut-off in larger E_p. An increase in level of the density fluctuations results in the shift of the $\langle E_p^2 \rangle$ toward lower values. However, the E_p still reaches the threshold for the three-wave decay.

It is interesting to notice that the results of our preliminary analysis are rather close to those obtained analyzing the experimental data of observations onboard satellites Cluster [Krasnoselskikh et al., 2007] and Wind [Cairns and Robinson, 1999].

It is worth noting that the results obtained in the framework of probabilistic model are very similar to those obtained in the Hamiltonian model of the beam-plasma interaction in the inhomogeneous solar wind. These last were already compared with the direct measurements of the waveforms onboard Wind and Stereo satellites, and were shown to reproduce quite well the data of observations [Krafft et al., 2014]. These numerical simulations show formation of the spikes of the electric field of Langmuir waves with a peak magnitudes several times above the mean. The model considers two-non linear effects, related to the presence of the density irregularities in the plasma, that can caused observed clumping phenomena. First effect consist of the break up of the conditions of the resonance interaction between electrons and Lanmguir waves. The second effect is related to the features of the wave propagation in the plasma with density fluctuations, namely, in the variation of the waves group velocity. The clumping effect is observed in both Hamiltonian model and in probabilistic model. Since the probabilistic model is operated by the averaged waves growth rate, γ, the gain of the wave energy takes place on the spatial scales much larger than the scale of the single density irregularity, and the model can not describe the significant amplification of $|E|^2$ on scales that correspond to the characteristic scales of the clumps. From this fact we conclude, that observed clumping structures appear due to the effects related to the propagation of the Langmuir waves in the inhomogeneous plasma rather than due to the oscillations of the waves growth rate.

5.7 Resume in French

Les ondes de Langmuir ont fait l'objet d'études intensives dans le vent solaire, en amont de choc terrestre et au voisinage d'autres chocs planétaires au cours des 6 dernières décennies. Dès le début, il a été remarqué que les ondes de plasma sont concentrées en "bouffées" avec des amplitudes maximales de typiquement trois ordres de grandeur au-dessus de la moyenne. Smith and Sime [1979] ont proposé une explication du phénomène de concentration en bouffées basée sur l'idée que le plasma est non-homogène, et possède, dans la plupart des régions où le faisceau peut exciter les ondes, des non-homogénéités dont la taille caractéristique est comparable à l'échelle caractéristique de croissance spatiale des ondes. En se basant sur cette idée, Robinson [1992], a proposé une modèle qui décrit l'interaction du faisceau d'électrons avec des ondes de Langmuir dans un tel plasma non-homogène. Le faisceau se propage en alternance dans des régions où le taux de croissance des ondes soit positif soit négatif, et ceci se traduit par des oscillations de la pente de fonction de distribution des électrons autour du niveau de stabilité marginale. En conséquence, les variations de taux de croissance ressemblent à une marche aléatoire. En prenant en compte que le taux de croissance correspond au logarithme de la densité de l'énergie des ondes avec une limite supérieure à peu près égale à la densité de l'énergie cinétique du faisceau, on peut en déduire que la statistique de cette caractéristique doit suivre une loi normale. Le modèle proposé a permis d'expliquer le phénomène observé de concentration en bouffées du champs électrique des ondes, et permet ainsi de faire une prédiction sur la distribution de probabilité des pics des amplitudes de ces bouffées. En utilisant le théorème de la limite centrale, on peut en déduire que la distribution des amplitudes maximales du champ électrique des enveloppes d'ondes de Langmuir obéit à la distribution log-normale.

Des études statistiques des événements, effectuées sur différentes données expérimentales obtenues à bord de plusieurs satellites et dans un plasma de laboratoire ont démontré que la répartition des amplitudes peut ressembler à la distribution log-normale. Cependant, différents processus non-linéaires, tels que la dégénérescence de l'onde électrostatique de Langmuir en une autre onde de Langmuir et une onde ionique sonore, peuvent aboutir à une déviation de la distribution log- normale. Récemment, Krasnoselskikh et al. [2007] ont proposé un modèle qui décrit l'interaction linéaire de paquets d'ondes de Langmuir avec un faisceau d'électrons et qui prend en compte deux effets importants causés par les irrégularités de la densité, à savoir: 1) la diffusion angulaire du vecteur d'onde causée par la diffusion sur les fluctuations de densité de faible amplitude, et 2) la suppression de l'instabilité provoquée par le déplacement dans l'espace des vitessesde l'onde, qui s'éloigne de la région correspondant à la résonance avec les particules pendant le passage de la perturbation de densité de relativement grande amplitude. Les auteurs ont montré que les distributions de logarithme de l'intensité de l'onde peuvent appartenir à une distribution Pearson du type IV plutôt qu'à la distri-

bution normale comme c'est le cas dans certaines circonstances. La principale raison la déviation des distributions par rapport à une distribution normale est due au faible nombre des régions où les ondes se développent qui empêche le théorème de la limite centrale de s'appliquer.

Nous avons effectué une analyse statistique préliminaire des résultats de simulations. Ces simulations sont réalisées avec notre modèle probabiliste de l'interaction d'un faisceau avec un plasma et en appliquant une densité de probabilité de fluctuations correspondante à celle observée dans le vent solaire. Les résultats que nous obtenons dans nos simulations sont les distributions statistiques des intensités d'ondes pendant le processus de développement et d'évolution de l'instabilité de faisceau avec un plasma. Nous ne faisons pas de calculs de phases des ondes et de leur distribution spatiale dans le système. Pour mener à bien l'analyse de la distribution statistique des ondes, nous avons créé un ensemble de données artificielles en utilisant le profil de densité ayant un spectre de puissance similaire à celui observé dans le vent solaire. Pour reconstruire la distribution spatiale du champ électrique, sur des échelles plus petites que l'échelle typique de la relaxation de faisceau, nous utilisons l'approximation WKB pour décrire la propagation d'ondes.

L'analyse statistique ayant pour l'objectif de déterminer les caractéristiques statistiques du champ d'onde pour différents niveaux de fluctuations de densité, a été réalisée pour deux niveaux de fluctuations de densité: $\left(\langle \delta n^2 \rangle\right)^{1/2} \sim 0.001 N_0$ et $\left(\langle \delta n^2 \rangle\right)^{1/2} \sim 0.03 N_0$. Cette analyse de la distribution des pics du champs électrique a montré que dans le cas de petites fluctuations de densité (avec un niveau moyen d'environ $0.001 N_0$), la distribution de $P(E_p^2)$ est assez semblable à une distribution log-normale, ce qui correspond à une statistique gaussienne pour le taux de croissance en accord avec l'hypothèse de base de théorie SGT. Par contre, quand le niveau de fluctuations est grand, la distribution des taux de croissance s'écarte d'une distribution normale assez fortement.

La distribution semblable à une log-normale a également été observée dans le cas de grandes fluctuations de densité d'amplitude ($\left(\langle \delta n^2 \rangle\right)^{1/2} / N_0 = 0.03$). Une augmentation du niveau des fluctuations de densité se traduit dans les faites par un décalage du pic de la distribution vers des valeurs plus faibles. Ce changement se produit parce que les fluctuations de grande amplitude peuvent supprimer ou fortement affaiblir le développement de l'instabilité du faisceau; par conséquence, l'énergie acquise par les ondes dans ce cas est inférieure au cas d'un plasma ayant un niveau de fluctuations plus faible.

De façon très différente, la distribution du champ électrique des ondes de Langmuir $E^p 2$ subit des modifications essentielles lorsque le niveau des fluctuations $\left(\langle \delta n^2 \rangle\right)^{1/2} / N_0$ augmente. Dans le cas de fluctuations de densité de faible amplitudes, $P(Re(E))$ obéit à la distribution normale avec une précision assez élevée. Dans le cas d'un niveau de fluctuations de densité plus grand la distribution statistique obtenue est plus proche de

la distribution de type IV de la classification de Pearson.

Nous avons effectué la même analyse avec les données de simulations obtenues en utilisant le code basé sur l'approche Hamiltonienne publié par Krafft et al. [2015]. Les résultats de l'analyse pour les champs de petites amplitudes sont très similaires à ceux obtenus avec le modèle probabiliste. Toutefois pour des amplitudes plus grandes et à partir d'un certain champ électrique critique E_c, la distribution décroît très rapidement lorsque les amplitudes deviennent plus grandes que E_c. Les simulations de Krafft et al. [2015] ont été réalisées avec un très faible amortissement de Landau pour les fluctuations la densité de basse fréquence, ce qui a permis d'observer un phénomène physique supplémentaire à savoir l'instabilité de décroissance des ondes de Langmuir primaires en onde de Langmuir secondaire plus une onde ionique sonore.

Ceci résulte dans la limitation de l'amplitude des ondes. Quand l'onde atteint une amplitude suffisament grande, et en particulier plus grande que le seuil de instabilité de décroissance, ce processus se développe assez rapidement et limite l'amplitude de l'onde. Cet effet explique la coupure et la décroissance rapide de la distribution quand les amplitudes sont supérieures à E_c. Pour les données obtenues dans la même modélisation avec un plus grand niveau des fluctuations de densité ($\left(\langle \delta n^2 \rangle\right)^{1/2} / N_0 = 0.03$), la distribution est similaire à une log-normale vers les petites amplitudes, et décroit rapidement pour des amplitudes plus grandes que E_c. Une augmentation du niveau des fluctuations de densité résulte dans le déplacement du maximum de la distribution $\langle E_p^2 \rangle$ vers des valeurs plus faibles. Le déplacement se produit parce que les grandes fluctuations de densité peuvent supprimer l'instabilité du faisceau, et ainsi la quantité d'énergie acquise par les ondes est inférieure quand le niveau de fluctuations est plus élevé. Cependant, l'amplitude du champ électrique en cas de faible amortissement atteint toujours le seuil de l'instabilité de décroissance.

Il faut noter que les résultats de notre analyse préliminaire sont assez proches de ceux obtenus sur les données expérimentales des observations à bord des satellites Cluster ([Krasnoselskikh et al., 2007]) et Wind ([Cairns and Robinson, 1999]).

Il convient de souligner que les résultats obtenus dans le cadre du modèle probabiliste sont très semblables à ceux obtenus en utilisant le modèle Hamiltonien de l'interaction faisceau-plasma dans le vent solaire non-homogène. Ce dernier a déjà été comparé avec les mesures directes des formes d'onde à bord des satellites WIND et STEREO, et il a été montré que les simulations reproduisent bien ces observations [Krafft et al., 2014]. Ces simulations numériques montrent la formation des pics localisés du champ électrique des ondes de Langmuir, avec des amplitudes plusieurs fois supérieures à la moyenne. Le modèle considère deux effets non-linéaires liés à la présence des irrégularités de densité dans le plasma, qui peuvent causer les phénomènes observés de formation de bouffées d'ondes. L'effet de concentration des ondes dans des paquets est observé aussi bien dans le modèle Hamiltonien que dans le modèle probabiliste.

Dans le modèle probabiliste, l'élément principal est le coefficient moyen du taux de croissance des ondes, γ. Le gain d'énergie des ondes a lieu sur des échelles spatiales plus grandes que l'échelle caractéristique de la fluctuation de densité localisée, et ceci indique que ce modèle ne peut pas décrire l'amplification significative de l'amplitude d'onde sur l'échelle de seul fluctuation. Finalement, nous concluons que les structures de bouffée d'ondes observées apparaissent à cause d'un effet lié à la propagation des ondes dans le plasma non-homogène, et que l'effet d'oscillations de taux du croissance est moins important.

Appendix B

Appendix

B.1 Normalization and numerical scheme

In the numerical simulations as well as in the presentation of the simulations results, the variables are normalized according to $\omega_p t$, z/λ_D, v/v_t, and $E_k/\sqrt{4\pi N_0 T_e}$ so that the normalized wave energy density is $|E|^2/(4\pi N_0 T_e)$, where T_e is electron temperature. Then Equations Equations 5.48, 5.51, 5.52 together with equations 5.30, 5.31 and 5.29 can be written in dimensionless form as, respectively (with the normalized damping factors $\tilde{\gamma}_k^{(e)}$ and $\tilde{\gamma}_k^{(i)}$ included),

$$\left(\frac{\partial}{\partial t} - \tilde{\gamma}_k^{(e)}\right) E_k = -i\left(\varpi_k E_k + \frac{(\rho E)_k}{2} + i\beta_k J_k\right), \tag{B.1}$$

$$\frac{\partial u_k}{\partial t} - 2\tilde{\gamma}_k^{(i)} u_k = ik\tilde{c}_s\left(\rho_k + \frac{\left(|E|^2\right)_k}{4}\right), \tag{B.2}$$

$$\frac{\partial}{\partial t}\rho_k = ik\tilde{c}_s(u_k + (\rho u)_k), \tag{B.3}$$

$$\frac{dz_p}{dt} = v_p, \quad \frac{dv_p}{dt} = -Re\sum kE_k \exp i(kz_p - \omega_k t), \tag{B.4}$$

where $\varpi_k = 3k^2/2$, $\beta_k(n_b/N_0)/k$ and $\tilde{c}_s = c_s/v_t \simeq m/m_i$.

Whereas equations B.4 are solved with the help of the classical leapfrog scheme, the numerical solution of equations B.1 - B.4 is performed using the following discretization schemes involving the Fourier components E_k, u_k, and ρ_k of the electric field, the plasma velocity, and the density fluctuations, respectively,

$$E_k^{n+1} = \frac{1 - i(\varpi_k - i\tilde{\gamma}_k^{(e)})\tau/2}{\varpi_k + i\tilde{\gamma}_k^{(e)})\tau/2}E_k - \frac{i\tau}{\varpi_k + i\tilde{\gamma}_k^{(e)})\tau/2}\left[\frac{(\rho E)_k}{2} + i\beta_k J_k\right]^n, \tag{B.5}$$

$$u_k^{n+1} = u_k^n\left(\frac{1 + \tilde{\gamma}_k^{(i)} - (k\tilde{c}_s\tau)^2/4}{1 - \tilde{\gamma}_k^{(i)} + (k\tilde{c}_s\tau)^2/4}\right) - \frac{ik\tilde{c}_s\tau}{1 - \tilde{\gamma}_k^{(i)} + (k\tilde{c}_s\tau)^2/4}\left(\rho_k^n + \frac{1}{4}\left(|E|^2\right)_k^n\right), \tag{B.6}$$

$$\rho_k^{n+1} = \rho_k^n - ik\tilde{c}_s\tau\left(\frac{u_k^{n+1} + u_k^n}{2} + (\rho u)_k^n\right), \tag{B.7}$$

where the subscript n (resp. $n+1$) indicates that the value is considered at time t_n (resp. t_{n+1}), with $t_{n+1} - t_n = \tau$; τ is the time step. To check the validity of the numerical procedures and their accuracy, the invariants presented in equations 5.43 and 5.46 have been monitored.

Chapter 6

General conclusions

6.1 Conclusions in English

We presented a self-consistent probabilistic model for describing the relaxation of an electron beam in a solar wind with random density irregularities having the same spectral properties as measured onboard satellites and by means of other techniques. We suppose that, the system has several characteristic scales related to the characteristic scale of density fluctuations. On a scale lower than the characteristic scale of density fluctuations, wave-particle interaction can be precisely determined for waves with known parameters: phase, frequency and amplitude. However, on scales sufficiently larger than the characteristic scale of density irregularities, wave and particle dynamics are described by their characteristics averaged over the velocity space, namely, by the growth/damping rate and by the particle diffusion coefficient. The procedure of averaging requires the knowledge of the probability distribution function of wave phase velocities that can be determined from the probability distribution of density fluctuations. To this end, we performed a statistical study of density fluctuations, deduced from measurements onboard satellites when they were in the solar wind. Our analysis indicates that on spatial scales of approximately $10^2\lambda_D$, the distribution of the fluctuations obeys a Pearson type II distribution. However, deviations from the normal distribution are rather small. The closeness of the density fluctuation distributions results in quite similar probability distribution functions for wave phase velocities. Numerical simulations for the electron beam plasma interaction for both cases of the Gaussian and non-Gaussian distribution do not lead to substantial difference. Thus, one can conclude that the normal distribution of density fluctuations may be used as a good approximation for studies of the beam relaxation in the solar wind.

Applying a model to the system having parameters relevant to typical solar type III events, we determined that depending on v_b^2/v_t^2 and $(\langle\delta n^2\rangle)^{1/2}/N_0$, three different scenarios for the relaxation process can take place:

(1) When the level of density fluctuations is sufficiently low, $(\langle\delta n^2\rangle)^{1/2}/N_0 \ll v_t^2/v_b^2$, the beam relaxation and the excitation of Langmuir waves are developed in a manner

similar to that of a homogeneous plasma. Relaxation only runs toward lower velocities and after plateau formation there is no energy transfer to accelerated particles. The energy of the waves increases in time until it reaches the saturation level, which is typically above several tens of percent from the initial energy of the beam.

(2) $(\langle \delta n^2 \rangle)^{1/2}/N_0 \sim v_t^2/v_b^2$- corresponding to the intermediate regime. The density fluctuations are high enough to impact the non-linear dispersion relationship of Langmuir waves and to cause absorption of the waves by particles from the tail of the electron velocity distribution function. As a result, the energy of waves decays after reaching a maximum value. The wave decrease is accompanied by an increase in the number of energetic particles.

(3) $(\langle \delta n^2 \rangle)^{1/2}/N_0 \gg v_t^2/v_b^2$ - the presence of density fluctuations strongly slows down beam relaxation. Resonant broadening allows a wave generated with a phase velocity, V, to interact resonantly with particles having velocities v_p smaller and larger than V, even with particles having much larger velocities. As a result, the saturation level of the wave energy is significantly reduced. The energy of waves at the end of relaxation can be five times less than the maximum value achieved during the relaxation process. The energy transfer from slow particles with velocities $v < v_b$ to energetic particles with velocities larger than v_b is very effective. The energy transferred to accelerated particles can reach levels up to 60% of the initial energy of the beam.

Thus, we conclude that even small amplitude density irregularities with spatial scales in the range of $10^3\lambda_D - 10^4\lambda_D$ play an important role in the process of the relaxation of solar energetic beams with beam velocities larger than $15v_t$. The results are in a good agreement with results obtained using computer simulations in the framework of a Hamiltonian description for beam-plasma interaction in the presence of random density fluctuations [Krafft et al., 2013].

Our study revealed very important characteristics for the beam plasma interaction for very energetic beams with beam velocities above $15v_t$. For these beams, the relaxation takes place in two stages process. The first stage has a relatively short duration, with characteristic time, t_r, typically below $10^7\pi/\omega_p$. This stage is characterized by an effective energy exchange between Langmuir waves and beam electrons. At the end of the first stage the system achieves a quasi-stable state. Despite the fact that the electron distribution function preserves a region with a positive gradient, the averaged growth rate for waves is close to zero, however, it keeps a small positive value over a very long time period. Even for very fast beams with beam velocities of approximately $20v_t$, the characteristic spatial scale of the first stage of relaxation is approximately $20 \cdot 10^7\lambda_D$, indicating that this stage takes place in the solar corona. However, as shown in our simulations, the second stage of relaxation is at least 500 times longer. Thus, one can expect that the electron distribution function will have a positive slope at distances up to several AU. This two stage process can explain the Sturrock paradox,

observations of weak beams and, associated with them, wave activity at distances from the Sun up to 5 AU. This result also indicates that beams can only be registered by very capable particle instruments, and provides an explanation as to why there are so few direct observations of the positive slope of the electron distribution function onboard satellites [Anderson et al., 1981, Lin et al., 1981, Fuselier et al., 1985].

At the end We have performed preliminary statistical analysis of the results of simulations carried out using equations derived in our probabilistic model of beam plasma interaction with probability distribution of density fluctuations corresponding to observed in solar wind. The results we obtain in our simulations are statistical distributions of the wave intensities in the process of development and evolution of the beam plasma instability in inhomogeneous plasma. To carry out the analysis of the statistical distribution of wave fields we created an artificial data set taking pre-selected density profile having power spectrum similar to that of the solar wind. To reconstruct the spatial distributions of the electric field, on the scales smaller than the typical scales of the beam relaxation, we used the WKB approximation. To take into account the influence of the density irregularities we calculated spatial distributions of the wave vector from the spatial distributions of the density fluctuations. Slow temporal changes in E were taken from the numerical simulation based of probabilistic model.

The statistical analysis aiming to determine statistical characteristics of wavefields for different levels of density fluctuations was performed for two levels of density fluctuations, low level $\left(\langle \delta n^2 \rangle\right)^{1/2} \sim 0.001 N_0$ and $\left(\langle \delta n^2 \rangle\right)^{1/2} \sim 0.03 N_0$. The statistical analysis of the distribution of the peaks in the electric field showed that in the case of small density fluctuations (with averaged level of approximately $0.001 N_0$) the distribution of the $P(E_p^2)$ is rather similar to log-normal distribution, corresponding to Gaussian statistics for the increment as is supposed in the framework of SGT. On larger amplitudes the distribution deviates rather strongly.

The distribution similar to log-normal was also observed in the case of large amplitude density fluctuations ($\left(\langle \delta n^2 \rangle\right)^{1/2} / N_0 = 0.03$). An increase in level of the density fluctuations results in the shift of the peak of the distribution toward lower values. The shift occurs because the large amplitude density fluctuations can suppress the beam instability, and thus, the amount of the energy gained by the waves is less in the plasma with higher level of fluctuations.

In the contrast to the distribution of the E_p^2 the distribution of the electric field of the Langmuir waves undergone essential changes with increase in $\left(\langle \delta n^2 \rangle\right)^{1/2} / N_0$. For the case of the low amplitude density fluctuation, the $P(Re(E))$ obeys the normal distribution with the high level of accuracy. For the case of the plasma with higher level of density fluctuation the obtained distribution is closer to the Pearson type IV distribution.

We carried out the very same analysis with the data of simulations carried out in

the framework of Hamiltonian approach obtained by Krafft et al. [2015], 2015. The results of the analysis for small amplitudes are very similar to those for probabilistic model, however for larger amplitudes to begin from some critical electric field E_c the distribution rapidly falls in range of amplitudes large than E_c. The simulations of Krafft et al. [2015] are carried out with very low Landau damping for low frequency density fluctuations, this allowed to observe additional physical phenomenon, decay instability of primary Langmuir wave on secondary Langmuir wave and ion sound wave. This leads to restriction of the wave amplitude, the waves having amplitudes larger than the threshold for decay instability decay. This effect explains the rapid cutoff of the distribution for amplitudes larger than E_c. For the data obtained in the same modeling with larger level of density fluctuations $\left(\left\langle \delta n^2 \right\rangle\right)^{1/2} / N_0 = 0.03$) the distribution was found to be also similar to log-normal for small amplitudes and with a cut-off in larger E_c. However, the E_p still reaches the threshold for the three-wave decay.

It is interesting to notice that the results of our preliminary analysis are rather close to those obtained analyzing the experimental data of observations onboard satellites Cluster [Krasnoselskikh et al., 2007] and Wind [Cairns and Robinson, 1999].

It is worth noting that the results obtained in the framework of probabilistic model are very similar to those obtained in the Hamiltonian model of the beam-plasma interaction in the inhomogeneous solar wind. These last were already compared with the direct measurements of the waveforms onboard Wind and Stereo satellites, and were shown to reproduce quite well the data of observations [Krafft et al., 2014]. These numerical simulations show formation of the spikes of the electric field of Langmuir waves with a peak magnitudes several times above the mean. The model considers two-non linear effects, related to the presence of the density irregularities in the plasma, that can caused observed clumping phenomena. First effect consist of the break up of the conditions of the resonance interaction between electrons and Lanmguir waves. The second effect is related to the features of the wave propagation in the plasma with density fluctuations, namely, in the variation of the waves group velocity. The clumping effect is observed in both Hamiltonian model and in probabilistic model. Since the probabilistic model is operated by the averaged waves growth rate, γ, the gain of the wave energy takes place on the spatial scales much larger than the scale of the single density irregularity, and the model can not describe the significant amplification of $|E|^2$ on scales that correspond to the characteristic scales of the clumps. From this fact we conclude, that observed clumping structures appear due to the effects related to the propagation of the Langmuir waves in the inhomogeneous plasma rather than due to the oscillations of the waves growth rate.

6.2 Conclusions in French

Dans cette thèse nous avons présenté un modèle probabiliste auto cohérent décrivant la relaxation d'un faisceau d'électrons dans un vent solaire dont les fluctuations aléatoires de la densité ont les mêmes propriétés spectrales que celles mesurées à bord de satellites. On a supposé que, le système possèdait différentes échelles caractéristiques en plus de l'échelle caractéristique des fluctuations de densité. Ceci nous a permis de décrire avec précision l'interaction onde-particule à des échelles inférieures à l'échelle caractéristique des fluctuations de densité en supposant que des paramètres d'onde sont connus: notamment, la phase, la fréquence et l'amplitude. Cependant, pour des échelles suffisamment plus grandes que l'échelle caractéristique des irrégularités de densité, l'interaction des ondes et des particules ne peut être caractérisée déterminé que par des quantités statistiques moyennes dans l'espace des vitesses à savoir: le taux de croissance/amortissement et le coefficient de diffusion des particules. La procédure d'évaluation de la moyenne nécessite la connaissance de la fonction de distribution de densité de probabilité des vitesses de phase des ondes, laquelle peut être déterminée à partir de la distribution de la densité de probabilité des fluctuations de densité électronique. À cette fin, nous avons réalisé une étude statistique des fluctuations de densité, déduites de mesures effectuées à bord des satellites dans le vent solaire. Notre analyse indique que, pour les échelles spatiale supérieures ou égales à environ $10^2\lambda_D$, la distribution des fluctuations obéit à la distribution de Pearson de type II. Cependant, les écarts entre cette distribution et la distribution normale sont plutôt petits. La proximité des distributions de fluctuations de la densité électronique se traduit par une relative similarité des fonctions de distribution de probabilités des vitesses de phase des ondes. Les simulations numériques décrivant l'interaction d'un faisceau d'électrons avec un plasma pour les deux cas (distribution Gaussienne et non-Gaussienne) ne montrent pas de différences notables. On en conclut, que la distribution normale des fluctuations de la densité électronique peut être utilisée comme une bonne approximation pour l'étude de la relaxation d'un faisceau d'électrons dans le vent solaire.

En appliquant au système un modèle ayant des paramètres semblables à ceux typiques pour des sources d'émissions radio solaires de type III, nous avons déterminé que, suivant le rapport entre v_b^2/v_t^2 et $(\langle\delta n^2\rangle)^{1/2}/N_0$, trois scénarios différents pour le processus de relaxation peuvent avoir lieu:

(1) Lorsque le niveau des fluctuations de densité est suffisamment faible, $(\langle\delta n^2\rangle)^{1/2}/N_0 \ll v_t^2/v_b^2$, la relaxation du faisceau d'électrons et l'excitation des ondes de Langmuir se font d'une façon très semblable à cequise produit dans un plasma homogène. La relaxation et la formation du plateau se développent seulement vers les vitesses plus petites que la vitesse du faisceau et, après la formation du plateau, il n'y a pas de transfert d'énergie aux particules accélérées. L'énergie des ondes augmente au cours du temps jusqu'à atteindre le niveau de saturation, lequel est typiquement est de l'ordre de quelques

dizaines de pourcent de l'énergie initiale du faisceau.

(2) Le niveau $(\langle \delta n^2 \rangle)^{1/2}/N_0 \sim v_t^2/v_b^2$- correspond au régime intermédiaire. Les fluctuations de densité sont suffisamment élevées pour influencer la relation de dispersion non linéaire des ondes de Langmuir. Ceci produit un effet d'absorption des ondes par les particules de la queue de la fonction de distribution des vitesses électroniques. En conséquence, l'énergie des ondes décroît après avoir atteint une valeur maximale. La baisse de l'énergie des ondes est accompagnée par une augmentation de nombre de particules énergétiques.

(3) En fin, pour $(\langle \delta n^2 \rangle)^{1/2}/N_0 \gg v_t^2/v_b^2$, la présence des fluctuations de densité ralentit fortement le processus de relaxation du faisceau. L'élargissement du domaine de résonance permet à une onde générée avec une vitesse de phase, V, d'interagir et d'être en résonance avec des particules ayant des vitesses v_p, plus petites que V aussi bien qu'avec des particules plus rapides (même avec des particules ayant des vitesses beaucoup plus grandes). En conséquence, le niveau de saturation de l'énergie des ondes est réduit de manière très significative. L'énergie des ondes à la fin de la relaxation peut être cinq fois inférieure à la valeur maximale atteinte pendant le processus de relaxation. Le transfert d'énergie des particules lentes (avec des vitesses $v < v_b$) aux particules énergétiques (avec des vitesses plus grandes que v_b) est très efficace. L'énergie transférée aux particules accélérées peut atteindre des niveaux allant jusqu'à 60% de l'énergie initiale du faisceau.

On en conclut que même les irrégularités de densité de petite d'amplitude, avec échelles spatiales dans la gamme de $10^3\lambda_D - 10^4\lambda_D$, jouent un rôle très important dans la relaxation de faisceaux d'électrons énergétiques solaires caractérisés par des vitesses plus grandes que $15v_t$. Ces résultats sont en bon accord avec les résultats des simulations numériques utilisant la description Hamiltonienne de l'interaction de faisceau-plasma en présence de fluctuations de densité aléatoires [Krafft et al., 2013].

Notre étude a révélé une caractéristique très importante de l'interaction faisceau-plasma dans le cas des faisceaux très énergétiques ayant des vitesses au-dessus de $15v_t$. Pour ces faisceaux, la relaxation se développe en deux étapes. La première étape a une durée relativement courte, avec un temps caractéristique, t_r, typiquement inférieure à $10^7\pi/\omega_p$. Cette phase est caractérisée par un échange d'énergie très efficace entre les ondes de Langmuir et les électrons du faisceau. À la fin de la première étape, le système atteint un état quasi stable. En dépit du fait que la fonction de distribution des électrons conserve une région de gradient positif dans l'espace de vitesses, mais le taux de croissance moyenne pour les ondes est assez proche de zéro. Cependant, cette petite valeur positive est gardée pendant une période de temps très longue. Même pour les faisceaux d'électrons très rapides avec des vitesses d'environ $20v_t$, l'échelle spatiale caractéristique de la première étape de relaxation est de l'ordre de $20 \cdot 10^7\lambda_D$, ce qui indique, que pour des éjections des particules dans des conditions solaire; cette

étape a lieu plutôt dans la couronne solaire. Comme les simulations l'indiquent, la seconde étape de la relaxation a une durée au moins 500 fois plus longue. On peut donc s'attendre à ce que la fonction de distribution des électrons garde une petite pente positive jusqu'à des distances allant jusqu'à plusieurs AU. Ce processus en deux étapes peut expliquer le paradoxe de Sturrock, notamment, les observations de faibles faisceaux d'électrons et d'ondes associées à des distances du Soleil allant jusqu'à 5 AU. Ce résultat indique également que les pentes positives de la fonction de distribution d'électrons ne peuvent être mises en évidence que par des instruments particules très sensibles. Ceci explique sans doute pourquoi il y a tellement peu d'observations directes de la pente positive de la fonction de distribution des électrons à bord de satellites [Anderson et al., 1981, Lin et al., 1981, Fuselier et al., 1985].

Nous avons effectué une analyse préliminaire des résultats de simulations basées sur notre modèle probabiliste de l'interaction faisceau-plasma dans le cas d'une distribution de la densité de probabilité des fluctuations correspondant à celle observée dans le vent solaire. Nous avons ainsi pu obtenir les distributions statistiques des intensités d'ondes pendant le processus de développement et d'évolution de l'instabilité de faisceau-plasma dans le cas d'un plasma non-homogène. Pour mener à bien l'analyse de la distribution statistique du champ d'ondes, nous avons créé un ensemble de données artificielles base sur le profil de densité présélectionné et présentant un spectre de puissance similaire à celui observé dans le vent solaire. Pour reconstruire la distribution spatiale du champ électrique sur des échelles plus petites que l'échelle typique de la relaxation de faisceau, nous utilisons l'approximation WKB pour décrire la propagation des ondes.

L'analyse statistique ayant pour objectif de déterminer les caractéristiques statistiques du champ d'onde pour différents niveaux de fluctuations de densité, l'etude a été réalisée pour deux niveaux de fluctuations de densité. Un premier niveau relativement faible $\left(\langle \delta n^2 \rangle\right)^{1/2} \sim 0.001 N_0$ et un deuxièmeplus fort $\left(\langle \delta n^2 \rangle\right)^{1/2} \sim 0.03 N_0$. L'analyse de la distribution des pics du champ électrique a montré que, dans le cas de petites fluctuations de densité (avec un niveau moyen d'environ $0.001 N_0$), la distribution de $P(E_p^2)$ est assez semblable à la distribution log-normale pour de faibles amplitudes du champ. Cette statistique Gaussienne pour le taux de croissance est en accord avec l'hypothèse de base de la théorie SGT. Pour des amplitudes plus grandes, la distribution des taux de croissance s'écarte assez fortement de la distribution normale.

La distribution semblable à la distribution log-normale a également été observée dans le cas des fluctuations de densité plus fortes (d'amplitude $\left(\langle \delta n^2 \rangle\right)^{1/2} / N_0 = 0.03$). Une augmentation du niveau des fluctuations de densité se traduit en fait par un décalage du pic de la distribution vers des valeurs plus faibles. Ce changement se produit parce que les fluctuations de grande amplitude peuvent supprimer ou fortement affaiblir le développement d'instabilité du faisceau. La conséquence, c'est que l'énergie acquise par les ondes dans ce cas est inférieure à celle acquise dans le cas du plasma avec le

niveau de fluctuations plus faible.

Par contre, la distribution du champ électrique des ondes de Langmuir E_p^2 subi des modifications très importantes lorsque le niveau des fluctuations $\left(\langle \delta n^2 \rangle\right)^{1/2} / N_0$ augmente. Dans le cas des fluctuations de densité de faible amplitude, $P(Re(E))$ obéit à la distribution normale avec un niveau de précision assez élevé. Quand le niveau des fluctuations de densité est plus grand, alors la distribution statistique obtenue est plus proche de la distribution du type IV de classification de Pearson.

Nous avons effectué la même analyse avec les données de simulations basées sur l'approche Hamiltonienne de Krafft et al. [2015]. Les résultats de l'analyse pour les champs de petites amplitudes sont très similaires à ceux de modèle probabiliste. Toutefois, pour des amplitudes plus grandes et à partir d'un certain champ électrique critique E_c, les distributions obtenues dans ces simulation montrent une décroissance très rapide pour les amplitudes supérieures à E_c. Les simulations de Krafft et al. [2015] étaient réalisées avec un très faible amortissement de Landau pour les fluctuations la densité de basse fréquence. En fait, ceci a permis d'observer un phénomène physique supplémentaire: l'instabilité de décroissance des ondes de Langmuir primaires en onde de Langmuir secondaire et onde ionique sonore.

Au final, il en résulte un effet de limitation de l'amplitude des ondes. Quand l'amplitude des ondes devient plus grande que le seuil de l'instabilité de décroissance, ce processus se développe assez rapidement ce qui à pour effet delimite l'amplitude des ondes. Cet effet explique la coupure et la décroissance rapide de la distribution quand les amplitudes du champ électrique sont supérieures à E_c. Pour les données obtenues avec la même modélisation mais avec un plus grand niveau des fluctuations de densité ($\left(\langle \delta n^2 \rangle\right)^{1/2} / N_0 = 0.03$), la distribution obtenue se trouve être similaire à la distribution log-normale obtenue pour les petites amplitudes, et rapidement décroissante pour des amplitudes plus grandes que E_c. Une augmentation du niveau des fluctuations de densité abouti au déplacement du maximum de distribution $\langle E_p^2 \rangle$ vers des valeurs plus faibles. Ce déplacement se produit parce que les grandes fluctuations de densité peuvent supprimer l'instabilité du faisceau, et ainsi, la quantité d'énergie acquise par les ondes est inférieure à celle acquise quand le niveau de fluctuations est plus élevé. Cependant, l'amplitude du champ électrique en cas de faible amortissement atteint toujours le seuil de l'instabilité de décroissance.

Il faut noter que les résultats de notre analyse préliminaire sont assez proches de ceux obtenus à partir des données expérimentales mesurées à bord des satellites Cluster [Krasnoselskikh et al., 2007] et Wind [Cairns and Robinson, 1999].

Il convient aussi de souligner que les résultats obtenus dans le cadre du modèle probabiliste sont très proches de ceux obtenus en utilisant le modèle Hamiltonien de l'interaction faisceau-plasma dans le vent solaire non-homogène. Ces derniers avaient déjà été comparés avec les mesures directes des formes d'onde faites à bord de satellites

WIND et STEREO. Ces comparaisons avaient permis de démontrer que les simulations reproduisent bien, on peut même dire en détail, les données d'observations [Krafft et al., 2014]. Ces simulations numériques mettent en évidence la formation de pics localisés du champ électrique d'ondes de Langmuir ayant des amplitudes plusieurs fois au-dessus de la moyenne. Le modèle considère deux effets non-linéaires, liées à la présence des irrégularités de densité dans le plasma, qui peuvent causer le phénomène de formation de bouffées d'ondes. L'effet de concentration d'ondes dans des paquets est observé dans le modèle Hamiltonien aussi bien que dans le modèle probabiliste. Dans le modèle probabiliste, l'élément important est le coefficient moyen du taux de croissance des ondes, γ. Le gain en l'énergie des ondes est obtenu via des échelles spatiales plus grandes que l'échelle caractéristique de la fluctuation de densité localisée, ce qui implique que ce modèle ne peut pas décrire l'amplification significative de l'amplitude des ondes a partir d'une échelle de fluctuation unique. En conséquence, nous pouvons conclure que, les structures de bouffée d'ondes observées sont principalement dues à l'effet lié à la propagation des ondes dans un plasma non-homogène, et que l'effet des oscillations du taux de croissance joue un rôle moins important.

Bibliography

A. I. Akhiezer. *Plasma electrodynamics - Vol.1: Linear theory; Vol.2: Non-linear theory and fluctuations.* 1975.

H. Alvarez, F. Haddock, and R. P. Lin. Evidence for Electron Excitation of Type III Radio Burst Emission. *Solar Phys.*, 26:468–473, Oct. 1972. doi: 10.1007/BF00165288.

K. A. Anderson and R. P. Lin. Observations on the Propagation of Solar-Flare Electrons in Interplanetary Space. *Physical Review Letters*, 16:1121–1124, June 1966. doi: 10.1103/PhysRevLett.16.1121.

R. R. Anderson, T. E. Eastman, D. A. Gurnett, L. A. Frank, and G. K. Parks. Plasma waves associated with energetic particles streaming into the solar wind from the earth's bow shock. *J. Geophys. Res.*, 86:4493–4510, June 1981. doi: 10.1029/JA086iA06p04493.

L. A. Artsimovich and R. Z. Sagdeev. Plasma physics for physicists. *Moscow Atomizdat*, 1979.

M. J. Aschwanden. Particle acceleration and kinematics in solar flares - A Synthesis of Recent Observations and Theoretical Concepts (Invited Review). *Space Sci. Rev.*, 101:1–227, Jan. 2002. doi: 10.1023/A:1019712124366.

D. R. Austin, M. J. Hole, P. A. Robinson, I. H. Cairns, and R. Dallaqua. Laboratory Evidence for Stochastic Plasma-Wave Growth. *Physical Review Letters*, 99(20): 205004, Nov. 2007. doi: 10.1103/PhysRevLett.99.205004.

S. D. Bale, D. Burgess, P. J. Kellogg, K. Goetz, and S. J. Monson. On the amplitude of intense Langmuir waves in the terrestrial electron foreshock. *J. Geophys. Res.*, 102: 11281–11286, June 1997. doi: 10.1029/97JA00938.

S. D. Bale, P. J. Kellogg, K. Goetz, and S. J. Monson. Transverse z-mode waves in the terrestrial electron foreshock. *Geophys. Res. Lett.*, 25:9–12, 1998. doi: 10.1029/97GL03493.

J. S. Bendat and A. G. Piersol. BOOK REVIEW: Random Data Analysis and Measurement Procedures. *Measurement Science and Technology*, 11:1825–1826, Dec. 2000. doi: 10.1088/0957-0233/11/12/702.

N. H. Bian, E. P. Kontar, and H. Ratcliffe. Resonance broadening due to particle scattering and mode coupling in the quasi-linear relaxation of electron beams. *Journal of Geophysical Research (Space Physics)*, 119:4239–4255, June 2014. doi: 10.1002/2013JA019664.

C. R. Boshuizen, I. H. Cairns, and P. A. Robinson. Stochastic growth theory of spatially-averaged distributions of Langmuir Fields in Earth's foreshock. *Geophys. Res. Lett.*, 28:3569–3572, 2001. doi: 10.1029/2000GL012709.

D. A. Brain. The bow shocks and upstream waves of Venus and Mars. *Advances in Space Research*, 33:1913–1919, Jan. 2004. doi: 10.1016/j.asr.2003.05.036.

B. N. Breizman and D. D. Ryutov. Influence of Inhomogeneity of Plasma on the Relaxation of an Ultrarelativistic Electron Beam. *Soviet Journal of Experimental and Theoretical Physics Letters*, 11:421, June 1970.

I. H. Cairns and D. B. Melrose. A theory for the 2f(p) radiation upstream of the earth's bow shock. *J. Geophys. Res.*, 90:6637–6640, July 1985. doi: 10.1029/JA090iA07p06637.

I. H. Cairns and J. D. Menietti. Stochastic growth of waves over Earth's polar cap. *J. Geophys. Res.*, 106:29515–29530, Dec. 2001. doi: 10.1029/2000JA000422.

I. H. Cairns and P. A. Robinson. Strong Evidence for Stochastic Growth of Langmuir-like Waves in Earth's Foreshock. *Physical Review Letters*, 82:3066–3069, Apr. 1999. doi: 10.1103/PhysRevLett.82.3066.

L. M. Celnikier, C. C. Harvey, R. Jegou, P. Moricet, and M. Kemp. A determination of the electron density fluctuation spectrum in the solar wind, using the ISEE propagation experiment. *A&A.*, 126:293–298, Oct. 1983.

L. M. Celnikier, L. Muschietti, and M. V. Goldman. Aspects of interplanetary plasma turbulence. *A&A.*, 181:138–154, July 1987.

C. H. K. Chen, C. S. Salem, J. W. Bonnell, F. S. Mozer, and S. D. Bale. Density Fluctuation Spectrum of Solar Wind Turbulence between Ion and Electron Scales. *Physical Review Letters*, 109(3):035001, July 2012. doi: 10.1103/PhysRevLett.109.035001.

W. A. Coles and J. K. Harmon. Interplanetary scintillation measurements of the electron density power spectrum in the solar wind. *J. Geophys. Res.*, 83:1413–1420, Apr. 1978. doi: 10.1029/JA083iA04p01413.

A. J. Conway, J. C. Brown, B. A. C. Eves, and E. Kontar. Implications of solar flare hard X-ray "knee" spectra observed by RHESSI. *A&A.*, 407:725–734, Aug. 2003. doi: 10.1051/0004-6361:20030897.

W. M. Cronyn. The Analysis of Radio Scattering and Space-Probe Observations of Small-Scale Structure in the Interplanetary Medium. *ApJ*, 161:755, Aug. 1970. doi: 10.1086/150576.

W. E. Drummond and D. Pines. Nonlinear plasma oscillations. *Annals of Physics*, 28: 478–499, July 1964. doi: 10.1016/0003-4916(64)90205-2.

G. A. Dulk. Radio emission from the sun and stars. *Ann. Rev. Astron. Astrophys.*, 23: 169–224, 1985. doi: 10.1146/annurev.aa.23.090185.001125.

A. G. Emslie, B. R. Dennis, A. Y. Shih, P. C. Chamberlin, R. A. Mewaldt, C. S. Moore, G. H. Share, A. Vourlidas, and B. T. Welsch. Global Energetics of Thirty-eight Large Solar Eruptive Events. *ApJ*, 759:71, Nov. 2012. doi: 10.1088/0004-637X/759/1/71.

R. E. Ergun, D. Larson, R. P. Lin, J. P. McFadden, C. W. Carlson, K. A. Anderson, L. Muschietti, M. McCarthy, G. K. Parks, H. Reme, J. M. Bosqued, C. D'Uston, T. R. Sanderson, K. P. Wenzel, M. Kaiser, R. P. Lepping, S. D. Bale, P. Kellogg, and J.-L. Bougeret. Wind Spacecraft Observations of Solar Impulsive Electron Events Associated with Solar Type III Radio Bursts. *ApJ*, 503:435–445, Aug. 1998. doi: 10.1086/305954.

R. E. Ergun, D. M. Malaspina, I. H. Cairns, M. V. Goldman, D. L. Newman, P. A. Robinson, S. Eriksson, J. L. Bougeret, C. Briand, S. D. Bale, C. A. Cattell, P. J. Kellogg, and M. L. Kaiser. Eigenmode Structure in Solar-Wind Langmuir Waves. *Physical Review Letters*, 101(5):051101, Aug. 2008. doi: 10.1103/PhysRevLett.101.051101.

M. A. Forman, R. T. Wicks, and T. S. Horbury. Detailed Fit of "Critical Balance" Theory to Solar Wind Turbulence Measurements. *ApJ*, 733:76, June 2011. doi: 10.1088/0004-637X/733/2/76.

L. A. Frank and D. A. Gurnett. Direct Observations of Low-Energy Solar Electrons Associated with a Type III Solar Radio Burst. *Solar Phys.*, 27:446–465, Dec. 1972. doi: 10.1007/BF00153116.

S. A. Fuselier, D. A. Gurnett, and R. J. Fitzenreiter. The downshift of electron plasma oscillations in the electron foreshock region. *J. Geophys. Res.*, 90:3935–3946, May 1985. doi: 10.1029/JA090iA05p03935.

A. A. Galeev, R. Z. Sagdeev, V. D. Shapiro, and V. I. Shevchenko. Langmuir turbulence and dissipation of high-frequency energy. *Soviet Journal of Experimental and Theoretical Physics*, 46:711, Oct. 1977a.

A. A. Galeev, R. Z. Sagdeev, V. D. Shapiro, and V. I. Shevchenko. Relaxation of high-current electron beams and the modulational instability. *Zhurnal Eksperimentalnoi i Teoreticheskoi Fiziki*, 72:507–517, Feb. 1977b.

V. L. Ginzburg and V. V. Zhelezniakov. On the Possible Mechanisms of Sporadic Solar Radio Emission (Radiation in an Isotropic Plasma). *Soviet Ast.*, 2:653, Oct. 1958.

M. V. Goldman. Progress and problems in the theory of type III solar radio emission. *Solar Phys.*, 89:403–442, Dec. 1983. doi: 10.1007/BF00217259.

M. V. Goldman, G. F. Reiter, and D. R. Nicholson. Radiation from a strongly turbulent plasma - Application to electron beam-excited solar emissions. *Physics of Fluids*, 23: 388–401, Feb. 1980. doi: 10.1063/1.862982.

D. B. Graham, I. H. Cairns, D. M. Malaspina, and R. E. Ergun. Evidence against the Oscillating Two-stream Instability and Spatial Collapse of Langmuir Waves in Solar Type III Radio Bursts. *ApJ Lett.*, 753:L18, July 2012. doi: 10.1088/2041-8205/753/1/L18.

R. J.-M. Grognard. Numerical simulation of the weak turbulence excited by a beam of electrons in the interplanetary plasma. *Solar Phys.*, 81:173–180, Nov. 1982. doi: 10.1007/BF00151988.

D. A. Gurnett, R. R. Anderson, F. L. Scarf, and W. S. Kurth. The heliocentric radial variation of plasma oscillations associated with type III radio bursts. *J. Geophys. Res.*, 83:4147–4152, Sept. 1978. doi: 10.1029/JA083iA09p04147.

E. L. Haydock, J. C. Brown, A. J. Conway, and A. G. Emslie. The effect of wave generation on HXR bremsstrahlung spectra from flare thick-target beams. *Solar Phys.*, 203:355–369, Nov. 2001. doi: 10.1023/A:1013389621784.

D. E. Hinkel-Lipsker, B. D. Fried, and G. J. Morales. Analytic expressions for mode conversion in a plasma with a linear density profile. *Physics of Fluids B*, 4:559–575, Mar. 1992. doi: 10.1063/1.860255.

S. A. Kaplan and V. N. Tsytovich. *Plasma astrophysics.* 1973.

J. Kašparová, E. P. Kontar, and J. C. Brown. Hard X-ray spectra and positions of solar flares observed by RHESSI: photospheric albedo, directivity and electron spectra. *A&A.*, 466:705–712, May 2007. doi: 10.1051/0004-6361:20066689.

P. J. Kellogg. Langmuir waves associated with collisionless shocks; a review. *Planet. Space Sci.*, 51:681–691, Sept. 2003. doi: 10.1016/j.pss.2003.05.001.

P. J. Kellogg and T. S. Horbury. Rapid density fluctuations in the solar wind. *Annales Geophysicae*, 23:3765–3773, Dec. 2005. doi: 10.5194/angeo-23-3765-2005.

P. J. Kellogg, K. Goetz, R. L. Howard, and S. J. Monson. Evidence for Langmuir wave collapse in the interplanetary plasma. *Geophys. Res. Lett.*, 19:1303–1306, June 1992. doi: 10.1029/92GL01016.

P. J. Kellogg, K. Goetz, S. J. Monson, and S. D. Bale. Langmuir waves in a fluctuating solar wind. *J. Geophys. Res.*, 104:17069–17078, Aug. 1999. doi: 10.1029/1999JA900163.

M. Kendall and A. Stuart. *The advanced theory of statistics. Vol.1: Distribution theory.* 1977.

E. P. Kontar. Dynamics of electron beams in the solar corona plasma with density fluctuations. *A&A.*, 375:629–637, Aug. 2001a. doi: 10.1051/0004-6361:20010807.

E. P. Kontar. Propagation of a fast electron cloud in a solar-like plasma of decreasing density. *Plasma Physics and Controlled Fusion*, 43:589–601, Apr. 2001b. doi: 10.1088/0741-3335/43/4/314.

E. P. Kontar and H. L. Pécseli. Nonlinear development of electron-beam-driven weak turbulence in an inhomogeneous plasma. *Phys. Rev. E*, 65(6):066408, June 2002. doi: 10.1103/PhysRevE.65.066408.

E. P. Kontar and H. A. S. Reid. Onsets and Spectra of Impulsive Solar Energetic Electron Events Observed Near the Earth. *ApJ Lett.*, 695:L140–L144, Apr. 2009. doi: 10.1088/0004-637X/695/2/L140.

E. P. Kontar, J. C. Brown, and G. K. McArthur. Nonuniform Target Ionization and Fitting Thick Target Electron Injection Spectra to RHESSI Data. *Solar Phys.*, 210: 419–429, Nov. 2002. doi: 10.1023/A:1022494318540.

E. P. Kontar, H. Ratcliffe, and N. H. Bian. Wave-particle interactions in non-uniform plasma and the interpretation of hard X-ray spectra in solar flares. *A&A.*, 539:A43, Mar. 2012. doi: 10.1051/0004-6361/201118216.

C. Krafft and A. Volokitin. Resonant three-wave interaction in the presence of suprathermal electron fluxes. *Annales Geophysicae*, 22:2171–2179, June 2004. doi: 10.5194/angeo-22-2171-2004.

C. Krafft and A. Volokitin. Stabilization of the fan instability: Electron flux relaxation. *Physics of Plasmas*, 13(12):122301, Dec. 2006. doi: 10.1063/1.2372464.

C. Krafft, A. S. Volokitin, and V. V. Krasnoselskikh. Interaction of Energetic Particles with Waves in Strongly Inhomogeneous Solar Wind Plasmas. *ApJ*, 778:111, Dec. 2013. doi: 10.1088/0004-637X/778/2/111.

C. Krafft, A. S. Volokitin, V. V. Krasnoselskikh, and T. D. de Wit. Waveforms of Langmuir turbulence in inhomogeneous solar wind plasmas. *Journal of Geophysical Research (Space Physics)*, 119:9369–9382, Dec. 2014. doi: 10.1002/2014JA020329.

C. Krafft, A. S. Volokitin, and V. V. Krasnoselskikh. Langmuir Wave Decay in Inhomogeneous Solar Wind Plasmas: Simulation Results. *ApJ*, 809:176, Aug. 2015. doi: 10.1088/0004-637X/809/2/176.

V. V. Krasnoselskikh, V. V. Lobzin, K. Musatenko, J. Soucek, J. S. Pickett, and I. H. Cairns. Beam-plasma interaction in randomly inhomogeneous plasmas and statistical properties of small-amplitude Langmuir waves in the solar wind and electron foreshock. *Journal of Geophysical Research (Space Physics)*, 112(11):A10109, Oct. 2007. doi: 10.1029/2006JA012212.

V. V. Krasnoselskikh, T. Dudok de Wit, and S. D. Bale. Determining the wavelength of Langmuir wave packets at the Earth's bow shock. *Annales Geophysicae*, 29:613–617, Mar. 2011. doi: 10.5194/angeo-29-613-2011.

S. Krucker and R. P. Lin. Relative Timing and Spectra of Solar Flare Hard X-ray Sources. *Solar Phys.*, 210:229–243, Nov. 2002. doi: 10.1023/A:1022469902940.

S. Krucker, E. P. Kontar, S. Christe, and R. P. Lin. Solar Flare Electron Spectra at the Sun and near the Earth. *ApJ Lett.*, 663:L109–L112, July 2007. doi: 10.1086/519373.

S. Krucker, P. H. Oakley, and R. P. Lin. Spectra of Solar Impulsive Electron Events Observed Near Earth. *ApJ*, 691:806–810, Jan. 2009. doi: 10.1088/0004-637X/691/1/806.

V. Krupar, E. P. Kontar, J. Soucek, O. Santolik, M. Maksimovic, and O. Kruparova. On the speed and acceleration of electron beams triggering interplanetary type III radio bursts. *A&A.*, 580:A137, Aug. 2015. doi: 10.1051/0004-6361/201425308.

R. M. Kulsrud. Magnetic reconnection in a magnetohydrodynamic plasma. *Physics of Plasmas*, 5:1599–1606, May 1998. doi: 10.1063/1.872827.

L. D. Landau and E. M. Lifshitz. *Electrodynamics of continuous media.* 1960.

B. Li, P. A. Robinson, and I. H. Cairns. Quasilinear calculation of Langmuir wave generation and beam propagation in the presence of density fluctuations. *Physics of Plasmas*, 13(8):082305, Aug. 2006. doi: 10.1063/1.2218331.

R. P. Lin. The Emission and Propagation of 40 keV Solar Flare Electrons. I: The Relationship of 40 keV Electron to Energetic Proton and Relativistic Electron Emission by the Sun. *Solar Phys.*, 12:266–303, May 1970. doi: 10.1007/BF00227122.

R. P. Lin. Non-relativistic Solar Electrons. *Space Sci. Rev.*, 16:189–256, June 1974. doi: 10.1007/BF00240886.

R. P. Lin. Energetic solar electrons in the interplanetary medium. *Solar Phys.*, 100: 537–561, Oct. 1985. doi: 10.1007/BF00158444.

R. P. Lin and R. A. Schwartz. High spectral resolution measurements of a solar flare hard X-ray burst. *ApJ*, 312:462–474, Jan. 1987. doi: 10.1086/164891.

R. P. Lin, D. W. Potter, D. A. Gurnett, and F. L. Scarf. Energetic electrons and plasma waves associated with a solar type III radio burst. *ApJ*, 251:364–373, Dec. 1981. doi: 10.1086/159471.

R. P. Lin, R. A. Mewaldt, and M. A. I. Van Hollebeke. The energy spectrum of 20 keV-20 MeV electrons accelerated in large solar flares. *ApJ*, 253:949–962, Feb. 1982. doi: 10.1086/159693.

R. P. Lin, W. K. Levedahl, W. Lotko, D. A. Gurnett, and F. L. Scarf. Evidence for nonlinear wave-wave interactions in solar type III radio bursts. *ApJ*, 308:954–965, Sept. 1986. doi: 10.1086/164563.

D. M. Malaspina and R. E. Ergun. Observations of three-dimensional Langmuir wave structure. *Journal of Geophysical Research (Space Physics)*, 113(12):A12108, Dec. 2008. doi: 10.1029/2008JA013656.

D. M. Malaspina, I. H. Cairns, and R. E. Ergun. Antenna Radiation near the Local Plasma Frequency by Langmuir Wave Eigenmodes. *ApJ*, 755:45, Aug. 2012. doi: 10.1088/0004-637X/755/1/45.

A. Mangeney, C. Salem, C. Lacombe, J.-L. Bougeret, C. Perche, R. Manning, P. J. Kellogg, K. Goetz, S. J. Monson, and J.-M. Bosqued. WIND observations of coherent electrostatic waves in the solar wind. *Annales Geophysicae*, 17:307–320, Mar. 1999. doi: 10.1007/s00585-999-0307-y.

D. B. Melrose. The emission mechanisms for solar radio bursts. *Space Sci. Rev.*, 26: 3–38, May 1980a. doi: 10.1007/BF00212597.

D. B. Melrose. *Plasma astrohysics. Nonthermal processes in diffuse magnetized plasmas - Vol.1: The emission, absorption and transfer of waves in plasmas; Vol.2: Astrophysical applications*. 1980b.

D. B. Melrose. Plasma emission - A review. *Solar Phys.*, 111:89–101, Mar. 1987. doi: 10.1007/BF00145443.

D. B. Melrose and M. V. Goldman. Microstructures in type III events in the solar wind. *Solar Phys.*, 107:329–350, Sept. 1987. doi: 10.1007/BF00152030.

D. B. Melrose, I. H. Cairns, and G. A. Dulk. Clumpy Langmuir waves in type III solar radio bursts. *A&A.*, 163:229–238, July 1986.

L. Muschietti, M. V. Goldman, and D. Newman. Quenching of the beam-plasma instability by large-scale density fluctuations in 3 dimensions. *Solar Phys.*, 96:181–198, Mar. 1985. doi: 10.1007/BF00239800.

M. Neugebauer. The enhancement of solar wind fluctuations at the proton thermal gyroradius. *J. Geophys. Res.*, 80:998–1002, Mar. 1975. doi: 10.1029/JA080i007p00998.

K. Nishikawa and D. D. Ryutov. Relaxation of relativistic electron beam in a plasma with random density inhomogeneities. *Journal of the Physical Society of Japan*, 41: 1757–1765, Nov. 1976.

T. M. O'Neil, J. H. Winfrey, and J. H. Malmberg. Nonlinear Interaction of a Small Cold Beam and a Plasma. *Physics of Fluids*, 14:1204–1212, June 1971. doi: 10.1063/1.1693587.

I. N. Onishchenko, A. R. Linetskii, N. G. Matsiborko, V. D. Shapiro, and V. I. Shevchenko. Contribution to the Nonlinear Theory of Excitation of a Monochromatic Plasma Wave by an Electron Beam. *Soviet Journal of Experimental and Theoretical Physics Letters*, 12:281, 1970.

K. Papadopoulos and H. P. Freund. Solitons and second harmonic radiation in type III bursts. *Geophys. Res. Lett.*, 5:881–884, Oct. 1978. doi: 10.1029/GL005i010p00881.

K. Papadopoulos, M. L. Goldstein, and R. A. Smith. Stabilization of Electron Streams in Type III Solar Radio Bursts. *ApJ*, 190:175–186, May 1974. doi: 10.1086/152862.

K. Pearson. Contributions to the Mathematical Theory of Evolution. II. Skew Variation in Homogeneous Material. *Royal Society of London Philosophical Transactions Series A*, 186:343–414, 1895. doi: 10.1098/rsta.1895.0010.

D. Píša, G. B. Hospodarsky, W. S. Kurth, O. Santolík, J. Souček, D. A. Gurnett, A. Masters, and M. E. Hill. Statistics of Langmuir wave amplitudes observed inside Saturn's foreshock by the Cassini spacecraft. *Journal of Geophysical Research (Space Physics)*, 120:2531–2542, Apr. 2015. doi: 10.1002/2014JA020560.

O. Podladchikova, B. Lefebvre, V. Krasnoselskikh, and V. Podladchikov. Classification of probability densities on the basis of Pearson's curves with application to coronal heating simulations. *Nonlinear Processes in Geophysics*, 10:323–333, 2003.

E. Priest and T. Forbes. *Magnetic Reconnection*. June 2000.

H. Ratcliffe, N. H. Bian, and E. P. Kontar. Density Fluctuations and the Acceleration of Electrons by Beam-generated Langmuir Waves in the Solar Corona. *ApJ*, 761:176, Dec. 2012. doi: 10.1088/0004-637X/761/2/176.

H. Ratcliffe, E. P. Kontar, and H. A. S. Reid. Large-scale simulations of solar type III radio bursts: flux density, drift rate, duration, and bandwidth. *A&A.*, 572:A111, Dec. 2014. doi: 10.1051/0004-6361/201423731.

H. A. S. Reid and E. P. Kontar. Solar Wind Density Turbulence and Solar Flare Electron Transport from the Sun to the Earth. *ApJ*, 721:864–874, Sept. 2010. doi: 10.1088/0004-637X/721/1/864.

H. A. S. Reid and E. P. Kontar. Evolution of the Solar Flare Energetic Electrons in the Inhomogeneous Inner Heliosphere. *Solar Phys.*, 285:217–232, July 2013. doi: 10.1007/s11207-012-0013-x.

H. A. S. Reid and E. P. Kontar. Stopping frequency of type III solar radio bursts in expanding magnetic flux tubes. *A&A.*, 577:A124, May 2015. doi: 10.1051/0004-6361/201425309.

H. A. S. Reid and H. Ratcliffe. A review of solar type III radio bursts. *Research in Astronomy and Astrophysics*, 14:773–804, July 2014. doi: 10.1088/1674-4527/14/7/003.

P. A. Robinson. Clumpy Langmuir waves in type III radio sources. *Solar Phys.*, 139: 147–163, May 1992. doi: 10.1007/BF00147886.

P. A. Robinson. Stochastic wave growth. *Physics of Plasmas*, 2:1466–1479, May 1995. doi: 10.1063/1.871362.

P. A. Robinson, I. H. Cairns, and D. A. Gurnett. Clumpy Langmuir waves in type III radio sources - Comparison of stochastic-growth theory with observations. *ApJ*, 407: 790–800, Apr. 1993. doi: 10.1086/172560.

D. D. Ryutov. Quasilinear Relaxation of an Electron Beam in an Inhomogeneous Plasma. *Soviet Journal of Experimental and Theoretical Physics*, 30:131, 1969.

R. Z. Sagdeev and A. A. Galeev. *Nonlinear Plasma Theory.* 1969.

D. F. Smith and D. Sime. Origin of plasma-wave clumping in type III solar radio burst sources. *ApJ*, 233:998–1004, Nov. 1979. doi: 10.1086/157463.

R. A. Smith, M. L. Goldstein, and K. Papadopoulos. On the theory of the type III burst exciter. *Solar Phys.*, 46:515–527, Feb. 1976. doi: 10.1007/BF00149880.

J. Soucek, O. Santolik, T. Dudok de Wit, and J. S. Pickett. Cluster multispacecraft measurement of spatial scales of foreshock Langmuir waves. *Journal of Geophysical Research (Space Physics)*, 114:A02213, Feb. 2009. doi: 10.1029/2008JA013770.

P. A. Sturrock. Type III Solar Radio Bursts. *NASA Special Publication*, 50:357, 1964.

T. Takakura and H. Shibahashi. Dynamics of a cloud of fast electrons travelling through the plasma. *Solar Phys.*, 46:323–346, Feb. 1976. doi: 10.1007/BF00149860.

G. Thejappa, R. J. MacDowall, M. Bergamo, and K. Papadopoulos. Evidence for the Oscillating Two Stream Instability and Spatial Collapse of Langmuir Waves in a Solar Type III Radio Burst. *ApJ Lett.*, 747:L1, Mar. 2012. doi: 10.1088/2041-8205/747/1/L1.

G. Thejappa, R. J. MacDowall, and M. Bergamo. Observational evidence for the collapsing Langmuir wave packet in a solar type III radio burst. *Journal of Geophysical Research (Space Physics)*, 118:4039–4052, July 2013. doi: 10.1002/jgra.50441.

A. N. Tikhonov. *Current problems of mathematical physics and computational mathematics*. 1982.

J. Šafránková, Z. Němeček, F. Němec, L. Přech, A. Pitňa, C. H. K. Chen, and G. N. Zastenker. Solar Wind Density Spectra around the Ion Spectral Break. *ApJ*, 803: 107, Apr. 2015. doi: 10.1088/0004-637X/803/2/107.

J. A. van Allen and S. M. Krimigis. Impulsive Emission of 40-kev Electrons from the Sun. *J. Geophys. Res.*, 70:5737–5751, Dec. 1965. doi: 10.1029/JZ070i023p05737.

A. A. Vedenov and D. D. Ryutov. Quasilinear Effects in Two-Stream Instabilities. In A. M. A. Leontovich, editor, *Reviews of Plasma Physics, Volume 6*, volume 6 of *Reviews of Plasma Physics*, page 1, 1975.

A. A. Vedenov, E. Velikhov, and R. Sagdeev. Quasilinear theory of plasma oscillations. *Nuclear Fusion Suppl.*, 2:465–475, 1962.

S. Vidojević, A. Zaslavsky, M. Maksimović, M. Dražić, and O. Atanacković. Statistical Analysis of Langmuir Waves Associated with Type III Radio Bursts: I. Wind Observations. *Baltic Astronomy*, 20:596–599, 2011.

A. Volokitin, V. Krasnoselskikh, C. Krafft, and E. Kuznetsov. Modelling of the beam-plasma interaction in a strongly inhomogeneous plasma. In G. P. Zank, J. Borovsky, R. Bruno, J. Cirtain, S. Cranmer, H. Elliott, J. Giacalone, W. Gonzalez, G. Li, E. Marsch, E. Moebius, N. Pogorelov, J. Spann, and O. Verkhoglyadova, editors, *American Institute of Physics Conference Series*, volume 1539 of *American Institute of Physics Conference Series*, pages 78–81, June 2013. doi: 10.1063/1.4810994.

A. Voshchepynets and V. Krasnoselskikh. Electron beam relaxation in inhomogeneous plasmas. *Annales Geophysicae*, 31:1379–1385, Aug. 2013. doi: 10.5194/angeo-31-1379-2013.

A. Voshchepynets and V. Krasnoselskikh. Probabilistic model of beam-plasma interaction in randomly inhomogeneous solar wind. *Journal of Geophysical Research (Space Physics)*, 120:10, Dec. 2015. doi: 10.1002/2015JA021705.

A. Voshchepynets, V. Krasnoselskikh, A. Artemyev, and A. Volokitin. Probabilistic Model of Beam-Plasma Interaction in Randomly Inhomogeneous Plasma. *ApJ*, 807: 38, July 2015. doi: 10.1088/0004-637X/807/1/38.

J. P. Wild, S. F. Smerd, and A. A. Weiss. Solar Bursts. *Ann. Rev. Astron. Astrophys.*, 1:291, 1963. doi: 10.1146/annurev.aa.01.090163.001451.

R. Woo and J. W. Armstrong. Spacecraft radio scattering observations of the power spectrum of electron density fluctuations in the solar wind. *J. Geophys. Res.*, 84: 7288–7296, Dec. 1979. doi: 10.1029/JA084iA12p07288.

P. H. Yoon, C. S. Wu, A. F. Vinas, M. J. Reiner, J. Fainberg, and R. G. Stone. Theory of 2 omega$_{pe}$ radiation induced by the bow shock. *J. Geophys. Res.*, 99:23481, Dec. 1994. doi: 10.1029/94JA02489.

V. V. Zaitsev, N. A. Mityakov, and V. O. Rapoport. A Dynamic Theory of Type III Solar Radio Bursts. *Solar Phys.*, 24:444–456, June 1972. doi: 10.1007/BF00153387.

V. E. Zakharov. Collapse of Langmuir Waves. *Soviet Journal of Experimental and Theoretical Physics*, 35:908, 1972.

A. Zaslavsky, C. Krafft, L. Gorbunov, and A. Volokitin. Wave-particle interaction at double resonance. *Phys. Rev. E*, 77(5):056407, May 2008. doi: 10.1103/PhysRevE.77.056407.

V. V. Zharkova and M. Gordovskyy. The Effect of the Electric Field Induced by Precipitating Electron Beams on Hard X-Ray Photon and Mean Electron Spectra. *ApJ*, 651:553–565, Nov. 2006. doi: 10.1086/506423.

L. F. Ziebell, P. H. Yoon, J. Pavan, and R. Gaelzer. Nonlinear Evolution of Beam-plasma Instability in Inhomogeneous Medium. *ApJ*, 727:16, Jan. 2011. doi: 10.1088/0004-637X/727/1/16.